AD-A067 514 CALIFORNIA UNIV LOS ANGELES DEPT OF CHEMICAL UNCLEAR--ETC F/G 10/3
THEORETICAL AND EXPERIMENTAL ANALYSIS OF ALKALINE ZINC BATTERIE--ETC(U)
JAN 79 D N BENNION, J NEWMAN, W G SUNU F44620-76-C-0098

UNCLASSIFIED UCLA-CNTE-1-1 AFOSR-TR-79-0472 NL

1 OF 2
ADA
067514

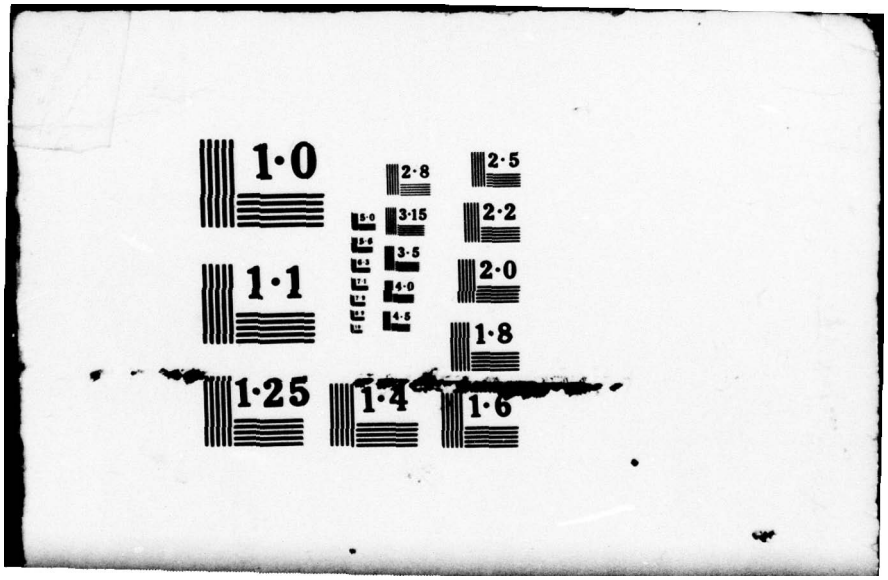
1·0
1·1
1·25
2·8
3·15
3·5
4·0
4·5
2·5
2·2
2·0
1·8
1·4
1·6

(18) AFOSR-TR-79-0472 APR 9 RECD

(19)

(14) UCLA-CNTE-1-1
January 1979

LEVEL II

(12)

(6) THEORETICAL AND EXPERIMENTAL ANALYSIS OF ALKALINE ZINC BATTERIES.

(10) Douglas N. Bennion, Principal Investigator
John Newman, Co-Principal Investigator
Won Sunu,
Siddhartha Ghosh
Bruce M. Eliash
Manojit Sinha

Guen

(11) Jan 79

(12) 286p.

(15) Contract No. F44620-76-C-0098 Mod P00006

(9) Final rept.
15 Apr 76 - 30 Sep 78

Distribution of this document is unlimited

(16) 2303

(17) A1

AIR FORCE OFFICE OF SCIENTIFIC RESEARCH (AFSC)
NOTICE OF TRANSMITTAL TO DDC
This technical report has been reviewed and is approved for public release IAW AFR 190-12 (7b).
Distribution is unlimited.
A. D. BLOSE
Technical Information Officer

Chemical, Nuclear, and Thermal Engineering Department
School of Engineering and Applied Science
University of California, Los Angeles
Los Angeles, California 90024

UNCLASSIFIED

SECURITY CLASSIFICATION OF THIS PAGE (When Data Entered)

REPORT DOCUMENTATION PAGE	READ INSTRUCTIONS BEFORE COMPLETING FORM
1. REPORT NUMBER: AFOSR-TR- 79-0472 / 2. GOVT ACCESSION NO.	3. RECIPIENT'S CATALOG NUMBER
4. TITLE (and Subtitle): THEORETICAL AND EXPERIMENTAL ANALYSIS OF ALKALINE ZINC BATTERIES	5. TYPE OF REPORT & PERIOD COVERED: Final 4/15/76-9/30/78
	6. PERFORMING ORG. REPORT NUMBER: UCLA-CNTE-1-1
7. AUTHOR(s): Douglas N. Bennion, John Newman, Won G. Sunu, Siddhartha Ghosh, Bruce M. Eliash, Manojit Sinha	8. CONTRACT OR GRANT NUMBER(s): F44620-76-C-0098
9. PERFORMING ORGANIZATION NAME AND ADDRESS: Chemical, Nuclear, & Thermal Engr. Dept. University of California Los Angeles, California 90024	10. PROGRAM ELEMENT, PROJECT, TASK AREA & WORK UNIT NUMBERS: 61102F 2303/A1
11. CONTROLLING OFFICE NAME AND ADDRESS: Air Force Office of Scientific Research/NC Bolling Air Force Base, DC 20332	12. REPORT DATE: January 1979
	13. NUMBER OF PAGES: 184
14. MONITORING AGENCY NAME & ADDRESS(if different from Controlling Office)	15. SECURITY CLASS. (of this report): Unclassified
	15a. DECLASSIFICATION/DOWNGRADING SCHEDULE

16. DISTRIBUTION STATEMENT (of this Report)

Approved for public release; distribution unlimited.

17. DISTRIBUTION STATEMENT (of the abstract entered in Block 20, if different from Report)

18. SUPPLEMENTARY NOTES

19. KEY WORDS (Continue on reverse side if necessary and identify by block number)

Batteries, Zinc, Zinc Oxide, Nickel Oxide, Separators, Potassium Hydroxide, Storage Batteries, Math Model

20. ABSTRACT (Continue on reverse side if necessary and identify by block number)

The processes that control the useful life time and performance rates in non-flowing zinc electrodes for electrical storage batteries have been investigated. In particular, the chemical reaction rates, concentration, and electrical potential distributions have been predicted theoretically and measured experimentally as functions of position in the electrode and time for both charge, discharge, and multiple cycles. Changes in crystal structure and solid distributions have also been measured and examined theoretically. Similar rates and distributions have been measured and correlated for RAI P2291 ion exchange

20. Abstract (continued)

membrane separators used in zinc secondary batteries such as the nickel-zinc battery ($Zn/KOH,H_2O/NiOOH$). Distributions in flow through electrodes were also observed experimentally and calculated theoretically, using the copper deposition reaction for experimental convenience. Work was begun on the theoretical description of the nickel oxide electrode. Experimental work is being planned to validate and revise our understanding of how the nickel electrode operates. Work is continuing on measurement of concentration profiles in zinc electrodes.

FOREWORD

This Final Report was prepared by Won G. Sunu, Manojit Sinha, Siddhartha Ghosh, Bruce M. Eliash, Douglas N. Bennion (Principal Investigator) and John Newman (Co-Principal Investigator). The report covers work done April 15, 1976, through September 30, 1978, on contract number F44620-76-C-0098. Advice and direction of Dr. David Pickett and other personnel at AFAPL, Wright Patterson Air Force Base, is gratefully acknowledged.

The principal, completed results of this work are reported in the Ph.D. dissertation of Dr. Won G. Sunu and the M.S. thesis of Mr. Manojit Sinha. Dr. Sunu's dissertation is included in its entirety as a part of this report. Three papers are being prepared based on Dr. Sunu's research. They will be submitted for publication in 1979. Mr. Sinha's thesis was condensed, modestly revised, and published in the *J. Electrochem. Soc.* A reprint of that paper is included as a part of this report.

Mr. Siddhartha Ghosh was supported primarily through work study funds from the University of California. Between 10 and 20% of his support was from this contract. His thesis is included as part of this report. A paper based on that work is to be submitted for publication in 1979.

Two projects are not yet complete. Mr. Bruce Eliash is continuing the work of Dr. Sunu. Mr. Eliash's work should be finished in late 1979 or early 1980. Publication of that work is expected in 1980. Mr. Manojit Sinha has begun his Ph.D. research work on the performance of the nickel oxide electrode in alkaline media. A preliminary theoretical model is proposed and a computer code has been written which allows calculations based on the model. The results of that work are included

with this report. Experimental work to test and improve the model is being started. Publication of these results is expected in 1980.

PAPERS PUBLISHED OR IN PREPARATION BASED ON WORK DONE ON THIS CONTRACT

Publications

Manojit Sinha and Douglas N. Bennion, "Transport Parameters for Potassium Hydroxide-Water Solution in a Cation Exchange Membrane", J. Electrochem. Soc., 125, 556-561 (1978).

Papers in Preparation

Won G. Sunu, Douglas N. Bennion, and John Newman, "Mass Transfer in Concentrated Ternary Electrolytes" (to be submitted Ind. Eng. Chem. Fundam., 1979).

Won G. Sunu and Douglas N. Bennion, "Transient and Failure Analysis of Porous Zinc Electrodes, I, Theoretical" (to be submitted J. Electrochem. Soc., 1979).

Won G. Sunu and Douglas N. Bennion, "Transient and Failure of Porous Zinc Electrodes, II, Experimental" (to be submitted J. Electrochem. Soc., 1979).

Siddhartha Ghosh and Douglas N. Bennion, "Removal of Copper from Dilute Solutions by a Flow-through Porous Electrode" (to be submitted J. Appl. Electrochem., 1979).

Papers in Preparation for which Experimental Work is Still Going on

Bruce M. Eliash and Douglas N. Bennion, "Zinc Electrode Concentration Profiles" (to be submitted J. Electrochem. Soc., 1980).

Manojit Sinha and Douglas N. Bennion, "Performance Controlling Processes in a Porous Nickel Oxide Battery Electrode" (to be submitted J. Electrochem. Soc., 1980).

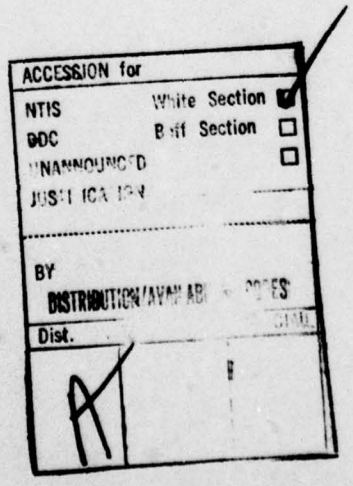

TABLE OF CONTENTS

Foreword

List of Publications

Table of Contents

Abstract

1. "Transient and Failure Analyses of Porous Zinc Electrodes" by W. G. Sunu and D. N. Bennion

2. "Transport Parameters for Potassium Hydroxide-Water Solution in a Cation Exchange Membrane" by Manojit Sinha and Douglas N. Bennion

3. "Study of a Flow-through Porous Electrode Having Perpendicular Direction of Current and Electrolyte Flow for Removal of Copper from Dilute Solution" by Siddhartha Ghosh and Douglas N. Bennion

4. "Zinc Electrode Concentration Profiles, A Preliminary Report" by Bruce M. Eliash and Douglas N. Bennion

5. "Performance Controlling Processes in a Porous Nickel Oxide Battery Electrode, A Preliminary Report" by Manojit Sinha and Douglas N. Bennion

ABSTRACT

The processes that control the useful life time and performance rates in non-flowing zinc electrodes for electrical storage batteries have been investigated. In particular, the chemical reaction rates, concentration, and electrical potential distributions have been predicted theoretically and measured experimentally as functions of position in the electrode and time for both charge, discharge, and multiple cycles. Changes in crystal structure and solid distributions have also been measured and examined theoretically. Similar rates and distributions have been measured and correlated for RAI P2291 ion exchange membrane separators used in zinc secondary batteries such as the nickel-zinc battery ($Zn/KOH,H_2O/NiOOH$). Distributions in flow through electrodes were also observed experimentally and calculated theoretically, using the copper deposition reaction for experimental convenience. Work was begun on the theoretical description of the nickel oxide electrode. Experimental work is being planned to validate and revise our understanding of how the nickel electrode operates. Work is continuing on measurement of concentration profiles in zinc electrodes.

A number of factors have been found to be important in the operation and control of zinc electrodes. During discharge, zinc metal (Zn) reacts with hydroxyl ions (OH^-) to yield water and electrons which are "pumped" into the external electrical circuit. Initially OH^- ions within the porous, zinc electrode are consumed. When those OH^- ions are consumed, further reaction must be supported by transport of OH^- across the separator from the counter electrode, nickel oxide, for example. For RAI P2291 membrane separators, it was found that reaction rates of 50 mA/cm^2 could

not be supported by the ion transport, but 20 mA/cm^2 could be supported. The supply of OH^- ions across the separator is one factor, along with the electric potential distribution, which causes the discharge reaction to concentrate in a narrow zone close to the membrane. At 20 mA/cm^2 the zone is about 0.3 mm across. At 50 mA/cm^2 the zone shrinks to about 0.1 mm. The reaction zone thickness has important implications for electrode design.

During charging of the zinc electrode, OH^- ions are produced within the porous electrode. This situation causes the OH^- ion concentration to increase in the depth of the porous electrode favoring a broad reaction zone and lower potential losses at higher current densities as compared to the discharge reaction. The implication is that the zinc electrode can be safely charged at higher rates than discharged. There are other considerations which enter, however. The nickel electrode becomes OH^- ion "starved" during charging and wild, dendritic type zinc deposits get worse at high charge rates. Thus high charge rates are not really possible.

Two types of zinc electrode passivation have been identified, surface coverage of otherwise reactive zinc area and pore blockage. Pore blockage will be discussed in later paragraphs. The exposed, reactive zinc is gradually covered up by ZnO precipitation as the discharge reaction proceeds. At modest current densities and reasonably high OH^- concentrations, above about 1.0 M, the precipitate is a porous, fluffy type deposit which slowly inhibits access to the active zonc. However, this form of surface coverage allows large, useful fractions of active zinc to continue to react. It appears that when the surface concentration of OH^- ions get too low, the form of the precipitate becomes monolithic,

impervious, and totally blanks off any further reaction. The electrode, or at least the affected area of the porous electrode, is passivated. More detailed observations of this passivation mechanism are needed; but the evidence is that OH^- ion concentration is a significant factor.

Porosity of the porous zinc electrode is shown to be a critical parameter. Zinc oxide (ZnO) has a much larger molar volume than zinc. As zinc is converted to zinc oxide, the local volume fraction of solid increases and the volume fraction of electrolytic solution (KOH, K_2ZnOH_4, H_2O) decreases. As has been shown, the reaction rate is largest at the face of the electrode leading to pore plugging at the face if there is not sufficient space for the ZnO to precipitate. When the face of the electrode plugs, further discharge is impossible. For a porosity (fraction of volume filled with electrolytic solution) of 0.33 pore plugging at the face was the failure mode. For a porosity of 0.6, pore plugging at the face did not occur. However, tests on cycling performance showed that with increasing number of cycles more and more zinc and zinc oxide accumulated in the high reaction rate region, that is, in the face of the electrode. Long term cycle tests have not yet been done, but the clear implication of our results is that as cycling proceeds zinc transports from the central region of the electrode to the surface. This transport of zinc causes increasing porosity in the central region and decreasing porosity at the face. When the face porosity goes below a critical value of about 0.5, failure by pore plugging will occur and electrode life can be expected to end.

The OH^- concentration distributions have been shown to control many factors which govern electrode performance. Experiments to measure experimentally the actual KOH and K_2ZnOH_4 concentrations are now under

way. An operating electrode is frozen, sectioned, and the sections analyzed. Preliminary, calibrating runs and technique development are complete. Actual measurements are expected over the next few months. The results will allow validation and possibly revisions to our present model of transport in a porous zinc electrode.

It can be shown that once zinc electrodes are produced which approximate the practical limit implied by our model calculations, the nickel oxide electrode will become performance limiting. A theoretical model of the nickel electrode has been completed which shows the interrelationships of water and OH^- ion transport along with potential and reaction rate distributions and their relation to properties of the nickel oxide film and associated charge transport steps. Future experiments are designed to help investigate the nickel valence states which can be achieved and what the limitations on charge transfer capacity are for practical electrodes. In addition the role of water and affects of water balance on the nickel oxide electrode will be considered.

Flow through porous electrodes are an alternative design to the more customary electrodes with limited or no convective flow. In convection designs, the working electrode is inert, and the ZnO precipitates in a storage tank external to the electrode stack. Experimental and theoretical work has been completed demonstrating the interrelationships between flow rates, applied potential, input and output concentration, electrode length, and electrode thickness with potential, current and reaction distribution and cost effectiveness. The experimental work was done with copper deposition at 600 ppm input concentration. The optimum conditions were found to be: electrode thickness of 0.6 cm, applied potential of 1.4 V, and superficial velocity of about 11 cm/s. The minimum in velocity was very broad.

UNIVERSITY OF CALIFORNIA

Los Angeles

Transient and Failure Analyses of Porous Zinc Electrodes

A dissertation submitted in partial satisfaction of the requirements for the degree Doctor of Philosophy in Engineering

by

Won Guen Sunu
and
Douglas N. Bennion
Thesis Director

1978

TABLE OF CONTENTS

LIST OF SYMBOLS v

LIST OF TABLES ix

LIST OF FIGURES x

ACKNOWLEDGMENTS xiv

VITA xv

ABSTRACT xvi

I. INTRODUCTION 1

II. THE MATHEMATICAL MODEL 10

II-1. Zinc Electrode Reaction 10

II-2. Ternary Electrolyte Theory 11

II-3. Description of the Model 18

II-4. Computation Procedures 30

III. ZINC ELECTRODE BEHAVIOR PREDICTED FROM THE MATHEMATICAL MODEL 36

III-1. Discharge Behavior 38

III-2. Behavior on Cycling 46

III-3. Zinc Electrode Failure Modes 54

IV. EXPERIMENTS

IV-1. Preparation of the Pressed Zinc Electrode . . . 57

IV-2. Potential Measurements 58

IV-3. Determination of Reaction Profiles 62

V. RESULTS

V-1. Reaction Profiles 66

V-2. Overpotentials of the Zinc Electrode 76

VI. DISCUSSION

VI-1. Failure During Discharge 91

VI-2. Depletion of Electrolytes 92

VI-3. Pore Plugging 95

VI-4. Passivation 99

VI-5. Failure During Charge 103

VI-6. Failure During Cycling 105

VII. CONCLUSION 110

REFERENCES 112

APPENDIX A

A-1. Ternary Transport Parameters as Functions of Friction Coefficients 120

A-2. Friction Coefficients as Functions of Six Transport Parameters 121

A-3. Transformation of the Transport Equations into the Other Four Component Systems 122

A-4. Ternary Transport Parameters Calculated from Two Sets of Binary Data 124

APPENDIX B Mass Transfer Coefficients (k_A, k_B, and k_s^*) . 128

APPENDIX C

C-1. Solubility of ZnO in KOH Solution 133

C-2. Conductivity of KOH Electrolytic Solution . . 134

C-3. Activity Coefficients of Potassium Hydroxide and Potassium Zincate 135

APPENDIX D

D-1. Input Data 136

D-2. Programming Parameters 139

D-3. Computer Program 142

LIST OF SYMBOLS

A	cross sectional area of zinc electrode, cm^2
a	specific surface area per unit volume of the electrode, cm^2/cm^3
a_m	active surface area for charge transfer reaction per unit volume of the electrode, cm^2/cm^3
a_s	active surface area for precipitation or dissolution of ZnO per unit volume of the electrode, cm^2/cm^3
c_i	concentration of species i, $mole/cm^3$
c_i^o	initial concentration of species i, $mole/cm^3$
c_i^{bl}	average concentration of species i within the boundary layer, $mole/cm^3$
c_2^{eq}	equilibrium or saturation concentration of zincate ion, $mole/cm^3$
c_i^s	concentration of species i at the active metal surface, $mole/cm^3$
d	thickness of the solution or membrane boundary layer, cm
$\mathscr{D}_{ij}$	binary diffusion coefficients, cm^2/sec
D_{ij}^o	diffusion coefficients with respect to solvent velocity, cm^2/sec
D_{ij}^{bl}	diffusion coefficients across the boundary layer (solution or membrane), cm^2/sec
F	Faraday's constant, 96,487 coul/equiv.
I	superficial applied current density, amp/cm^2
i_1	superficial current density in matrix phase, amp/cm^2
i_2	superficial current density in solution phase, amp/cm^2
i_0^o	exchange current density based on initial concentrations of c_2^o and c_3^o, amp/cm^2
i_0	exchange current density, amp/cm^2
j	local transfer current density based on unit area of active zinc surface, amp/cm^2

K_{ij} friction coefficients, interaction of species i and j, Joule-sec/cm^5

k_A mass transfer coefficients of potassium zincate from active sites to bulk in the pores or vice versa, cm/sec

k_B mass transfer coefficients of potassium hydroxide from active sites to bulk in the pores or vice versa, cm/sec

k_{XTL} rate constant for precipitation or dissolution of ZnO, cm/sec

k_s^* rate constants combining mass transfer of zincate, k_A, with chemical rate constant, k_{XTL}, cm/sec

L electrode thickness, cm

L_{ij} multicomponent transport parameters, $mole^2$/sec-cm-Joule

L_{ii}^{bl} mass transfer coefficients of species i across the boundary layer used in Table I and equation (55), cm/sec

M_i chemical symbol for species i

m_i molality of species i, mole/Kg of water

N_i flux of species i in the x-direction, mole/cm^2-sec

N_i^{bl} flux of species i across the boundary layer, mole/cm^2-sec

N_i^L flux of species i across the electrode surface (x=L), mole/cm^2-sec

n number of electrons transferred in electrode reaction

n_k^i number of moles of species i in k th sectioned sample

p, q shape factor, dimensionless

RT gas constant multiplied by absolute temperature, Joule/mole

R_i source term of species i in equation (35), mole/cm^3-sec

s_i stoichiometric number of species i for charge transfer reaction, defined in equation (10)

s_i^* stoichiometric number of species i for precipitation or dissolution of ZnO, defined as in equation (10)

t, t^*	tortuosity factor
t_i^o	transference number of species i referred to solvent velocity
t_i^{bl}	transference number of species i across the boundary layer
$\bar{V}_i$	partial molar volume of species i, cm^3/mole
V	volume of electrolytic solution reservoir between the membrane and the zinc electrode surface, cm^3
v_i	velocity of species i in solution, cm/sec
$v^{\square}$	superficial volume average velocity, $\Sigma_i c_i \bar{V}_i v_i$, cm/sec
x	distance from the backing plate, cm
z_i	charge number of species i

Greek Symbols

α_a	a kinetic parameter
α_c	a kinetic parameter
γ	exponent in zincate concentration dependence of the exchange current density
γ_i	mean molal activity coefficient of species i
δ	characteristic diffusion length between the active metal surface and the bulk in the pores, cm
ϵ	electrode porosity
ϵ_i	volume fractions of solid species i
ζ	exponent in OH^- concentration dependence of the exchange current density
κ	conductivity of solution, mho/cm
κ^m	conductivity of solution in the membrane, mho/cm
ν_i^k	number of ionic species i per molecule of electrolyte "k"

ν_k number of ions produced by the dissociation of one molecule of electrolyte k. $\nu_A=\nu_1^A+\nu_2^A=3$ for potassium zincate and $\nu_B=\nu_1^B+\nu_3^B=2$ for potassium hydroxide.

μ_i chemical potential of species i, Joule/mole

σ_i conductivity of solid species i, mho/cm

ϕ_1 potential in metal phase, volts

ϕ_2 potential in solution phase , volts

ϕ_2^s potential of solution at the active metal surface, volts

Subscripts

i any arbitrary species i; 1 for potassium ion, 2 for zincate ion, 3 for hydroxide ion, A for potassium zincate, and B for potassium hydroxide.

o solvent

LIST OF TABLES

No.	Title	Page
I	Transport Parameters Applied to the Various Boundary Layers	37
II	Measured and Calculated Transference Numbers . . .	126

LIST OF FIGURES

No.	Title	Page
1.	Geometric features of the porous electrode (for anodic reaction)	19
2.	Overpotential, $\phi_1(o)- \phi_2(L)$, of zinc electrode during constant current discharge for type I membrane boundary (I=50 mA/cm^2, L=0.1 cm, ε^o=0.4, ε^o_{Zn}=0.5, ε^o_{ZnO}=0.1) .	39
3.	Concentration profiles during constant current discharge for type I membrane boundary (I=50 mA/cm^2, A for one minute polarization and B,C, and D for 10%, 20%, and 30% depth of discharge, respectively)	40
4.	Concentration profiles of KOH after 10% depth of discharge (I=50 mA/cm^2 and A, B, and C for solution boundary, type I membrane boundary, and type II membrane boundary, respectively)	42
5.	Distribution of local charge transfer current, j(mA/cm^2), for type I membrane boundary (I=50 mA/cm^2, L=0.1 cm, and A,B,C,and D represent 0%, 10%, 20%, and 40% depth of discharge, respectively)	43
6.	Distribution of Zn and ZnO plotted as volume fractions (cm^3/cm^3) for type I membrane boundary (I=50 mA/cm^2, and A, B, C, and D represent 10%, 20%, 30%, and 40% depth of discharge, respectively)	44
7.	Distribution of Zn and ZnO plotted as volume fractions (cm^3/cm^3) for solution boundary (I=50 mA/cm^2, and A, B, C, and D represent 10%, 20%, 30%, and 40% depth of discharge, respectively)	45
8.	Concentration profile during constant current charge for type I membrane boundary (I=50 mA/cm^2, L=0.1 cm, and A for one minute polarization and B and C for 10% and 20% depth of charge, respectively)	48
9.	Distribution of local charge transfer current density, j(mA/cm^2), during the first cycle for type I membrane boundary (I=50 mA/cm^2, L=0.1 cm, and A, B, and C represent 0%, 10%, 20% depth of discharge or charge, respectively)	49
10.	Overpotential, $\phi_1(o)- \phi_2(L)$, of zinc electrode with time during three cycles for type I membrane boundary. A, 1st cycle; B, 2nd cycle; C, 3rd cycle (I=50 mA/cm^2,	

L=0.1 cm, ε^{o}=0.4, ε^{o}_{Zn}=0.5, ε^{o}_{ZnO}=0.1) 50

11. Distribution of Zn and ZnO plotted as volume fractions (cm^3/cm^3) during two cycles for type I membrane boundary (I=50 mA/cm^2, L=0.1 cm, ε^{o}_{Zn}=0.5, ε^{o}_{ZnO}=0.1) 51

12. Distribution of Zn and ZnO plotted as volume fractions (cm^3/cm^3) during two cycles for solution boundary (I= 50 mA/cm^2, L=0.1 cm, ε^{o}_{Zn}=0.5, ε^{o}_{ZnO}=0.1) 52

13. Distribution of Zn and ZnO plotted as volume fractions at two current densities for type I membrane boundary. ---, after one cycle; —— , after two cycles. 53

14. Test cell assembly 59

15. Electrical circuit for operation of cell 61

16. Weight percent of the dissolved zinc in 1 M NH_4Cl-NH_4OH within 6 or 7 minutes contact time 64

17. Profiles of Zn and ZnO for the low porosity electrode discharged to 8% depth at 50 mA/cm^2. ○ and ⬡, measured profiles for Zn; histograms, measured profiles for ZnO; smooth curves, predicted profiles for Zn and ZnO 68

18. Profiles of Zn (circles and hexagons) and ZnO (histograms) for the low porosity electrode discharged at 20 mA/cm^2. ○ and histogram A, measured profiles after 10% depth; ⬡ and histogram B, measured profiles after 23% depth; smooth curves, predicted profiles after 10% and 23% depths of discharge 69

19. Profiles of Zn and ZnO for the high porosity electrode discharged to 10% depth at 50 mA/cm^2. ○ and ⬡, measured profiles for Zn; histograms, measured profiles for ZnO; smooth curves, predicted profiles for Zn and ZnO 71

20. Profiles of Zn and ZnO for the high porosity electrode discharged to 21% depth at 50 mA/cm^2. ○ and ⬡, measured profiles for Zn; histograms, measured profiles for ZnO; smooth curves, predicted profiles for Zn and ZnO 72

21. Profiles of Zn (circles and hexagons) and ZnO (histograms) measured for the high porosity electrode discharged at 20 mA/cm^2. ○ and histogram A for 10% depth of discharge; ⬡ and histogram B for 22% depth of discharge 73

22. Profiles of Zn (circles and hexagons) and ZnO (histograms) measured for the low porosity electrode discharged at 50 mA/cm^2. ○ and histogram A for 20% depth of discharge for the electrode having thickness of 0.05 cm; ⬡ and histogram B for 8% depth of discharge for the electrode having thickness of 0.1 cm 74

23. Profiles of Zn (top line) and ZnO (bottom line) measured for the low porosity electrode after one cycle. At each half cycle, 50 mA/cm^2 and 10% depth of initial zinc were applied 75

24. Overpotentials at the face of the zinc electrode (x=L) on discharge at 50 mA/cm^2. ——— and ---, measured overpotentials; ○, predicted overpotentials for L50-ZMD, ● , predicted overpotentials for L50-ZDM. L and H represent low porosity and high porosity electrodes, respectively, and Z, M, and D represent zinc electrode, membrane, and dynel, respectively (Figure notation L50-ZDM represents a low porosity zinc electrode having a dynel beneath the membrane discharged at 50 mA/cm^2) . . 78

25. Overpotentials at the face of the zinc electrode (x=L) on discharge at 20 mA/cm^2. ——— and ---, measured overpotentials; ○ and ●, predicted overpotentials for L20-ZDM without and with corrections for swelling, respectively. Explanation of figure notation is given in Figure 24 caption. 80

26. Photographs of the electrode surface. A, unused zinc electrode; B, L50-ZMD electrode after discharge failure . 82

27. Photographs of the electrode surface after discharge failure. A, L20-ZMD (low porosity electrode discharged at 20 mA/cm^2); B, H20-ZDM (high porosity electrode discharged at 20 mA/cm^2) 83

28. Overpotentials measured at four different positions on discharge of L50-ZDM electrode at 50 mA/cm^2. Curves A, B, and C represent the overpotentials measured at the backing plate, at the face of the test electrode, and above the membrane, respectively. Curve D is the potential difference between the zinc test and the zinc counter electrodes 85

29. Overpotentials measured at four different positions on charge of L50-ZDM electrode at 50 mA/cm^2. Explanation of curves A, B, C, and D is given in Figure 28 caption. The gaps F-C and C-E are the overpotentials across the the membrane and across the solution in the counter electrode compartment, respectively 86

30. Overpotentials measured at the face of the electrode (L50-ZDM) on charge at 50 mA/cm^2. Explanation of figure notation is given in Figure 24 caption. The previous discharge time prior to onset of charge is 39.4 minutes for L50-ZMD, 69.6 minutes for L50-ZDM, 84.5 minutes for H50-ZDM, and 138.5 minutes for L50-ZD. 88

31. Photographs of the dynel cloth after one discharge-charge cycle. Current density was 50 mA/cm^2. Zinc deposit penetrates the dynel towards the counter electrode. A for L50-ZDM and B for L50-ZD 90

32. Normalized average KOH concentration as a function of operation time. Curve A is for one layer of RAI P2291 membrane, porosity of 0.3, and electrode thickness of 0.1 cm; curve B is for two layers of RAI P2291 membrane, porosity of 0.3, and electrode thickness of 0.1 cm; curve C is for two layers of RAI P2291 membrane, porosity of 0.6, and electrode thickness of 0.1 cm 96

33. Transference numbers of ions in a 0.1 M HCl-KCl ternary solution. Data points are the measured values (67) and solid curves are the calculated values 127

34. Diffusion path during charge near the solid surface within the pores; (A) zinc deposition by charge transfer reaction and (B) dissolution of ZnO by chemical reaction. Dashed lines represent the direction of zincate movement during charge 129

ABSTRACT OF THE DISSERTATION

Transient and Failure Analyses of Porous

Zinc Electrodes

by

Won Guen Sunu

Doctor of Philosophy in Engineering

University of California, Los Angeles, 1978

Professor Douglas N. Bennion, Chairman

A one dimensional mathematical model, perpendicular to the electrode surface, of a porous zinc electrode has been developed on the basis of concentrated ternary electrolyte theory. Numerical techniques were used to predict the galvanostatic behavior and thus the failure mechanisms of porous zinc electrodes under conditions similar to those of secondary zinc batteries. Profiles of zinc and zinc oxide and electrode overpotentials during galvanostatic operation of pressed zinc electrodes having two different porosities were measured at superficial current densities of 20 and 50 mA/cm^2. A membrane was used to separate the zinc test and counter electrode compartments. The experimental observations are in good agreement with the theoretical predictions.

Discharge at 50 mA/cm^2 caused electrode failure due to the depletion of hydroxide ions within the zinc electrode compartment. At a lower current density of 20 mA/cm^2, discharge continued until pore plugging (blockage of the 1st kind) or passivation (blockage of the 2nd kind) caused the zinc electrode to fail. In both cases, the reac-reaction profiles are highly nonuniform and the reaction zone, located

near the electrode surface, is very thin. On repeated cycling, the difference between the anodic and cathodic reaction distributions caused the movement of zinc and zinc oxide in the direction perpendicular to the electrode surface. This may be a limiting factor in the losses in cell capacity of secondary zinc batteries which are designed to eliminate dendrite penetration and shape change.

I. INTRODUCTION

The zinc electrode has been commonly used as a negative electrode in primary cells such as Leclanche dry cells and alkaline zinc manganese dioxide cells. It also has received considerable attention, during the last decade, as a negative plate in secondary batteries, e.g., zinc-nickel, zinc-silver oxide, zinc-bromine, and zinc-chlorine cells. The use of zinc electrodes in secondary batteries is attractive because of its availability, its low cost, and its ability to deliver high energy and power density. However, secondary cells using zinc electrodes have poor cycle life, limited by zinc electrode failure. Any improvements on the cycle life of the zinc electrode can be applicable to its use in Zn-Ni or Zn-AgO rechargeable batteries which are potential applications for use in electric vehicle propulsion or aerospace.

Failure of the zinc electrode can be attributed to a variety of causes. Two major causes of failure are zinc dendrite formation and shape change. The zinc dendrites which are formed during charge penetrate the separator and cause short circuits to the counter electrode. Much of the work to date on improving zinc electrode behavior during charge has been associated with zinc deposit morphology, deposit adherency, and mechanism of dendrite growth as discussed in a review by Oswin and Blurton (1). Zinc dendrite growth appears to be controlled by the mass transfer of zincate ions (2) and is characterized by a critical current density (3). The preferential dendrite growth at the top of a porous zinc electrode observed by Oxley (4) has been attributed to zincate depletion of the electrolytic solution in that region (1). The results of these studies have suggested that the use of low charge

rate, pulse charging, and metallic or organic additives have some beneficial effects on preventing the formation of dendritic zinc deposits (5). The detrimental dendrite penetration, however, has been successfully reduced by use of an appropriate membrane material (6) such as commercially available grafted polyethylene ion exchange membrane.

Another failure known as shape change is the redistribution of solid zinc species during cycling over the electrode surface, which eventually decreases the effective surface area and thus cell capacity of the zinc electrode. Previous investigators (7,8,9) have indicated that the solid species moves from the top and sides to the bottom and center of the zinc porous electrode during cycling and that loose packing, compared to tight packing, of the cell promotes more rapid redistribution of zinc.

A mechanism based on gravitational effects has been proposed (10), but this mechanism is not consistent with the fact that shape change is independent of cell orientation. Other investigators (7,9,11) suggested concentration cell effects as a mechanism of shape change. McBreen (7) has suggested that a concentration cell is generated by the differences in the current distribution during charge and discharge.

Recently, Choi et al. (12,13) have proposed that the main reason for the shape change is the convective flow driven by membrane electroosmotic effect as a dominant factor. The shape change was explained by the concentration cell caused by the differences in the convective flow pattern during cycling, i.e., flow of supersaturated zincate solution towards the zinc electrode center during discharge and flow of undersaturated zincate solution towards the electrode edge (or solution reservoir) during charge. The agreement between their experimental

results and theoretical predictions demonstrated that sealing or tight packing of the cell, preventing convection, successfully eliminated the shape change.

The simple approaches mentioned above have been effective in extending cycle life, but the resulting cycle life appears still to be limited by other factors. Initial loss of cell capacity as well as rapid decrease in cell capacity with continued cycling were observed even for the sealed cells for which chemical analysis for zinc species confirmed no shape change (13). This indicates that there are further reasons for cell failure to be explained and minimized in order to gain further cycle life improvements. A first step toward disclosing other failure modes and mechanism is to understand and be able to predict the zinc behavior within the porous negative electrode.

A number of workers investigated extensively the anodic zinc behavior in alkaline solution, using polycrystalline, flat plate electrodes. The major efforts have been concentrated on the studies of anodic passivation of the planar zinc electrode. It has been generally accepted that the applied current density can be fitted to a linear relationship with the inverse square root of the passivation time (14,15,16,17). A linear relationship based on the Sand equation (18) implies that diffusion of zincate ion away from the electrode is the controlling process for passivation. Therefore, passivation is expected to occur when the layer of electrolytic solution adjacent to the zinc surface reaches a critical concentration of zincate (16,17).

Porous electrodes involve much more complicated and interrelated phenomena than the planar electrode. In addition to passivation, conver-

sion of zinc into ZnO during discharge of the porous electrode decreases the pore size and thus the transport of electrolyte into the interior of the porous electrode. Some workers (19,20) have observed that utilization of zinc depends strongly on the initial porosity of the zinc electrode. Membranes, which have been used to prevent zinc dendrite penetration, can limit the transport of electrolyte species to and from the counter electrode as was discussed by Shaw and Remanick (21). Porous electrodes have highly nonuniform current distribution with an effective reaction zone which is very thin, resulting in local, high current density. The remaining part of the electrode acts as an inert matrix which does not contribute to the cell capacity. Nonuniform distribution can also accelerate the decrease in pore size in the reaction zone. In order to understand such processes and further identify the failure mechanisms, it is helpful to develop a mathematical model which describes properly the transient behavior of the porous zinc electrode.

Various mathematical models have been proposed to describe the behavior of the porous electrodes as summarized by Newman and Tiedemann (22). Winsel (23) described battery discharge by considering a single pore electrode of constant porosity and assuming uniform concentration and conductivity in the solution. Newman and Tobias (24) included the effects of a matrix resistance and concentration changes in their steady state analysis of a one dimensional homogeneous mixture model.

An attempt to consider structural changes in the pores was initiated by Alkire, Grens, and Tobias (25). Using a straight pore geometry, they investigated the effects of changes in porosity, concentration, and fluid flow on the dissolution of a porous copper electrode in

sulfuric acid solution. Dunning et al. (26) proposed a mathematical model which predicted discharge and cycling behavior of a Ag/AgCl electrode in NaCl solution and a $Cd/Cd(OH)_2$ electrode in KOH solution. They considered the effects of complexing of the sparingly soluble salt with the bulk electrolyte anion and the detailed structural effects on mass transfer parameter on the limiting species. However, the concentration derivative term was neglected and they applied a so-called pseudo steady state approximation to describe the transient behavior. Recently, Gu et al. (27) extended the model of Dunning et al. for Ag/AgCl electrode to include surface diffusion of the adsorbed complex ion and more realistic active surface area based on their experimental measurements. The transient behavior of the model was solved without using the pseudo steady state approximation.

Simonsson (28,29) applied his model to predict the failure mode of of the positive electrode of the lead acid battery. He showed that the discharge of the positive lead dioxide electrode at high current load failed by the severe depletion of sulfuric acid at the pore mouth, while Gidaspow and Baker (30) emphasized the pore plugging as a major cause of battery failure. A mathematical model which predicts the transient behavior of the porous zinc electrode has not been reported as yet except that of Choi et al. (12). The results of their model which includes a convection term in the y-direction, parallel to the electrode surface, successfully predicted the mechanism of the failure called "shape change".

In the present work, a mathematical model is developed to describe the transient behavior of the porous zinc electrode in the direction

perpendicular to the electrode surface. It also describes failure mechanisms during discharge and cycling operation other than shape change. The porous electrode is treated as the superposition of two continua, solution and solid phases, by use of a macroscopic averaging technique (22). This model resembles real electrodes when particle and pore dimensions are on the order of one micrometer.

The products produced during discharge of the $Cd/Cd(OH)_2$, Ag/AgCl, and $PbO_2/PbSO_4$ electrodes are believed to be sparingly soluble in the corresponding electrolytic solutions. For the zinc electrode, the discharge product ZnO is highly soluble in KOH solution. The electrolytic solution generally used for secondary batteries using zinc negative electrodes is highly concentrated KOH solution (about 10M) saturated with ZnO (about 1M). Furthermore, the electrolytic solution in contact with a discharging zinc electrode can become supersaturated with zincate (31), resulting in the concentrated potassium hydroxide-potassium zincate-water ternary mixture. Therefore, fundamental equations necessary for describing the concentrated ternary solution are developed based on irreversible thermodynamic principles (32). The resulting equations can also be applied to other multi-component systems such as molten salt and membrane transport.

Commercial zinc-nickel or zinc-silver oxide batteries, in general, have separators between the two electrode compartments which affect significantly the concentration variations inside the porous electrodes. The effect of the membrane separator and the electrolytic solution reservoir on the zinc electrode performance are included in the model to predict the mathematical behavior under conditions similar to a

practical battery system. The mathematical model presented here consists of Ohm's law in the solution phase, Ohm's law in the matrix phase, kinetic rate expression, conservation of charge, and conservation equations of hydroxide ion, zincate ion, water, and solid species. The effect of local mass transfer between the electrode active surface and the bulk solution in the pores, changes in porosity, variations of active surface area, and convection arising from the differences in molar volumes of reactants and products are included. The results of the numerical solution are used to suggest certain modes of failure and performance limitations of the zinc electrode.

Experimental measurements of zinc electrode overpotentials and current distribution were carried out using galvanostatic operation at two different current densities; 20 and 50 mA/cm^2. Those results were compared with the mathematical model predictions for zinc electrode failure.

There are several alternate procedures for fabricating porous zinc electrodes. They include pressing of ZnO powder mix (ZnO, HgO, and some other additives) which gives the zinc electrode in the discharged state (33), pressing of amalgamated zinc powder (34), metal spraying process, and electrodeposition process which result in the zinc electrode in the charged state. Determination of failure modes during discharge and cycling is the primary objective of this work. The porosity and volume of electrolyte reservoir of the electrode should be carefully controlled during preparation in order to obtain reproducible electrode performance and failure mechanism. The pressing techniques developed by Morrell and Smith (34) satisfy most of the above mentioned require-

ments and yield an electrode in the charged state.

There are three approaches for the experimental determination of current distribution. The first approach is the direct measurement of potential distribution by using numerous reference electrodes along the electrode. This approach was employed by Brodd (35) in the study of current distribution in a manganese dioxide electrode. The second approach is the direct measurement of the current distribution by using a sectioned electrode and measuring the current in each section as was used by Coleman (36) for MnO_2 electrode and by Gagnon and Austin (37) for Ag/Ag_2O electrode. The third approach is to measure the reaction distribution of the discharged electrode by electrode sectioning followed by the analysis of each section. The charge state of each section can be analyzed using chemical analysis as shown by Nagy and Bockris (38) for the zinc electrode, Bro and Kang (39) for the cadmium electrode, and Alkire (40) for the copper electrode.

The first two direct approaches have the advantage of allowing continuous measurements during operation, however, reference electrode probes or a discontinuous sectioned matrix may disturb the real current distribution and can lead to distorted results. The third approach is limited to one experimental data set per electrode, and the sectioning procedure can result in a net reduction and redistribution of material. The sectioning approach seems to be one of the promising experimental techniques required for battery development since its modification (so called freezing technique) allows determining the distribution of both solid and liquid species. By freezing the electrolyte in the boundary layer, followed by sectioning and chemical analysis, Brenner (41) and

Flatt et al. (42) successfully determined the concentration profiles in solution at dissolving anode surfaces and at a depositing cathode surface, respectively. In the present study, zinc and zinc oxide profiles are measured using the sectioning method with EDTA titration. Freezing was not tried.

II. THE MATHEMATICAL MODEL

II-1. Zinc Electrode Reaction

The process occurring in the zinc electrode in alkaline solution has been described by a dissolution-precipitation mechanism (43,44):

$$Zn + 4\,OH^- \rightleftharpoons Zn(OH)_4^= + 2\,e^- \quad (A)$$

$$Zn(OH)_4^= \rightleftharpoons ZnO + 2OH^- + H_2O \quad (B)$$

Discharge of the zinc electrode produces supersaturated zincate solution by electrochemical reaction (A), from which ZnO is precipitated by a chemical reaction (B). The reverse process occurs during charge. Several investigators (44,45) have attempted to determine the rate of the precipitation reaction. However, exact values of rate constants are not precisely known.

The electrochemical reaction mechanism for zinc amalgam electrode in alkaline media has been studied by previous investigators (46,47,48) to give

$$Zn(Hg) + 2OH^- \rightleftharpoons Zn(OH)_2 + 2e^- \quad (C)$$

$$Zn(OH)_2 + 2OH^- \rightleftharpoons Zn(OH)_4^= \quad (D)$$

For a pure zinc electrode in alkaline solution, the exchange reaction mechanism is more complicated due to the lattice disruption and other imperfections. A number of investigators (49,50,51,52) have studied the kinetic mechanism for the solid zinc electrode. The mechanism proposed by Bockris et al. (52) is as follows.

$$Zn + OH^- \rightleftharpoons Zn(OH) + e^- \quad (E)$$

$$Zn(OH) + OH^- \rightleftharpoons Zn(OH)_2^- \quad (F)$$

$$Zn(OH)_2^- + OH^- \rightleftharpoons Zn(OH)_3^- + e^- \quad (G)$$

$$Zn(OH)_3^- + OH^- \rightleftharpoons Zn(OH)_4^{=} \quad (H)$$

where reaction step (G) is the rate controlling step.

In a concentrated KOH solution saturated with ZnO, it is possible for the following complexes of zinc species to be present as intermediate compounds: Zn^{++}, $Zn(OH)^+$, $Zn(OH)_2$, $Zn(OH)_3^-$, $Zn(OH)_4^{=}$ ... $Zn(OH)_n^{2-n}$. These complexes are formed according to the following equation

$$Zn^{++} + nOH^- \rightleftharpoons Zn(OH)_n^{2-n} \quad (I)$$

The equilibrium constants reported by Butler (53) are $10^{4.15}$ for n=1, $10^{10.15}$ for n=2, $10^{14.25}$ for n=3, and 10^{15} for n=4. Using these values, Boden et al. (54) concluded that the only species present to any appreciable extent in KOH solution was $Zn(OH)_4^{=}$ ion. Other workers (55,56,57) also confirmed that the predominant species was zincate ion. Therefore, in the present work, the electrolytic solution is considered as a four component system containing K^+, OH^-, $Zn(OH)_4^{=}$, and H_2O.

II-2. Ternary Electrolyte Theory

It is shown that the solution under consideration is a ternary mixture containing potassium hydroxide as well as potassium zincate. The solution for use in alkaline zinc batteries is, in general, highly concentrated KOH solution (about 40 wt%) saturated with ZnO. The ZnO is highly soluble in KOH solution, and it is generally agreed that anodic discharge of zinc in KOH solution produces a supersaturated zincate solution which is often greater by a factor of two than the equilibrium zincate concentration (31).

As the concentration of an ionic species become large, interactions between ions and solvent and ion-ion interactions become important. Newman et al. (58) have developed a binary electrolyte theory for concentrated solution. The following analysis of a four component system will parallel that of a binary electrolyte considered by Newman et al.

The general concept of relating a driving force per unit volume on a species i, $d_i (= c_i \nabla \mu_i)$, to a linear sum of frictional interactions exerted on species i by species j, $K_{ij}(v_j - v_i)$, was proposed by Maxwell, often referred to as the Stefan-Maxwell equation (59).

$$d_i = c_i \nabla \mu_i = \sum_j K_{ij} (v_j - v_i) \qquad (1)$$

where v_i is the velocity of species i, c_i is the concentration of species i, and μ_i is the chemical potential or, in case of ionic species, μ_i is to be interpreted as electrochemical potentials as suggested by by Guggenheim (60). The friction coefficients K_{ij} are, in general, quite concentration dependent. However, they can be defined in terms of binary diffusion coefficients $\mathscr{D}_{ij}$, which are found to be less condentration dependent (58,59)

$$K_{ij} = \frac{RT\, c_i c_j}{c_T \mathscr{D}_{ij}} \qquad (2)$$

where c_T is the total concentration of the solution. From Newton's Third Law of Motion, Onsager's reciprocal relation is satisfied (61); $K_{ij} = K_{ji}$. Therefore, the number of independent friction coefficients for the n component system are n(n-1)/2.

For the four component system under consideration, i.e., common cation K^+ (species "1"), anions $Zn(OH)_4^=$ (species "2") and OH^- (species

"3"), water (species "o"), the multicomponent transport equation (1) can be represented as follows:

$$c_1 \nabla\mu_1 = K_{12}(v_2-v_1) + K_{13}(v_3-v_1) + K_{1o}(v_o-v_1) \tag{3}$$

$$c_2 \nabla\mu_2 = K_{21}(v_1-v_2) + K_{23}(v_3-v_2) + K_{2o}(v_o-v_2) \tag{4}$$

$$c_3 \nabla\mu_3 = K_{31}(v_1-v_3) + K_{32}(v_2-v_3) + K_{3o}(v_o-v_3) \tag{5}$$

The fourth equation for water is not an independent equation due to the Gibbs-Duhem equation, $\Sigma_i c_i \nabla\mu_i = 0$.

The chemical potentials of electrolytes A and B are defined by the following equations.

$$\nabla\mu_A = \nu_1^A \nabla\mu_1 + \nu_2^A \nabla\mu_2 \tag{6}$$

$$\nabla\mu_B = \nu_1^B \nabla\mu_1 + \nu_3^B \nabla\mu_3 \tag{7}$$

where the electrolyte A ($K_2Zn(OH)_4$) contains ν_1^A number of species "1" (K^+) and ν_2^A number of species "2" ($Zn(OH)_4^=$). Likewise, ν_1^B and ν_3^B are defined by the number of species "1" (K^+) and species "3" (OH^-), respectively, per molecule of electrolyte B (KOH). Electroneutrality requires $z_1\nu_1^A + z_2\nu_2^A = 0$ and $z_1\nu_1^B + z_3\nu_3^B = 0$ (or $z_1c_1 + z_2c_2 + z_3c_3 = 0$).

The current density is written as

$$i = F \sum_i z_i N_i = Fz_1c_1v_1 + Fz_2c_2v_2 + Fz_3c_3v_3 \tag{8}$$

If the electrical potential ϕ is defined by the potential of a suitable reference electrode at a point in the solution measured with respect to a similar reference electrode at a fixed point in the solution, thermodynamic principles yield

$$- nF \nabla\phi = s_1 \nabla\mu_1 + s_2 \nabla\mu_2 + s_3 \nabla\mu_3 + s_o \nabla\mu_o \tag{9}$$

The s_i coefficients are the stoichiometric coefficients of species i for the electrode reaction represented by

$$\sum_i s_i M_i^{z_i} = ne^- \tag{10}$$

where M_i is a symbol representing the chemical formula of species i.

Equations (3) to (8) are six linear equations containing ten variables; $v_1, v_2, v_3, v_o, \mu_1, \mu_2, \mu_3, \mu_A, \mu_B$, and i. The rearrangement of equations (3) to (8) in terms of fluxes N_i (or $c_i v_i$) is straightforward but quite involved. The above system of four components is very similar to those considered by Bennion (membrane, single salt, and water)(62), by Tiedemann and Bennion (cation, anion, neutral salt, and water)(63), and by Miller (two salts with common cation and water)(64).

Using the reference velocity as the solvent velocity v_o, the resulting rearrangement through matrix inversion is given by the following equations.

$$N_1 = -\left(\nu_1^A L_{AA} + \nu_1^B L_{AB}\right)\nabla\mu_A - \left(\nu_1^A L_{AB} + \nu_1^B L_{BB}\right)\nabla\mu_B + \frac{t_1^o}{z_1 F} i + c_1 v_o \tag{11}$$

$$N_2 = -\nu_2^A L_{AA} \nabla\mu_A - \nu_2^A L_{AB} \nabla\mu_B + \frac{t_2^o}{z_2 F} i + c_2 v_o \tag{12}$$

$$N_3 = -\nu_3^B L_{AB} \nabla\mu_A - \nu_3^B L_{BB} \nabla\mu_B + \frac{t_3^o}{z_3 F} i + c_3 v_o \tag{13}$$

$$N_o = c_o v_o \tag{14}$$

The arrangement of Equation (9) for potential coupled with equation (11) through (14) results in the following equation.

$$i = -\kappa\nabla\phi - \frac{\kappa}{nF}\left[\frac{s_2}{\nu_2^A} + \frac{n}{z_2\nu_2^A}t_2^o - \frac{s_o}{c_o}c_A\right]\nabla\mu_A$$

$$- \frac{\kappa}{nF}\left[\frac{s_3}{\nu_3^B} + \frac{n}{z_3\nu_3^B}t_3^o - \frac{s_o}{c_o}c_B\right]\nabla\mu_B \qquad (15)$$

where transport parameters L_{AA}, L_{AB}, L_{BB}, t_1^o, t_2^o (or t_3^o), and κ are expressed as a function of the K_{ij} and concentration in Appendix A-1. The reverse relations, i.e., K_{ij} as a function of the six measurable transport parameters are also shown in Appendix A-2. Appendix A-3 shows how the equations (11) to (15) can be transformed to represent transport equations for the other systems such as single salt-membrane-water and single salt-neutral salt-water.

The flux equations containing the diffusion coefficients, which are usually reported, are expressed in terms of concentration gradients. The chemical potential gradient is related to concentration gradients as

$$\frac{d\mu_i}{dx} = \left(\frac{\partial\mu_i}{\partial c_A}\right)\frac{dc_A}{dx} + \left(\frac{\partial\mu_i}{\partial c_B}\right)\frac{dc_B}{dx} \qquad (16)$$

The solvent velocity v_o has been chosen as a reference velocity in the above treatment. In some cases, such as in porous electrodes, it is more convenient to use volume average velocity $v^{\square}$ as a reference velocity. The volume average velocity is defined by

$$v^{\square} = \frac{\sum_i c_i v_i \overline{V}_i}{\sum_i c_i \overline{V}_i} = \sum_i N_i \overline{V}_i \qquad (17)$$

where $\overline{V}_i$ is the partial molar volume of species i.

The flux equations referred to the volume average velocity, using concentration gradients, are shown below:

$$\frac{N_2}{\nu_2^A} = - D_{AA} \frac{dc_A}{dx} - D_{AB} \frac{dc_B}{dx} + \frac{t_2}{z_2 \nu_2^A F} i + c_A v^{\square} \tag{18}$$

$$\frac{N_3}{\nu_3^B} = - D_{BA} \frac{dc_A}{dx} - D_{BB} \frac{dc_B}{dx} + \frac{t_3}{z_3 \nu_3^B F} i + c_B v^{\square} \tag{19}$$

$$N_o = + D_{OA} \frac{dc_A}{dx} + D_{OB} \frac{dc_B}{dx} - c_o t_o^* \frac{i}{F} + c_o v^{\square} \tag{20}$$

where

$$\left.\begin{aligned}
D_{AA} &= D_{AA}^o - \frac{c_A}{c_o} D_{OA} \quad ; \quad D_{AA}^o = L_{AA} \frac{\partial \mu_A}{\partial c_A} + L_{AB} \frac{\partial \mu_B}{\partial c_A} \\
D_{AB} &= D_{AB}^o - \frac{c_A}{c_o} D_{OB} \quad ; \quad D_{AB}^o = L_{AA} \frac{\partial \mu_A}{\partial c_B} + L_{AB} \frac{\partial \mu_B}{\partial c_B} \\
D_{BA} &= D_{BA}^o - \frac{c_B}{c_o} D_{OA} \quad ; \quad D_{BA}^o = L_{AB} \frac{\partial \mu_A}{\partial c_A} + L_{BB} \frac{\partial \mu_B}{\partial c_A} \\
D_{BB} &= D_{BB}^o - \frac{c_B}{c_o} D_{OB} \quad ; \quad D_{BB}^o = L_{AB} \frac{\partial \mu_A}{\partial c_B} + L_{BB} \frac{\partial \mu_B}{\partial c_B} \\
D_{OA} &= c_o (\bar{V}_A L_{AA} + \bar{V}_B L_{AB}) \frac{\partial \mu_A}{\partial c_A} + c_o (\bar{V}_A L_{AB} + \bar{V}_B L_{BB}) \frac{\partial \mu_B}{\partial c_A} \\
D_{OB} &= c_o (\bar{V}_A L_{AA} + \bar{V}_B L_{AB}) \frac{\partial \mu_A}{\partial c_B} + c_o (\bar{V}_A L_{AB} + \bar{V}_B L_{BB}) \frac{\partial \mu_B}{\partial c_B} \\
t_2 &= t_2^o - z_2 c_2 t_o^* \\
t_3 &= t_3^o - z_3 c_3 t_o^* \quad ; \quad t_o^* = \frac{\bar{V}_1 t_1^o}{z_1} + \frac{\bar{V}_2 t_2^o}{z_2} + \frac{\bar{V}_3 t_3^o}{z_3}
\end{aligned}\right\} \tag{21}$$

For the solvent velocity reference frame, the parameters D_{OA}, D_{OB}, and t_o^* disappear from the above equations. The quantities D_{ij}, t_i, and $v^{\square}$ should be replaced with D_{ij}^o, t_i^o, and v_o, respectively, to represent the flux equations referred to the solvent velocity v_o.

The partial molar volumes of the ions shown in the parameter t_o^* satisfy

$$\bar{V}_A = \nu_1^A \bar{V}_1 + \nu_2^A \bar{V}_2 \tag{22}$$

$$\bar{V}_B = \nu_1^B \bar{V}_1 + \nu_3^B \bar{V}_3 \tag{23}$$

These relations are not sufficient to determine the partial molar volumes of ions separately. Consequently, we let

$$\bar{V}_1 = \frac{t_2^o}{\nu_1^A} \bar{V}_A + \frac{t_3^o}{\nu_3^B} \bar{V}_B \tag{24}$$

This choice is based solely on convenience (65), and no physical significance should be attached to it. With this choice, t_o^* becomes zero, and t_i in equations (18) and (19) reduce to t_i^o.

The expressions of Appendix A-1 enable us to calculate the transport parameters for a ternary mixture from the data of binary electrolytes. Tabulated data for K_{ij} (or $\mathscr{D}_{ij}$) for 1:1 and 1:2 binary electrolytes have been compiled by Chapman (66). The transference numbers and conductivities calculated from the two sets of binary data showed good agreement with the experimental data for the ternary mixtures. An example is shown in Appendix A-4 where measured transference numbers for HCl-KCl solution (67) are compared with the transference numbers estimated from the binary data (66).

However, successful prediction of the diffusion coefficients, D_{ij},

for ternary mixtures requires the knowledge of the ternary activity coefficients as indicated by equations (21). The activity coefficients for a mixed solution may be approximated by use of Newman's treatment (68). Some workers (64,69,70) have used experimental ternary activity coefficients to show reasonable agreements between the measured and the predicted diffusion coefficients. They applied the multicomponent transport equations of Miller (64), which were derived based on an inverse description of the equation (1) of the form : $J_i = \Sigma_i l_{ij} X_j$ where X_j is the thermodynamic driving force, J_i is the molar flux of species i, and l_{ij} are the phenomenological or transport coefficients. The flux equations (18),(19), and (20) and current equation (15) will be used to describe the mathematical model of the porous zinc electrode.

II-3. Description of the Model

A one dimensional mathematical model of a porous zinc electrode has been proposed which predicts OH^- concentration c_3, $Zn(OH)_4^=$ concentration c_2, superficial current density in the solution i_2, transfer current density j, porosity ε, superficial volume average velocity $v^{\square}$, potential in the solution ϕ_2, and potential in the matrix ϕ_1 as a function of time and position perpendicular to the surface of the electrode. The geometric features of the model are shown in Figure 1. A backing plate is located at x=0 and the membrane or external boundary layer is at x=L. The effects of membrane as well as volume of solution reservoir between the electrode surface and membrane on the electrode performance were included to predict zinc electrode behavior under conditions similar to a practical battery system. The porous

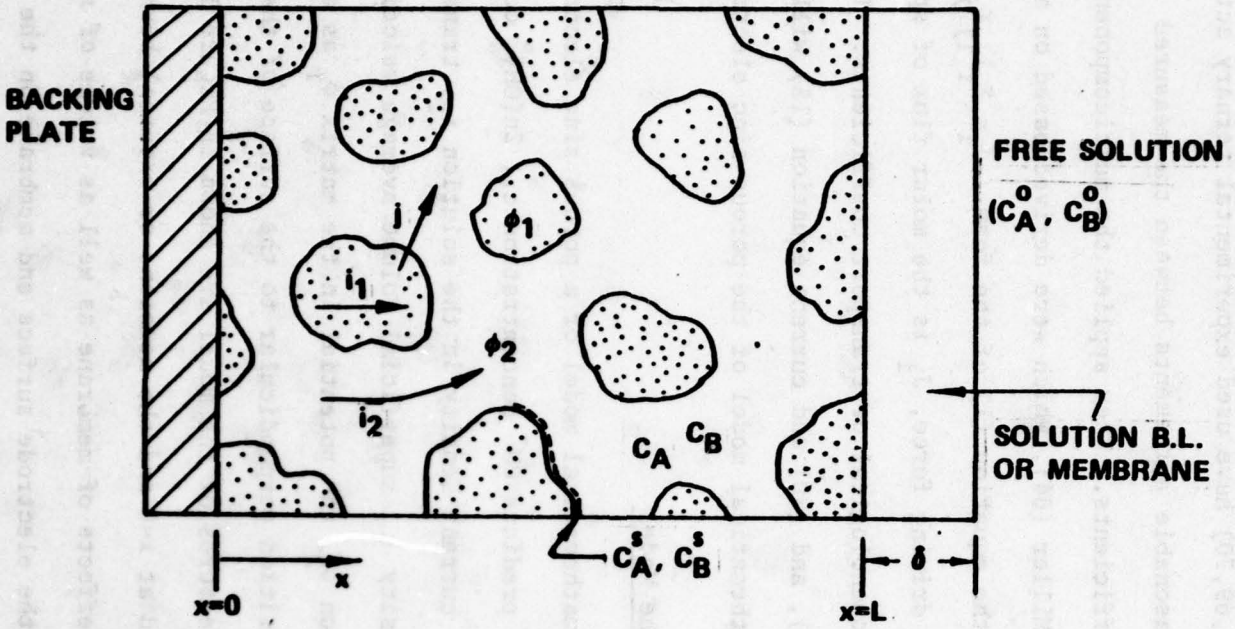

Figure 1 . Geometric Features of the Porous Electrode (for Anodic Reaction).

electrode is treated as a homogeneous mixture of the ionically conducting solution phase denoted by subscript "2" and an electronically conducting matrix phase denoted by subscript "1". The solid matrix might contain zinc, zinc oxide, and inert conducting materials (for example, graphite) or any combinations of the three. The equations developed in the previous section can be applied only to the pure homogeneous solution phase (porosity of unity). In the porous electrode, effects of porosity and tortuosity on the transport equations must be included.

The macroscopic averaging technique performed over the volume of pores within the electrode has been described in detail by Newman and Tiedemann (22) and Dunning (71). This macroscopic averaging treatment is applied to the present model by disregarding the actual geometric details of the pores. For example, consider c_i as the concentration of species i averaged over the volume of solution in the pores. Then the superficial concentration, averaged over the unit volume of the electrode, is ϵc_i where ϵ is the porosity of the electrode. If N_i is defined by the superficial flux based on the unit cross sectional area of the electrode, N_i/ϵ represents the flux through the unit area of solution phase in the pores. Similarly, $v^{\square}/\epsilon$ is the velocity in the solution phase if $v^{\square}$ is a superficial bulk fluid velocity.

The use of averaged quantities (N_i/ϵ, i_2/ϵ, and $v^{\square}/\epsilon$) into equations (18), (19), and (20) yields the following equations.

$$\frac{N_2}{\nu_2^A} = - D_{AA}\epsilon^{1+t}\frac{dc_A}{dx} - D_{AB}\epsilon^{1+t}\frac{dc_B}{dx} + \frac{t_2^o}{z_2\nu_2^A F} i_2 + c_A v^{\square} \qquad (25)$$

$$\frac{N_3}{\nu_3^B} = - D_{BA}\varepsilon^{1+t}\frac{dc_A}{dx} - D_{BB}\varepsilon^{1+t}\frac{dc_B}{dx} + \frac{t_3^o}{z_3\nu_3^B F} i_2 + c_B v^{\square} \quad (26)$$

$$N_o = D_{OA}\varepsilon^{1+t}\frac{dc_A}{dx} + D_{OB}\varepsilon^{1+t}\frac{dc_B}{dx} + c_o v^{\square} \quad (27)$$

where t_i^o is the transference number of species i, t is the tortuosity factor, c_i is the bulk concentration of species i averaged over the volume of solution, and N_i, i_2, and $v^{\square}$ refer to the superficial quantities based on the unit cross sectional area of both matrix and pores. The diffusion coefficients D_{ij} are replaced with $D_{ij}\varepsilon^{1+t}$ to account for the tortuosity correction. Schofield and Dakshinamurti (72) have suggested that the effective diffusion coefficients are proportional to $\varepsilon^{1.5}$ (or t=0.5).

The basic equations of the model to be discussed are Ohm's law in the solution phase, redox kinetic expression, conservation of zincate, conservation of hydroxide ion, overall conservation, and Ohm's law in the matrix phase.

Ohm's Law in the Solution Phase

A modified Ohm's law applied to the ternary electrolyte solution in the porous electrode is obtained from equation (15).

$$i_2 = - \kappa\varepsilon^{1+t}\frac{d\phi_2}{dx} - \frac{\kappa\varepsilon^{1+t}}{n F}\left(\frac{s_2}{\nu_2^A} + \frac{n t_2^o}{z_2\nu_2^A} - \frac{s_o}{c_o} c_A\right)\frac{d\mu_A}{dx}$$

$$- \frac{\kappa\varepsilon^{1+t}}{n F}\left(\frac{s_3}{\nu_3^B} + \frac{n\, t_3^o}{z_3\nu_3^B} - \frac{s_o}{c_o} c_B\right)\frac{d\mu_B}{dx} \quad (28)$$

where ϕ_2 is the potential of a reference electrode of the same kind as

the working electrode placed in the bulk solution within the pores of the porous electrode; κ is the conductivity of solution in the pores at concentration c_i; c_i is the concentration of species i where subscript o refers to solvent; μ_i is the chemical potential of species i; and s_i, n, and z_i have meanings as defined in equation (10). The effective solution conductivity corrected for tortuosity considered here is represented by $\kappa\varepsilon^{1+t}$. Meredith and Tobias (73) and Gagnon (74) suggested t as 0.5, while t=2.0 was observed by Ksenzhek et al. (75). Simonsson (28) and Romanova and Selitsky (76) observed an effective conductivity which is only about one tenth of the conductivity of the free electrolytic solution. They attributed this great reduction to the gas bubbles left in the pores.

Redox Electrochemical Rate Expression

The rate of the charge transfer reaction A at the solid-solution interface can be represented by the following equation.

$$j = i_0^o \left(\frac{c_2^s}{c_2^o}\right)^{\gamma} \left(\frac{c_3^s}{c_3^o}\right)^{\zeta} \left(e^{\frac{\alpha_a F}{RT}(\phi_1 - \phi_2^s)} - e^{-\frac{\alpha_c F}{RT}(\phi_1 - \phi_2^s)} \right) \qquad (29)$$

where α_a and α_c are the effective anodic and cathodic transfer coefficients, respectively; j is the local transfer current per unit area of active zinc surface which acts as active sites for reaction (A); i_0^o is the exchange current density evaluated at reference concentrations c_2^o and c_3^o; γ and ζ are the orders of dependence of the exchange current density i_0 on zincate and hydroxide concentrations, respectively; ϕ_1 is the potential of the matrix phase; and ϕ_2^s is the potential of the reference electrode of the same kind as the working electrode located

just outside the double layer.

The conservation of charge requires

$$a_m j = \frac{di_2}{dx} \tag{30}$$

where a_m is the solid-solution interface area per unit volume of electrode which acts as active sites for reaction (A).

If the diffusion of a species to or from the reaction sites is assumed to proceed through a well defined characteristic diffusion length, δ, the concentration of zincate ion (c_2^s) and hydroxide ion (c_3^s) at the metal surface can be determined from the following equations.

$$\frac{di_2}{dx} = -\frac{nF}{s_2} a k_A (c_2^s - c_2) \tag{31}$$

$$\frac{di_2}{dx} = -\frac{nF}{s_3} a k_B (c_3^s - c_3) \tag{32}$$

where a is the solid-solution interface area per unit volume of the electrode, k_i is the mass transfer coefficient (in cm/sec) of species i from the bulk solution in the pores to the reaction sites which are active for charge transfer reaction (A) or vice versa.

The potential at the metal surface, ϕ_2^s, is assumed to be the same as the potential of the bulk solution in the pores, ϕ_2. Equations (29) through (32) are combined to give

$$\frac{di_2}{dx} = a_m i_0^o \left(\frac{c_2}{c_2^o} - \frac{s_2 \frac{di_2}{dx}}{nFak_A c_2^o} \right)^{\gamma} \left(\frac{c_3}{c_3^o} - \frac{s_3 \frac{di_2}{dx}}{nFak_B c_3^o} \right)^{\zeta} \left[e^{\frac{\alpha_a F}{RT}(\phi_1 - \phi_2)} - e^{-\frac{\alpha_c F}{RT}(\phi_1 - \phi_2)} \right] \tag{33}$$

The constants γ, ζ, α_a, and α_c, corresponding to the reaction mechanism (E) to (H) of Bockris et al. (52), are 0.75, 0.0, 1.5, and 0.5, respectively. The exchange current density, i_0^o, reported by a number of investigators (52,77,78,79,80) has the values in the range of 10 to 300 mA/cm^2.

Species Conservation Equation

The use of appropriate averaging quantities yields the following conservation equation.

$$\frac{\partial \varepsilon c_i}{\partial t} = - \frac{d N_i}{dx} + R_i \qquad (34)$$

where R_i represents production or consumption of species i due to the electrode reaction. During discharge, zincate ion is produced by charge transfer reaction (A) and consumed by precipitation reaction (B). On the other hand, hydroxide ion is consumed by reaction (A) and produced by reaction (B). The reaction source R_i can be written as

$$R_i = - \frac{s_i}{nF} \frac{di_2}{dx} + s_i^* a k_s^* (c_2 - c_2^{eq}) \qquad (35)$$

where k_s^*, during discharge, is defined by the rate constant combining mass transfer of zincate ions from bulk solution in the pores to the reaction sites with chemical rate constant for precipitation of ZnO; c_2^{eq} is the equilibrium (or saturation) concentration of zincate ion at the solid-solution interface which are active for reaction (B); and s_i and s_i^* are the stoichiometric coefficients of species i for the reaction (A) and for the reaction (B), respectively, defined by equation (10). Substitution of equation (35) into equation (34) yields

$$\frac{\partial \varepsilon c_2}{\partial t} = - \frac{d N_2}{dx} + \frac{1}{n F} \frac{di_2}{dx} - a k_s^* (c_2 - c_2^{eq}) \tag{36}$$

$$\frac{\partial \varepsilon c_3}{\partial t} = - \frac{d N_3}{dx} - \frac{4}{n F} \frac{di_2}{dx} + 2 a k_s^* (c_2 - c_2^{eq}) \tag{37}$$

$$\frac{\partial \varepsilon c_o}{\partial t} = - \frac{d N_o}{dx} + a k_s^* (c_2 - c_2^{eq}) \tag{38}$$

where $s_2 = -s_2^* = -1$, $s_3 = 4$, $s_3^* = -2$, $s_o = 0$, and $s_o^* = -1$ have been substituted.

Overall Conservation Equation

The porosity of the electrode will increase as zinc dissolves and decrease as ZnO precipitates. A material balance on the solid phases shows how the porosity changes with time as shown below.

$$\frac{\partial \varepsilon}{\partial t} = \frac{1}{nF} \sum_{\substack{i \\ \text{solid} \\ \text{species}}} \bar{V}_i s_i \frac{di_2}{dx} + \sum_{\substack{i \\ \text{solid} \\ \text{species}}} \bar{V}_i s_i^* a k_s^* (c_2 - c_2^{eq}) \tag{39}$$

where $\bar{V}_i$ is the partial molar volume of species i.

Similarly, a material balance on the species in the solution phase gives the following electrolyte continuity equation.

$$\frac{\partial \varepsilon}{\partial t} + \frac{dv^{\square}}{dx} = - \left(\frac{\bar{V}_A t_2^o}{z_2 \nu_2^A} + \frac{\bar{V}_B t_3^o}{z_3 \nu_3^B} + \frac{\bar{V}_A s_2}{n \nu_2^A} + \frac{\bar{V}_B s_3}{n \nu_3^B} + \frac{\bar{V}_o s_o}{n} \right) \frac{1}{F} \frac{di_2}{dx}$$

$$- a k_s^* \left(\frac{s_2^* \bar{V}_A}{\nu_2^A} + \frac{s_3^* \bar{V}_B}{\nu_3^B} + \bar{V}_o s_o^* \right) (c_2 - c_2^{eq}) \tag{40}$$

This equation is obtained by adding equations (36), (37), and (38) which have been multiplied by $\bar{V}_A / \nu_2^A$, $\bar{V}_B / \nu_3^B$, and $\bar{V}_o$, respectively, and

using the relations of $c_A\bar{V}_A+c_B\bar{V}_B+c_o\bar{V}_O=1$, $\bar{V}_AD_{AA}+\bar{V}_BD_{BA}-\bar{V}_oD_{OA}=0$, and $\bar{V}_AD_{AB}+\bar{V}_BD_{BB}-\bar{V}_oD_{OB}=0$. The last two relations for D_{OA} and D_{OB} are obtained from equations (21).

From equations (39) and (40), the convective bulk flow motion in the porous electrode can be described by the following overall continuity equation.

$$\frac{dv^{\square}}{dx} = -\frac{1}{nF}\left[\bar{V}_{Zn}+4\bar{V}_B-\bar{V}_A-2\left(\frac{t_2^o\bar{V}_A}{\nu_1^A}+\frac{t_3^o\bar{V}_B}{\nu_1^B}\right)\right]\frac{di_2}{dx}$$

$$+ ak_s^*\left[\bar{V}_{ZnO}+\bar{V}_o+2\bar{V}_B-\bar{V}_A\right](c_2-c_2^{eq}) \qquad (41)$$

The second bracket term is the volume change of reaction (B). The first bracket term represents the volume change due to reaction (A) if equation (24) is applied.

Ohm's Law in the Solid Matrix

Ohm's law in the solid matrix can be written as

$$i_1 = I - i_2 = -\sigma\epsilon_m\frac{d\phi_1}{dx} \qquad (42)$$

where ϕ_1 is the potential of the solid matrix, and ϵ_m is the volume of conducting material per unit volume of the electrode (not necessarily equal to $1-\epsilon$). The superficial current density in the solid phase i_1 and that in the solution phase i_2 are related to the total applied current density as $i_1+i_2=I$. The conductivity of solid matrix is approximated by

$$\sigma = \sigma_{Zn}^o(\epsilon_{Zn})^{t^*}+\sigma_{ZnO}^o(\epsilon_{ZnO})^{t^*}+\sigma_I^o(\epsilon_I)^{t^*} \qquad (43)$$

where σ_{Zn}^o, σ_{ZnO}^o, and σ_I^o are the conductivities of the zinc metal, zinc

oxide, and inert materials in the pure solid state, respectively, and ε_{Zn}, ε_{ZnO}, and ε_I are the volumes of zinc, zinc oxide, and inert materials, respectively, per unit volume of the electrode.

Mass Transfer Coefficients (k_A, k_B, and k_s^*)

The reaction rate is determined by the rate of mass transfer of a limiting species between bulk solution within the pores and the active reaction sites. During discharge, hydroxide ion is depleted at the metal surface, producing zincate ion. The zincate ions are expected to diffuse into the bulk solution in the pores resulting in a supersaturated zincate solution. At the same time, the zincate ions in the supersaturated solution will diffuse to the ZnO surface to precipitate as ZnO. The limiting species at the metal surface during charge is the zincate ions which must be supplied from the bulk in the pores. The solution becomes undersaturated with ZnO and solid ZnO will dissolve into the solution.

Based on the assumption that there exists a characteristic diffusion length, δ, which is the distance between the solid-solution interface and the bulk solution inside the pores, mass transfer coefficients k_A, k_B, and k_s^* defined in equations (30), (31), and (35) are described by the following equations (see Appendix B for derivation)

$$k_A = k_A^o \frac{1 - \frac{a_m}{a}}{\ln(\frac{a}{a_m})} \quad ; \; k_A^o = \frac{D_{AA}}{\delta}$$

$$k_B = k_B^o \frac{1 - \frac{a_m}{a}}{\ln(\frac{a}{a_m})} \quad ; \; k_B^o = \frac{D_{BB}}{\delta} \qquad (44)$$

$$\frac{1}{k_s^*} = \frac{1}{k_A^o \dfrac{1-a_s/a}{\ln(\frac{a}{a_s})}} + \frac{1}{\dfrac{a_s}{a} k_{XTL}}$$

where k_A and k_B are the mass transfer coefficients of potassium zincate and potassium hydroxide, respectively, transferring from metal surface to the bulk within the pores or vice versa, δ is the characteristic diffusion length, k_s^* is the rate constant combining mass transfer of zincate from bulk to ZnO surface with chemical rate constant for precipitation of ZnO, and D_{AA} and D_{BB} are the diffusion coefficients of the potassium zincate and potassium hydroxide, respectively. The area a_m and a_s represent the interfacial areas which are active for electrochemical reaction (A) and for chemical reaction (B), respectively.

Surface Area (a_m, a_s, and a)

The value of the true electrochemically active area is difficult to determine. To a first approximation, it is assumed that the macroscopic averaged particles with uniform radius are arranged in face centered cubic closed packed positions. For a given reference porosity ε^o and radius R^o, the solid-solution interface area a^o per unit volume of the electrode can be estimated from the relation of $a^o=3(1-\varepsilon^o)/R^o$. The specific surface area of the electrode at any state having porosity of ε can be related to the reference interface area a^o as $a/a^o=(1-\varepsilon)R^o/(1-\varepsilon^o)/R$. Since the ratio R/R^o is equal to $(a/a^o)^{0.5}$, the specific area a can be represented as follows:

$$a = a^o \left(\frac{1-\varepsilon}{1-\varepsilon^o} \right)^{2/3}$$

The specific interface area a is the sum of the area a_m which is active for charge transfer reaction (A) and the area a_s which is the active site for dissolution or precipitation of ZnO.

In the absence of the inert conducting material, the area a_m and a_s become a_{Zn} (zinc area) and a_{ZnO} (ZnO area), respectively. They are approximated by the following equation.

$$a_{Zn} \text{ (or } a_m) = a - z_{ZnO} = a \frac{(\varepsilon^*_{Zn})^p}{(\varepsilon^*_{Zn})^p + (\varepsilon_{ZnO})^q} \tag{46}$$

where ε_{ZnO} is the volume fraction of ZnO, ε^*_{Zn} is the volume fraction of active zinc which can be converted into ZnO, and p and q are the constants relating volume to surface area which depend on morphology of the crystals ($p=q=\frac{2}{3}$ for cubical or spherical crystals). The volume fraction of active zinc, ε^*_{Zn}, is defined by

$$\varepsilon^*_{Zn} = \varepsilon_{Zn} - (\varepsilon^{plug}_{Zn} + \varepsilon^{covr}_{Zn}) \tag{47}$$

where ε^{plug}_{Zn} and ε^{covr}_{Zn} represent the volume fractions of nonactive zinc caused by pore plugging (blockage of the 1st kind) and complete coverage on zinc surface by ZnO (usually called passivation or blockage of the 2nd kind), respectively.

The quantity ε^{covr}_{Zn} is approximated by

$$\varepsilon^{covr}_{Zn} = \lambda (\varepsilon^{max}_{Zn} - \varepsilon^{plug}_{Zn}) \tag{48}$$

where

$$\varepsilon^{max}_{Zn} = \varepsilon_{Zn} + \varepsilon_{ZnO} \frac{\bar{V}_{Zn}}{\bar{V}_{ZnO}}$$

$$\varepsilon^{plug}_{Zn} = \varepsilon_{Zn} - (\varepsilon) \bar{V}_{Zn} / (\bar{V}_{ZnO} - \bar{V}_{Zn})$$

The meaning of the various volume fractions is explained by using the following example.

Let us consider a local section of the electrode having porosity of 0.3, 60% Zn by volume, and 10% ZnO by volume. The partial molar volumes of zinc and zinc oxide are 9.15 and 14.51 cm^3/mole, respectively. Due to the differences in the partial molar volumes, 85.3% conversion of Zn into ZnO results in pore plugging, i.e., $\epsilon=0$, $\epsilon_{Zn}=0.088$, and $\epsilon_{ZnO}=0.912$. The remaining Zn can not be converted into ZnO, and is denoted by $\epsilon_{Zn}^{plug}(=0.088)$. However, complete surface coverage of zinc by ZnO might occur before pore plugging. If complete conversion of ZnO into Zn occurs during cycling due to a local deep charge, the maximum amount of zinc in the fully charged state, ϵ_{Zn}^{max}, becomes 0.663. The maximum amount of active zinc which can be utilized, $\epsilon_{Zn}^{max}-\epsilon_{Zn}^{plug}$, is 0.575. The fractional constant λ is defined based on this quantity to describe the failure due to passivation.

When inert conducting material is present in the matrix, a constant value is used for the surface area of the inert material a_I with the relation of $a=a_{Zn}+a_{ZnO}+a_I$. In this case, a_m becomes $a_{Zn}+a_I$ and a_s becomes a_{ZnO} during charge. On discharge, a_m and a_s are taken as a_{Zn} and $a_{ZnO}+a_I$, respectively.

II-4. Computation Procedures

The six equations; two second order equations (36) and (37) and four first order equations (28), (33), (41), and (42); form a set of nonlinear, coupled differential equations. The six unknown variables are i_2, ϕ_2, c_2, c_3, $v^{\square}$, and ϕ_1, which are functions of time and posi-

tion. The six equations can be solved by use of numerical techniques with the following initial and boundary conditions.

Initial conditions at time=0

$$c_2 = c_2^o$$
$$c_3 = c_3^o \qquad (49)$$
$$v^{\square} = 0$$

For the other variables, the analytical solutions of the following approximated equations are used to estimate the initial profiles of i_2, ϕ_1, and ϕ_2.

$$i_2 = -\kappa^o(\varepsilon^o)^{1+t}\frac{d\phi_2}{dx}$$
$$\frac{di_2}{dx} = a_m^o i_0^o \frac{(\alpha_a + \alpha_c)F}{RT}(\phi_1 - \phi_2) \qquad (50)$$
$$i_1 = I - i_2 = -\sigma^o\varepsilon_m^o\frac{d\phi_1}{dx}$$

where the superscript o refers to the values evaluated at time=0, and I is the applied current density. The solution of equation (50) can be written as follows (e.g., for current distribution)

$$\frac{di_2}{dy} = I\chi\left(\frac{\sigma_e}{\kappa_e+\sigma_e}\frac{\text{Cosh }\chi y}{\text{Sinh }\chi} + \frac{\kappa_e}{\kappa_e+\sigma_e}\frac{\text{Cosh }\chi(1-y)}{\text{Sinh }\chi}\right) \qquad (51)$$

where

$$\chi = L\sqrt{\frac{(\alpha_a+\alpha_c)Fi_0^o a_m^o}{RT}\left(\frac{1}{\kappa_e}+\frac{1}{\sigma_e}\right)}$$

where y is the dimensionless distance from the backing plate (x/L), L is the electrode thickness, σ_e is the effective matrix conductivity ($\sigma^o\varepsilon_m^o$),

and κ_e is the effective solution conductivity ($\kappa^o(\varepsilon^o)^{1+t}$).

The boundary conditions at x=0 are as follows:

$$\frac{d\phi_2}{dx} = 0 \text{ (or } i_2=0)$$

$$\frac{dc_2}{dx} = 0$$

$$\frac{dc_3}{dx} = 0 \qquad (52)$$

$$v\square = 0$$

$$\phi_1 = 0$$

At the boundary x=L, the current density in the solution phase (i_2) is the same as the applied current density (I). For the species boundary conditions, the limited mass transfer of the various species across the boundary layer should be accounted for to give a better approximation to an actual battery system. Most of the aqueous secondary batteries have a separator adjacent to the electrode surface. Membranes have been used as separators. In some cases, porous, inert materials (for example, dynel cloth) which contain excess solution reservoir are placed between the electrode surface and the membrane.

If the solution reservoir is assumed to be completely mixed, the changes in amount of species i with time in the solution reservoir are equal to the flux of species i across the boundary at x=L, N_i^L, minus the flux of species i across the boundary layer (or membrane), N_i^{bl}. Based on this concept, the boundary conditions at x=L can be written as follows:

At x=L $\quad i_2 = I$

$$\frac{\partial}{\partial t}(Vc_2) = A(N_2^L - N_2^{bl}) \qquad (53)$$

$$\frac{\partial}{\partial t}(Vc_3) = A(N_3^L - N_3^{bl})$$

where A is the cross sectional area of the electrode and V is the volume of solution reservoir located between the electrode surface and the membrane. If excess solution reservoir is absent (i.e., V=0), the above boundary conditions simply represent the conservation of fluxes at the boundary , i.e., $N_2^L = N_2^{bl}$ and $N_3^L = N_3^{bl}$.

The fluxes N_2^L and N_3^L are given by equations (25) and (26), respectively, modified to describe the fluxes at the boundary at x=L. The fluxes N_2^{bl} and N_3^{bl} are written as follows:

$$\frac{N_2^{bl}}{\nu_2^A} = \frac{D_{AA}^{bl}}{d}(c_A^L - c_A^o) + \frac{t_2^{bl}}{z_2 \nu_2^A F} I + c_A^{bl} v^{bl}$$

$$\frac{N_3^{bl}}{\nu_3^B} = \frac{D_{BB}^{bl}}{d}(c_B^L - c_B^o) + \frac{t_3^{bl}}{z_3 \nu_3^B F} I + c_B^{bl} v^{bl} \qquad (54)$$

where d is the thickness of the boundary layer (or membrane).

The six equations can be solved by numerical techniques developed by Newman (81,82) subject to the initial conditions (49) and (50) and the boundary conditions (52) through (54). The electrode length of L was divided into NJ mesh points separated by a distance h between mesh points. The boundaries were at J=1 (x=0) and J=NJ (x=L). Mesh point J refers to a distance of (J-1)h from the backing plate. In the computer programming, the variables were denoted as follows:

$$C(1,J) = i_2(J)$$

$$C(2,J) = \phi_2(J)$$

$$C(3,J) = c_2(J) \text{ or } c_A(J)$$

$$C(4,J) = c_3(J) \text{ or } c_B(J)$$

$$C(5,J) = \sqrt{\square}(J)$$

$$C(6,J) = \phi_1(J)$$

In order to apply Newman's technique, the six equations were linearized about a trial solution and put into finite difference form. Central difference form was used for equations (36) and (37). Forward difference form for equation (28) and backward difference form for equations (33), (41), and (42) were employed with the coefficients of terms being averaged between two appropriate mesh points. The resulting six finite difference equations are correct to second order, h^2.

At the boundaries J=1 and J=NJ, the following finite difference forms were used for the first order boundary conditions.

For J=1,

$$a(J)\frac{dC(K,J)}{dx} = a(J)\frac{-3C(K,J)+4C(K,J+1)-C(K,J+2)}{2h} + O(h^2)$$

For J=NJ

$$a(J)\frac{dC(K,J)}{dx} = a(J)\frac{C(K,J-2)-4C(K,J-1)+3C(K,J)}{2h} + O(h^2)$$

where K refers to the unknown variable and J refers to the mesh point.

The Crank-Nicolson implicit method (83) was used for averaging time derivatives in equations (36) and (37). For example, considering the following equation,

$$\frac{\partial c_3}{\partial t} = a\frac{\partial^2 c_3}{\partial x^2}$$

the finite difference form used is

$$\frac{C(3,J)-Z(3,J)}{\Delta t} = \frac{1}{2}a(J)\,\frac{C(3,J+1)+C(3,J-1)-2C(3,J)}{2h} + \frac{1}{2}za(J)\,\frac{Z(3,J+1)+Z(3,J-1)-2Z(3,J)}{2h}$$

where Z and za represent the values of C and a of the previous time step, respectively.

The resulting matrix was solved using numerical techniques developed by Newman (81,82). The convergence criterion used was 10^{-5} which is defined by the ratio of the difference between the two successive solutions to the present solution.

The numerical calculations require a knowledge of the various parameters used in the mathematical model. The conductivity of the electrolytic solution (84), solubility of ZnO in KOH solution (85), and activity coefficients of KOH and potassium zincate (68,86) were expressed as a function of concentration based on the data taken from various literature reports. Those formulas and references are described in Appendix C. Other chemical and physical parameters pertinent to the system under consideration are described in Appendix D-1. The computer programs and the control parameters are shown in Appendix D. The numerical solutions were carried out in double precision on the UCLA IBM 360/91 digital computer.

III. ZINC ELECTRODE BEHAVIOR PREDICTED FROM THE MATHEMATICAL MODEL

The mathematical model described in the previous section was solved to predict the behavior and failure modes of the porous zinc electrode having the following initial conditions. The electrolytic solution initially contained in the pores is taken as 8M KOH solution (about 35 wt%) saturated with zincate (c_A^o=0.66M). The electrode under consideration is initially 40% void volume, 50% zinc, and 10% ZnO by volume (ε^o= 0.4, ε_{Zn}^o=0.5, ε_{ZnO}^o=0.1, and ε_I^o=0). The zinc electrode behavior during galvanostatic operation with superficial current densities of 50 and 20 mA/cm^2 were considered. These current densities are believed to be high enough to represent those required during operation of common secondary batteries and low enough to eliminate anodic passivation, at least in the initial stages. Therefore, it is assumed that complete coverage of the zinc surface by precipitated ZnO (passivation) does not occur; ε_m^{covr} is zero.

A general membrane boundary case, where a membrane is placed between the zinc electrode surface and the free solution, is considered by taking the parameters shown in Table 1 (type I). However, some of the results for the other boundaries, when they appear to be useful, are also included; for example, solution boundary (the third column) and cation exchange RAI P2291 membrane boundary (the fourth column of Table I). The other parameters used in this calculation are shown in Appendix D-1. The predicted results during galvanostatic discharge of a porous zinc electrode are shown in Figures 2 to 7. Figures 8 to 13 illustrate the summarized zinc electrode behavior during cycling.

Table I. Transport Parameters Applied to the Various Boundary Layers

	Type I Membrane Boundary	Solution Boundary	Type II Membrane (RAI P2291)*
t_1^{bl}	0.5	0.23	0.5
t_2^{bl}	0.0	0.05	0.0
t_3^{bl}	0.5	0.72	0.5
D_{AA}^{bl} (cm^2/s)	2.5×10^{-8}	6.0×10^{-6}	1.0×10^{-8}
D_{BB}^{bl} (cm^2/s)	2.5×10^{-7}	2.0×10^{-5}	7.5×10^{-8}
d (cm)	0.0025	0.005	0.0025
L_{AA}^{bl} (cm/s)	1.0×10^{-5}	0.0012	4.0×10^{-6}
L_{BB}^{bl} (cm/s)	1.0×10^{-4}	0.004	3.0×10^{-5}

* Transport parameters for RAI P2291 membrane were taken from the data of Sinha and Bennion.(87). The parameter L_{ii}^{bl} is defined by D_{ii}^{bl}/d (refer to equation 54).

III-1. Discharge Behavior

Figure 2 shows the anodic overpotentials, $\phi_1(o) - \phi_2(L)$, defined by the potential of the backing plate minus the potential in the solution at the electrode surface, as a function of time or depth of discharge. The shape of potential-time curve resembles those reported by Elsdale et al. (88). In contrast to the sharp increase at a point of passivation on a planar zinc electrode (for example, see references 14 and 15), the potential-time curve is characterized by an initial gradual rise in overpotential followed by a steeper rise at a later stage. The overpotential goes up substantially in the region of 40% depth of discharge. It is to be noticed that even in the idealized model, only 40% of initial zinc metal can be converted into ZnO prior to electrode failure. The electrode failure at 40% depth of discharge is caused by high ohmic loss in the solution due to the decrease in pore size as well as KOH concentration and partly by high activation and concentration overpotentials.

Figure 3 shows how the concentration profiles for KOH (top curves) and potassium zincate (bottom curves) develop during discharge at 50 mA/cm^2 current density. Initial concentration of the solution was 8M KOH saturated with zincate (0.66M) as shown by dotted lines. After one minute polarization, KOH concentration decreases and zincate becomes supersaturated (curve A). On further discharge, KOH concentration decreases further to give curves B for 10%, C for 20%, and D for 30% depth of discharge. Saturation concentration of zincate decreases as KOH concentration decreases. Therefore, zincate solution concentration also decreases as discharge continues; however, there is always some

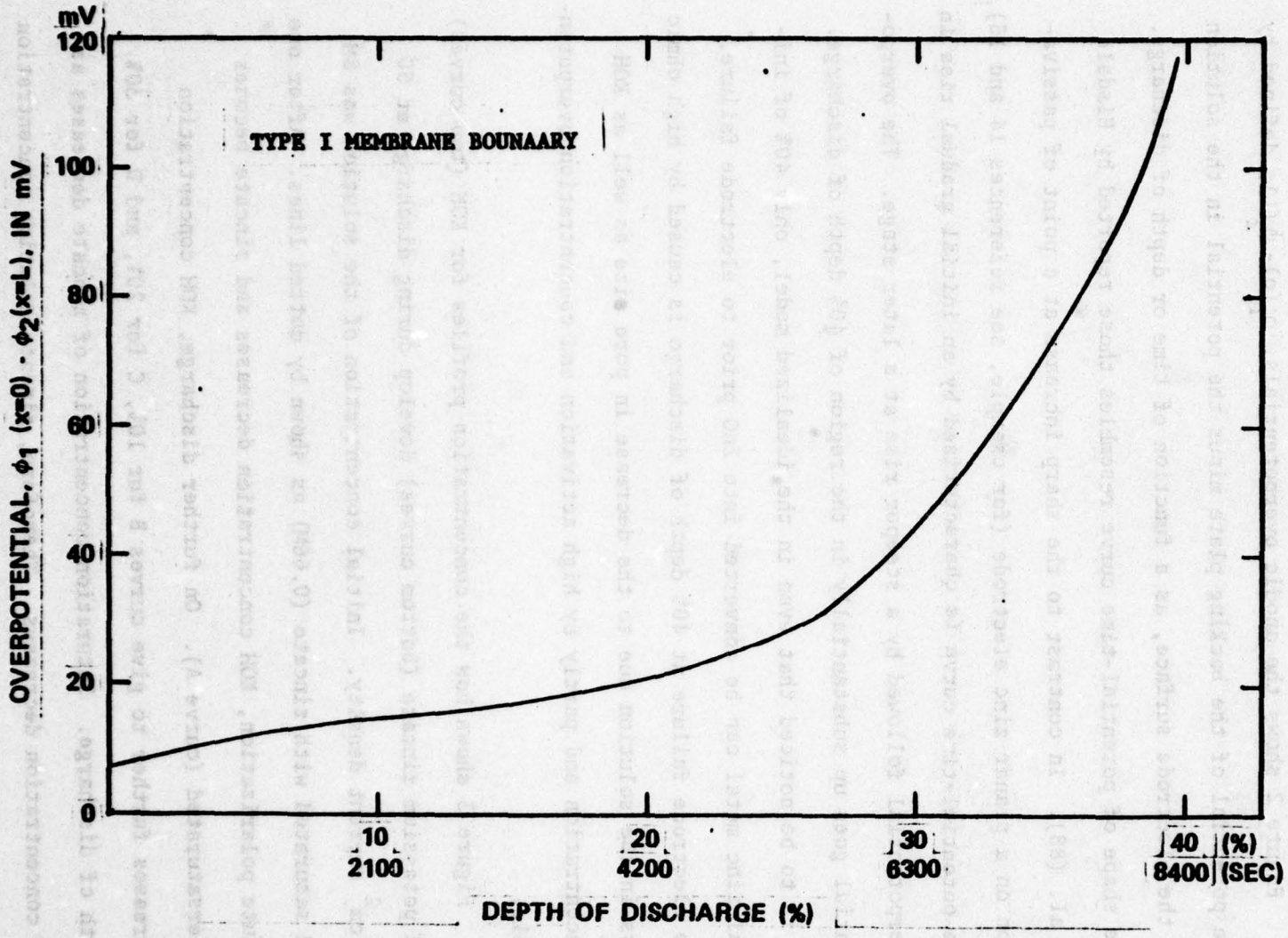

Figure 2. Overpotential, $\phi_1(o)-\phi_2(L)$, of Zinc Electrode During Constant Current Discharge for Type I Membrane Boundary (I=50 mA/cm^2, L=0.1 cm, $\epsilon^o=0.4$, $\epsilon^o_{Zn}=0.5$, $\epsilon^o_{ZnO}=0.1$)

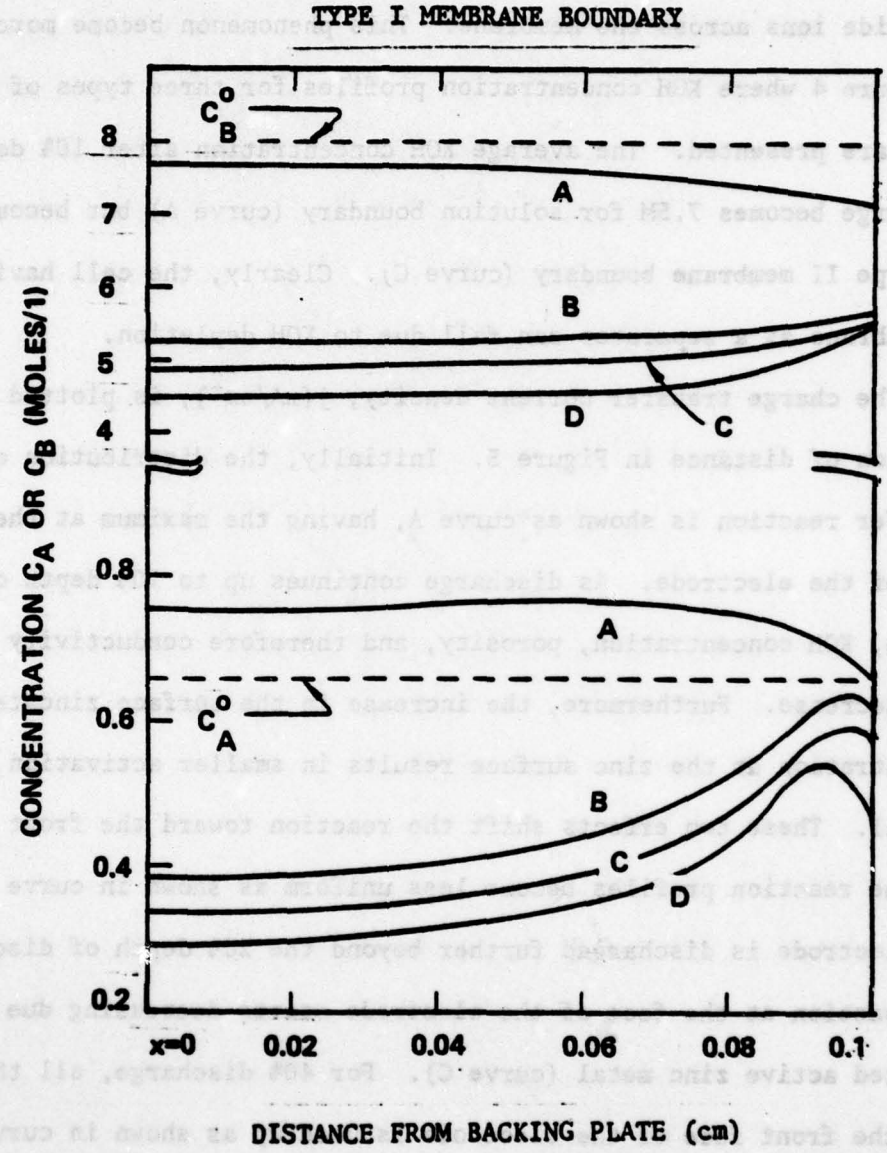

Figure 3. Concentration Profiles During Constant Current Discharge for Type I Membrane Boundary (I=50 mA/cm^2, A for One Minute Polarization and B,C, and D for 10%, 20%, and 30% Depth of Discharge, respectively)

degree of supersaturation. The significant depletion of KOH electrolyte, e.g., 4.5M at 30% depth of discharge is due to the restricted flux of hydroxide ions across the membrane. This phenomenon become more obvious in Figure 4 where KOH concentration profiles for three types of boundaries are presented. The average KOH concentration after 10% depth of discharge becomes 7.5M for solution boundary (curve A) but becomes 2.0M for type II membrane boundary (curve C). Clearly, the cell having type II membrane as a separator can fail due to KOH depletion.

The charge transfer current density, $j(mA/cm^2)$, is plotted as a function of distance in Figure 5. Initially, the distribution of charge transfer reaction is shown as curve A, having the maximum at the front face of the electrode. As discharge continues up to 10% depth of discharge, KOH concentration, porosity, and therefore conductivity of solution decrease. Furthermore, the increase in the surface zincate concentration at the zinc surface results in smaller activation overpotential. These two effects shift the reaction toward the front face and the reaction profiles become less uniform as shown in curve B. If the electrode is discharged further beyond the 20% depth of discharge, the reaction at the face of the electrode starts decreasing due to the depleted active zinc metal (curve C). For 40% discharge, all the zinc near the front face of the electrode is used up as shown in curve D. The reaction profile is highly nonuniform and the effective reaction zone moves step by step from the face of the electrode toward the backing plate. Similar profiles are obtained for the other two boundaries.

The distribution of solid zinc and zinc oxide, in terms of volume fractions, is plotted in Figure 6 for type I membrane and in Figure 7

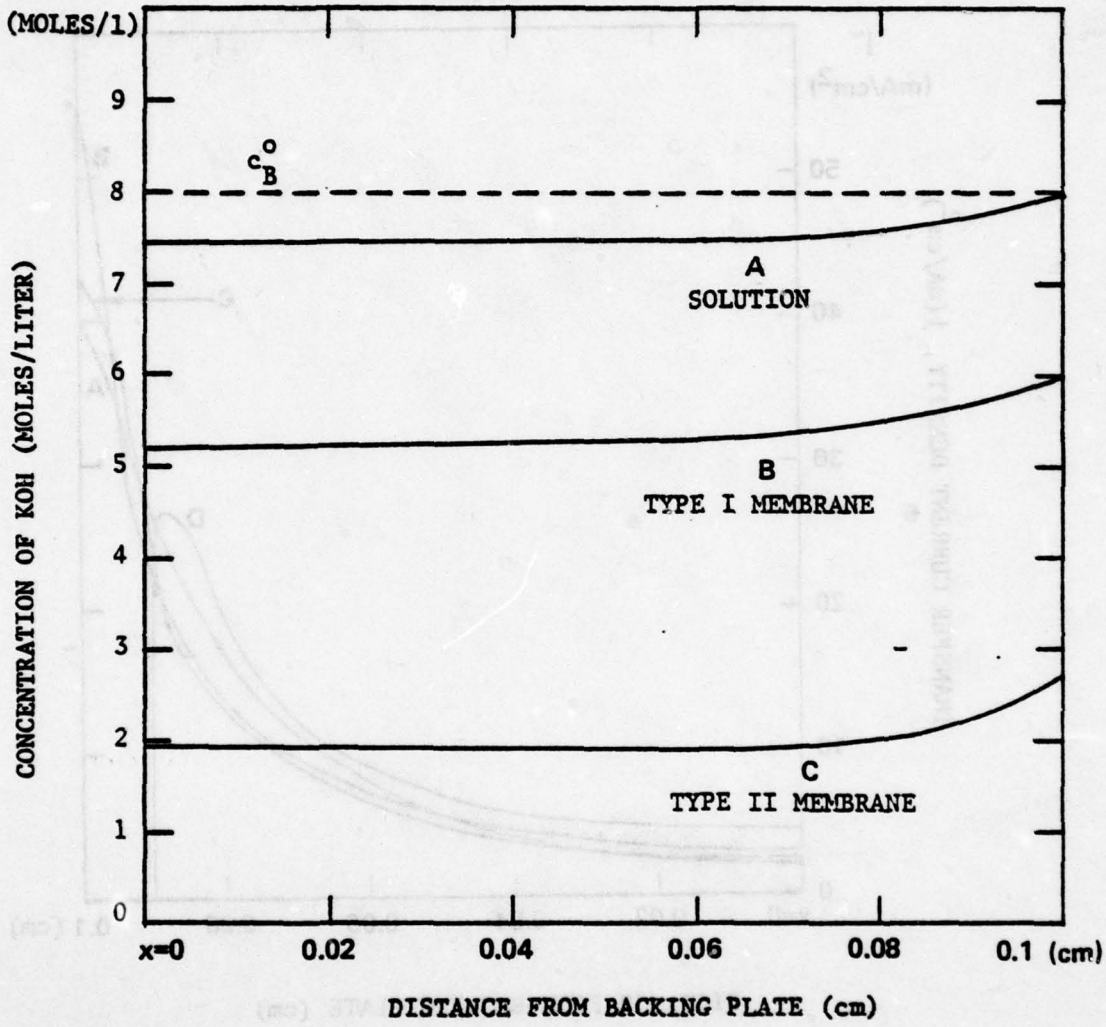

Figure 4. Concentration Profiles of KOH After 10% Depth of Discharge (I=50 mA/cm^2 and A,B,and C for Solution Boundary, Type I Membrane Boundary, and Type II Membrane Boundary, Respectively)

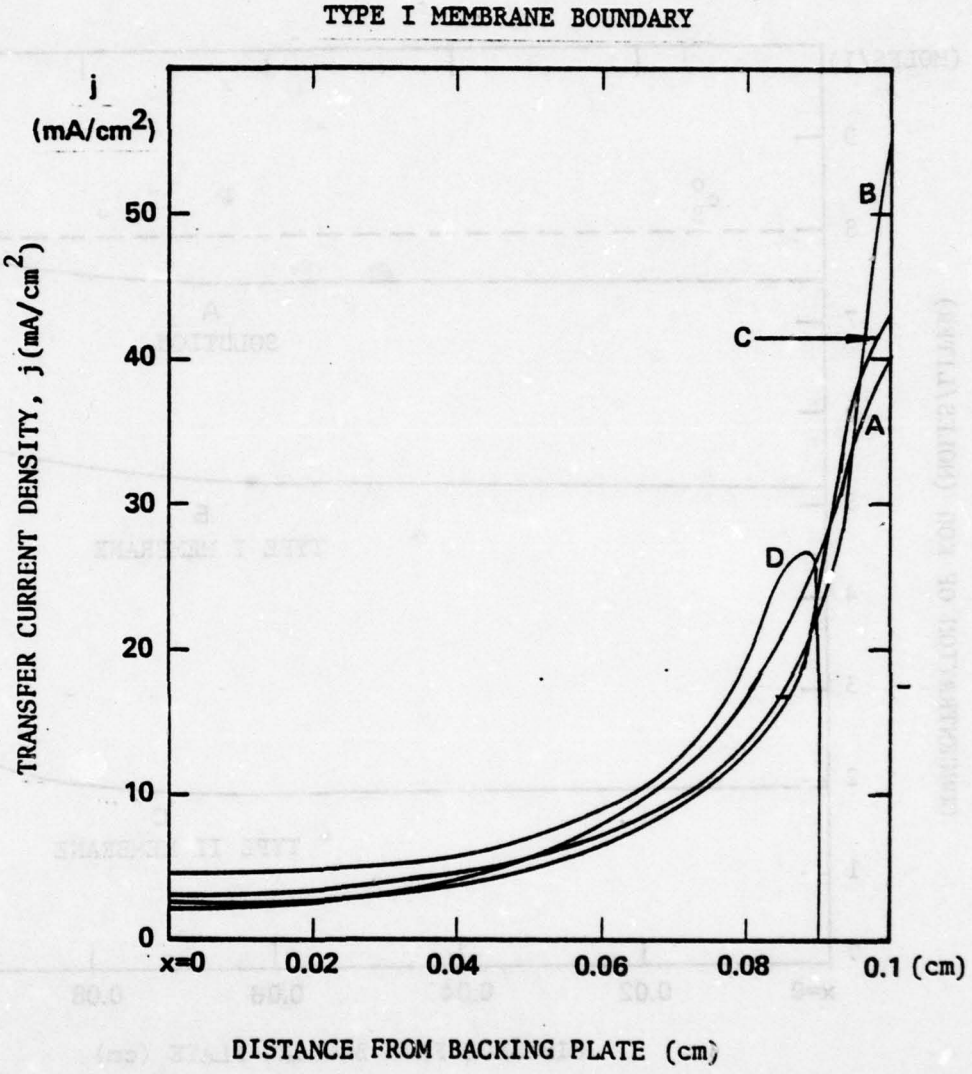

Figure 5. Distribution of Local Charge Transfer Current, j(mA /cm^2), for Type I Membrane Boundary (I=50 mA/cm^2, L=0.1 cm, and A,B,C,and D Represent 0%,10%,20%, and 40% Depth of Discharge, Respectively)

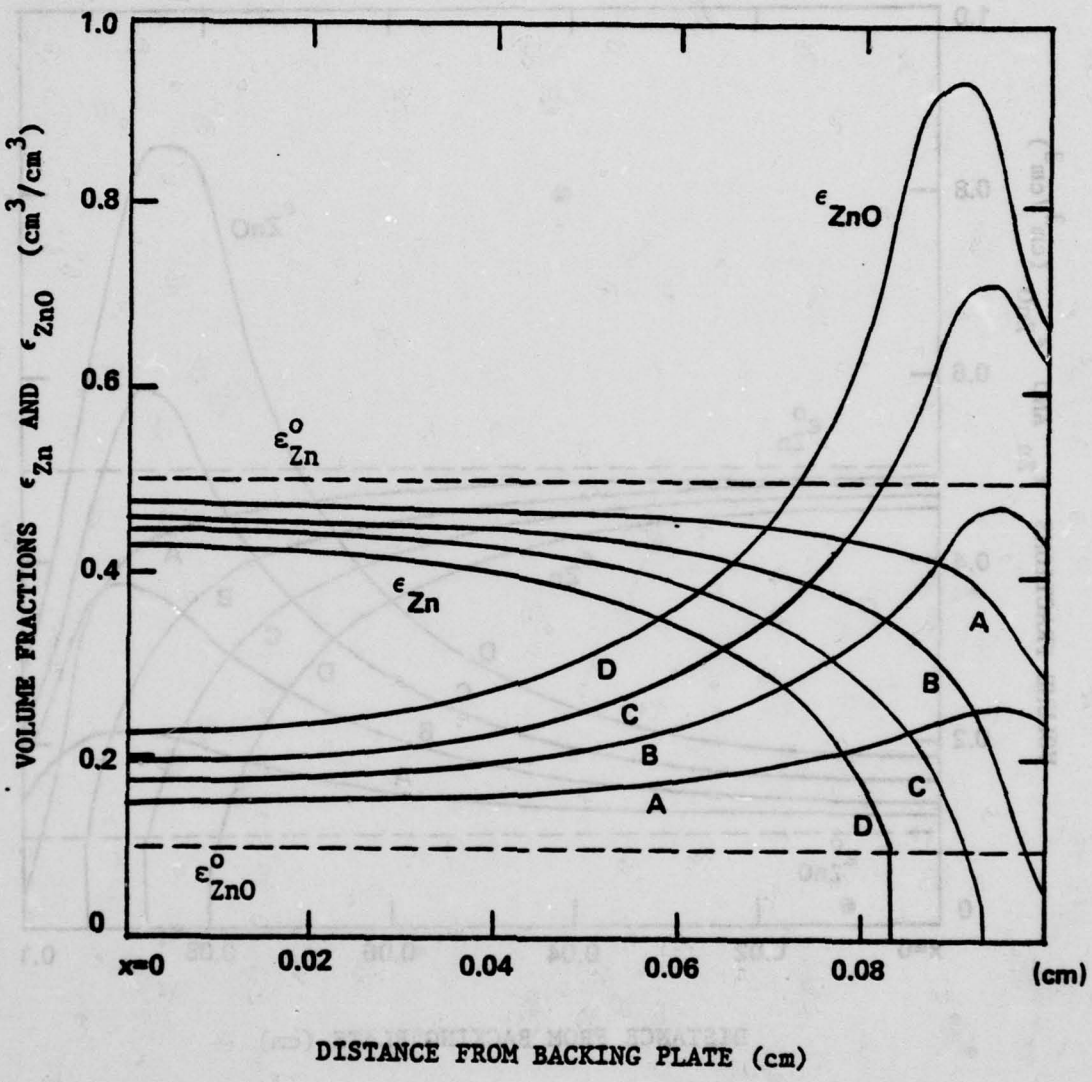

Figure 6. Distribution of Zn and ZnO Plotted As Volume Fractions (cm^3/cm^3) for Type I Membrane Boundary ($I=50\ mA/cm^2$, and A,B,C,and D Represent 10%,20%,30%,and 40% Depth of Discharge, Respectively)

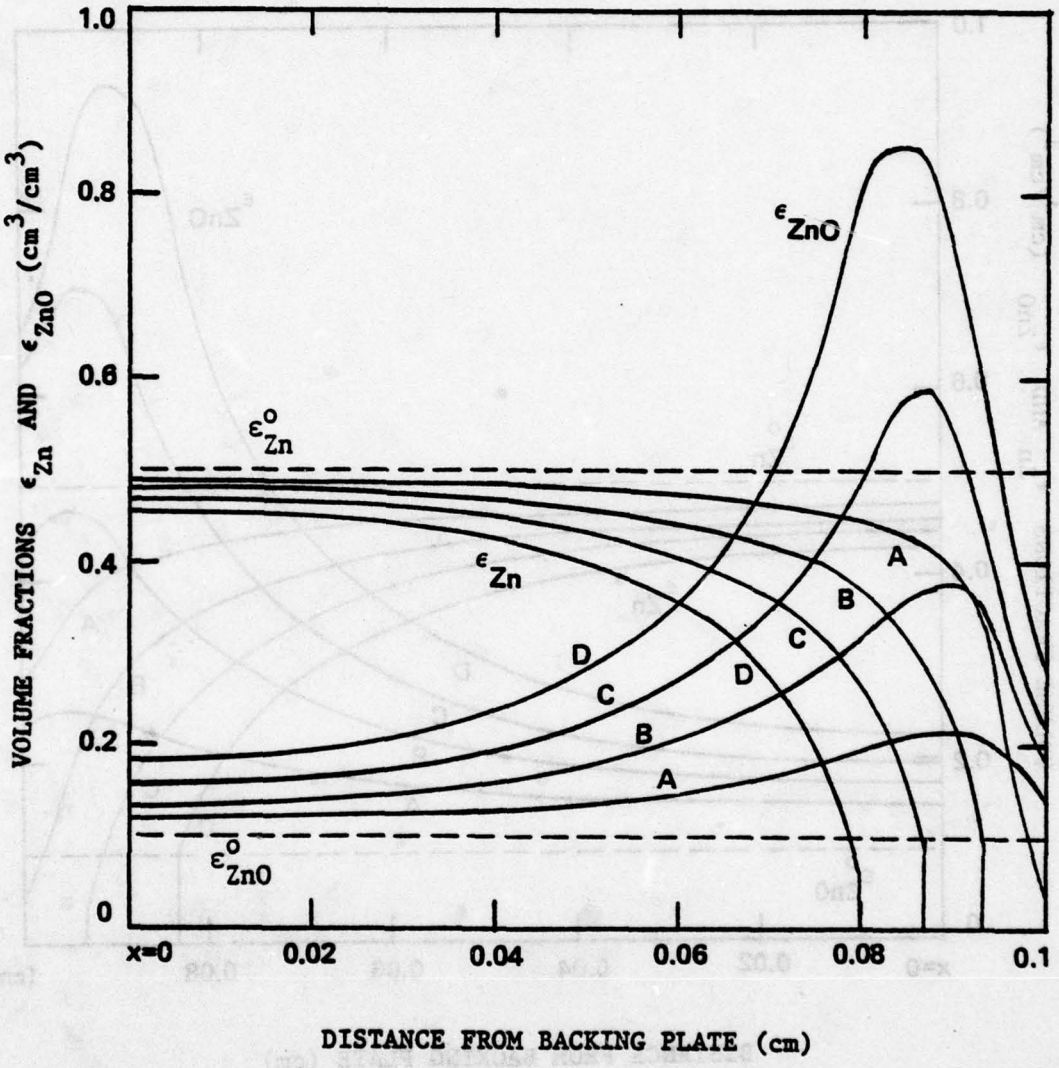

Figure 7. Distribution of Zn and ZnO Plotted as Volume Fractions (cm^3/cm^3) for Solution Boundary ($I=50$ mA/cm^2, and A,B, C,and D Represent 10%,20%,30%,and 40% Depth of Discharge, Respectively)

for solution boundary. As shown in Figure 5, solid zinc is consumed mainly near the face of the electrode and used up after only 23% discharge for the membrane boundary (Figure 6) and 10% discharge for the solution boundary (Figure 7). During discharge, solid zinc dissolves into solution by charge transfer reaction (A), producing supersaturated zincate solution from which ZnO is precipitated by chemical reaction step (B). Consequently, the total conversion of zinc into zincate ion at a specified time t, i.e., the integrated area between the dotted line (denoted by ε^{o}_{Zn}) and the curve ε_{Zn} at time t, must be the same for both cases. However, the total amount of ZnO precipitated, i.e., the integrated area of ZnO profile, is smaller for the solution case than for the membrane case. For example, after 40% depth of discharge, the amount of precipitated ZnO obtained from Figure 6 and Figure 7 are 95% and 55%, respectively, of the total amount of the consumed zinc which is calculated from the current applied during the operation period (8400 seconds). The missing zinc oxide is lost into the counter electrode compartment as a soluble species, zincate ion, before precipitation occurs.

III-2. Behavior on Cycling

The electrode initially composed of 40% liquid filled pores, 50% Zn, and 10% ZnO by volume was cycled with constant current density of 50 mA/cm^2. For each cycle, 20% depth of discharge followed by 20% depth of charge are applied. At the beginning of each discharge or charge step, the concentrations of zincate and hydroxide ions are assumed to be c^{o}_{2}(0.66M) and c^{o}_{3}(8M), respectively. This assumption is not significant

since the time required to reach c_2^o or c_3^o is negligible compared to the total operation time at each half cycle. For example, at the end of 20% discharge of the first cycle, the solution is 5M KOH for type I membrane boundary case and 7.4M KOH for the solution boundary case. The time required after cycle reversal for the solution to reach 8M KOH is about 3 minutes for type I membrane boundary and 30 seconds for the solution boundary case.

Figure 8 shows the concentration profiles of hydroxide (top curves) and zincate (bottom curves) during charge of the first cycle. In Figure 9, transfer current distribution on charging is compared to that on discharging for type I membrane boundary case. Current distribution during charge becomes more uniform since precipitated ZnO initially reduces the active zinc surface area and shifts the reaction towards the backing plate. The overpotential is plotted as a function of time in Figure 10. The anodic overpotentials increase to give 20 mV, 24mV, and 32mV at the end of discharge of the 1st, 2nd, and 3rd cycle, respectively. Similar but less significant increase in overpotential is observed during charge. This increase in overpotential, namely, the decrease in cell capacity with cycling is due to the redistribution of zinc and zinc oxide which causes pore plugging near the front face of the electrode.

The volume fractions of zinc and zinc oxide during two cycles are plotted as a function of distance in Figure 11 for the type I membrane boundary and Figure 12 for the solution boundary. The distribution of zinc and zinc oxide becomes less uniform as cycling continues. This nonuniformity is more serious for the solution boundary (Figure 12) than for the membrane boundary (Figure 11). The volume fractions of Zn and

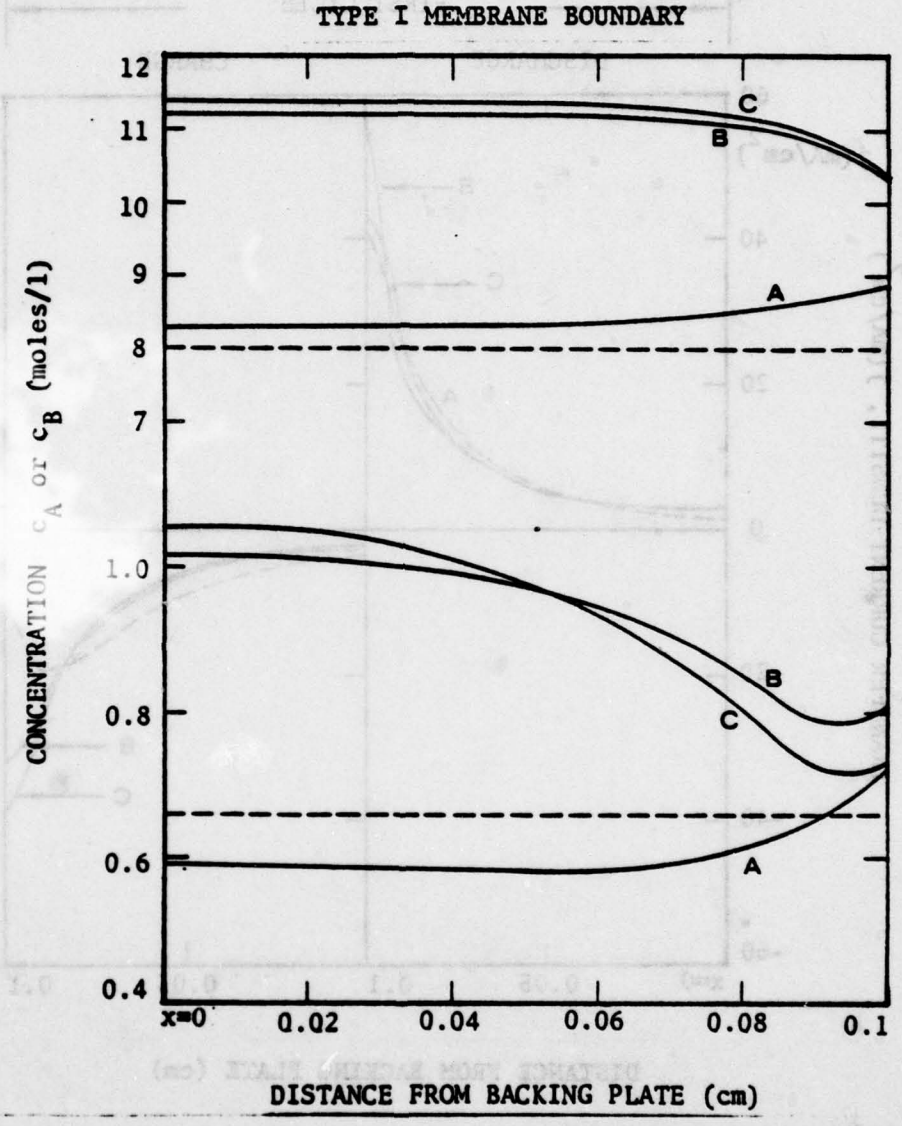

Figure 8. Concentration Profile During Constant Current Charge for Type I Membrane Boundary (I=50 mA/cm^2, L=0.1 cm, and A for One Minute Polarization and B and C for 10% and 20% Depth of Charge, Respectively)

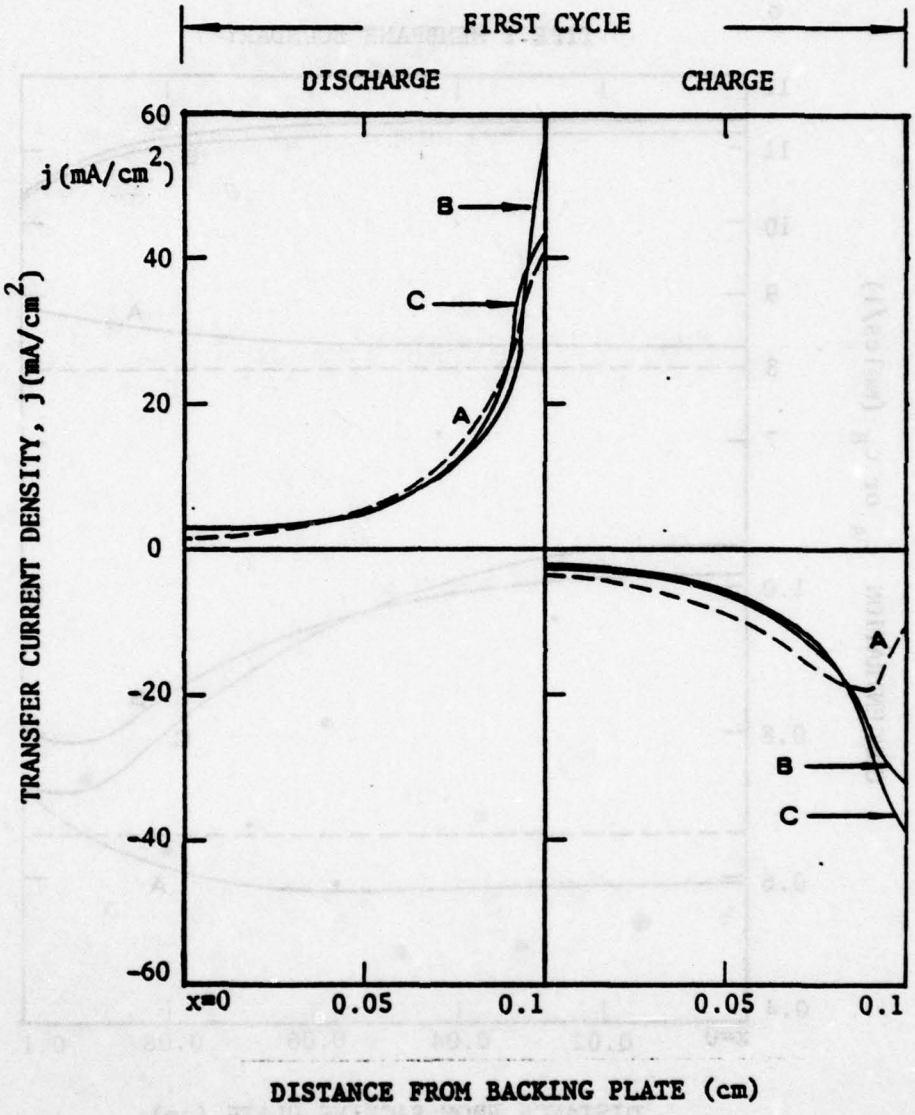

Figure 9. Distribution of Local Charge Transfer Current Density, j(mA/cm^2), During the First Cycle for Type I Membrane Boundary (I=50 mA/cm^2, L=0.1 cm, and A,B,and C Represent 0%,10%, and 20% Depth of Discharge or Charge, Respectively)

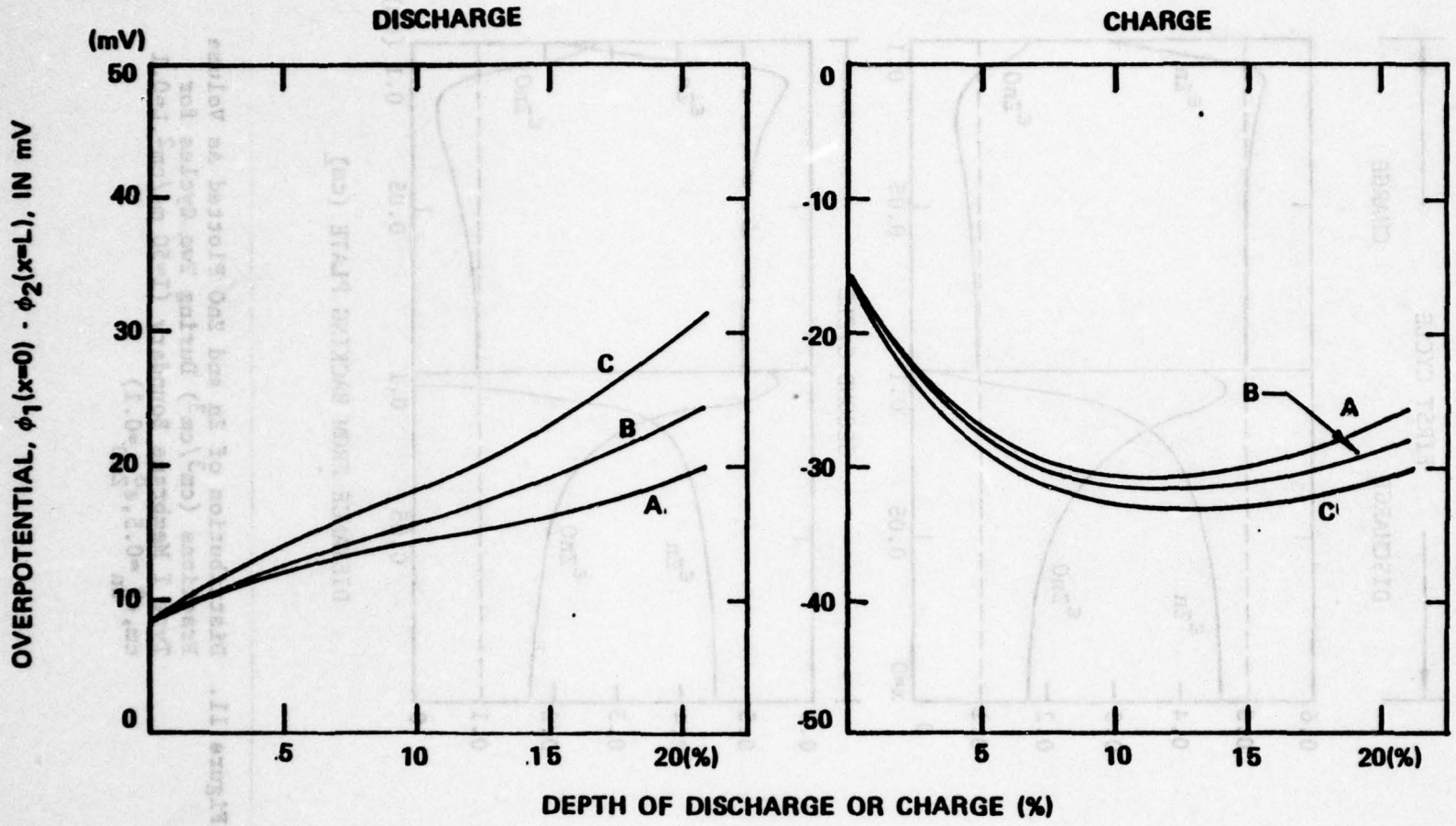

Figure 10. Overpotential, $\phi_1(o)-\phi_2(L)$, of Zinc Electrode with Time During Three Cycles for Type I Membrane Boundary. A, 1st Cycle; B, 2nd Cycle; C, 3rd Cycle. ($I=50$ mA/cm^2, $L=0.1$ cm, $\epsilon^o=0.4$, $\epsilon^o_{Zn}=0.5$, $\epsilon^o_{ZnO}=0.1$)

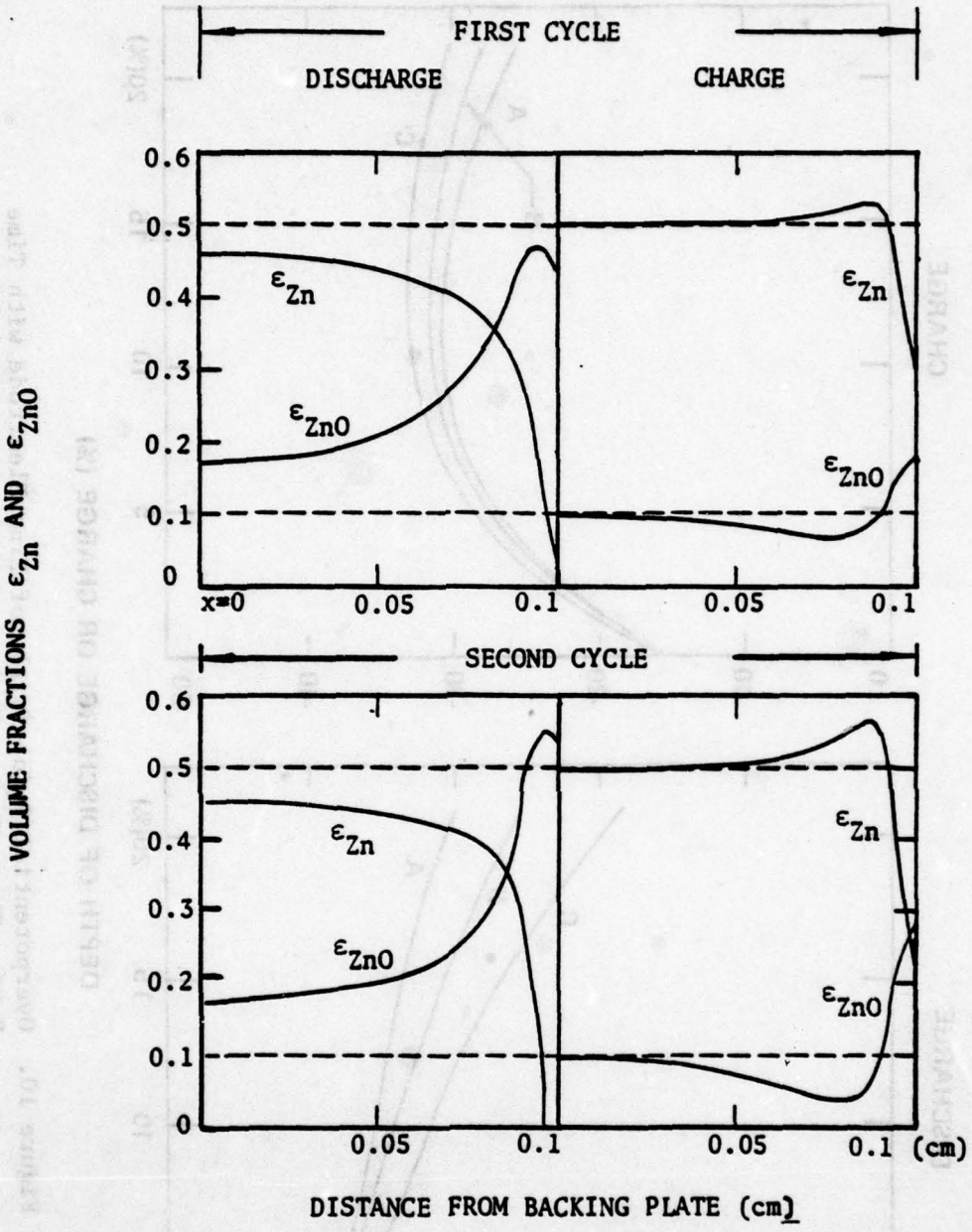

Figure 11. Distribution of Zn and ZnO Plotted As Volume Fractions (cm^3/cm^3) During Two Cycles for Type I Membrane Boundary ($I=50\ mA/cm^2, L=0.1$ cm, $\epsilon^o_{Zn}=0.5, \epsilon^o_{ZnO}=0.1$)

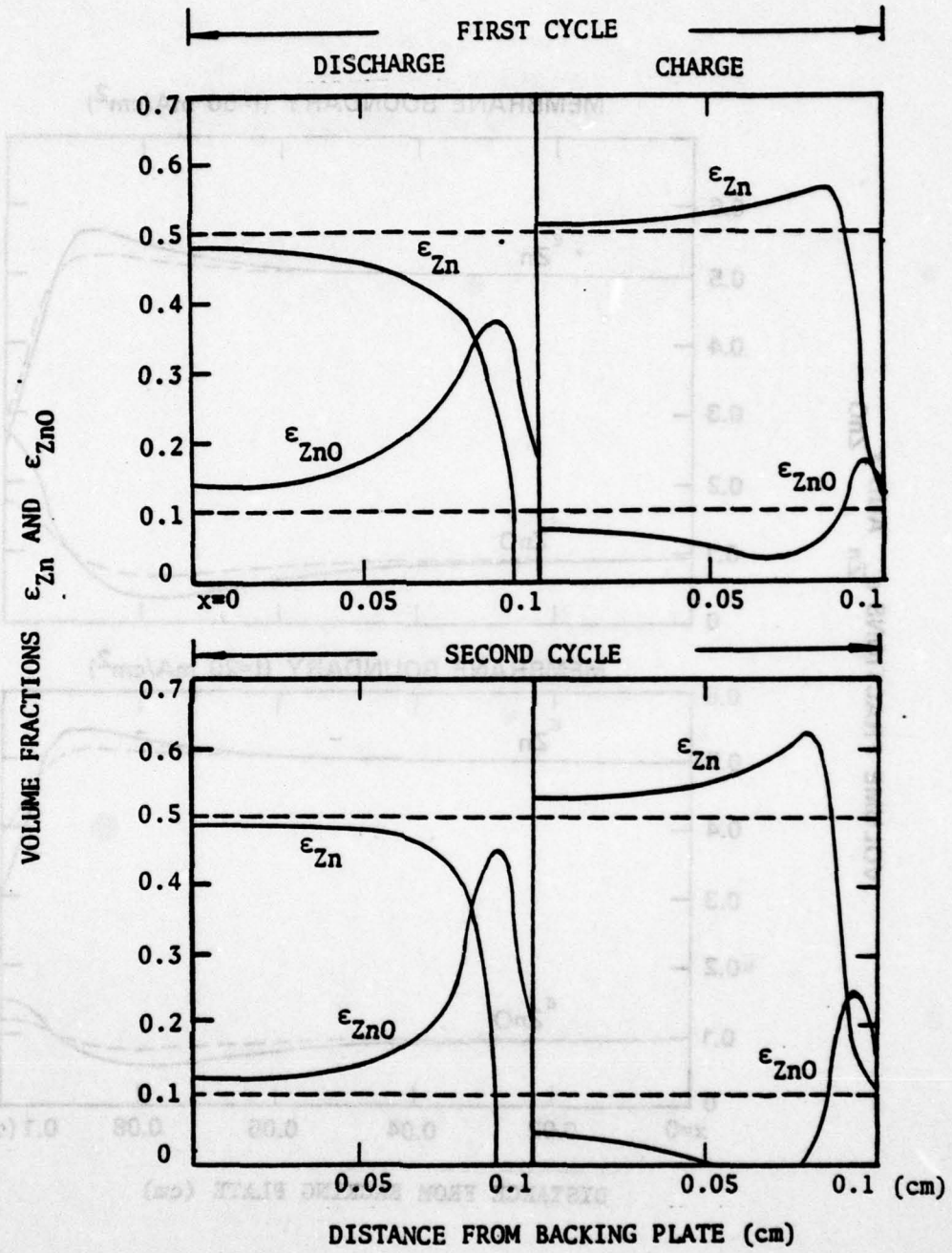

Figure 12. Distribution of Zn and ZnO Plotted As Volume Fractions (cm^3/cm^3) During Two Cycles for Solution Boundary (I=50 mA/cm^2, L=0.1 cm, ϵ^o_{Zn}= 0.5, ϵ^o_{ZnO}=0.1)

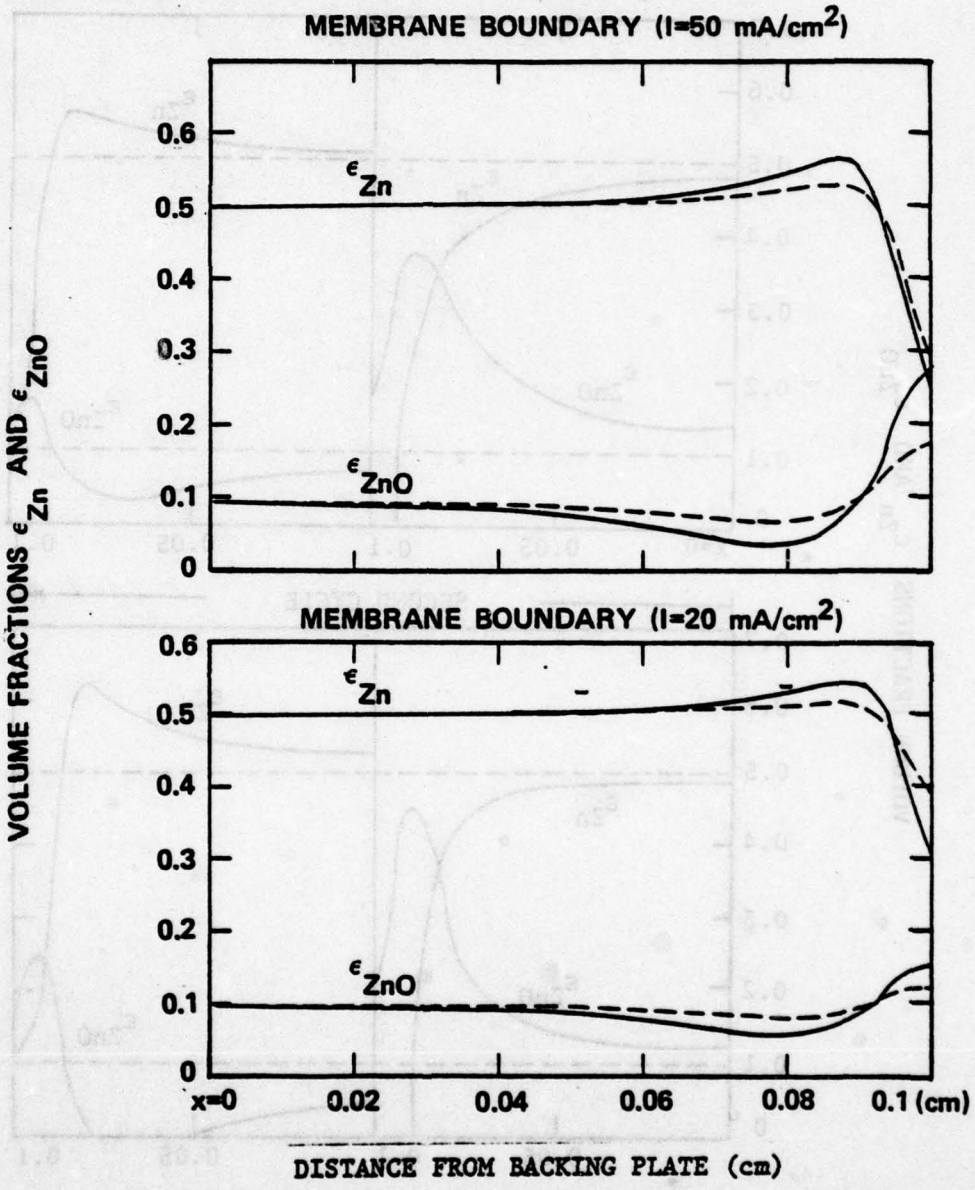

Figure 13. Distribution of Zn and ZnO Plotted As Volume Fractions At Two Current Densities for Type I Membrane Boundary. ---, After One Cycle; ——, After Two Cycles.

ZnO for the low current density of 20 mA/cm^2 are compared with those for the high current density of 50 mA/cm^2 in Figure 13. For each cycle, 20% depth of discharge followed by 20% depth of charge was applied. Profiles of Zn and ZnO are clearly more uniform for the low current density compared to those for the high current density.

III-3. Zinc Electrode Failure Modes

Zinc electrode behavior occurring during cycling has been predicted by a mathematical model. The model predicts that discharge of the zinc electrode having porosity of 0.4 with current density of 50 mA/cm^2 failed after only 40% depth of discharge (see Figure 2) due to pore plugging (blockage of the 1st kind) as shown in Figure 6. The model also predicts that the reaction distribution is highly nonuniform, and the effective reaction zone is very thin (Figure 5). This nonuniform reaction distribution will accelerate the failure due to pore plugging at the face of the electrode. Furthermore, the zinc metal in the region outside the effective reaction zone serves simply as an inert matrix and does not contribute to the cell capacity. Therefore, thin electrodes are required for design of industrial cells in order to have high cell capacity per unit weight of electrode.

The loss of ZnO species into the counter electrode compartment during discharge is very large for cells without a membrane (see Figure 7), while for the cell with a membrane (Figure 6), mass transfer of zincate ion into the counter electrode compartment was restricted. During charge, for the cell without a membrane or with a punctured membrane, the zincate ions which have moved towards the counter elec-

trode on discharging are expected to move back towards the zinc test electrode. This type of mass transport leads to zinc dendrite formation which eventually causes short circuits to the counter electrode. This is, probably, the main reason along with preventing zinc metal nucleation within the membrane why industrial cells having appropriate membranes successfully reduce dendrite formation and short circuits.

However, for cells having a membrane such as RAI P2291 cation exchange membrane, KOH concentration was depleted significantly during discharge, which can be a cause of electrode failure. Discharge failure due to KOH depletion was predicted in Figure 4 (curve C).

Shape change, i.e., the redistribution of solid zinc species in the y-direction, has been successfully explained by the differences in convective flow and the degree of super- (or under-) saturation of zincate ion during cycling (12,13). Similarly, redistribution of solid zinc species in the x-direction is predicted as shown in Figures 11 to 13. ZnO precipitated during discharge was not completely dissolved during charge but accumulated at the electrode surface as cycling continues. This movement may be a limiting factor in the loss of cell capacity after many cycles.

Based on the zinc electrode behavior predicted by the present mathematical model, failure modes occurring in the zinc electrode are summarized as follows;

Failure during discharge

(1)* Blockage of the 1st kind (pore plugging)

(2)* Blockage of the 2nd kind (passivation or surface coverage on zinc surface by the precipitated ZnO)

(3)* Depletion of KOH solution

(4) Gas evolution

Failure during charge

(1)* Depletion of zincate

(2) Zinc dendrite formation

(3) Gas evolution

Failure during cycling

(1) Zinc dendrite formation and short circuit

(2) Shape change in the y-direction

(3)* Redistribution of Zn species in the x-direction

(4) Accumulated gas evolution

where symbol "*" denotes the failure modes to be considered in the present work.

IV. EXPERIMENTS

IV-1. Preparation of the Pressed Zinc Electrode

The test electrodes were prepared from pure zinc powder (Plasmadyne Co.) with particle sizes between 250 and 325 mesh (60-44 microns). The zinc powder was amalgamated with mercury in a mercuric acetate solution containing an amount of mercury equal to 2.5 wt% of the zinc weight. The amalgamation solution also contains one percent glacial acetic acid. Complete amalgamation was confirmed by adding a mixture of NH_4Cl and NH_4OH to a small sample of the solution, where any dissolved mercury would form a white precipitate. After amalgamation is complete, the zinc powder is rinsed, dried in a vacuum oven, and stored in a desicator.

The test zinc electrodes were prepared by pressing amalgamated zinc powder onto a backing plate. The backing plate consisted of a titanium foil (0.001 inches thick) upon which a silver screen (0.004 inches thick) had been spot welded. Electrodes with two different porosities were tested; low porosity and high porosity electrodes. The low porosity electrodes were obtained by pressing the Zn(Hg) powder in a stainless steel mold using 13000 psi. The resultant electrode contained about 0.5 grams of zinc amalgam and had a porosity of about 0.3 to 0.35. The high porosity electrodes were prepared by the procedure given by Morrell and Smith (34). A mixture of NaCl powder and Zn(Hg) powder having the weight ratio of 40 NaCl-60 Zn(Hg) was pressed onto a backing plate using 20000 psi. The NaCl powder used as a filler had a particle size of 250 to 325 mesh. After pressing, the resultant electrode was soaked in distilled water for 24 hours. Complete dissolution of NaCl was con-

firmed during this period. This gave a highly porous, stable structure having a porosity of about 0.6. After the electrode was dried, a white precipitate formed, which may be zinc-oxychloride, zinc-hydroxy chloride, or zinc-hydroxy carbonate. This compound was easily dissolved by dipping it in dilute HCl solution. The resultant electrode contained about 0.3 g of zinc.

The electrodes made by the above procedures were disks having a cross sectional area of 1 cm^2 and thickness of about 0.1 to 0.11 cm. Small cross sectional area, 1 cm^2, was chosen in order to minimize the effect of nonuniform current distribution in the direction parallel to the electrode surface.

IV-2. Potential Measurements

A schematic drawing of the test cell is shown in Figure 14. The main body of the cell was made of Plexiglas. The test zinc electrode was completely sealed by two O-rings when the cell is assembled by tightening screws. A silver screen having a zinc deposit was used as a counter electrode. Two layers of RAI P2291 (40/20) cation exchange membrane (thickness of 0.001 inches) and one layer of dynel (thickness of 0.005 inches), used as separators, were placed on top of the test electrode. The RAI membrane is a beta radiation cross linked low density polyethylene film which has been gamma-radiation grafted with methacrylic acid. The dynel is a porous non-woven acrylonitrile which is resistant to oxidation in the cell environment. The sealed test zinc electrode contained limited electrolytic solution (about 0.03 to 0.11 cm^3), while the counter electrode compartment contained effectively a large amount of solution (about 1.5 cm^3).

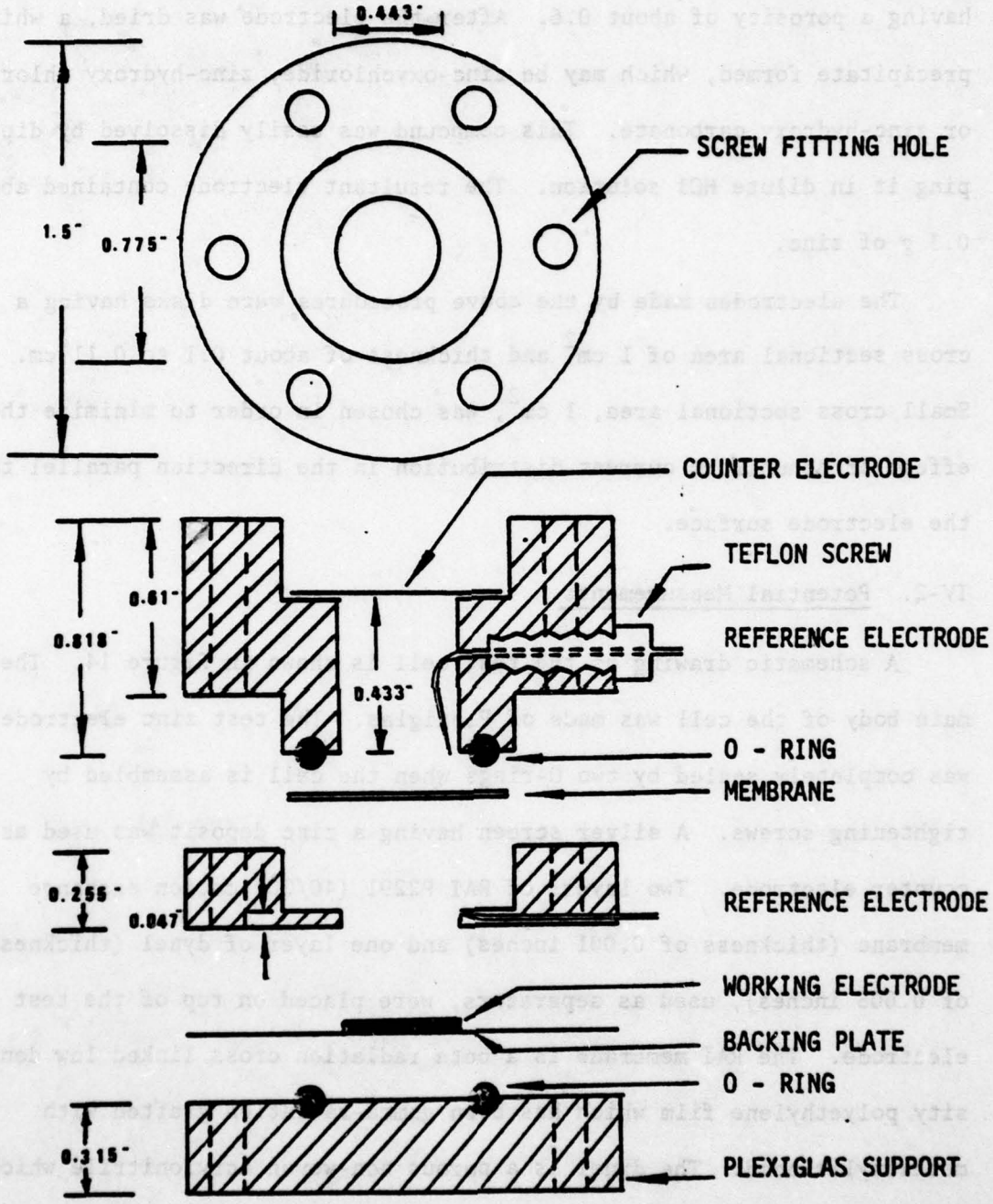

Figure 14. Test Cell Assembly

The teflon capillaries lead to the Hg/HgO reference electrodes. The Hg/HgO reference electrodes were made by the procedure given by Falk and Salkind (89). The H-shaped glass tube contained 40 wt% KOH solution which contacted with a mercury oxide-mercury- platinum wire couple. A dynel fiber plug was inserted into the end of the capillary tube to minimize the flow of electrolytic solution from the zinc electrode compartment into the reference electrode or vice versa.

After evacuation, filling the cell with solution, and assembling the cell, the test electrodes were discharged galvanostatically in a 40 wt% KOH solution saturated with ZnO. Figure 15 is the basic circuit used in operation of the cell. The overpotentials of the test zinc electrode were measured with respect to Hg/HgO reference electrodes using a Keithley Model 602 electrometer and one channel of a Varian Associate G2000 two-channel recorder. Three Hg/HgO reference electrodes were used to measure the zinc electrode potentials at three different positions; one above the membrane, one on the electrode surface, and one on the backing plate. An automatic multipole switch and a Flexopulse HG 108A6 timer were used to allow periodic measurements at three positions with intervals of 20 seconds. An external zinc-mercury cell was connected in series in the electrometer circuit to cancel out the equilibrium potential of the zinc electrode with respect to Hg/HgO reference electrode. This arrangement allowed zero potential at open circuit and the sensitivity of the potential data was improved. Potential differences between the zinc test and the zinc counter electrodes were recorded continuously using the other channel of the recorder. The integrated current passed was counted by a coulometer, Model 541

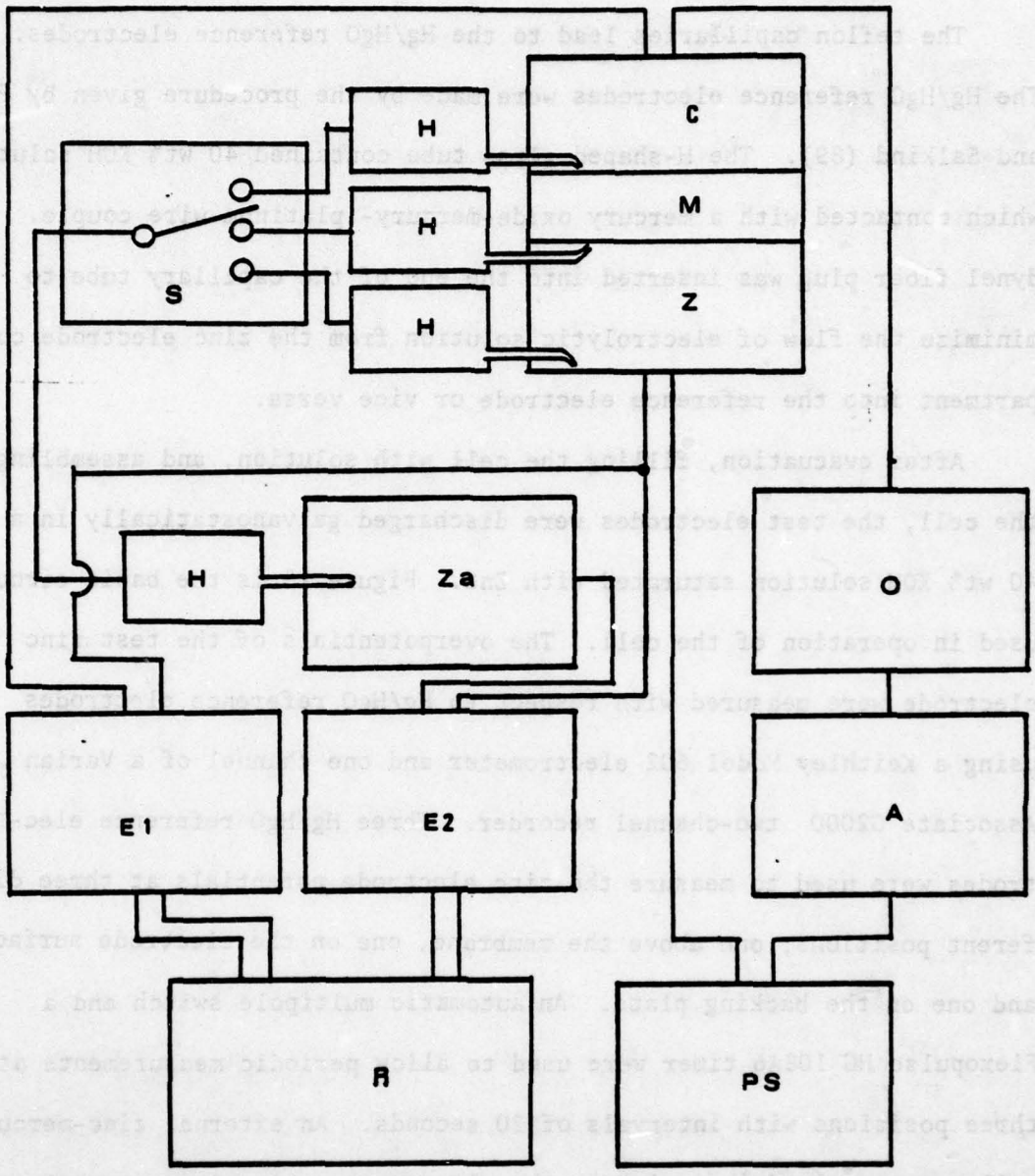

Figure 15. Electrical Circuit for Operation of Cell. A, ammeter; C, counter electrode; E1, electrometer for monitoring test to counter electrode potential difference; E2, electrometer for measuring overpotentials at three different positions; H, Hg/HgO reference electrodes (40 wt% KOH solution); M, separators; O, resistor; PS, constant current power supply; R, two channel recorder; Z and Za, zinc test and zinc auxiliary electrodes (40 wt% KOH-saturated zincate), respectively.

Koslow Scientific Co.

IV-3. Determination of Reaction Profiles

Some electrodes were sectioned using the technique developed by Bro and Kang (39). The discharged electrode was fitted into a fixture having a microadvancing screw. This allowed the electrode to be advanced 0.025 inches per revolution. The electrode having thickness of 0.1 to 0.11 cm was then machined off, by use of a milling machine, in the direction parallel to the electrode surface. This sectioning operation resulted in about 5 to 10 sections. The machined chips per each section were collected and analyzed to determine the amount of zinc and zinc oxide.

The standard technique for analyzing zinc and zinc oxide with EDTA titration has been described in detail by Welcher (90). The sectioned chips were dissolved and stirred vigorously in 10 ml of 1M NH_4Cl-NH_4OH buffer solution for five minutes. Previous investigators (38,91) have suggested that this solution dissolves ZnO completely but attacks zinc negligibly during this period. The solution was vacuum filtered and washed six times with distilled water. About 5 ml of 1M NH_4Cl-NH_4OH was added to the filtrate and the resulting solution was titrated with 0.1M disodium EDTA. Near the end point, 0.01M disodium EDTA was used to give a more accurate titration. The indicator used was 0.2% solution of Eriochrome Black T in triethanolamine. The color of indicator changes from red to blue at the end point. The weight of ZnO equivalent to 1 ml of 0.1M disodium EDTA is 8.138 mg. Following the analysis of the ZnO, the filtered zinc powder was dissolved in 1 to 2 ml of 10M HCl solution for several hours. The solution was adjusted to pH=7 by adding 1M KOH

solution and then pH=10 by adding 1M NH_4Cl-NH_4OH solution, and titrated with 0.1M (and 0.01M) disodium EDTA. The equivalent weight of zinc for 1 ml of 0.1M disodium EDTA is 6.538 mg.

The error associated with the above procedure was estimated from the following experiments. Samples containing known weights of Zn or ZnO were titrated without filtration. For ZnO the results of the titration agreed with the known weight of the ZnO sample within 0.5%. For the sampled zinc powder, titration error was within 1%. However, when a sample containing a mixture of known amounts of Zn and ZnO is analyzed by the above procedure, it appears that the vigorous stirring, used to ensure the complete dissolution of ZnO, increases the dissolution rate of Zn. In order to quantify the error caused by the dissolution of Zn, samples of amalgamated zinc powder were vigorously stirred in 10 ml of 1M NH_4Cl-NH_4OH solution for five minutes and vacuum filtered for one or two minutes. The filtered solution was titrated with disodium EDTA. It was observed that the dissolution of zinc in 1M NH_4Cl-NH_4OH solution was about 4 wt% of the initial zinc within 6 or 7 minutes contact time as shown in Figure 16. Thus, when the amount of dissolved zinc during selective dissolution of ZnO from a Zn-ZnO mixture is accounted for, titration errors remain within 1% unless the sampled chips require less than about 0.02 ml of 0.1M disodium EDTA for titration.

The reaction profiles are represented by the absolute volume fractions of Zn and ZnO as a function of distance. During discharge, the electrode thickness generally increased as much as 10% depending on the porosity and depth of discharge. Therefore, the fractional thickness of the sectioned electrode was taken as the moles of Zn and ZnO in the chip

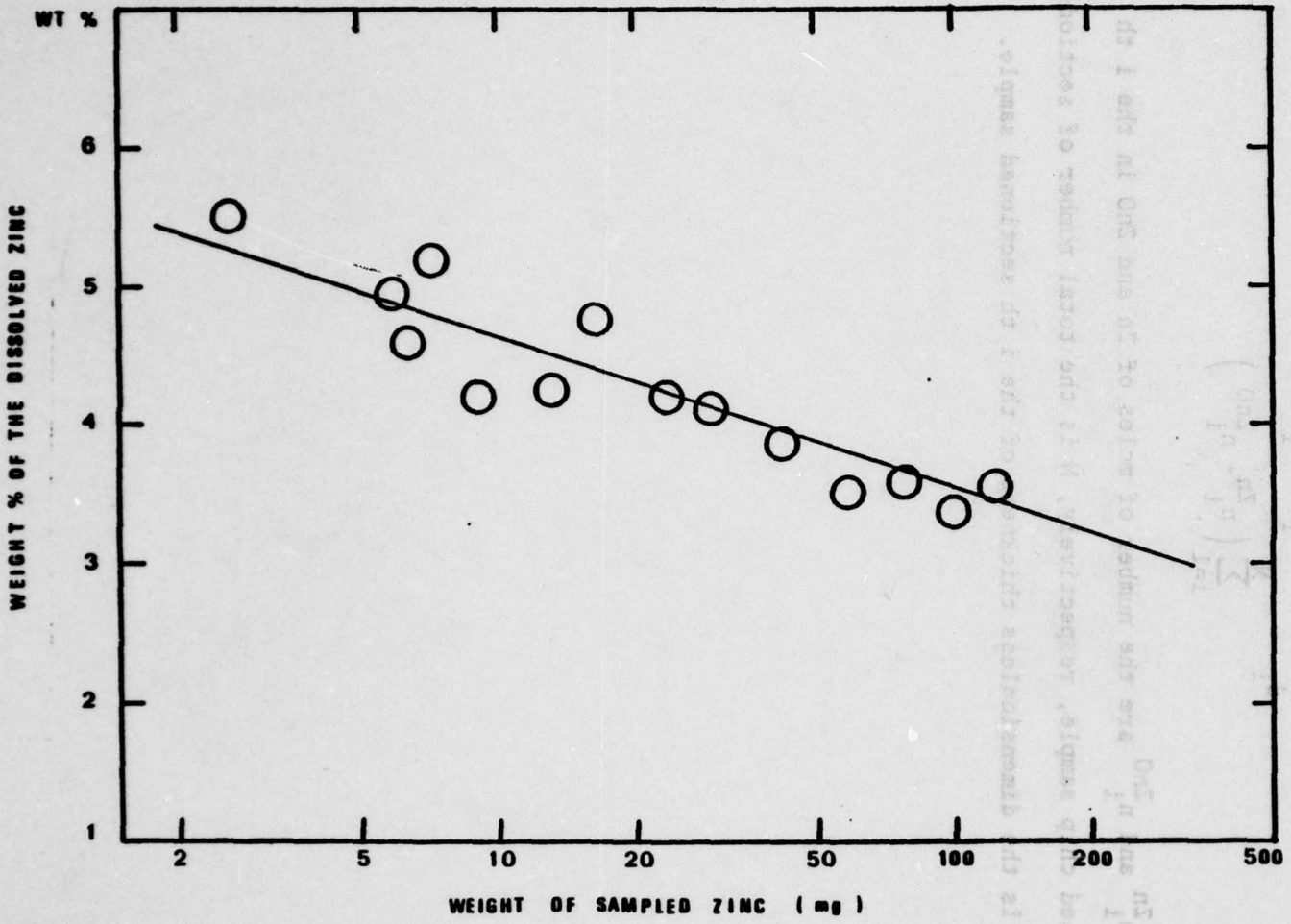

Figure 16. Weight Percent of the Dissolved Zinc in 1M NH_4Cl-NH_4OH Within 6 or 7 Minutes Contact Time

sample divided by the total moles of Zn and ZnO.

$$d_i = \frac{n_i^{Zn} + n_i^{ZnO}}{\sum_{i=1}^{N} \left(n_i^{Zn} + n_i^{ZnO} \right)}$$

where n_i^{Zn} and n_i^{ZnO} are the number of moles of Zn and ZnO in the i th sectioned chip sample, respectively, N is the total number of sections, and d_i is the dimensionless thickness of the i th sectioned sample.

V. RESULTS

V-1. Reaction Profiles

The reaction distribution, in terms of the volume fractions of Zn and ZnO, is shown in Figures 17 to 23. In all of these experiments, a dynel cloth was placed between the test electrode surface and the membrane. This arrangement is designated by "ZDM" configuration throughout this report. The measured volume fractions of ZnO are represented by the histograms and those of zinc are plotted as circles and hexagons, which are located at the center of each level of the ZnO histogram.

Some of the measured profiles are compared with the profiles predicted from the mathematical model. The data of Appendix D-1 are used for the numerical calculations. Some of the important parameters are as follows: the initial specific surface area, a^o=300 cm^2/cm^3; initial KOH concentration, c_3^o=10 M; initial porosity, ε^o=0.33 for the low porosity electrode and ε^o=0.6 for the high porosity electrode; initial volume fractions of ZnO and the inert conducting material, ε_{ZnO}^o=0 and ε_I^o=0; exchange current density, i_0^o=0.1 amp/cm^2 (taken from reference 52); tortuosity factor, t=0.5; transport parameters of hydroxide ions across the two layers of RAI P2291 membrane, t_3^m=0.5 and L_{BB}^m=1.5x10^{-5} cm/sec (taken from reference 87).

All the parameters used are taken from experimental data reported in the literature or are estimated from theoretical considerations. One exception is the effective conductivity of the electrolytic solution which was chosen to give the best fit between experimental and theoretical results. The effective conductivities are taken as 27%

(for the low porosity electrode) and 12% (for the high porosity electrode) of the conductivity of the free electrolytic solution. This choice may not be unreasonable considering the observations of Simonsson (28) and Romanova and Selitsky (76). They observed an effective conductivity which is only about one tenth of the conductivity of the free solution. They attributed this large reduction in conductivity to the gas generaged in the pores.

Figure 17 shows the volume fractions of zinc (circles and hexagons) and zinc oxide (histograms) measured for low porosity electrode (ZDM configuration) discharged to 8% depth at 50 mA/cm^2. The predicted profiles are shown as the smooth curves. The reaction profiles are highly nonuniform resulting in a very thin reaction zone. The observed as well as predicted reaction profiles, discharged at a low current density of 20 mA/cm^2, are shown in Figure 18. Circles and solid line A are measured after 10% depth and hexagons and solid line B are measured after 23% depth of discharge. Even for the 20 mA/cm^2 discharge, a thin reaction zone is still observed. After 23% depth of discharge (4.51 hour), all the zinc at the electrode face is used up and reaches the region for pore plugging. Discharge failure occurs at about 22% depth in the theoretical calculation but at about 32% depth in our experiments. Cracking or swelling of the electrode observed during operation allows further discharge to 32% depth (6.3 hour discharge) before the electrode fails due to pore plugging. It is to be noticed that only one fifth of the electrode is effectively utilized prior to electrode failure.

The zinc and zinc oxide profiles for the high porosity electrode

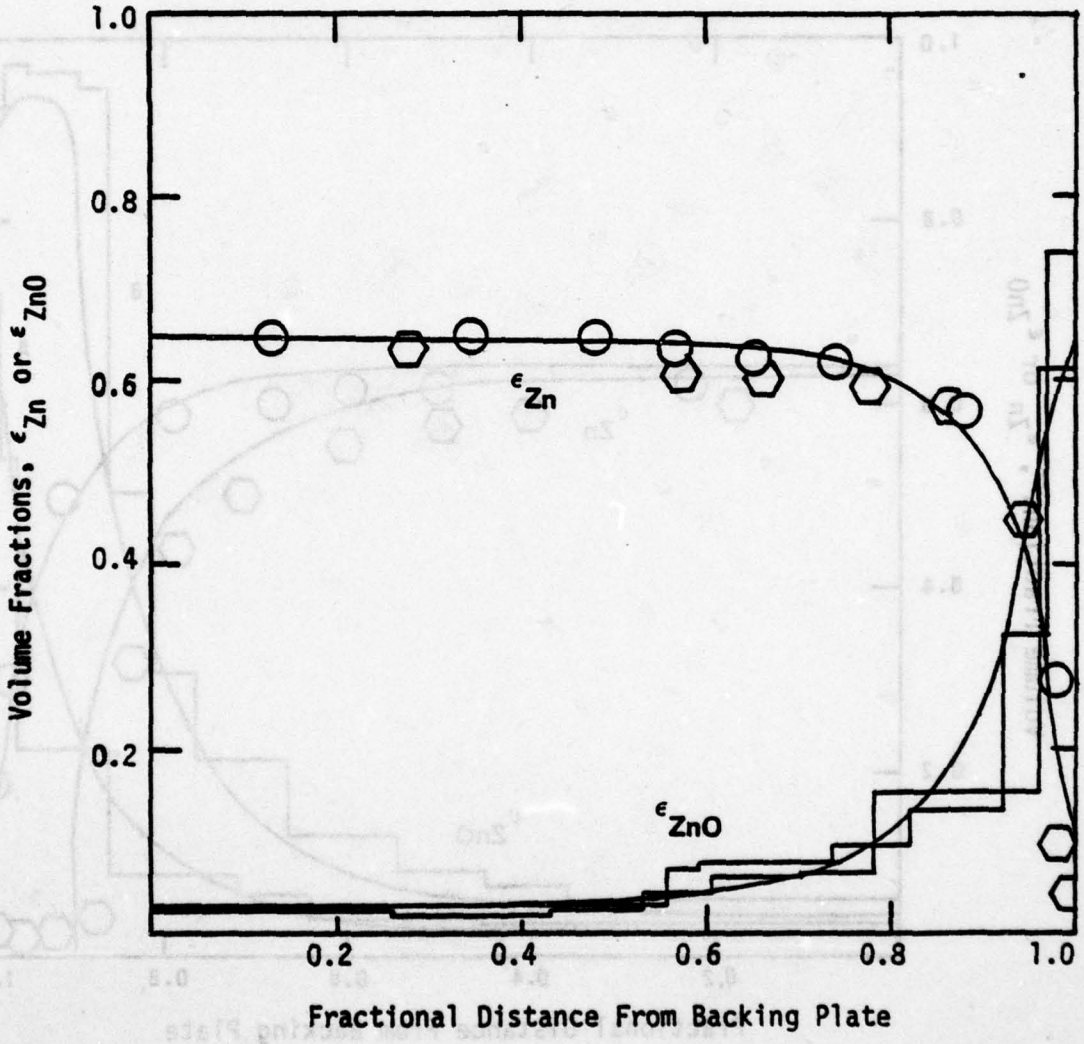

Figure 17. Profiles of Zn and ZnO for the Low Porosity Electrode Discharged to 8% Depth at 50 mA/cm^2. ◯ and ⬡, Measured Profiles for Zn; Histograms, Measured Profiles for ZnO; Smooth Curves, Predicted Profiles for Zn and ZnO.

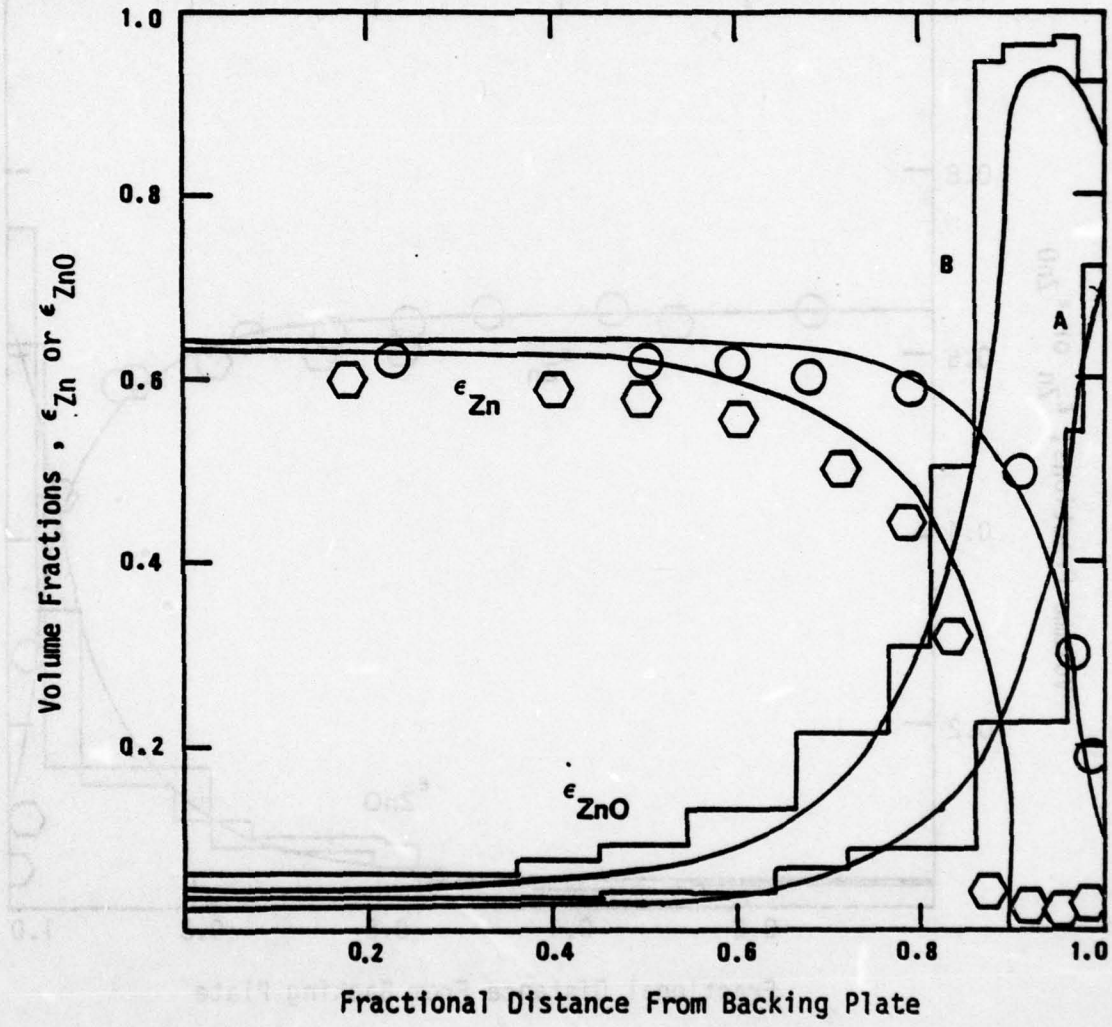

Figure 18. Profiles of Zn (Circles and Hexagons) and ZnO (Histograms) for the Low Porosity Electrode Discharged at 20 mA/cm^2. ◯ and Histogram A, Measured Profiles After 10% Depth; ⬡ and Histogram B, Measured Profiles After 23% Depth; Smooth Curves, Predicted Profiles After 10% and 23% Depths of Discharge.

to 10% depth at 50 mA/cm^2 are shown in Figure 19. Further discharge up to 21% depth (one hour discharge) results in the profiles in Figure 20. Two sets of data as well as the predicted profiles are presented. For the high porosity electrode, ohmic loss as well as concentration overpotentials through the solution are smaller than those for the low porosity electrode. This small solution resistance shifts the reaction profile towards the backing plate to produce a more uniform profile. Agreement between the measured and the predicted profiles becomes poor compared to that for the low porosity electrode. This is due to the severe swelling of the high porosity electrode which is weak in mechanical strength. Evidently, porosities for this electrode are large enough to eliminate the failure due to pore plugging, at least in the short cycle range.

In Figure 21, the measured profiles for 20 mA/cm^2 discharge are shown. Curve A is for 10% depth of discharge and curve B is for 22% depth of discharge (2.6 hour operation). Since the mechanical strength of this electrode discharged to 22% depth was very weak, the electrode was broken into pieces during sectioning process of the missing portion of solid line B. Discharge of this electrode at 20 mA/cm^2 continued to more than 68% depth (8 hour operation).

In Figure 22, the measured profiles of zinc and zinc oxide for the low porosity electrode having thickness of 0.05 cm is compared to that for the electrode having thickness of 0.1 cm.

The profiles shown in Figure 23 are measured after one cycle for a low porosity electrode with an applied current density of 50 mA/cm^2. The total charge passed at each half cycle was equivalent to 10% conver-

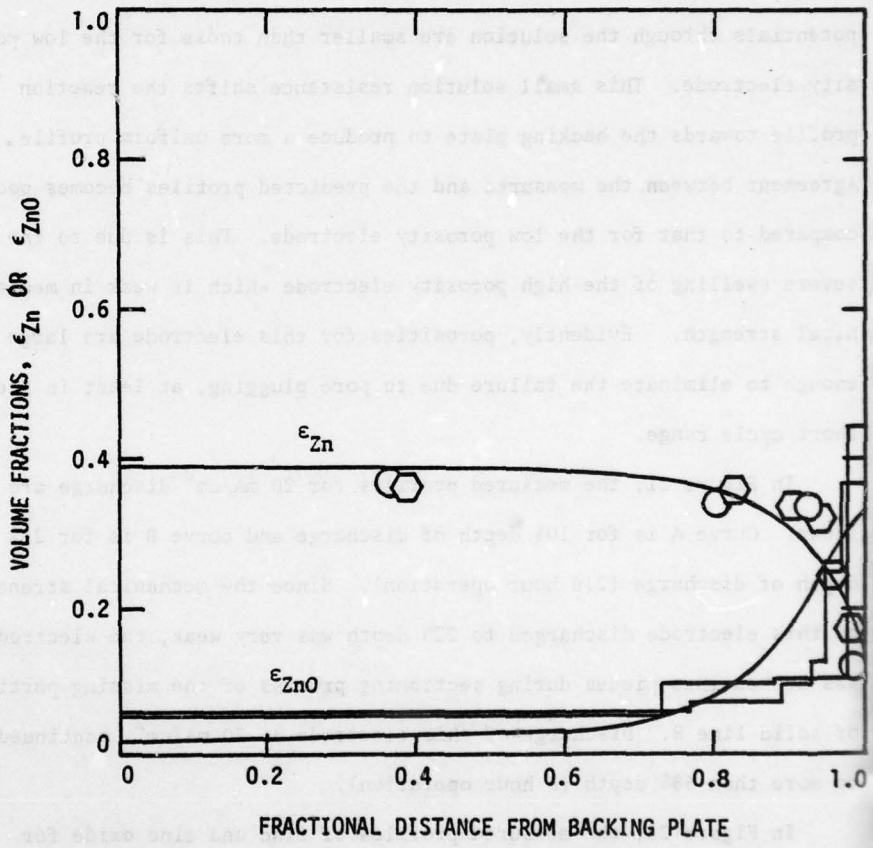

Figure 19. Profiles of Zn and ZnO for the High Porosity Electrode Discharged to 10% Depth at 50 mA/cm^2. ○ and ⬡, Measured Profiles for Zn; Histograms, Measured Profiles for ZnO; Smooth Curves, Predicted Profiles for Zn and ZnO.

AD-A067 514 CALIFORNIA UNIV LOS ANGELES DEPT OF CHEMICAL UNCLEAR--ETC F/G 10/3
THEORETICAL AND EXPERIMENTAL ANALYSIS OF ALKALINE ZINC BATTERIE--ETC(U)
JAN 79 D N BENNION, J NEWMAN, W G SUNU F44620-76-C-0098

UNCLASSIFIED UCLA-CNTE-1-1 AFOSR-TR-79-0472 NL

2 OF 2
ADA
067514

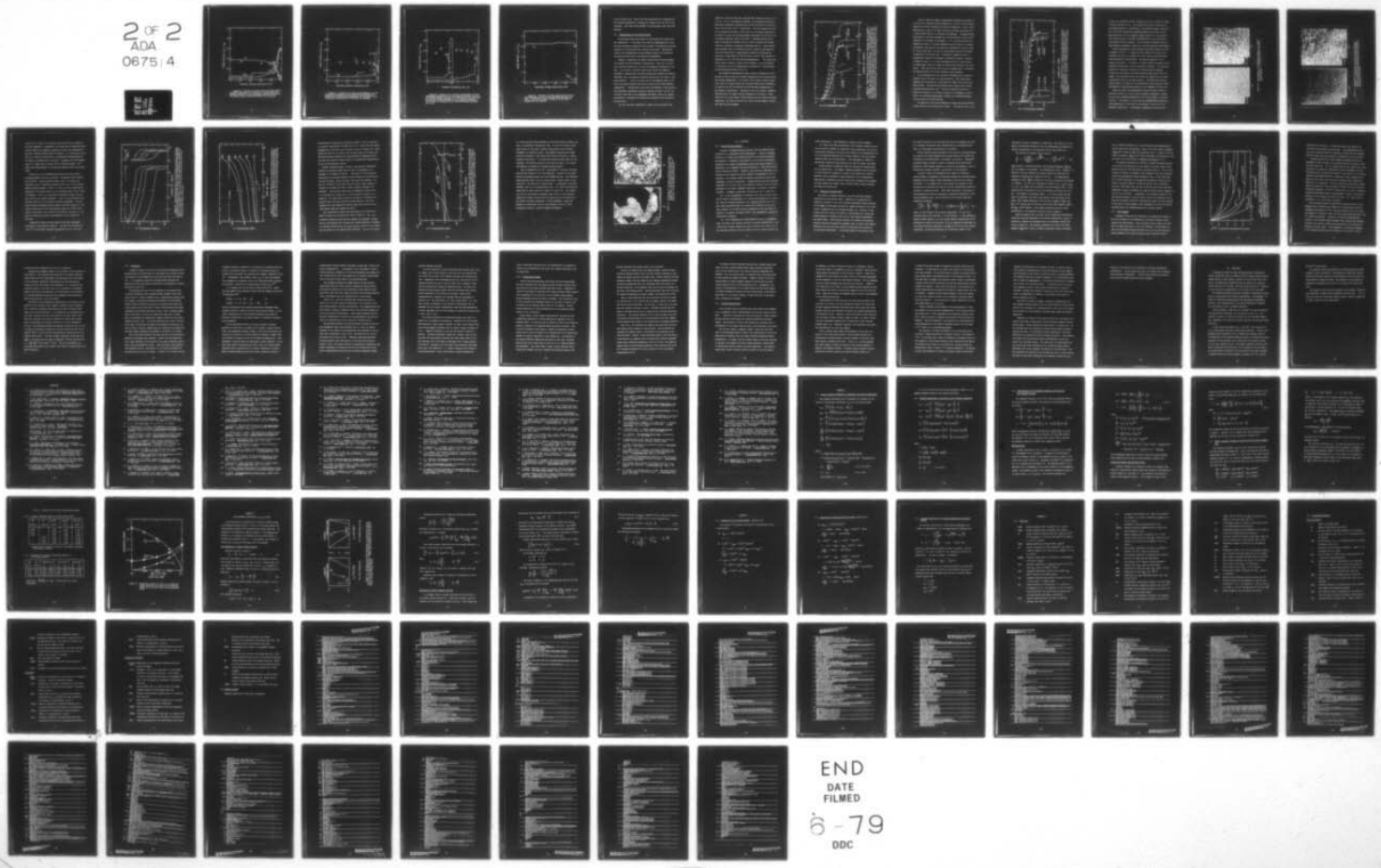

END
DATE FILMED
6-79
DDC

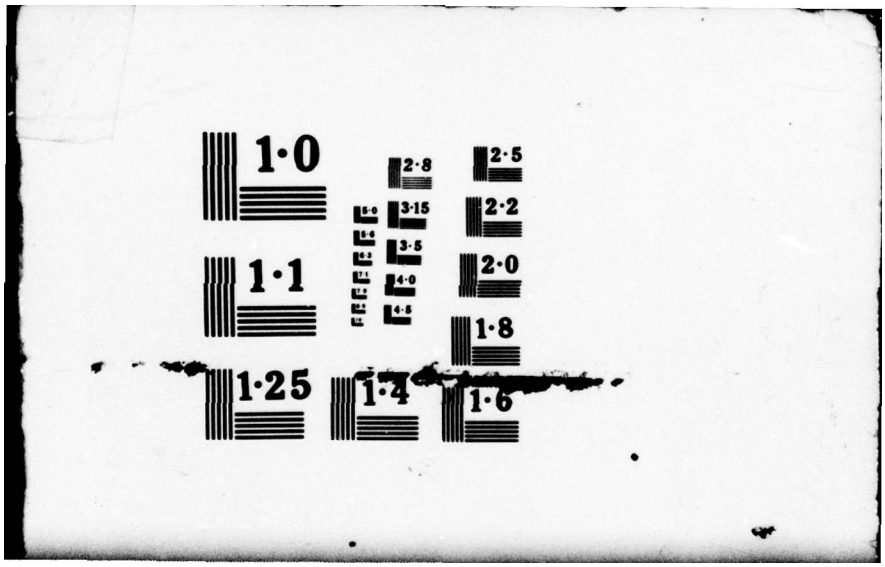
1·0
1·1
1·25
1·4
1·6
1·8
2·0
2·2
2·5
2·8
3·15
3·5
4·0

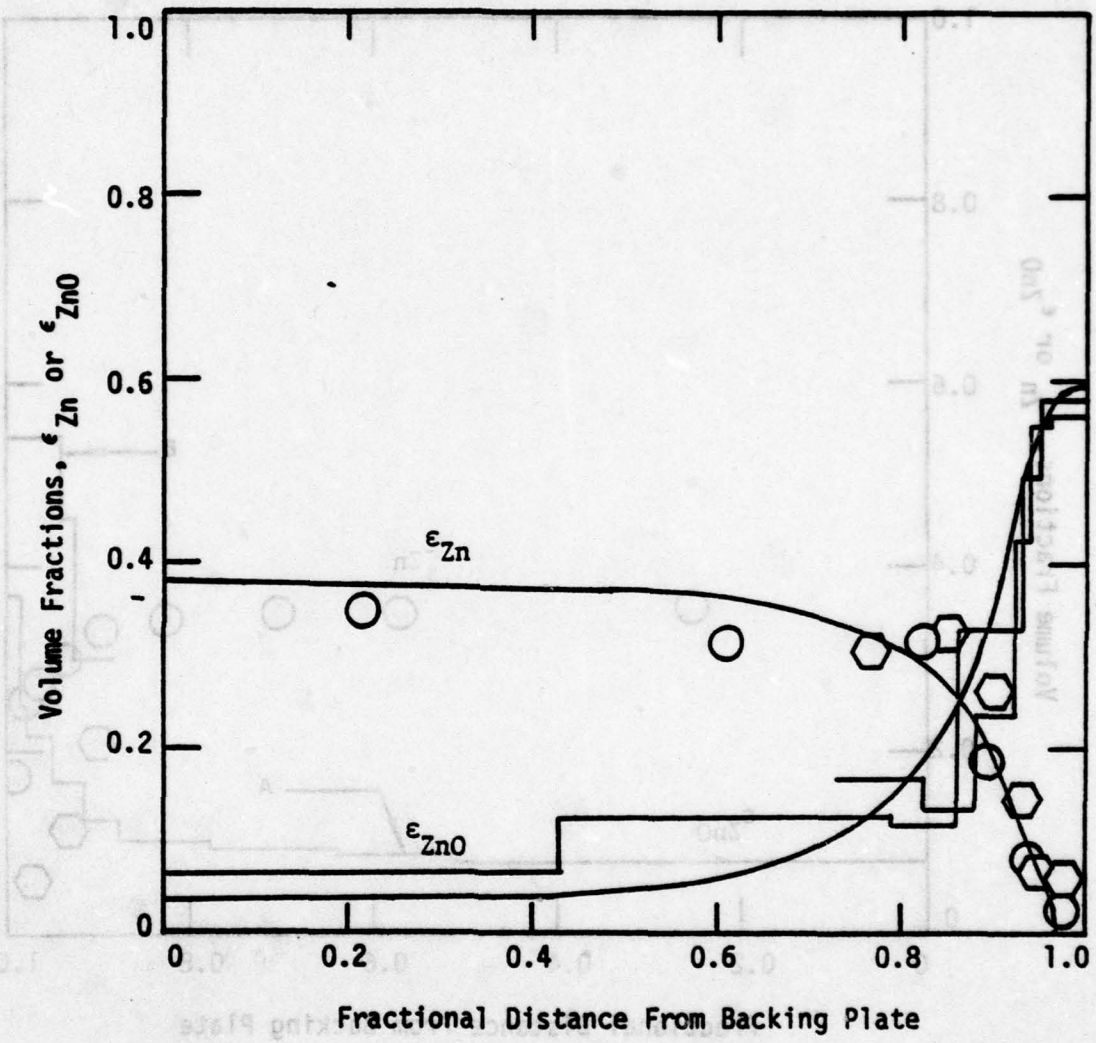

Figure 20. Profiles of Zn and ZnO for the High Porosity Electrode Discharged to 21% Depth at 50 mA/cm^2. ○ and ⬡, Measured Profiles for Zn; Histograms, Measured Profiles for ZnO; Smooth Curves, Predicted Profiles for Zn and ZnO.

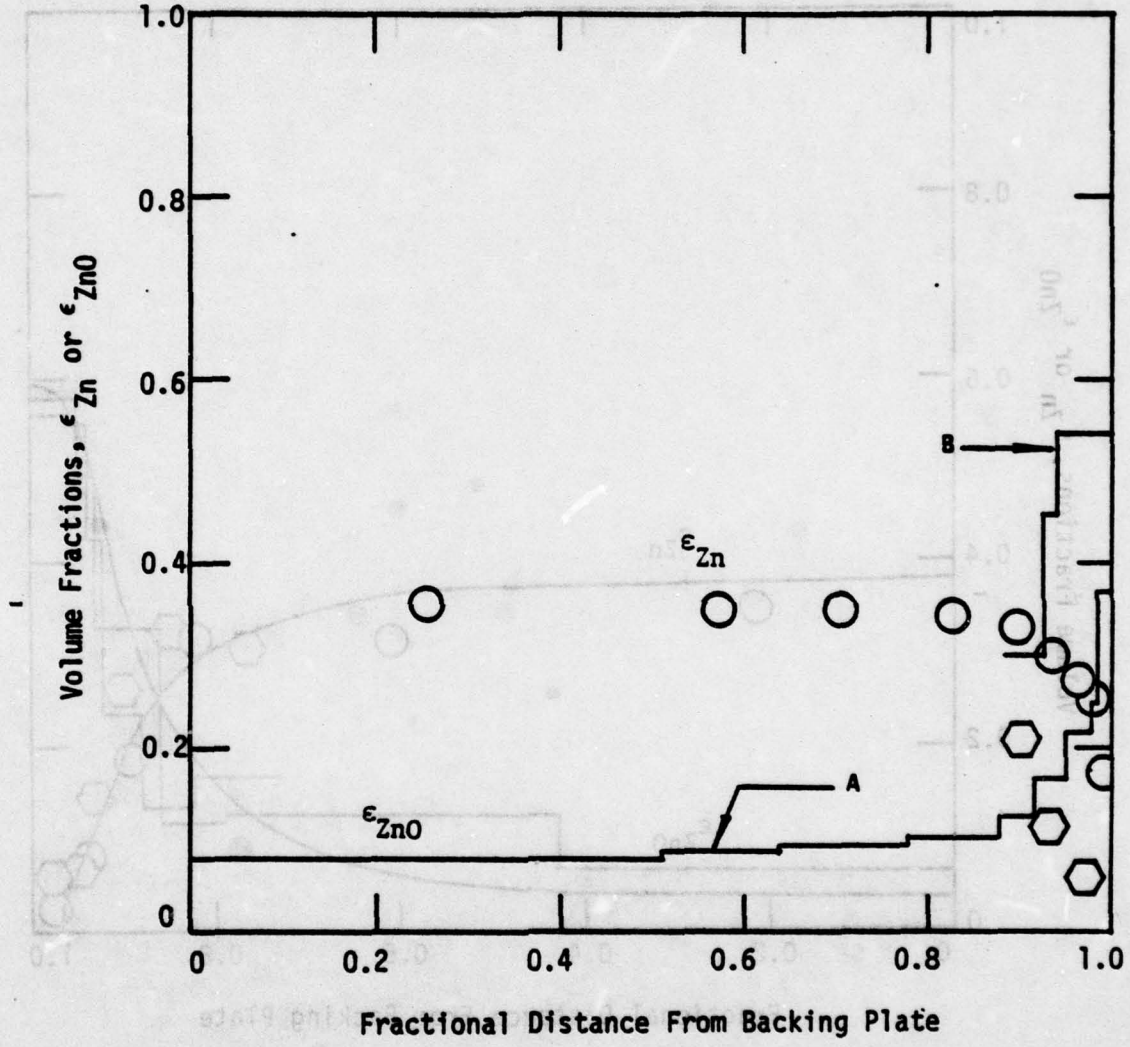

Figure 21. Profiles of Zn (Circles and Hexagons) and ZnO (Histograms) Measured for the High Porosity Electrode Discharged At 20 mA/cm^2. ◯ and Histogram A for 10% Depth of Discharge; ⬡ and Histogram B for 22% Depth of Discharge.

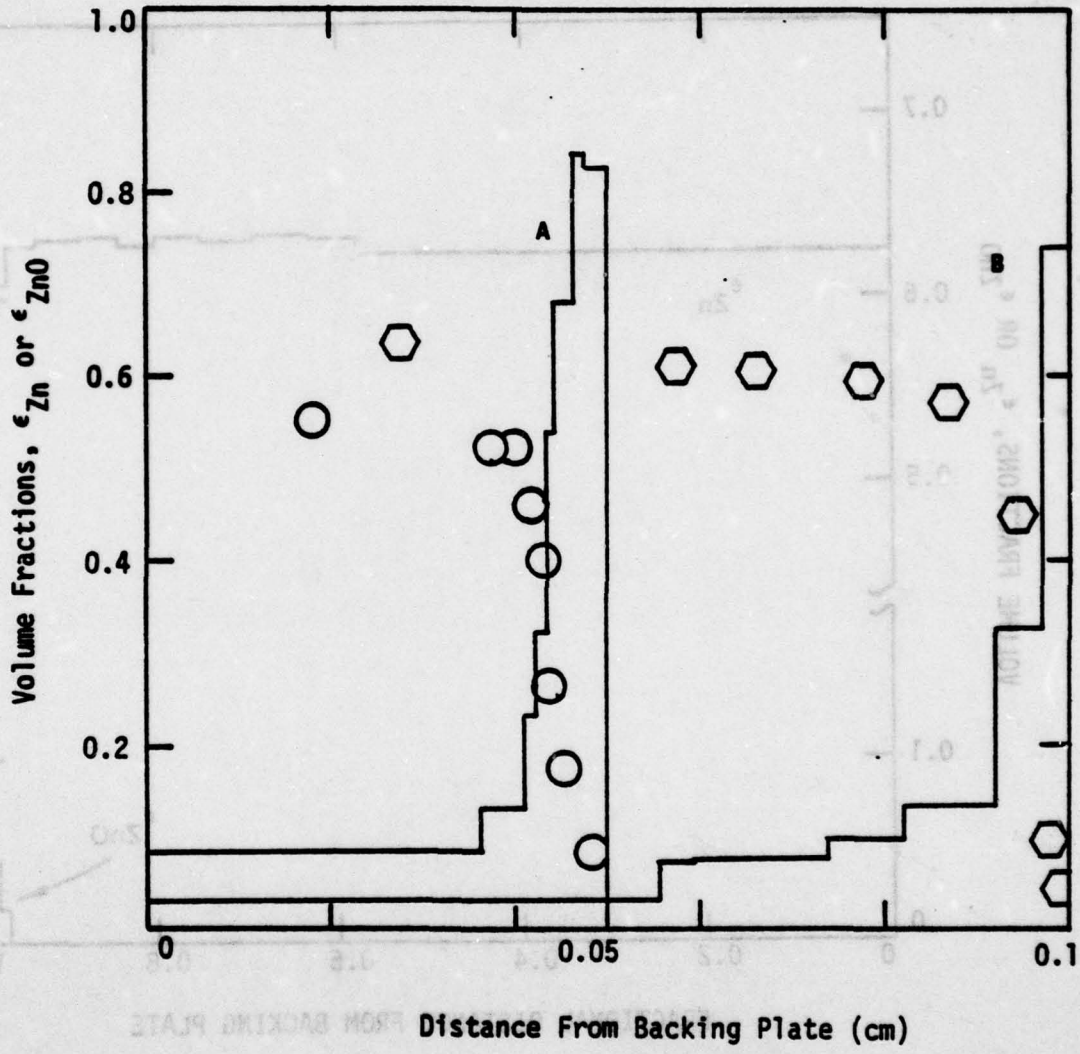

Figure 22. Profiles of Zn (Circles and Hexagons) and ZnO (Histograms) Measured for the Low Porosity Electrode Discharged At 50 mA/cm^2. ○ and Histogram A for 20% Depth of Discharge for the Electrode Having Thickness of 0.05 cm; ⬡ and Histogram B for 8% Depth of Discharge for the Electrode Having Thickness of 0.1 cm.

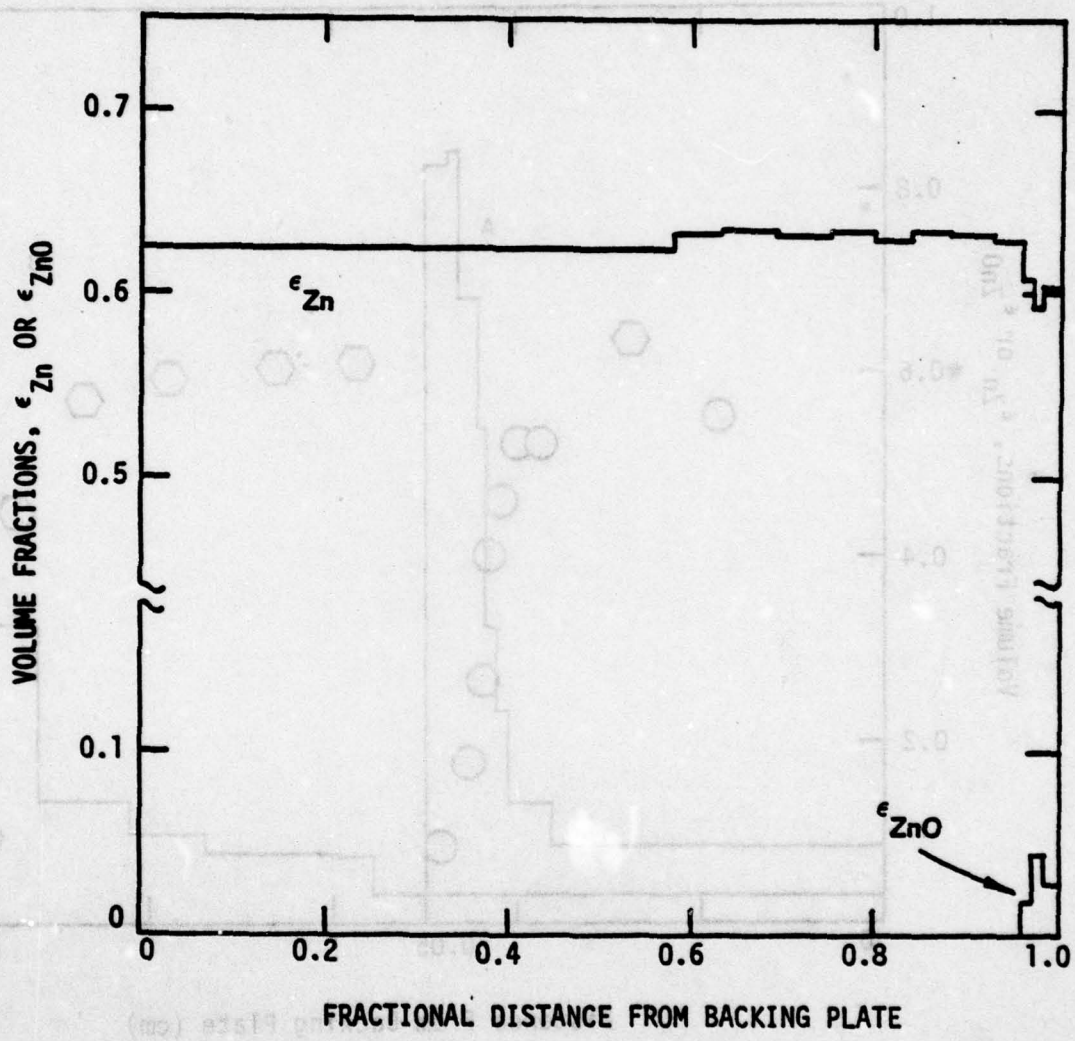

Figure 23. Profiles of Zn (Top Line) and ZnO (Bottom Line) Measured for the Low Porosity Electrode After One Cycle. At Each Half Cycle, 50 mA/cm^2 and 10% Depth of Initial Zinc were Applied.

sion of initial zinc. Some of the ZnO precipitated on discharging was not dissolved completely on charging but remained near the face of the electrode. This type of ZnO movement on cycling might cause long time failures.

V-2. Overpotentials of the Zinc Electrode

The potential data taken during the preliminary test period were not reproducible. It was found later that the reproducibility of the data was successfully improved when the amount of electrolytic solution accessible to the electrode was carefully controlled. Consequently, several cell configurations having different amounts of electrolytic solution have been used in the potential measurements.

Figure 24 illustrates the anodic overpotentials during discharge at 50 mA/cm^2 for four different configurations. They are a low porosity electrode having dynel on top of the membrane (designated by L50-ZMD), a low porosity electrode having dynel beneath the membrane (L50-ZDM), a high porosity electrode having dynel beneath the membrane (H50-ZDM), and a low porosity electrode having dynel but without a membrane (L50-ZD). For all the cases, dynel and membrane refer to the use of one layer of dynel cloth and two layers of RAI P2291 membrane, respectively. Placing dynel cloth below the membrane in ZDM configuration provides an additional solution reservoir of about 0.03 cm^3, but the dynel cloth used in an arrangement ZMD simply serves as a supporting material to minimize the difficulties associated with swelling of the electrode.

The zinc electrode compartment is about 0.12 cm thickness (see

Figure 14), while the zinc test electrode has thickness of about 0.1 to 0.11 cm. For 0.1 cm thickness electrodes, the configurations ZMD and ZDM using low porosity electrode (ε=0.3) have electrolytic solution of about 0.05 cm^3 and 0.08 cm^3, respectively. The total capacity for the the low porosity electrode is 23.6 A-min (or 471 minutes operation at 50 mA/cm^2) and that for the high porosity electrode is 14.05 A-min (or 281 minutes operation time at 50 mA/cm^2). Discharge failure occurs after 33 minutes for L50-ZMD (curve A), after 62 minutes for L50-ZDM (curve B), and after 70 minutes for H50-ZDM (curve C). These observations indicate that the electrode failure is caused by KOH depletion since the failure time is approximately doubled by increasing the electrolyte volume from 0.05 cm^3 for ZMD to 0.08 cm^3 (for L50-ZDM configuration) or 0.11 cm^3 (for H50-ZDM configuration). The theoretical result shown in Figure 4 (curve C) also indicates that the discharge to 10% depth of the cell configuration corresponding to ZMD decreases the KOH concentration from 8 M to 2 M.

The predicted overpotentials using the data of Appendix D-1 were plotted as white circles for L50-ZMD configuration and as black circles for L50-ZDM configuration. The volume of the external solution reservoir, which is located between the electrode surface and the membrane, is taken as 0.01 cm^3 for ZMD and 0.05 cm^3 for ZDM configurations in the numerical calculations. Discharge for the cell without a membrane (L50-ZD)(curve D in Figure 24) was continued to 137 minutes. Since there will be a large supply of KOH solution from the counter electrode compartment, the failure observed for L50-ZD electrode might be associated with the pore plugging.

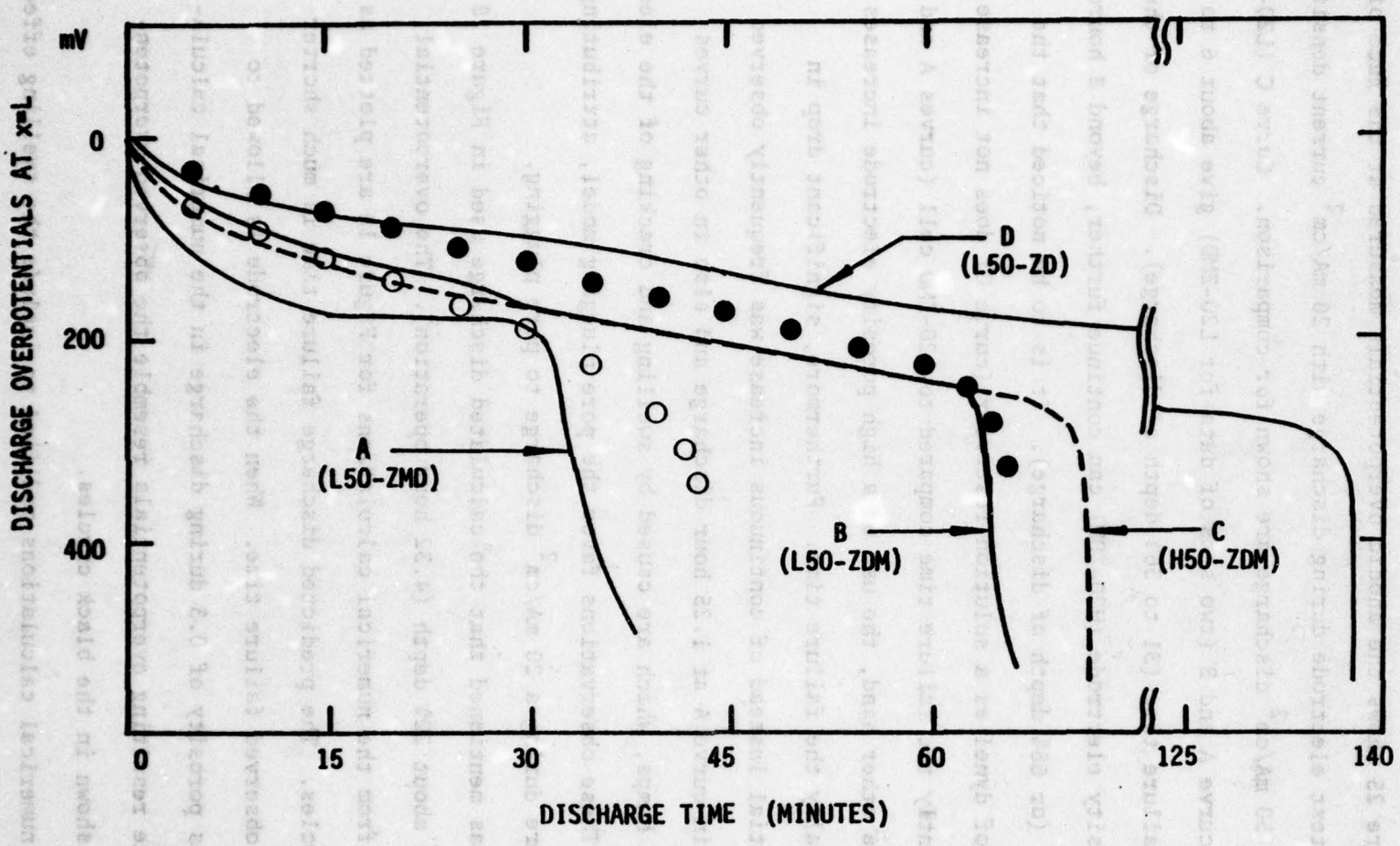

Figure 24. Overpotentials at the Face of the Zinc Electrode (x=L) On Discharge at 50 mA/cm^2. ___ and ---, Measured Overpotentials; ○, Predicted Overpotentials for L50-ZMD; ●, Predicted Overpotentials for L50-ZDM. L and H Represent Low Porosity and High Porosity Electrodes, Respectively, and Z,M,and D Represent Zinc Electrode, Membrane, and Dynel, Respectively (Figure Notation L50-ZDM Represents a Low Porosity Zinc Electrode Having a Dynel Beneath the Membrane Discharged at 50 mA/cm^2)

Figure 25 shows the anodic overpotentials measured at the face of the zinc test electrode during discharge with 20 mA/cm^2 current density. Those for 50 mA/cm^2 discharge are shown for comparison. Curve C (L20-ZDM) and curve A and B (two sets of data for L20-ZMD) give about 6 to 7 hours failure time (31 to 36% depth of discharge). Discharge of the high porosity electrode (H20-ZDM) can continue further, beyond 8 hours operation (or 68% depth of discharge). It is to be noticed that the addition of dynel as a solution reservoir (curve C) does not increase significantly the failure time compared to L20-ZMD cell (curves A and B) On the other hand, the use of a high porosity electrode increases substantially the failure time. Furthermore, significant drop in overpotential instead of continuous increase was frequently observed as shown in curve A at 1.25 hour discharge and also in other curves as smooth humps, which are caused by swelling and cracking of the electrode. These observations favor the pore plugging model, attributing the failure during a 20 mA/cm^2 discharge to pore plugging.

It was mentioned that the calculated discharge used in Figure 18 failed at about 22% depth (4.32 hour operation). The overpotential obtained from the numerical calculations for Figure 18 are plotted as white circles. The predicted discharge failure time is much shorter than the observed failure time. When the electrode is allowed to retain its porosity of 0.3 during discharge in the numerical calculations, the resulting overpotentials resemble the observed overpotentials as shown in the black circles.

The numerical calculations modified to include the swelling effect (black circles) can be described as follows. The reaction zone of the

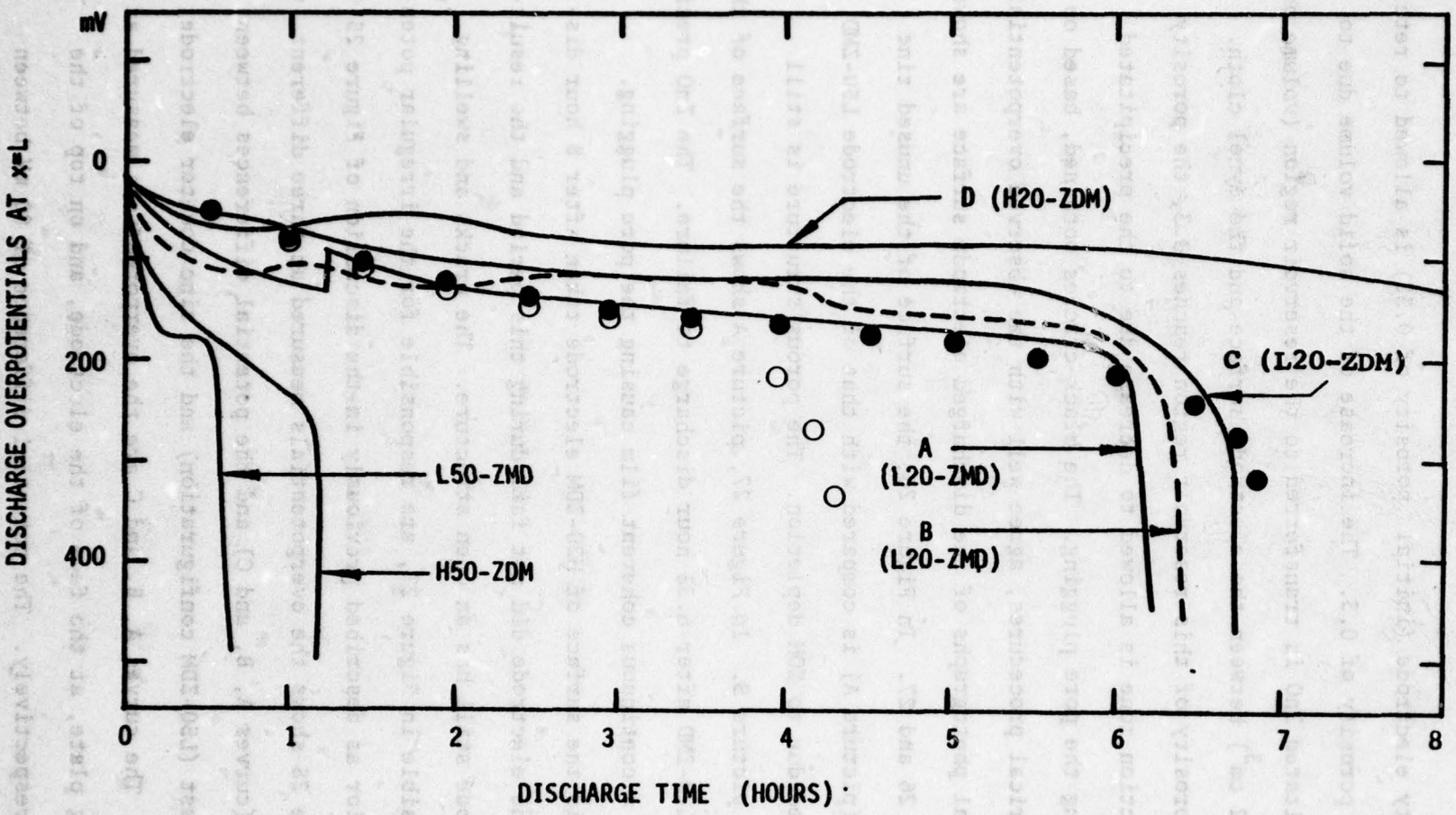

Figure 25. Overpotentials at the Face of the Zinc Electrode (x=L) On Discharge at 20 mA/cm^2. —— and ---, Measured Overpotentials; ○ and ●, Predicted Overpotentials for L20-ZDM Without and With Corrections for Swelling, Respectively. Explanation of Figure Notation is Given in Figure 24 Caption.

low porosity electrode (initial porosity of 0.33) is allowed to retain a constant porosity of 0.3. The increase of the solid volume due to the precipitated ZnO is transferred to the reservoir region (volume of $0.01 \sim 0.02\ cm^3$) between the electrode surface and the dynel cloth. When the porosity of this reservoir region reaches 0.3, the porosity of the reaction zone is allowed to decrease due to the precipitated ZnO, causing the pore plugging. The black circles obtained, based on these numerical procedures, agree well with the observed overpotentials.

Several photographs of the discharged electrode surface are shown in Figures 26 and 27. In Figure 26, the surface of the unused zinc electrode (picture A) is compared with that of the electrode L50-ZMD which failed due to KOH depletion. The porous structure is still visible in picture B. In Figure 27, picture A shows the surface of the electrode L20-ZMD after 6.33 hour discharge to failure. The ZnO precipitated as a continuous coherent film causing the pore plugging. Picture B is the surface of H20-ZDM electrode taken after 8 hour discharge. The electrode did not fail during this period and the resulting electrode still has an open structure. The cracks and swelling, clearly visible in Figure 27, are responsible for the irregular potential behavior as described previously in the discussion of Figure 25.

Figure 28 shows the overpotentials measured at three different positions (curves A, B, and C) and the potential differences between the zinc test (L50-ZDM configuration) and the zinc counter electrode (curve D). The curves A, B, and C are the overpotentials measured at the backing plate, at the face of the electrode, and on top of the membrane, respectively. The potential difference of 80 mV between

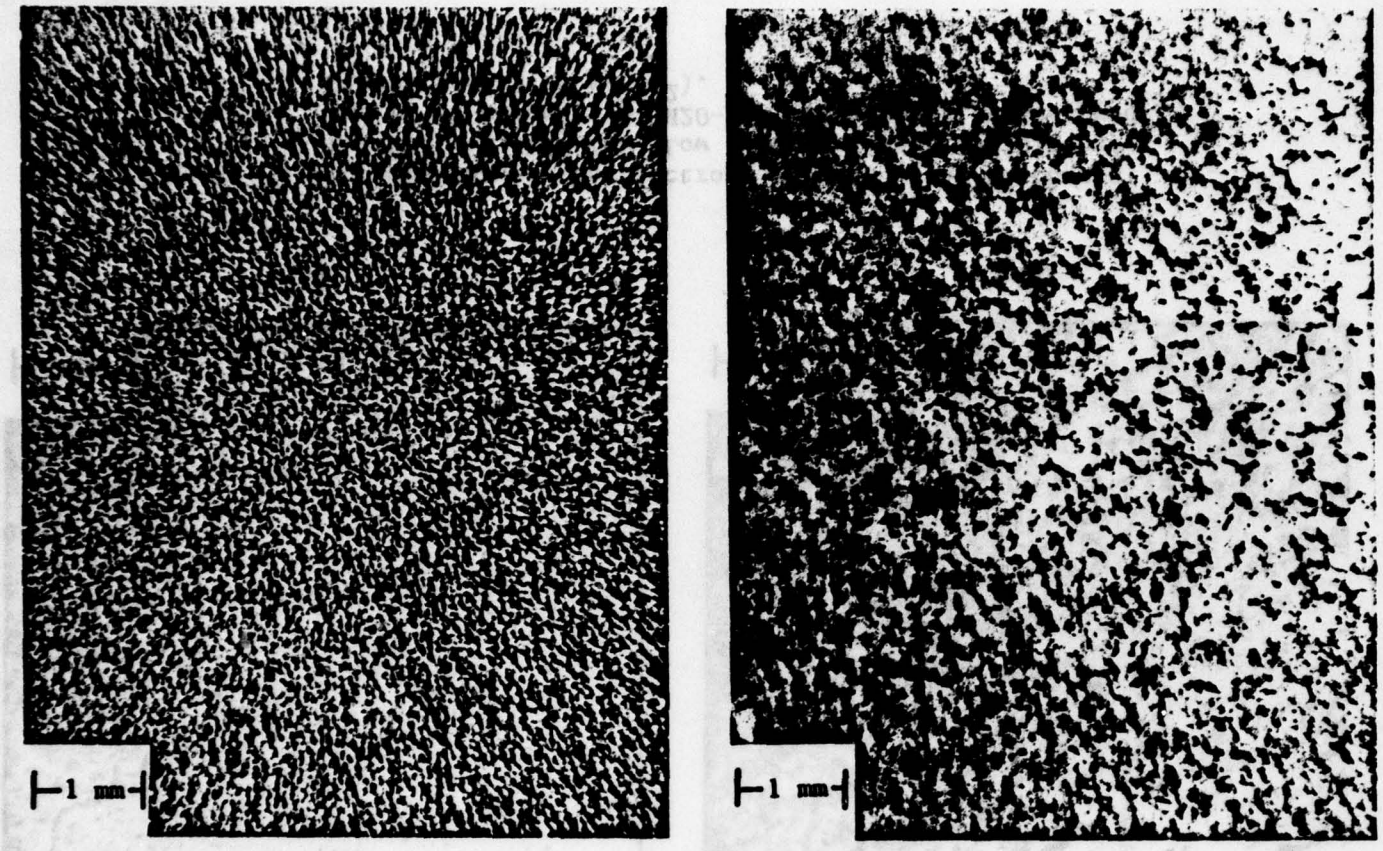

(A) (B)

Figure 26. Photographs of the Electrode Surface. A, Unused Zinc Electrode; B, L50-ZMD Electrode After Discharge Failure.

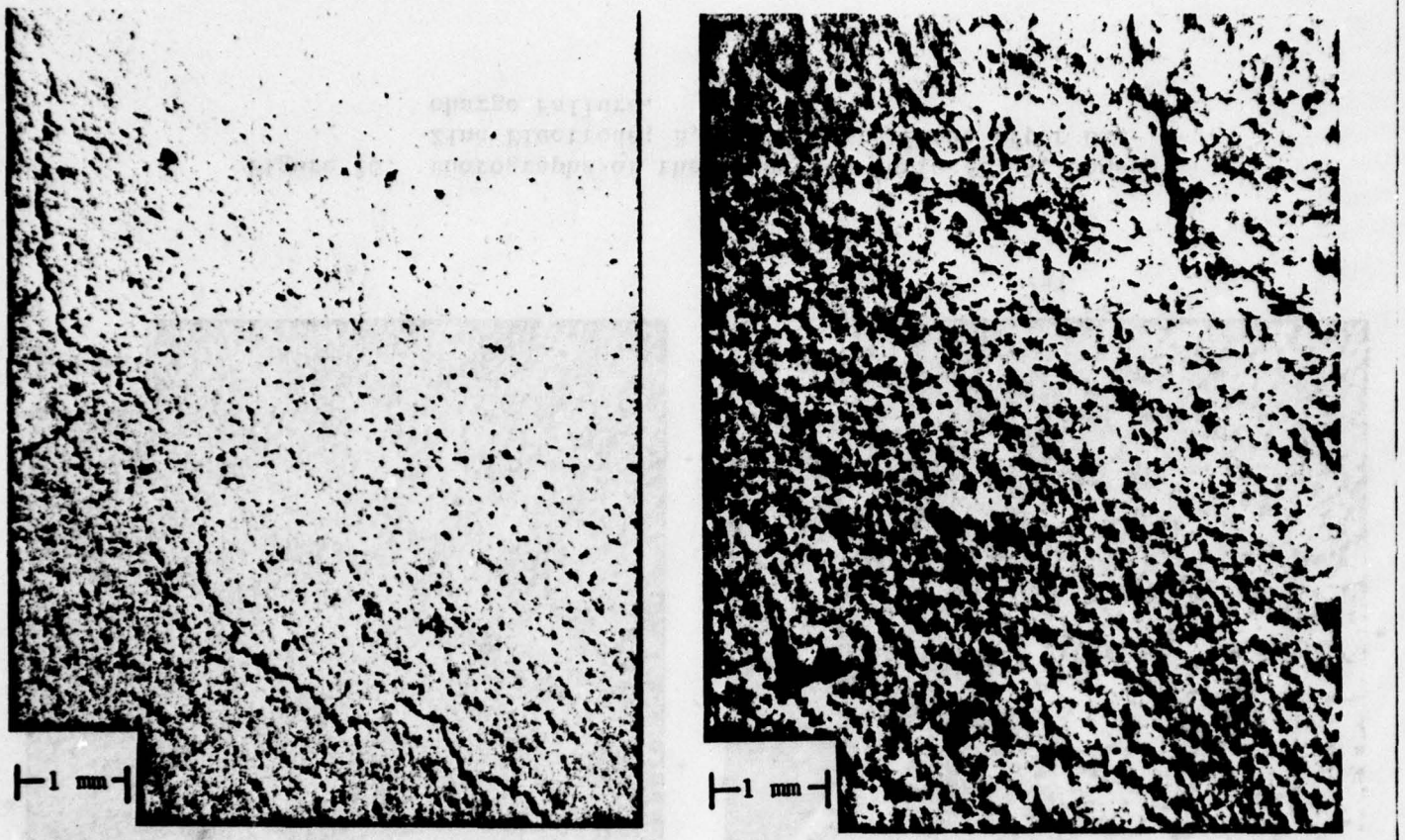

Figure 27. Photographs of the Electrode Surface After Discharge Failure. A, L20-ZMD (Low Porosity Electrode Discharged at 20 mA/cm^2); B, H20-ZDM (High Porosity Electrode Discharged at 20 mA/cm^2).

lines B and C, which is the potential drop across the two layers of RAI P2291 membrane, is comparable to the ohmic loss of about 90 mV calculated based on the measured conductivity across this membrane (87). The first discharge failed after 67.5 minutes. By allowing the cell to rest for 8 minutes at open circuit, an additional discharge time of 12 minutes is obtained prior to failure. Increase in the rest period leads to a longer time tc failure for the second discharge. This implies that KOH depletion is the failure mechanism under these conditions.

Figure 29 is the corresponding potential-time curves during continued charge of the test electrode. The applied current density was 50 mA/cm^2. During continued charge, about 3.9 A-minute was recovered, prior to significant potential drop, out of 3.98 A-minute applied during discharge. Curves A, B, and C are the overpotentials measured at the backing plate, at the electrode surface, and on top of the membrane. Curve D is the potential difference between the zinc test and the zinc counter electrodes. Curve E is drawn based on the solution ohmic loss in the counter electrode compartment. The distance between the membrane and the counter electrode surface (1.1 cm) and the conductivity of 10 M KOH solution (about 0.51 $\Omega^{-1}cm^{-1}$)(84) results in the ohmic loss of about 110 mV which is the gap C-E. The gap D-E represents the anodic overpotentials of the counter zinc electrode.

Comparison of Figure 28 with Figure 29 provides some useful information of the potential behavior. The test zinc electrode has 0.08 cm^3 of electrolytic solution and porosity of 0.33, while the

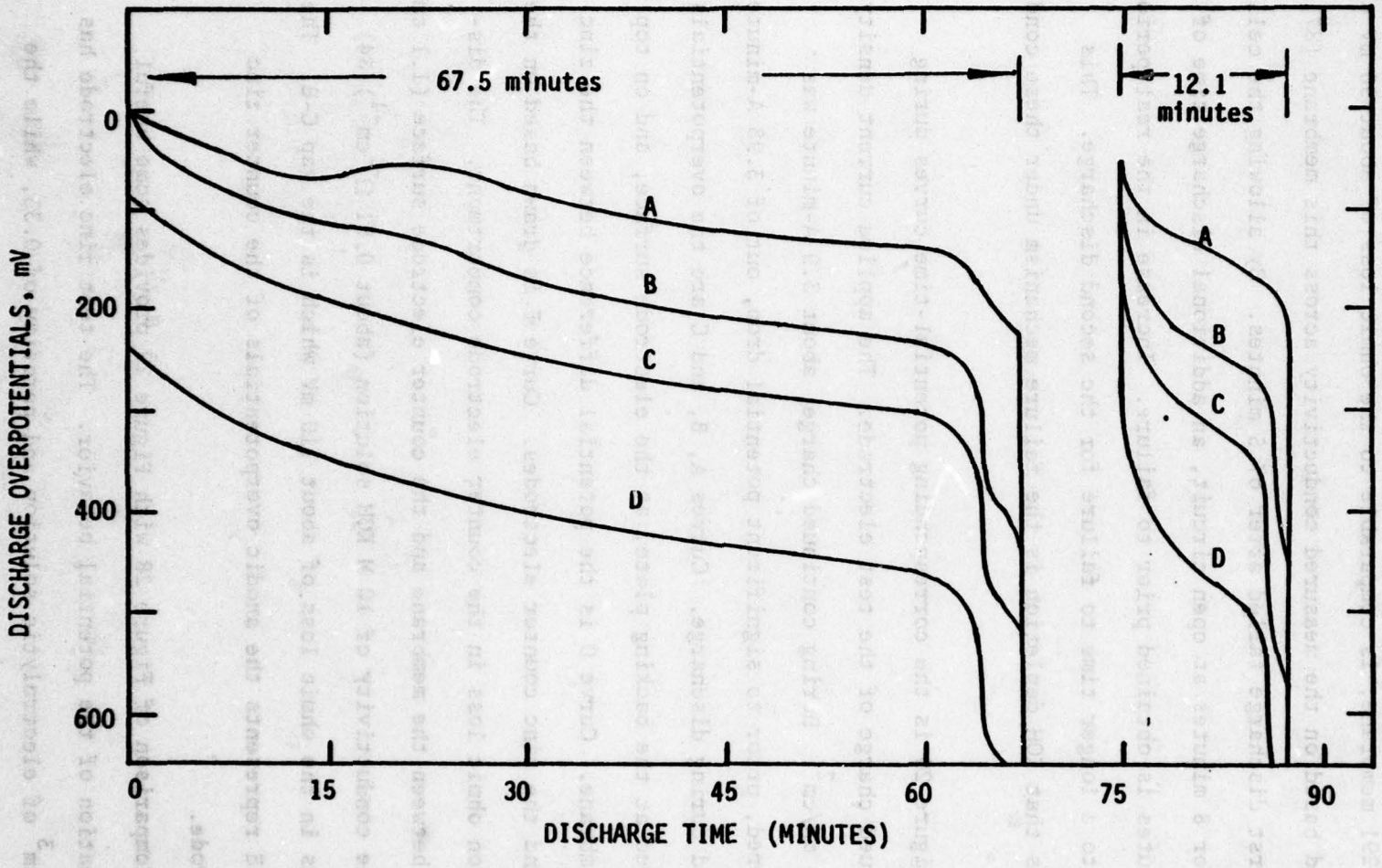

Figure 28. Overpotentials Measured at Four Different Positions On Discharge of L50-ZDM Electrode at 50 mA/cm^2. Curves A,B,and C Represent the Overpotentials Measured at the Backing Plate, at the Face of the Test Electrode, and Above the Membrane, Respectively. Curve D is the Potential Difference Between the Zinc Test and the Zinc Counter Electrodes.

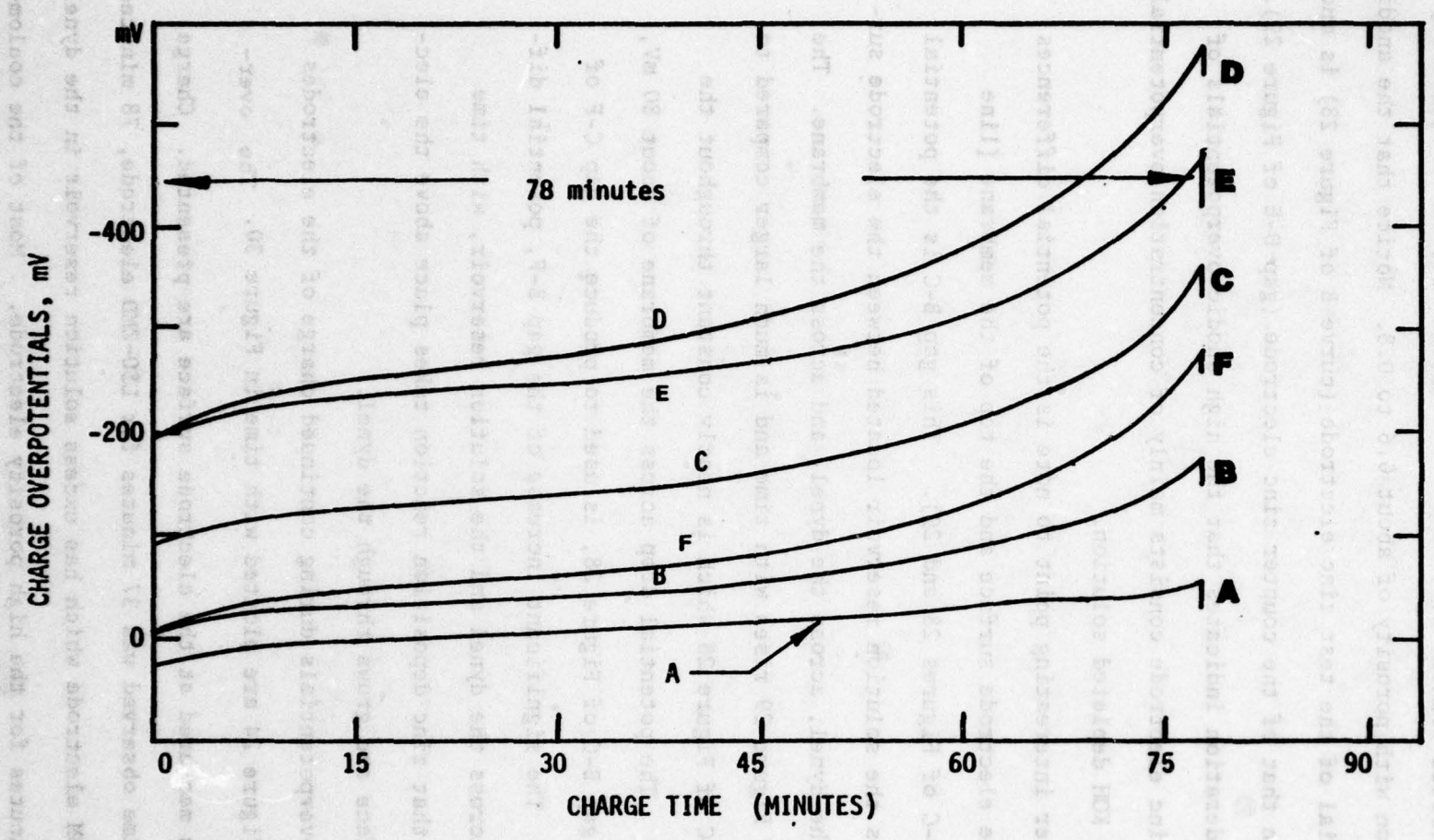

Figure 29. Overpotentials Measured at Four Different Positions On Charge of L50-ZDM Electrode at 50 mA/cm^2. Explanation of Curves A,B,C,and D is given in Figure 28 Caption. The Gaps F-C and C-E are the Overpotentials Across the Membrane and Across the Solution in the Counter Electrode Compartment, Respectively.

electrodeposited counter zinc electrode contains 1.5 cm^3 of electrolytic solution with porosity of about 0.6 to 0.8. Notice that the anodic overpotential of the test zinc electrode (curve B of Figure 28) is much larger than that of the counter zinc electrode (gap D-E of Figure 29). This consideration indicates that the high anodic overpotentials of the test zinc electrode consists mainly of concentration overpotential due to the KOH depleted solution.

Another interesting point to note is the potential differences between the electrode surface and the top of the membrane (line spacings B-C of Figures 28 and 29). This gap B-C is the potential drop across the solution reservoir located between the electrode surface and the dynel, across the dynel, and across the membrane. The gap B-C of Figure 29 rises with time and is much larger compared to the gap B-C of Figure 28 which is nearly constant throughout the operation. The potential drop across the membrane of about 80 mV, i.e., the gap B-C of Figure 28, is used to produce the gap C-F of Figure 29. The significant increase of the gap B-F, potential differences across the dynel and the solution reservoir, with time indicates that zinc deposition reaction takes place above the electrode surface and grows through the dynel.

The overpotentials during continued charge of the electrodes shown in Figure 24 are plotted with time in Figure 30. The overpotentials measured at the electrode surface are presented. Charge failure time observed was 37 minutes for L50-ZMD electrode, 78 minutes for L50-ZDM electrode which has excess solution reservoir in the dynel, and 112 minutes for the high porosity electrode. Most of the coulom-

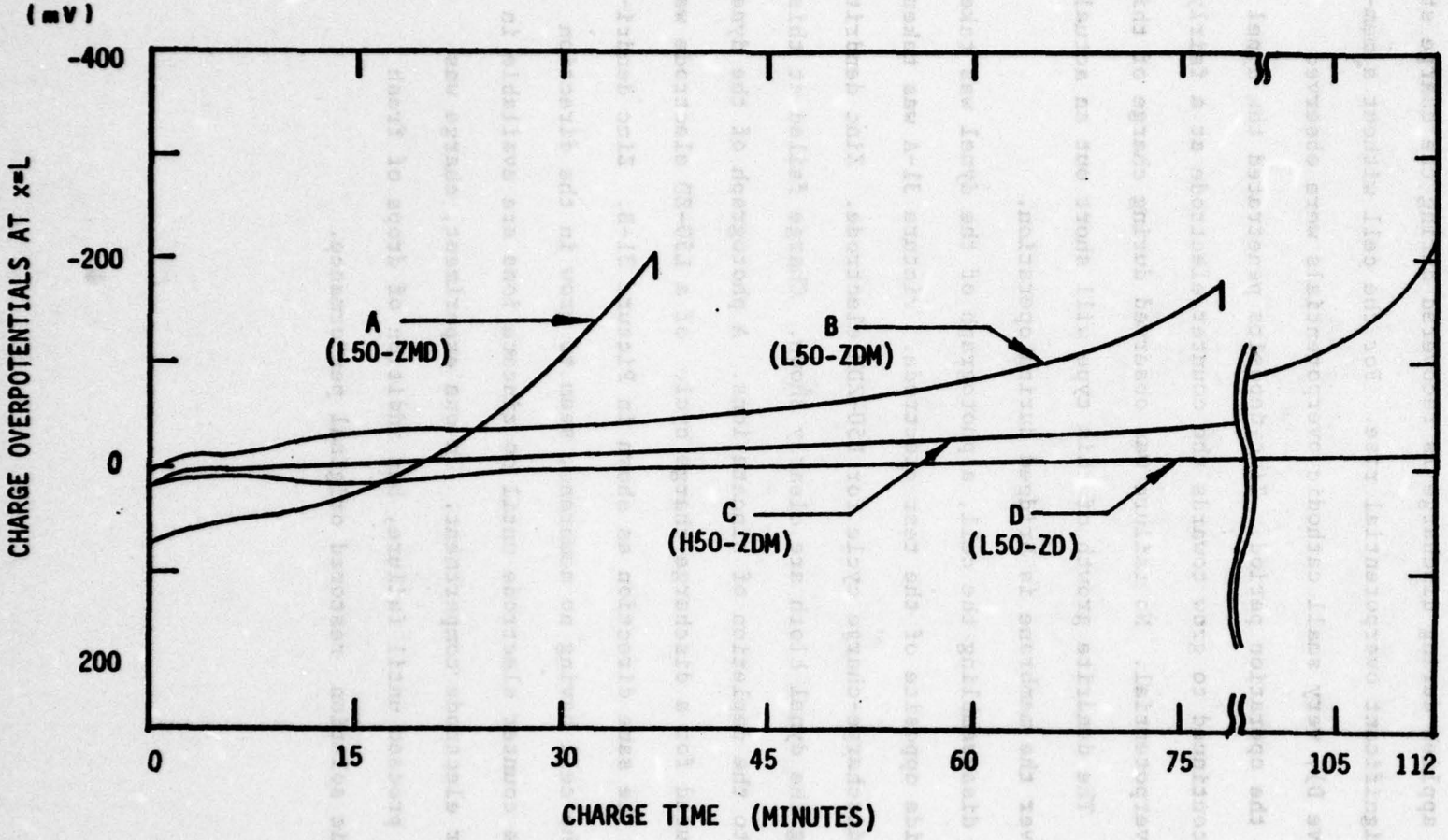

Figure 30. Overpotentials Measured at the Face of the Electrode (L50-ZDM) On Charge at 50 mA/cm^2. Explanation of Figure Notation is Given in Figure 24 Caption. The previous Discharge Time prior to Onset of Charge is 39.4 minutes for L50-ZMD, 69.6 Minutes for L50-ZDM, 84.5 Minutes for H50-ZDM, and 138.5 Minutes for L50-ZD.

bic charge applied during discharge is recovered during the charge step prior to significant overpotential rise. For the cell without a membrane (curve D), very small cathodic overpotentials were observed throughout the operation period. Zinc deposits penetrated the dynel cloth and continued to grow towards the counter electrode at a fairly constant overpotential. No failure was observed during charge of this electrode. The dendrite growth of this type will short out an actual cell whenever the membrane is bridged during operation.

After disassembling the cell, a photograph of the dynel was taken from the side opposite of the test electrode. Picture 31-A was taken after one discharge-charge cycle for L50-ZDM electrode. Zinc dendrites penetrating the dynel cloth are clearly shown. Charge failed at this stage due to the depletion of zincate ions. A photograph of the dynel separator used for a discharge-charge cycle of a L50-ZD electrode was taken from the same direction as shown in Picture 31-B. Zinc dendrites, for the cell having no membrane, seem to grow in the direction towards the counter electrode until no zincate ions are available in the counter electrode compartment. In one experiment, charge was allowed to proceed until failure, but addition of drops of fresh electrolytic solution restored original performance.

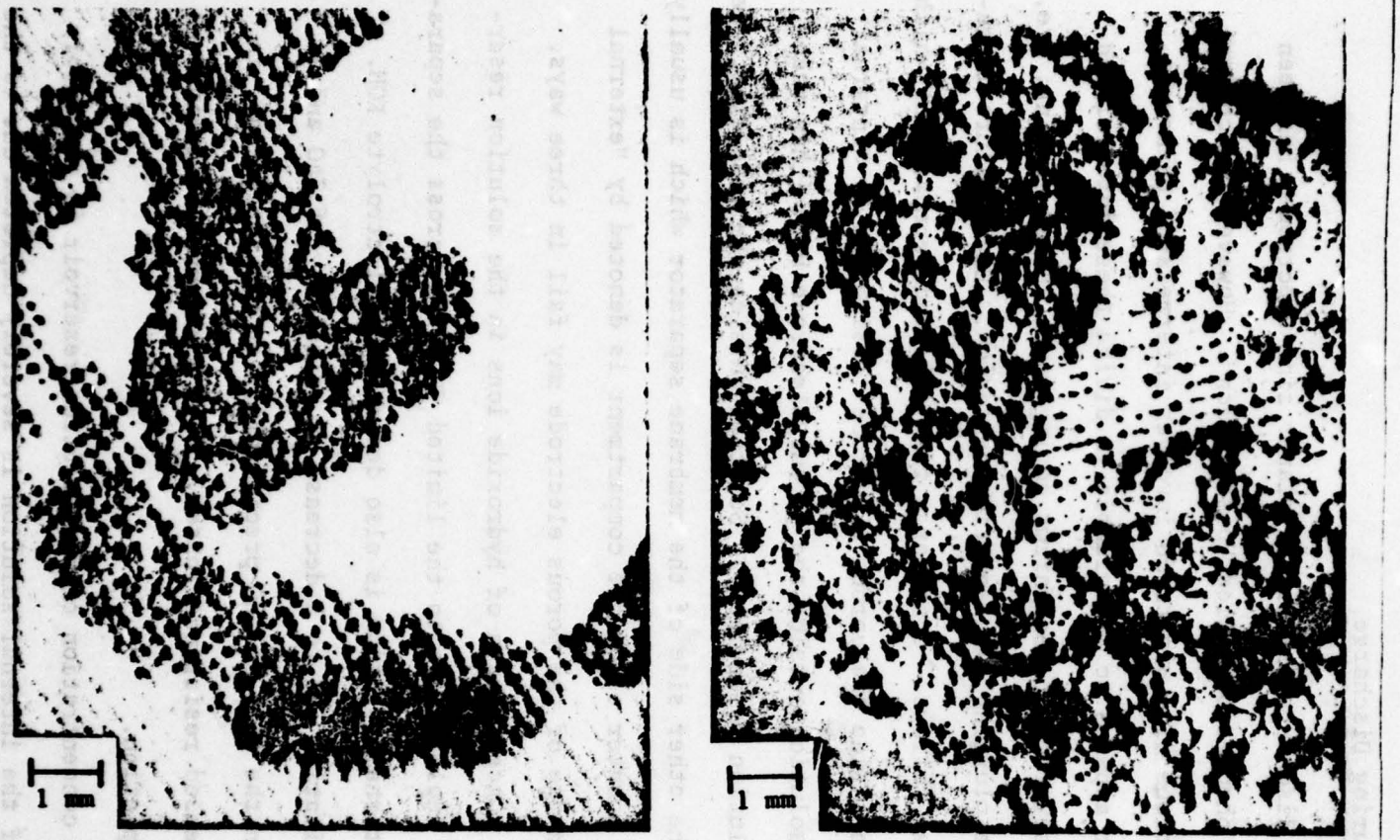

Figure 31. Photographs of the Dynel Cloth After One Discharge-Charge Cycle. Current Density Was 50 mA/cm^2. Zinc Deposit Penetrates the Dynel Towards the Counter Electrode. A, for L50-ZDM and B for L50-ZD.

VI. DISCUSSION

VI-1. Failure During Discharge

In general, discharge failure of planar zinc electrodes has been interpreted as a phenomenon called "passivation". However, discharge failure of the porous zinc electrode involves interrelated phenomena, and therefore, it appears to be valuable to divide these interrelated mechanisms into several sub-mechanisms having more precise meaning, i.e., passivation, pore plugging, and solution depletion. Each failure mechanism is defined as follows. Consider a test electrode compartment which contains solution inside the porous electrode (designated by "internal solution"), and solution outside the porous electrode but within that compartment ("solution reservoir"). Solution outside the test electrode compartment on the other side of the membrane separator which is usually contained in the counter electrode compartment is denoted by "external solution". Discharge of the porous electrode may fail in three ways.

(1) If the concentration of hydroxide ions in the solution reservoir is severely depleted due to the limited OH^- flux across the separator, then the internal solution is also depleted of electrolyte KOH. This causes passivation due to a decrease in solubility of ZnO and a rapid increase in the rate of ZnO precipitation on the zinc metal, in addition to increased resistance losses. This phenomenon is defined as concentration depletion.

(2) If the concentration of the solution reservoir is reasonably high, but that of the internal solution is severely depleted due to the limited mass transfer through the porous structure near either side of the electrode surfaces, then the internal solution becomes depleted and

causes passivation. This phenomenon is defined as pore plugging.

(3) Even if the KOH concentration of the internal solution as well as the solution reservoir is appreciably high, passivation can occur by the physical blocking of the active zinc surface by the precipitated ZnO or by the depleted hydroxide ion or excess zincate at the zinc surface caused by high local current density. This phenomenon is defined as passivation, having the same meaning as was used for planar electrodes.

Failure causes or parameters which are expected to eliminate failure now become clear. For example, membrane parameters can be adjusted to allow faster OH^- transport or volume of the electrolytic solution reservoir can be increased to reduce depletion of OH^- concentration. High porosity electrodes allow for swelling and eliminate pore plugging, and high surface area reduces local transfer current density reducing the chance for passivation.

VI-2. Depletion of Electrolytes

The overall discharge reaction of the zinc electrode consumes hydroxide ions and produces water. Hydroxide ion concentration is expected to decrease in the zinc electrode compartment during discharge if the supply of hydroxide ion from the counter electrode is not sufficient to compensate for the consumed hydroxide ion. Depletion of KOH becomes even more serious for sealed or tight packed cells having membranes designed to minimize failure due to zinc dendrite penetration and shape change. Tight packing decreases the volume of electrolytic solution reservoir and generally membranes used to prevent zinc dendrite formation also limit the mass transfer of hydroxide ions between the two electrode compartments. A restricted amount of electrolytic solu-

tion and/or limited flux of hydroxide ions across the membrane can lead to a situation in which the zinc electrode fails on discharge earlier than if a large amount of electrolyte is available.

Failure observed during discharge of the zinc test electrode having two layers of RAI P2291 membrane with current density of 50 mA/cm^2 was attributed to the KOH depletion (see Figure 24-A,B,and C). Theoretical prediction shown in Figure 4 (curve C) confirmed these observations. Depletion of KOH strongly depends on the type of the membrane, volume of electrolytic solution reservoir, and porosity of the electrode.

In order to make such information more useful for industrial battery design, an approximate relationship between the electrode design parameters and the change in KOH concentration with time was obtained as follows. It is assumed that all the zincate ions produced by zinc dissolution are converted into ZnO and that OH^- concentration inside the electrode is completely mixed. Under these conditions, the decrease in KOH concentration inside the electrode, allowing for hydroxide ion flux from the boundary layer, can be written by the following simplified conservation equation.

$$\frac{V}{A}\frac{\partial \varepsilon c_3}{\partial t} = -\frac{N_3^{bl}}{\nu_3^B} + \frac{N_3(x=0)}{\nu_3^B} - \frac{I}{F} = -\left[-L_{BB}^{bl}(c_3^o - c_3) + \frac{t_3^{bl}}{z_3 \nu_3^B F} I\right] - \frac{I}{F} \qquad (55)$$

where V is the volume of the electrode compartment, A is the cross sectional area of the electrode, ε is the porosity, I is the superficial applied current density, c_3 is the average (mixed) concentration of the hydroxide ion inside the electrode, c_3^o is the hydroxide concentration in the counter electrode compartment, and L_{BB}^{bl} and t_3^{bl} are the mass transfer coefficient of potassium hydroxide and transference number of the

hydroxide ion across the membrane, respectively. The ratio V/A is the same as the electrode thickness L and the concentration c_3^o becomes the initial concentration of the hydroxide ion for the present cell.

The solution of equation (55) is given by

$$\frac{c_3}{c_3^o} = 1 - \frac{(1-t_3^{bl})I}{F\, L_{BB}^{bl}\, c_3^o}\left(1 - e^{-\frac{L_{BB}^{bl}}{V\varepsilon}At}\right) = 1 - \frac{1-t_3^{bl}}{M}\left(1-e^{-M\frac{t}{\tau}}\right) \quad (56)$$

where porosity, electrode thickness, and transport parameters L_{BB}^{bl} and t_3^{bl} are assumed to be constant. The characteristic time τ ($=c_3^o F\varepsilon L/I$) is defined by the time required for complete depletion of KOH when the boundary is insulated with respect to OH^- flux. The dimensionless parameter M ($=c_3^o\ F\ L_{BB}^{bl}/I$) corrects for the flux of hydroxide ion through the boundary. For the cell configuration L50-ZMD (ε=0.4, ε_{Zn}=0.5, ε_{ZnO}= 0.1, L=0.1 cm, c_3^o=8M, and I=50 mA/cm^2), the characteristic time τ is 617 seconds which is equivalent to only 3% conversion of initial zinc into ZnO. This number is surprisingly small. If the flux across the membrane is considered, the ratio c_3/c_3^o becomes, after 10% depth of discharge (2100 seconds operation), 0.68 for type I membrane (t_3^m=0.5 and $L_{BB}^m = 10^{-4}$ cm/sec) and 0.14 for one layer of RAI P2291 membrane (t_3^m=0.5 and $L_{BB}^m = 3\times10^{-5}$ cm/sec). This simple calculation provides a good approximation to the numerical solutions shown in Figure 4.

Based on equation (56), the ratio of the average KOH concentration inside the zinc test electrode to the initial concentration, c_3/c_3^o, is plotted as a function of discharge time at two different current densities in Figure 32. The transport parameters for type II RAI P2291 membrane (L_{KOH}^m=3x10^{-5} cm/sec and t_3^m=0.5) measured by Sinha and Bennion

(87), electrode thickness of 0.1 cm, and initial KOH concentration of 10M are used in the calculations. Curve A is for one layer of membrane ($L^m_{KOH}=3x10^{-5}$ cm/sec and $t^m_3=0.5$) and porosity of 0.3. Curve B is for two layers of membrane ($L^m_{KOH}=1.5x10^{-5}$ cm/sec and $t^m_3=0.5$) and porosity of 0.3, and curve C is for two layers of membrane and porosity of 0.6.

The average concentration of KOH for 50 mA/cm^2 discharge decreases to zero after 30 minutes for the low porosity electrode (curve B) and after one hour for the high porosity electrode (curve C). The two fold increase in porosity (or amount of KOH contained in the zinc electrode) doubles the concentration limited operation time. On the other hand, for 20 mA/cm^2 discharge, the average KOH concentration inside the low porosity electrode remains 3.14M KOH at infinite time of operation (curve B), which means that the flux of KOH from the counter electrode compartment through the membrane can supply the KOH solution consumed in the zinc test electrode. Consequently, the predicted (Figure 32) and the observed (Figures 24 and 25) results lead to the conclusion that at high rate discharge (50 mA/cm^2), KOH depletion causes the zinc electrode to fail prior to pore plugging, while discharge at low rate (20 mA/cm^2) continues until pore plugging causes zinc electrode failure.

VI-3. Pore Plugging

Discharge of most battery electrodes is accompanied by changes in pore sizes because of the differences in the molar volumes of solid reactant and solid product. Since the molar volume of ZnO (14.51 cm^3/mole) is larger than that of zinc (9.15 cm^3/mole), the conversion of zinc into ZnO during discharge decreases the pore size and eventually causes plugging of the porous structure unless sufficient space is

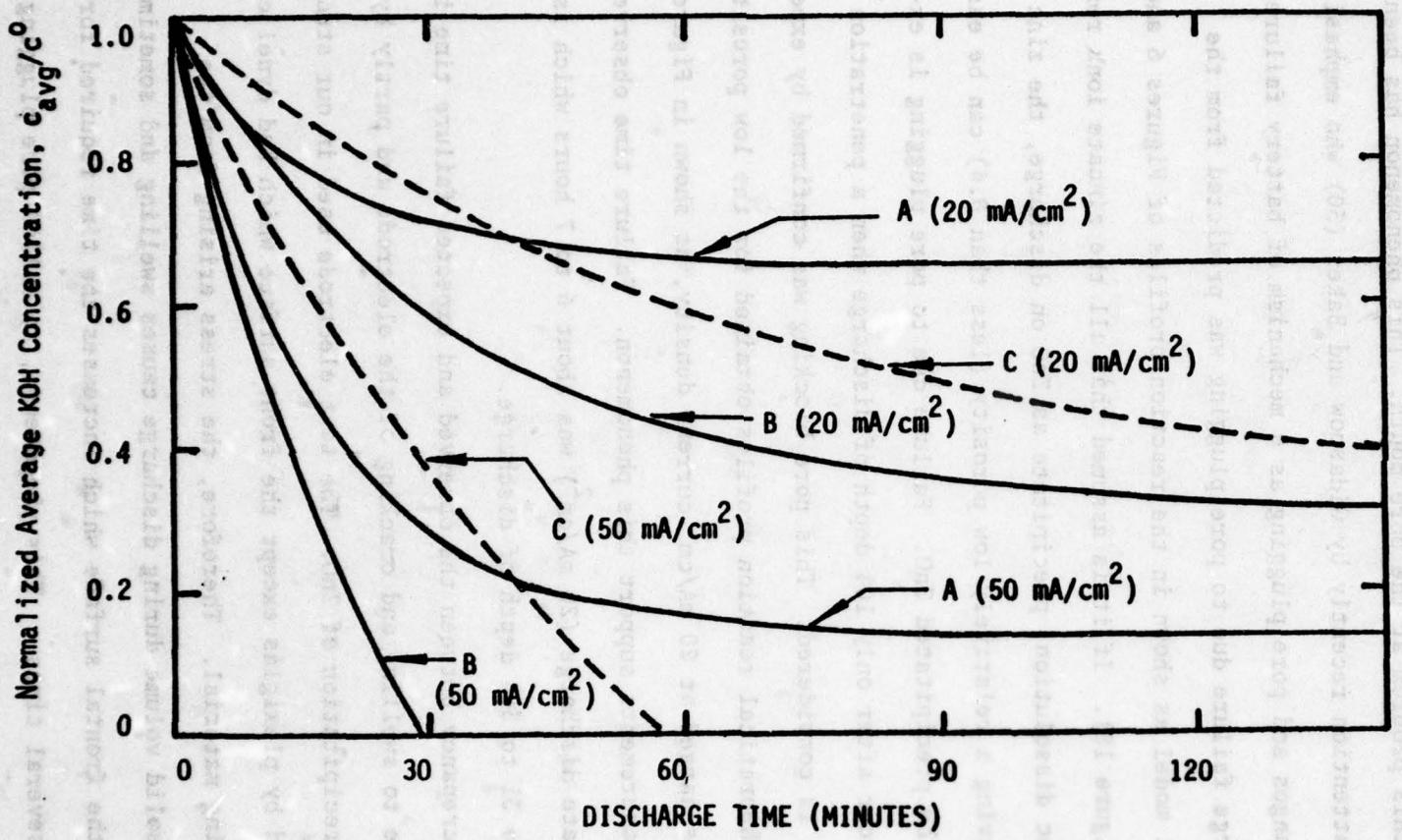

Figure 32. Normalized Average KOH Concentration As a Function of Operation Time. Curve A is for One Layer of RAI P2291 Membrane, Porosity of 0.3, and Electrode Thickness of 0.1 cm; Curve B is for Two Layers of RAI P2291 Membrane, Porosity of 0.3, and Electrode Thickness of 0.1 cm; Curve C is for Two Layers of RAI P2291 Membrane, Porosity of 0.6, and Electrode Thickness of 0.1 cm.

provided for the swelling. A nonuniform current distribution will accentuate this problem at the pore mouth. This phenomenon has been given some attention recently by Gidaspow and Baker (30) who emphasize porosity changes and pore plugging as a mechanism of battery failure.

Discharge failure due to pore plugging was predicted from the mathematical model as shown in the reaction profiles of Figures 6 and 7 (see also Figure 18). If it is assumed that all the zincate ions resulting from zinc dissolution precipitate as ZnO on discharge, the zinc electrode having a relatively low porosity (less than 0.4) can be easily blocked by the precipitated ZnO. Failure due to pore plugging is expected to occur after only 10% depth of discharge when a penetration depth of 0.1 is considered. This pore blocking was confirmed by experimental and theoretical reaction profiles obtained for the low porosity electrode discharged at 20 mA/cm^2 current density, as shown in Figure 18. Potential measurements support this phenomenon. Failure time observed during low rate discharge (20 mA/cm^2) was about 6 to 7 hours which is equivalent to 31 to 36% depth of discharge.

The discrepancy between the observed and expected failure time is primarily due to swelling and cracking of the electrode and partly by incomplete precipitation of ZnO. The test electrode used in our study was supported by plexiglas except the front surface which had dynel cloth as a supporting material. Therefore, the stress arising from the increase in solid volume during discharge causes swelling and sometimes cracking of the frontal surface which increases the time required for plugging by several times. This phenomenon, so called pore plugging, is also observed during high rate discharge (at 50 mA/cm^2) of L50-ZD

electrode having no membrane (see curve D of Figure 24).

Complete pore plugging leading to zero porosity is not necessary to cause failure. The electrode face having pore size smaller than some certain value can limit significantly the KOH supply into the interior of the electrode, resulting in KOH depletion and then passivation. Simonsson (28,29) has proposed this phenomenon, i.e., blocking of the electrode surface in the outer layer of the electrode by a discharge product followed by acid depletion in the inner part of the electrode, as a failure mechanism during high rate discharge of the porous PbO_2 positive electrode in a lead acid battery.

The effect of pore plugging on concentration of electrolyte in the interior of the electrode can be roughly estimated by use of equation (56). Consider a situation which might occur after 20% depth of discharge of an L20-ZDM electrode. It is assumed that an electrode with a unit cross sectional area ($A=1\ cm^2$) consists of an outer layer of ZnO which has a porosity of 0.05 and a thickness of 0.02 cm and an inner layer of unattacked zinc having a porosity of 0.3 and a thickness of 0.08 cm. The following parameters are applied to equation (56): $A=1\ cm^2$, V (volume of electrolytic solution of the inner part)$=0.024\ cm^3$, $I=0.02$ amp/cm^2, $t_3^{bl}=0.7$, and c_3^o (initial concentration of KOH outside the electrode)$=0.005$ mole/cm^3. The mass transfer coefficient across the outer (L_{BB}^{bl}) is evaluated using the values of $D_{BB}^o=2\times10^{-5}\ cm^2/sec$ and $d=0.02$ cm, i.e., $L_{BB}^{bl}=D_{BB}^o\varepsilon^{1.5}/d=1.118\times10^{-5}$ cm/sec. The OH^- concentration, c_3, calculated from equation (56) becomes 3.95 M after 8.3 minutes and 1.63 M after 33 minutes.

VI-4. Passivation

A number of workers (14,15,16,17) have reported discharge failure associated with the passivation of a flat plate zinc electrode in alkaline solution as was summarized by Jolas (92) and Powers and Breiter (93). It is generally agreed that the passivated electrodes are physically blocked from further dissolution by the presence of a passivating film of ZnO (14).

Two possibilities exist for the formation of the passive film; (a) direct formation on the electrode surface through a solid state reaction and (b) indirect formation from a supersaturated zincate solution through a dissolution-precipitation mechanism (51,93,94,95,96). Further studies (94,95,96) on planar zinc electrodes have shown that a white porous film of ZnO (type I) forms by precipitation from supersaturated solution before passivation occurs, while a coherent compact film of ZnO (type II) with color varying from light grey to black, which is responsible for passivation, appears directly on the surface beneath the type I film. It was also indicated that a type I film and then a type II film could be formed in the absence of convection, but only the type II film was observed when the conditions for supersaturation were largely removed by the presence of convection or stirring.

Only a few works (88,94,97) have been reported on the passivation behavior of the porous zinc electrode. Breiter (97) has found that only a small fraction of the interior of the porous electrodes participate in the electrochemical process. Nagy and Bockris (38) explained their measured reaction distribution by introducing the effects of the passive film on the zinc surface. Elsdale et al. (88,98) observed

a gradual increase in potential in the vicinity of transition from the active to the passive region, in contrast to the abrupt increase in potential for the planar zinc electrode (for example, references 14 and 15). Consequently, they defined a time, $t_{0.3}$, as the time required for attainment of a potential rise of 0.3 V from the initial potential and provided a linear plot of current density versus $(t_{0.3})^{-0.5}$.

It is assumed that the two types of passive film (i.e., porous film and compact film) observed by Powers (95) are formed by the following mechanisms (99).

$$Zn(OH)_2 \longrightarrow ZnO + H_2O \qquad (a)$$

$$Zn(OH)_4^{=} \longrightarrow ZnO + H_2O + 2OH^- \qquad (b)$$

Previous investigators have explained passivation phenomenon using transport process of zincate ions away from the metal surface. A very useful interpretation of the passivation mechanism can be made if hydroxide concentration at the metal surface is included in the passivation mechanism.

If the concentration of OH^- at the zinc surface is severely depleted or if the ratio of zincate to OH^- exceeds a certain critical value, the intermediate species, $Zn(OH)_2$, of the zinc dissolution reactions can not dissolve in the KOH solution but produces a compact film of ZnO (type II) directly on the solid surface by mechanism (a). This phenomenon is expected with very high anodic current operation. On the other hand, when the concentration of OH^- at the zinc surface remains reasonably high as expected with low current dissolution, the intermediate species $Zn(OH)_2$ dissolves in the KOH solution to produce a

supersaturated zincate solution from which a porous type I film of ZnO forms by mechanism (b). If the porous type I film grows to reach a certain thickness, transport of zincate and hydroxide ions between the zinc surface and the bulk in the pores will be limited, causing formation of the type II film, which is the passivating film.

This mechanism explains the common feature of most previous observations (99) that linear relation (between the current density and inverse of square root of the passivation time) holds for short passivation time, while for longer passivation time deviation from the linear relationship with less reproducibility in data occurs.

Popova et al. (100,101) concluded that passivation occurs by either (a) or (b) when zincate concentration in the vicinity of the zinc surface exceeds a critical concentration. They suggested that the molar ratio of zincate to hydroxide ions at the electrode surface was 0.16 at the instant of passivation. Other workers reported that the critical concentration of zincate ion was approximately half the hydroxide ion concentration in the electrolytic solution (16,17).

The passivation effects on electrode failure included in the present mathematical model (see equations (46) to (48)) are surface coverage of zinc surface by the precipitated ZnO (blockage of the 2nd kind) which corresponds to type I film. Our model does not include passivation due to type II film. Therefore, predicted potentials increase gradually until KOH solution in the bulk of the pores decreases to zero. The abrupt increase in overpotentials observed in the present experiments (see Figure 24 and 25) are believed due to this type II passivating film when the zinc electrode compartment becomes

severely depleted with KOH.

It was not possible to observe precisely when a porous type I film or compact type II film started to form since the test electrode was not visible and covered by the membrane and dynel cloth during operation. Immediately after disassembling the cell, the color of the discharged electrode was grey in the wet state, but it changed to white when the electrode was washed and completely dried. The grey color observed during discharge implies that the film formed under KOH depleted conditions is very similar to the type II film of ZnO. Considering that a separator was excluded from the experiments by Elsdale et al. (98) and Coates et al. (88), their results, i.e., gradual increase in potential in the vicinity of passivation, are in agreement with the present interpretation since the KOH concentration in their experiments may not have decreased to below the critical value to form a type II film.

The failure observed for the H20-ZDM electrode (see curve D of Figure 25) is attributed to passivation. Porosity of 0.6 for the H20-ZDM electrode is large enough to prevent, at least in the initial first cycle, pore plugging (blockage of the 1st kind) as shown in Figures 19 to 21. Complete conversion of zinc into ZnO results in about 0.4 porosity. Potential measurement (Figure 25), however, seems to indicate that the high porosity electrode also fails after about 8 to 10 hour operation (68 to 85% depth of discharge) with a current density of 20 mA/cm^2. Discharge up to the range of this operation time might cause type I film formation, i.e., surface coverage of zinc metal by the precipitated ZnO. Type I film having a certain thickness can

cause a significant decrease in OH^- ion concentration, an increase in zincate ion concentration at the active zinc surface, and finally type II passivation.

VI-5. Failure During Charge

Most of the work concerning the failure initiated during charge has been associated with zinc dendrite growth and short circuits which have been one of the major problems after many cycles. Comparison of Figure 30 with Figure 24 indicates that charge continues without significant overpotential rise until most of the coulombic charge applied during discharge has been recovered on charging. This observation leads to the conclusion that discharge products in any form of zincate, ZnO, or $Zn(OH)_2$ can be converted easily into zinc on charging. However, zincate depletion as a failure mechanism can not be neglected simply because of this observation.

During charge, zincate becomes undersaturated, and under certain circumstances depletion of zincate might play an important role as a limiting factor. If solid ZnO can not dissolve as fast as zinc deposits, zincate is expected to be depleted inside the porous electrode. Even if solid ZnO dissolves fast enough to replace the depositing zincate, zincate ions at the zinc surface can be depleted due to the limited mass transfer of zincate, especially at high charge rate. The increase in the zincate diffusion length from ZnO source to zinc sink, resulting from the high molar volume ratio of ZnO to Zn (1.5), might accelerate this phenomenon. The latter effect, namely, zincate depletion due to limited mass transfer, was not a dominant factor during charge of the

present electrode with current density up to 50 mA/cm^2.

Picture 31-A implies that zinc deposit growth, instead of being limited by depleted zincate ion at the zinc surface, continues to grow toward the zincate source in the dynel cloth. Similar behavior has been observed by Hamby (102) who found the zinc dendrite penetration through the porous polyethylene film (1/8" thickness) which was placed, as a solution reservoir, on the opposite side from the counter electrode (on the side of the backing plate). These observations leave only one possible reason for depletion of zincate, namely, slow dissolution of ZnO.

There is some indication that the dissolution direction of chemical reaction (B) is slow (103,104,105) on charge; however, the kinetic data has not been established. The fact that it takes one or two days even with vigorous stirring to obtain a saturated solution from ZnO powder in 10M KOH solution gives a rough idea how slow the dissolution reaction is. The zincate depletion of this type may cause the initial low capacity during charge of an electrode made of pure ZnO, commonly used as negative zinc plates in the construction of secondary batteries.

Choi et al. (13) observed cell capacity less than 30% of ZnO present during initial charge of a ZnO electrode. They attributed the resulting low capacity mainly to the failure of the positive silver oxide electrode. However, zincate depletion seems to have some effect on the initial low capacity since the electrolytic solution contained inside their electrode corresponds to only 0.37 A-hour (3.1% depth of charge) based on the following parameters; cross sectional area of 66 cm^2, electrode thickness of 0.16 cm, porosity of 0.65, and zincate concentration of 1 M.

On charge of L50-ZD electrode (Picture 31-B), without using a membrane, the cell accepted charge without rapid increase in potential until all the zincate ions in the counter electrode compartment was depleted. The zinc reaction front, in dendritic form, then moves step by step towards the counter electrode. Complete recovery of the discharge product on charge (compare Figures 24 and 30) does not prove zincate depletion due to slow dissolution of ZnO. Consequently, the success in interpretation of the charge failure outlined above depends on further knowledge of whether the rate of dissolution of the precipitated ZnO or, if it exists, $Zn(OH)_2$ is faster than that of ZnO powder used in forming the electrode.

VI-6. Failure During Cycling

Zinc electrode failure occurring after many cycles can be referred to as a phenomenon called "redistribution of solid zinc species (Zn and ZnO)". Inability of reforming the solid zinc species in their original position during cycling causes zinc dendrite penetration and shape change. High solubility of ZnO in KOH solution may accentuate the redistribution of zinc species from one part of the electrode to the other.

For the cell without a membrane, Figure 7 shows that only half (55%) of the discharge product (zincate ion) precipitates as ZnO and the remaining half diffuses into the counter electrode compartment before precipitation. On charge, once the zincate source in the zinc electrode is depleted, zinc deposits will grow towards additional zincate which is transferring from the counter electrode compartment. Zinc deposits formed under zincate limiting conditions similar to this are known to

be dendritic, as shown in Figure 31-B (see also references 1 and 2). On the other hand, if a membrane is used as a separator, 95% of the discharge product precipitates as ZnO as shown in Figure 6. Some of the remaining 5% of the zincate ion stays in the zinc electrode compartment and the remainder is lost into the counter electrode. Use of a membrane restricts zincate movement away from the test electrode. Charge of this electrode is less likely to cause dendrite growth through the separator because the source of zincate ions remains in the zinc test electrode. Comparison of these two examples shows an effect of the membrane on zinc dendrite penetration.

Redistribution of solid zinc and zinc oxide from one part of the electrode to the other can occur through the movement of zincate ions. The most important processes involving zincate ions include the charge transfer reaction, mass transfer of zincate, and chemical precipitation or dissolution of ZnO. Therefore, current distribution which characterizes the charge transfer reaction, degree of super- (or under-) saturation which determines precipitation or dissolution of ZnO, and mass transfer modes (e.g., diffusion, migration, and convection) will govern the redistribution of solid zinc species.

Let us consider shape change (redistribution of the solic zinc species in the y-direction parallel to the electrode surface) of a vented porous electrode having a solution reservoir on top and a membrane directly attached on one side. Choi et al. (12) has proposed that shape change is caused by convective flows driven primarily by membrane electroosmotic effects. Discharge induced convective flow of electrolytic solution towards the counter electrode results in a

decrease of the total volume of electrolytic solution inside the zinc electrode. If the electrode is vented, the solution in the reservoir will flow downwards. The solution picks up zincate ions along the flow path causing greater precipitation rates in the direction of flow. On the other hand, on charge, the increase of total volume of electrolytic solution inside the zinc electrode will push the undersaturated solution towards the reservoir. Notice that the solution in the reservoir now becomes undersaturated and greater dissolution is expected near the vent or reservoir. Repeated cycling causes movement of solid zinc species from near the reservoir portion of the electrode to positions remote from the reservoir. If the electrode is sealed, convective flow, and thus shape change will be limited.

Similar treatment can be applied to the redistribution of solid zinc species in the x-direction perpendicular to the electrode surface. The present work, in both experimental and theoretical aspects, deals with a sealed electrode to minimize the convective flow driven by the membrane. Under this condition, the convective flow arising from the volume changes due to the overall electrode reaction is on the order of 10^{-7} cm/sec and is considered negligible.

The reaction or current distribution in the x-direction during discharge is highly nonuniform as confirmed by Figure 5 and Figures 17 to 22. On the other hand, current distribution on charging is more uniform compared to that during discharge, since precipitated ZnO reduces the effective zinc surface area and shifts the reaction towards the backing plate (refer to Figure 9 for detailed comparison). On repeated cycling, this difference of anodic and cathodic current distributions

together with differences in the degree of super- (or under-) saturation causes the redistribution of solid zinc species and thus significant distortion of the electrode structure occurs as cycling progresses. The distorted structure is shown in Figures 11 to 13 (theoretical) and also in Figure 23 (experimental). The results are shown as an accumulation of ZnO at the electrode surface. If convective flow due to membrane pumping is allowed, more serious redistribution is expected. Similarly, allowing free movement of zincate ion into the counter electrode, by eliminating the membrane, may accelerate this effect as shown in Figures 11 and 12.

The result of Figure 10, namely, substantial overpotential rise with repeated cycling, predicts that the redistribution of zinc and zinc oxide in the x-direction is a limiting factor in the loss of cell capacity observed for cells designed to minimize shape change and dendrite penetration.

Comparison of Figure 28 with Figure 29 shows that the present cell exhibits much higher overpotentials during discharge compared to those during charge. Similar behavior has been observed by Hamby (102). He has concluded that the overpotentials during charge remain essentially constant but those on discharging increase significantly with large differences in overpotential between different positions. These observations imply that failure during anodic discharging may control the overall zinc electrode failure. This means that the redistribution of zinc species may cause overpotential rise through discharge failure mechanisms such as pore plugging, KOH depletion, and passivation. The ZnO accumulated for many cycles can decrease pore size, at least locally, resulting in high ohmic overpotential and eventually deplete the elec-

trolytes in the interior of the electrode to increase concentration overpotential. It also reduces the active zinc surface area, promoting high activation overpotential. Similar adverse effects are expected due to the gas trapped inside the porous electrode.

VII. CONCLUSION

A mathematical model has been developed using the concentrated ternary electrolyte theory to predict the local charge transfer current, current density in the solution, potential in the solution and in the matrix, concentrations of hydroxide ions and zincate ions, porosity, volume fractions of Zn and ZnO, and bulk solution velocity as a function of time and position perpendicular to the surface of the electrode.

The predicted behaviors have been confirmed by galvanostatic experiments on overpotentials and reaction distributions. The agreement between the theoretical predictions and the experimental observations provides a good interpretation of the failure mechanisms of negative zinc electrodes for use in secondary batteries.

During discharge at high rate (at 50 mA/cm^2) for both low porosity and high porosity electrodes, the utilization of zinc is severely limited by depletion of electrolyte within the zinc electrode compartment, depending on the volume of solution reservoir and the type of membrane used.

At lower current densities (e.g., 20 mA/cm^2), the utilization of zinc is much higher than that at high current densities. However, pore plugging plays an important role in limiting the discharge capacity. The predicted and the observed reaction profiles on discharge are highly nonuniform and the reaction zone, located near the electrode surface, is very thin, typically 0.2 mm. This highly nonuniform reaction distribution accentuates the failure due to pore plugging at the pore mouth. Low current density discharge of the high porosity electrode, designed to remove failure due to pore plugging, continued until the electrode

failed due to passivation.

The predicted reaction distribution on charge become more uniform compared to that on discharge. The difference of anodic and cathodic reaction distribution caused the redistribution of solid zinc and zinc oxide species on repeated cycling. This movement of solid species is predicted to contribute to the loss in cell capacity for long cycled cells.

The results of this work can be applied to the design of industrial zinc electrodes to improve their performance and cycle life. The results also point out areas where further research should be emphasized in order to gain cycle life improvements.

REFERENCES

1. H. G. Oswin and K. F. Blurton, "The Morphology of Zinc Electrodeposited from Alkaline Electrolyte," Zinc-Silver Oxide Batteries, A. Fleischer and J. J. Lander editors, John Wiley & Sons, Inc., New York, Chap. 6 (1971)

2. J. O'M. Bockris and G. A. Razumney, Fundamental Aspects of Electrocrystallization, Plenum Press, New York, Chap. 6 (1967)

3. R. D. Naybour, "Morphologies of Zinc Electrodeposited from Zinc-saturated Aqueous Alkaline Solution," Electrochimica Acta, 13, p. 763 (1968)

4. J. E. Oxley and C. W. Fleischmann, "Improvement of Zinc Electrodes for Electrochemical Cells," Contract NAS5-9591, First Quarterly Report, 21 pp., N66-13568 (September 1965)

5. S. Arouete, K. F. Blurton, and H. G. Oswin, "Controlled Current Deposition of Zinc From Alkaline Solution," J. Electrochem. Soc., 116, p. 166 (1969)

6. H. K. Farmery and W. A. Smith, "Some Material Problems in the Silver-Zinc Secondary Battery," Batteries, D. H. Collins editor, Pergamon Press, Inc., New York, p. 179 (1963)

7. James McBreen, "Zinc Electrode Shape Change in Secondary Cell," J. Electrochem. Soc., 119, p. 1620 (1972)

8. J. J. Lander, "Failure Modes and Mechanism," Zinc-Silver Oxide Batteries, A. Fleischer and J. J. Lander editors, John Wiley & Sons, Inc., New York, p. 457 (1971)

9. G. A. Dalin, "Improvement of Performance of Zinc Electrode," Zinc-Silver Oxide Batteries, A. Fleischer and J. J. Lander editors, John Wiley & Sons, Inc., New York, p. 87 (1971)

10. D. P. Boden, V. J. Spera, and R. B. Wiley, "Potential Distribution over the Surface of Planar Zinc Electrode During Charge and Discharge at Constant Current," Extended Abstracts, No. 13, The Electrochemical Society Meeting, Detroit (October, 1969).

11. J. McBreen and G. A. Dalin, "The Mechanism of Zinc Shape Change in Secondary Batteries," Extended Abstracts, No.45, The Electrochemical Society Meeting, Philadelphia (October 1966).

12. K. W. Choi, D. N. Bennion, and J. Newman, "Engineering Analysis of Shape Change in Zinc Secondary Electrode, I. Theoretical," J. Electrochem. Soc., 123, p. 1616 (1976)

13. K. W. Choi, D. Hamby, D. N. Bennion, and J. Newman, "Engineering Analysis of Shape Change in Zinc Secondary Electrodes, II. Experimental," J. Electrochem. Soc., 123, p. 1628 (1976)

14. N. A. Hampson, M. J. Tarbox, J. T. Lilley, and J. P. G. Farr, "The Passivation of Vertical Zinc Anodes in Potassium Hydroxide Solution," Electrochem. Tech., 2, p. 309 (1964)

15. N. A. Hampson and M. J. Tarbox, "The Anodic Behavior of Zinc in KOH Solution, I. Horizontal Anodes," J. Electrochem. Soc., 110, p. 95 (1963)

16. M. Eisenberg, H. F. Bauman, and D. M. Brettner, "Gravity Field Effects on Zinc Anode Discharge," J. Electrochem. Soc., 108, p. 909 (1961)

17. N. A. Hampson, P. E. Shaw, and R. Taylor, "Anocid Behavior of Zinc in Potassium Hydroxide Solution, II. Horizontal Anodes in Electrolytes Containing Zn(II)," Br. Corr. J., 4, p. 207 (1969)

18. H. J. S. Sand, Phil. Mag., Ser. 6, Vol. 1, p. 45 (1901)

19. F. Pryzbyla and F. J. Kelley, "Low Temperature Performance of the Zinc-Mercuric Oxide System," Sixth International Power Source Symposium, Brighton, Sussex, Pergamon Press, p. 373 (1969)

20. D. H. Morrel and D. W. Smith, "The Fabrication of Battery Plates Directly from Metal Powders," Fifth International Power Source Symposium, Brighton, Sussex, Pergamon Press, p. 207 (1967)

21. M. Shaw and A. H. Remanick, "Mass Transfer Properties of Membranes and Their Effect on Alkaline Battery Performance," Zinc-Silver Oxide Batteries, A. Fleischer and J. J. Lander editors, John Wiley & Sons, Inc., New York, p. 233 (1971)

22. J. Newman and W. Tiedemann, "Porous-Electrode Theory with Battery Applications," Am. Inst. Chem. Eng. J., 21, p. 25 (1975)

23. A. Winsel, "Beiträge zur Kenntnis der Stromverteilung in Porösen Elektroden," Z. Elektrochem., 66, p. 287 (1962)

24. J. Newman and C. W. Tobias, "Theoretical Analysis of Current Distribution in Porous Electrodes," J. Electrochem. Soc., 109. p. 1183 (1962)

25. R. C. Alkire, E. A. Grens II., and C. W. Tobias, "A Theory for Porous Electrodes Undergoing Structural Change by Anodic Dissolution," J. Electrochem. Soc., 116, p. 1328 (1969)

26. J. Dunning, D. N. Bennion, and J. Newman, "Analysis of Porous Electrodes with Sparingly Soluble Reactants," J. Electrochem.

Soc., 120, p. 906 (1973)

27. H. Gu, D. N. Bennion, and J. Newman, "Analysis of Porous Electrodes with Sparingly Soluble Reactants, III. Short Time Transients," J. Electrochem. Soc., 123, p. 1364 (1976)

28. D. Simonsson, "Current Distribution in the Porous Lead Dioxide Electrode," J. Electrochem. Soc., 120, p. 151 (1973)

29. D. Simonsson, "A Mathematical Model for the Porous Lead Dioxide Electrode," J. Appl. Electrochem., 3, p. 261 (1973)

30. D. Gidaspow and B. S. Baker, "A Model for Discharge of Storage Batteries," J. Electrochem. Soc., 120, p. 1005 (1973)

31. T. P. Dirkse, "Electrolytic Oxidation of Zn in Alkaline Solutions," J. Electrochem. Soc., 102, p. 497 (1955)

32. J. O. Hirschfelder, C. F. Curtiss, and R. B. Bird, Molecular Theory of Gases and Liquids, John Wiley & Sons, Inc., New York, p. 714 (1954)

33. J. A. Keralla, "Zinc Electrode Manufacture," Zinc-Silver Oxide Batteries, A. Fleischer and J. J. Lander editors, John Wiley & Sons, Inc., New York, p. 183 (1971)

34. D. H. Morrel and D. W. Smith, "The Fabrication of Battery Plates Directly from Metal Powders," Fifth International Power Source Symposium, Brighton, Sussex, Pergamon Press, p. 207 (1967)

35. R. J. Brodd, "Experimental Current Distribution in Porous Battery Electrodes," Electrochimica Acta, 11, p. 1107 (1966)

36. J. J. Coleman, "Distribution of Current in Porous Electrodes," J. Electrochem. Soc., 98, p. 26 (1951)

37. E. C. Gagnon and L. G. Austin, "Low-Temperature Cathode Performance of Porous Ag/AgO Electrodes," J. Electrochem. Soc., 118, p. 497 (1971)

38. Z. Nagy and J. O'M Bockris, "On the Electrochemistry of Porous Zinc Electrodes in Alkaline Solutions," J. Electrochem. Soc., 119, p. 1129 (1972)

39. P. Bro and H. Y. Kang, "Discharge Profiles in a Porous Cadmium Electrode," J. Electrochem. Soc., 118, p. 519 (1971)

40. R. C. Alkire, "Reaction Distribution in a Dissolving Porous Anode," Ph. D. Dissertation, University of California, Berkeley (1968)

41. A. Brenner, Electrodeposition of Alloys, Vol.1, Academic Press, London, p. 295 (1963)

42. R. K. Flatt, R. W. Wood, and P. A. Brook, "The Concentration Profiles in Solution at Dissolving Anode Surfaces (1) Zinc, Copper, and Brasses by the Freezing Techniques," J. Appl. Electrochem., 1, p. 35 (1971)

43. T. P. Dirkse, "Chemistry of the Zinc/Zinc Oxide Electrode," Zinc-Silver Oxide Batteries, A. Fleischer and J. J. Lander editors, John Wiley & Sons, Inc., New York, p. 19 (1971)

44. T. P. Dirkse, L. A. Vander Lugt, and N. A. Hampson, "Exchange in the Zinc, Zincate, ZnO System," J. Electrochem. Soc., 118, p. 1606 (1971)

45. D. D. Justice and R. M. Hurd, "Electrochemical Dissolution of ZnO Single Crystals," J. Electrochem. Soc., 118, p. 1417 (1971)

46. H. Gerischer, "Kinetic der Entlandung einfacher und Komplexer Zin-Ionen," Z. Physik. Chem., 202, p. 302 (1953)

47. J. P. G. Farr and N. A. Hampson, "The Exchange Reaction Zn(II)/Zn(Hg) in Alkali," J. Electroanal. Chem., 18, p. 407 (1968)

48. D. A. Payne and A. J. Bard, "The Mechanism of the Zinc (II)-Zinc Amalgam Electrode Reaction in Alkaline Media as studied by Chronocoulometric and Voltammetric Techniques," J. Electrochem. Soc., 119, p. 1665 (1972)

49. J. P. G. Farr and N. A. Hampson, "Evaluation of the Characteristics of Exchange Reaction. I. Exchange Reaction at a Solid Zinc Electrode in Alkali," J. Electroanal. Chem., 13, p. 433 (1967)

50. J. P. G. Farr and N. A. Hampson, "Reactions at Solid Metal Electrodes, Part-I. Faradaic Impedance of Zinc Electrodes in Alkaline Solution," Trans. Farad. Soc., 62, p. 3493 (1966)

51. R. D. Armstrong and G. M. Bullman, J. Electroanal. Chem., 25, p. 121 (1970)

52. J. O'M. Bockris, Z. Nagy, and A. Damjanovic, "On the Deposition and Dissolution of Zinc in Alkaline Solutions," J. Electrochem. Soc., 119, p. 285 (1972)

53. J. N. Butler, Ionic Equilibrium-A Mathematical Approach, Addison-Wesley Publ. Co., Inc., Chap. 8-3, p. 285 (1964)

54. D. P. Boden, R. B. Wylie, and V. J. Spera, "The Electrode Potential of Zinc Amalgamation in Alkaline Zincate Solution," J. Electrochem. Soc., 118, p. 1298 (1971)

55. T. P. Dirkse, C. Postmus, Jr., and R. Vandenbosch, "A Study of Alkaline Solution of Zinc Oxide," J. Am. Chem. Soc., 76, p. 6022 (1954)

56. A. O. Gubeli and J. Ste-Marie, "Stabilité des Complexes Hydroxo et Produits de Solubilité des Hydroydes de Metaux I. Argent et Zinc, "Can. J. Chem., 45, p. 827 (1967)

57. W. Van Doorne and T. P. Dirkse, "Supersaturated Zincate Solution," J. Electrochem. Soc., 112, p. 1 (1975)

58. J. Newman, D. N. Bennion, and C. W. Tobias, "Mass Transfer in Concentrated Binary Electrolytes," Berichte der Bunseng., Bd. 69, p. 608 (1965)

59. R. B. Bird, W. E. Stewart, and E. N. Lightfoot, Transport Phenomena, John Wiley & Sons, Inc., New York, p. 570 (1960)

60. E. A. Guggenheim, Thermodynamics, Amsterdam, North-Holland Publishing Co., (1959)

61. L. Onsager, "Reciprocal Relations in Irreversible Processes, I.," Phys. Rev., 38 (1), p. 2265 (1931)

62. D. N. Bennion, "Mass Transport of Binary Electrolyte Solutions in Membranes," School of Engineering and Applied Sciences, University of California, Los Angeles, Report-6617 (1966)

63. W. Tiedemann and D. N. Bennion, "The Application of Concentrated Electrolyte Theory to Transference Number Measurements in a Centrifuge," UCLA-ENG-7078, University of California, Los Angeles, pp. 115-133 (December 1970)

64. D. G. Miller, "Application of Irreversible Thermodynamics to Electrolyte Solutions, II. Ionic Coefficients l_{ij} for Isothermal Vector Transport Processes in Ternary Systems," J. Phys. Chem., 71, p. 616 (1967)

65. J. Newman and T. W. Chapman, "Restricted Diffusion in Binary Solutions," Am. Inst. Chem. Engr. J., 19, p. 343 (1973)

66. T. W. Chapman, "The Transport Properties of Concentrated Electrolytic Solutions," Ph.D. Dissertation, University of California, Berkeley (November 1967)

67. D. A. MacInnes, The Principles of Electrochemistry, Dover Publ., Inc., New York, p. 86 (1961)

68. J. Newman, Electrochemical System, Prentice-Hall, Inc., Englewood Cliffs, N. J., pp. 78-106 (1973)

69. C. Carman, "Intrinsic Mobilities and Independent Fluxes in Multicomponent Isothermal Diffusion, II. Complex Darken Systems," J. Phys. Chem., 72, p. 1713 (1968)

70. H. Kim, F. Reinfelds, and L. J. Gosting, "Isothermal Diffusion Studies of Water-Potassium Chloride-Hydrogen Chloride and Water-Sodium Chloride-Hydrogen Chloride Systems at 25 ° C., J. Phys. Chem., 77, p. 934 (1973)

71. J. S. Dunning, "Analysis of Porous Electrodes with Sparingly Soluble Reactants," Ph.D. Dissertation, University of California, Los Angeles, p. 98 (December 1971)

72. R. K. Schofield and C. Dakshinamurti, "Ionic Diffusion and Electrical Conductivity in Sands and Clays," Diss. Farad. Soc., No.3, p. 56 (1948)

73. R. E. Meredith and C. W. Tobias, "Conduction in Heterogeneous Systems," C. W. Tobias editor, Adv. Electrochem. Electrochem. Eng., 2, p. 15 (1962)

74. E. G. Gagnon, "The Triangular Voltage Sweep Method for Determining Double-Layer Capacity of Porous Electrodes, II. Porous Silver in Potassium Hydroxide," J. Electrochem. Soc., 120, p. 1052 (1973)

75. O. S. Ksenzhek, E. A. Kalinovskii, and E. L. Baskin, "Provodimost' elektrolita v poristykh nikelevykh elektrodakh," Zh. Prik. Khim., 37, p. 1045 (1964)

76. N. A. Hampson, G. H. Herdman, and R. Talor, "Some Kinetic and Thermodynamic Studies of the System Zn/Zn(II), OH^-," J. Electroanal. Chem., 25, p. 9 (1970)

77. J. P. G. Farr and N. A. Hampson, "Evaluation of the Characteristics of Exchange Reaction, I. Exchange Reaction at a Solid Zinc Electrode in Alkali," J. Electroanal. Chem., 13, p. 433 (1967)

78. J. P. G. Farr and N. A. Hampson, "The Exchange Reaction Zn(II)/Zn(Hg) in Alkali," J. Electroanal. Chem., 18, p. 407 (1968)

79. J. O'M. Bockris, Z. Nagy, and A. Damjanovic, "On the Deposition and Dissolution of Zinc in Alkaline Solutions," J. Electrochem. Sbc., 119, p. 285 (1972)

80. T. P. Dirkse and N. A. Hampson, "The Zn(II)/Zn Exchange Reaction in KOH Solution-II. Exchange Current Density Measurements Using the Double-Impulse Method," Electrochimica Acta, 17, p. 383 (1972)

81. J. Newman, "Numerical Solution of Coupled, Ordinary Differential Equations," Ind. Engr. Chem., Fundam., Vol. 7, p. 514 (1968)

82. J. Newman, Numerical Solution of Coupled, Ordinary Differential Equations," UCRL-17739, Lawrence Radiation Laboratory, University of California, Berkeley (August 1967)

83. J. Crank and P. Nicolson, "A Practical Method for Numerical Evaluation of Solutions of Partial Differential Equations of the Heat Conduction Type," Cambr. Phil. Soc. Proceed., 43, p. 50 (1947)

84. D. N. Bennion, "Phenomena at a Gas-Electrode-Electrolyte Interface," PH.D. Dissertation, University of California, Berkeley, Table A (1964)

85. W. F. Linke, Solubilities of Inorganic and Metal Organic Compounds, Vol. 2, 4th ed., Amer. Chem. Soc., Washington D. C., p. 1672 (1965)

86. R. A. Robinson and R. H. Stokes, Electrolyte Solutions, 2nd ed., Butterworths, London, p. 501 (1959)

87. M. Sinha and D. N. Bennion, "Transport Parameters for Potassium Hydroxide-Water Solution in a Cation Exchange Membrane," J. Electrochem. Soc. (to be pulished)

88. R. N. Elsdale, N. A. Hampson, P. C. Jones, and N. A. Strachan, "The Anodic Behavior of Porous Zinc Electrodes," J. Appl. Electrochem., 1, p. 213 (1971)

89. S. Uno Falk and A. J. Salkind, Alkaline Storage Batteries, John Wiley & Sons, Inc., New York, p. 532 (1969)

90. F. J. Welcher, The Analytical Uses of EDTA, Van Nostrand, Princeton, N. J., p. 149 (1958)

91. N. Marinicic and P. Bro, Paper 368 presented at The Electrochemical Society Meeting, Montreal, October (1968)

92. F. Jolas, "Electrodes De Zinc En Milieu Alkalin," Electrochim. Acta, 13, p. 2207 (1968)

93. R. W. Powers and M. W. Breiter, "The Anodic Dissolution and Passivation of Zinc in Concentrated Potassium Hydroxide Solutions," J. Electrochem. Soc., 116, p. 719 (1969)

94. M. W. Breiter,"Film Formation and Reduction on Zinc Electrodes in Concentrated Potassium Hydroxide Solutions," Electrochimica Acta, 16, p. 1169 (1971)

95. R. W. Powers, "Film Formation and Hydrogen Evolution on the Alkaline Zinc Electrode," J. Electrochem. Soc., 118, p. 685 (1971)

96. M. N. Hull, J. E. Ellison, and J. E. Toni, "The Anodic Behavior of Zinc Electrodes in KOH Electrolytes," J. Electrochem. Soc., 117, p. 192 (1970)

97. M. W. Breiter, "Dissolution and Passivation of Vertical Porous Zinc Electrodes in Alkaline Solution," Electrochimica Acta, 15, p. 1297 (1970)

98. G. Coates, N. A. Hampson, A. Marshal, and D. F. Porter, "The Anodic Behavior of Porous Zinc Electrodes, II. The Effects of Specific Surface Area of the Zinc Compact Material," J. Appl. Electrochem., 4, p. 75 (1974)

99. N. A. Hampson, "Kinetics of the Zinc Electrode," Zinc-Silver Oxide Batteries, A. Fleischer and J. J. Lander editors, John Wiley & Sons, Inc., New York, p. 51 (1971)

100. T. I. Popova, V. S. Bagotskii, and B. N. Kabanov, "The Anodic Passivation of Zinc in Alkali, I. Measurements at Constant Current Densities," Russ. J. Phys. Chem., 36, p. 766 (1962)

101. T. I. Popova, V. S. Bagotskii, and B. N. Kabanov, "The Anodic Passivation of Zinc in Alkali, II. Potentiostatic and Alternating Current Measurements; Determination of Charging Curves," Russ. J. Phys. Chem., 36, p. 770 (1962)

102. D. C. Hamby, "Research on Alkaline Zinc Secondary Electrodes with Emphasis on Life Improvement," Eleventh Monthly Report (June 1977) and Annual Progress Report (March 1977), under DOE Contract No. Ey-76-S-06-2434, Linfield Research Institute, McMinnville, Oregon.

103. T. P. Dirkse, "Electrode Migration and Reaction Processes Occurring within Alkaline Zinc Batteries, " Seventh Quarterly Report, AD-820273 (September 1967)

104. T. P. Dirkse, L. A. Vander Lugt, and N. A. Hampson, "Exchange in the Zn, Zincate, ZnO System," J. Electrochem. Soc., 118, p. 1606 (1971)

105. D. D. Justice and R. M. Hurd, "Electrochemical Dissolution of ZnO Single Crystals, " J. Electrochem. Soc., 118, p. 1417 (1971)

106. E. A. Guggenheim and J. C. Turgeon, "Specific Interaction of Ions," Trans. Farad. Soc., 51, p. 747 (1955)

APPENDIX A

A-1. Ternary Transport Parameters as Functions of Friction Coefficients

The transport parameters used in equations (11) through (15) are related to the friction coefficients K_{ij}'s in the following forms

$$L_{AA} = \frac{c_A^2}{D}\left(C_1^2 M_3 + 2C_1C_3K_{13} + C_3^2M_1 \right)$$

$$L_{AB} = L_{BA} = \frac{c_Ac_B}{D}\left(C_1^2(K_{13}+K_{23})+C_1C_3(2K_{13}+K_{1o})+C_3^2M_1\right)$$

$$L_{BB} = \frac{c_B^2}{D}\left(C_1^2(K_{13}+K_{23}+K_{1o}+K_{2o})+2C_1C_3(K_{13}+K_{1o})+C_3^2M_1 \right)$$

$$t_1^o = \frac{C_1}{D}\left(C_1(K_{2o}M_3+K_{23}K_{3o}) + C_3(K_{13}K_{2o} - K_{12}K_{3o}) \right)$$

$$\frac{t_2^o}{z_2\nu_2^A} = \frac{c_A}{D}\left(C_2(M_3K_{1o}+K_{3o}K_{13}) + C_3(K_{23}K_{1o} - K_{12}K_{3o}) \right)$$

$$\frac{t_3^o}{z_3\nu_3^B} = \frac{c_B}{D}\left(C_3(M_1K_{2o}+K_{1o}K_{21}) + C_1(K_{13}K_{2o}-K_{23}K_{1o}) \right)$$

$$\kappa = \frac{F^2\,D}{E}$$

where

$$D = C_1^2(M_3M_o-K_{3o}^2)+2C_1C_3(M_oK_{13}+K_{1o}K_{3o})+C_2^3(M_1M_o-K_{1o}^2)$$

$$E = M_o(K_{12}K_{13}+K_{12}K_{23}+K_{13}K_{23}) + K_{1o}K_{2o}(K_{13}+K_{23}) + K_{23}K_{3o}(K_{12}+K_{13}) + K_{1o}K_{3o}(K_{12}+K_{23}) + K_{1o}K_{2o}K_{3o}$$

$$M_i = \sum_{j\neq i} K_{ij} \qquad ; i,j= 1,2,3, \text{ and } o$$

$$C_i = z_ic_i \qquad ; i=1,2, \text{ and } 3$$

(for example, $M_1 = K_{1o}+K_{12}+K_{13}$)

It is to be noticed that one of the transference numbers is a dependent parameter because of the relation $t_1^o+t_2^o+t_3^o=1$.

A-2. Friction Coefficients as Functions of Six Transport Parameters

$$K_{12} = - C_1C_2 \frac{F^2}{\kappa} + \frac{C_1c_A}{L}\left(L_{BB}t_A^o - L_{AB}t_B^o - \frac{C_2}{c_A} H\right)$$

$$K_{13} = - C_1C_3 \frac{F^2}{\kappa} + \frac{C_1c_B}{L}\left(L_{AA}t_B^o - L_{AB}t_A^o - \frac{C_3}{c_B} H\right)$$

$$K_{23} = - C_2C_3 \frac{F^2}{\kappa} + \frac{c_Ac_B}{L}\left(L_{AB}t_1^o + \frac{C_3}{c_B} L_{BB}t_A^o + \frac{C_2}{c_A} L_{AA}t_B^o - \frac{C_2C_3}{c_Ac_B} H\right)$$

$$K_{1o} = \frac{C_1}{L}\left(-(c_AL_{BB}-c_BL_{AB})t_A^o - (c_BL_{AA}-c_AL_{AB})t_B^o\right)$$

$$K_{2o} = \frac{c_A}{L}\left((c_AL_{BB}-c_BL_{AB})(1-\frac{C_2}{c_A}t_2^o) - \frac{C_2}{c_A}(c_BL_{AA}-c_AL_{AB})t_B^o\right)$$

$$K_{3o} = \frac{c_B}{L}\left((c_BL_{AA}-c_AL_{AB})(1-\frac{C_3}{c_B}t_3^o) - \frac{C_3}{c_B}(c_AL_{BB}-c_BL_{AB})t_A^o\right)$$

where

$$L = L_{AA}L_{BB} - L_{AB}L_{AB}$$

$$H = L_{AA}t_B^ot_B^o - 2L_{AB}t_A^ot_B^o + L_{BB}t_A^ot_A^o$$

$$t_A^o = t_2^o/(z_2\nu_2^A)$$

$$t_B^o = t_3^o/(z_3\nu_3^B)$$

$$C_i = z_ic_i \qquad ; i=1,2, \text{ and } 3$$

A-3. Transformation of the Transport Equations into the Other Four Component Systems.

The transport equations (12) to (15), which are expressed based on the solvent reference velocity, are rewritten in more convenient forms as follows:

$$N_A = \frac{N_2}{\nu_2^A} = - L_{AA}\nabla\mu_A - L_{AB}\nabla\mu_B + \frac{t_A^o}{F} i + c_A v_o$$

$$N_B = \frac{N_3}{\nu_3^B} = - L_{AB}\nabla\mu_A - L_{BB}\nabla\mu_B + \frac{t_B^o}{F} i + c_B v_o \qquad \text{(A.3.1)}$$

$$i = - \kappa \nabla\phi - \frac{\kappa}{nF}\left((s_A + nt_A^o - \frac{s_o}{c_o} c_A)\nabla\mu_A + (s_B + nt_B^o - \frac{s_o}{c_o} c_B)\nabla\mu_B\right)$$

where new parameters defined by $t_A^o = t_2^o/(z_2\nu_2^A)$, $t_B^o = t_3^o/(z_3\nu_3^B)$, $s_A = s_2/\nu_2^A$, and $s_B = s_3/\nu_3^B$ include the effects of charge of the individual species. The equations (A.3.1) are transformed into several forms to describe the transport equations of similar four component systems.

Membrane System

A system consisting of salt A (cation "1" and anion "2"), solvent "o", and membrane "m" is considered. It appears to be convenient to select the reference velocity as the membrane velocity v_m which is zero rather than solvent velocity v_o. Therefore, the symbol "o" of equations (A.3.1) is replaced with the symbol "m". The remaining species "B" of equations (A.3.1) corresponds to the solvent species "o" of the membrane system. The parameter C_3 used in the relations of Appendix A-1 and A-2 is taken as zero, i.e., $C_3 = z_3 c_3 = 0$. The resulting equations are

$$N_A = - L_A^m \nabla\mu_A - L_{Ao}^m \nabla\mu_o + \frac{t_2^m}{z_2 \nu_2^A F} i + c_A v_m$$

$$N_o = - L_{Ao}^m \nabla\mu_A - L_o^m \nabla\mu_o + t_o^m \frac{i}{F} + c_o v_m \qquad \text{(A.3.2)}$$

$$i = - \kappa^m \nabla\phi - \frac{\kappa^m}{nF} \left(\left(\frac{s_2}{\nu_2^A} + \frac{n t_2^m}{z_2 \nu_2^A} \right) \nabla\mu_A + (s_o + n t_o^m) \nabla\mu_o \right)$$

where

$$L_A^m = c_A^2 (K_{1o} + K_{2o} + K_{mo})/D^m \quad ; \quad D^m = (K_{1o}+K_{2o}+K_{mo})(K_{1m}+K_{2m}+K_{om}) - K_{om}^2$$

$$L_{Ao}^m = c_A c_o (K_{1o} + K_{2o})/D^m$$

$$L_o^m = c_o^2 (K_{1o} + K_{2o} + K_{1m} + K_{2m})/D^m$$

$$t_o^m = \frac{c_o}{z_1 c_1} (K_{1o} K_{2m} - K_{2o} K_{1m})/D^m$$

$$t_2^m = (K_{1m}(K_{1o} + K_{2o} + K_{om}) + K_{1o} K_{om})/D^m$$

$$\frac{nF^2 D^m}{\kappa^m} = (K_{m1} + K_{m2} + K_{mo})(K_{12} K_{1o} + K_{12} K_{2o} + K_{1o} K_{2o}) + K_{1m} K_{2m} (K_{1o} + K_{2o})$$

$$+ K_{2o} K_{om} (K_{12} + K_{1o}) + K_{1m} K_{om} (K_{12} + K_{2o}) + K_{1m} K_{2m} K_{om}$$

The transference number t_1^m is related to t_2^m by the relation $t_1^m + t_2^m = 1$. These equations are the same as those developed by Bennion (62).

Single Salt-Neutral Species-Water System

A similar treatment can be applied to obtain the transport equations of a system which contains single salt (cation "1" and anion "2"), neutral species "N", and water "o". The velocity of the solvent is chosen as the reference velocity. If the symbols "m" and "o" are

replaced with the symbols "o" and "N", respectively, equations (A.3.2) reduce to the following equations (for example, for the current equation):

$$i = -\kappa\nabla\phi - \frac{\kappa}{nF}\left(\left(\frac{s_2}{\nu_2^A} + \frac{nt_2^o}{z_2\nu_2^A} - \frac{s_o}{c_o}c_A\right)\nabla\mu_A + \left(s_N + nt_N^o - \frac{s_o}{c_o}c_N\right)\nabla\mu_N\right) \qquad (A.3.3)$$

where

$$t_1^o = 1 - t_2^o = (K_{2o}(K_{N1} + K_{N2} + K_{No}) + K_{2N}K_{No})/D$$

$$t_N^o = \frac{c_N}{z_1c_1}(K_{1N}K_{2o} - K_{2N}K_{1o})/D$$

$$D = (K_{N1} + K_{N2} + K_{No})(K_{o1} + K_{o2} + K_{oN}) - K_{No}^2$$

The transference numbers t_1^o and t_2^o are positive, but t_N^o can be positive or negative. Equations (A.3.3) together with the corresponding flux equations are the same as those developed by Tiedemann (63).

A-4. Ternary Transport Parameters Calculated from Two Sets of Binary Data

The transport parameters $\mathcal{D}_{ij}$ for binary electrolytic solution have been compiled by Chapman (66). Some of the data for HCl and KCl electrolytes are shown in Table II. If Cl^- ion, H^+ ion, and K^+ ion are denoted by species "1", "2", and "3", respectively, a mixture containing 0.025 M HCl (salt "A") and 0.075 M KCl (salt "B") have the following values for $\mathcal{D}_{ij}$.

$$\mathcal{D}_{1o}^A = 1.984\times10^{-5}\ ,\ \mathcal{D}_{2o} = 9.258\times10^{-5},\ \mathcal{D}_{12} = 1.178\times10^{-6}$$

$$\mathcal{D}_{1o}^B = 2.063\times10^{-5}\ ,\ \mathcal{D}_{3o} = 1.978\times10^{-5},\ \mathcal{D}_{13} = 3.311\times10^{-7}$$

$$c_1 = 0.1\times10^{-3}\ ,\ c_2 = 0.025\times10^{-3},\ c_3 = 0.075\times10^{-3}$$

and $c_o = (\rho - c_A M_A - c_B M_B)/M_o$, $\rho = \rho_o + A_1 c_A + A_2 c_B$

where ρ is the density of the ternary solution (ρ_o is the density of pure solvent, and A_1 and A_2 are the best fit parameters calculated from the densities of two binary solutions), M_i is the molecular weight of the species i, and the subscripts "o", "A", and "B" represent water, HCl, and KCl, respectively. The parameter $\mathscr{D}_{23}$ is missing but parameter $\mathscr{D}_{1o}$ has two different values. For $\mathscr{D}_{1o}$, the following mixing rule is employed.

$$\mathscr{D}_{1o} = \frac{c_A \mathscr{D}_{1o}^{A} + c_B \mathscr{D}_{1o}^{B}}{c_A + c_B}$$

The parameter $\mathscr{D}_{23}$ is approximated by the following form.

$$\mathscr{D}_{23} = -\sqrt{\mathscr{D}_{2o}\,\mathscr{D}_{3o}} = 2.0431 \times 10^{-5}$$

The minus sign is chosen due to the repulsion forces arising between two different cations.

The friction coefficients K_{ij}'s, obtained from these six $\mathscr{D}_{ij}$'s by use of equation (2), are substituted into the relations of Appendix A-1. The calculated transference numbers of individual ions are compared to those reported by MacInnes et al. (67) in Table II-2 and Figure 33. Calculated transference numbers based on the arbitrarily chosen value of $\mathscr{D}_{23} = -100$ are also shown in Table II-2.

Table II. Measured and Calculated Transference Numbers

II-1. Transport Parameters $\mathscr{D}_{ij}$'s of Binary Electrolytes*

HCl (mole/l)	KCl (mole/l)	$\mathscr{D}_{-o} \times 10^5$ (cm^2/s)	$\mathscr{D}_{+o} \times 10^5$ (cm^2/s)	$\mathscr{D}_{+-} \times 10^6$ (cm^2/s)
0.025	-	1.984	9.258	1.178
0.05	-	1.964	9.270	1.702
0.075	-	1.951	9.289	2.058
-	0.025	2.051	1.969	0.1776
-	0.05	2.058	1.974	0.2653
-	0.075	2.063	1.978	0.3311

* These data are provided by Professor John Newman, University of California, Berkeley.

II-2. Measured and Calculated Transference Numbers for 0.1 M HCl-KCl Mixture

HCl (mol/l)	KCl (mol/l)	Measured (67) $t^o_{H^+}$	Measured (67) $t^o_{K^+}$	Calculated [a] $t^o_{H^+}$	Calculated [a] $t^o_{K^+}$	Calculated [b] $t^o_{H^+}$	Calculated [b] $t^o_{K^+}$
0.075	0.025	0.7456	0.0503	0.7579	0.0404	0.7577	0.0405
0.05	0.05	0.6198	0.1242	0.6286	0.1164	0.6281	0.1167
0.025	0.075	0.4109	0.2477	0.4051	0.2486	0.4045	0.2490

where $\mathscr{D}_{23} = -\sqrt{\mathscr{D}_{2o}\,\mathscr{D}_{3o}}$ and $\mathscr{D}_{23} = -100$ are used for a and b, respectively.

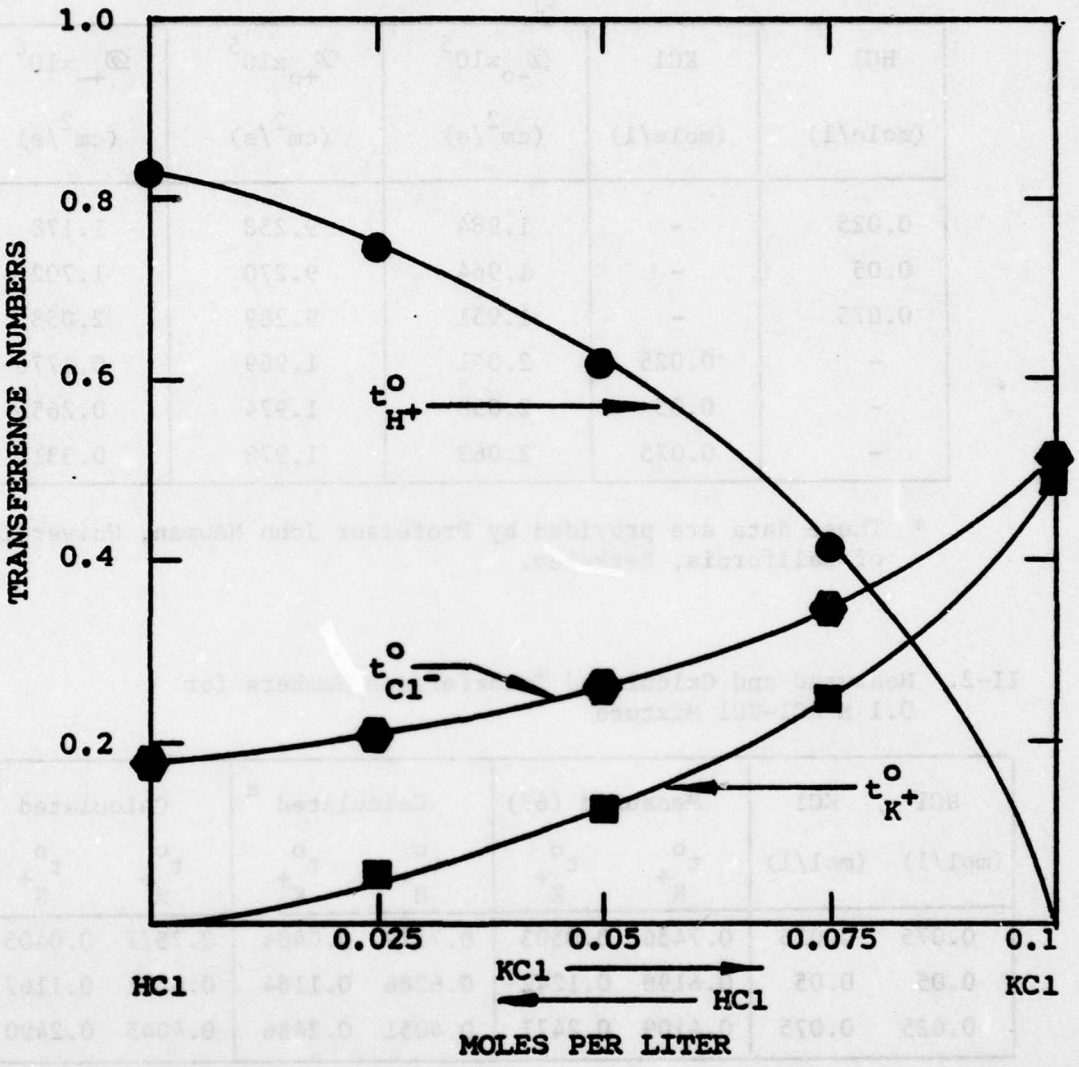

Figure 33. Transference Numbers of Ions in a 0.1M HCl-KCl Ternary Solution. Data Points are the Measured Values (67) and Solid Curves are the Calculated Values.

APPENDIX B

MASS TRANSFER COEFFICIENTS (k_A, k_B, and k_s^*)

It is assumed that the diffusion of a species proceeds through a well defined diffusion layer, δ, which is the distance between the solid-solution interface and the bulk solution inside the pores. The geometry of the situation is shown in Figure 34. The dimensionless distance, ξ, is defined by the distance from the solid surface, y, divided by the diffusion layer, δ. As an example, mass transfer of zincate ions occurring during charge will be considered.

Zinc Deposition by Charge Transfer Reaction

Electrode reaction is given by

$$Zn + 4OH^- \longleftarrow Zn(OH)_4^= + 2e^- \qquad (A)$$

where the stoichiometric coefficients have been defined in equation (10) to give the values of $s_2=-1$, $s_3=4$, and $n=2$. During charge, zincate ions in the solution diffuse into the area, a_m, to deposit as zinc. Within the diffusion layer, the flux of a species is given by Fick's law

$$N_2 = -D_{AA} \frac{dc_2}{dy} = -\frac{D_{AA}}{\delta} \frac{dc_2}{d\xi} \qquad (B.1)$$

Species conservation equation within the control volume at ξ can be written as

$$\frac{d}{d\xi}\left(\{ a_m + (a - a_m) \} N_2 \right) = 0 \qquad (B.2)$$

with boundary conditions;

$$c_2 = c_2^s \text{ at } \xi = 0 \quad \text{and} \quad c_2 = c_2^b \text{ at } \xi = 1.$$

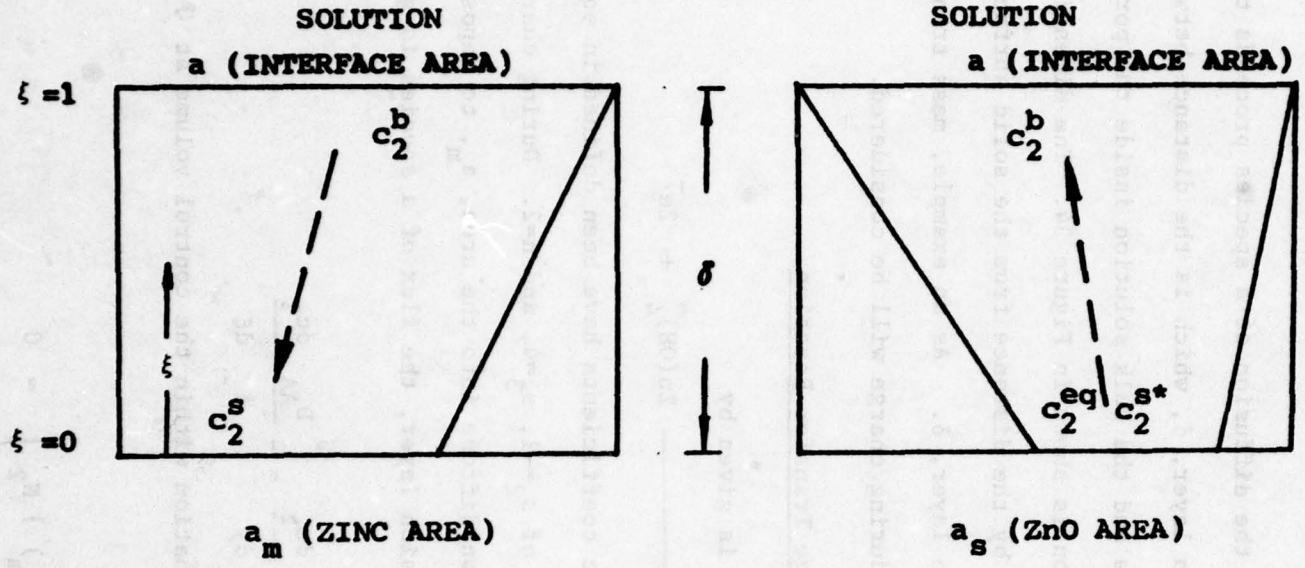

Figure 34. Diffusion Path During Charge Near the Solid Surface Within the Pores; (A) Zinc Deposition by Charge Transfer Reaction and (B) Dissolution of ZnO by Chemical Reaction. Dashed Lines Represent the Direction of Zincate Movement During Charge.

Integrating equation (B.2) yields the following concentration profile.

$$\frac{c_2 - c_2^s}{c_2^b - c_2^s} = \frac{\ln\left(1+\left(\frac{a-a_m}{a_m}\right)\xi\right)}{\ln\left(\frac{a}{a_m}\right)} \qquad (B.3)$$

The flux of zincate ion at $\xi=0$ across the metal area, a_m, or across the interface area, a, becomes

$$a_m N_2(\xi=0) = a_m\left[-\frac{D_{AA}}{\delta}\left(\frac{dc_2}{d\xi}\right)\right]_{\xi=0} = \frac{D_{AA}}{\delta}\frac{a-a_m}{\ln\left(\frac{a}{a_m}\right)}(c_2^s-c_2^b)$$

The charge transfer current per unit area of metal surface, j, is related to the zincate flux as follows:

$$\frac{di_2}{dx} = a_m j = \left(\frac{nF}{-s_2}\right)a_m N_2(\xi=0) = -\frac{nF}{s_2} a\, k_A\,(c_2^s-c_2^b) \qquad (B.4)$$

where

$$k_A = k_A^o\,\frac{1-\frac{a_m}{a}}{\ln\left(\frac{a}{a_m}\right)} \quad : \quad k_A^o = \frac{D_{AA}}{\delta} \qquad (B.5)$$

Equation (B.4) and equation (B.5) are equal to equations (31) and (44), respectively.

Similarly, mass transfer coefficient for hydroxide ion can be obtained to give

$$k_B = k_B^o\,\frac{1-\frac{a_m}{a}}{\ln\left(\frac{a}{a_m}\right)} \quad : \quad k_B^o = \frac{D_{BB}}{\delta}$$

Dissolution of ZnO by Chemical Reaction

On charging, solution becomes undersaturated with ZnO due to the charge transfer reaction (A). Under this condition, ZnO will dissolve into the solution by chemical reaction. Phase change from

ZnO crystal into the zincate ion at the ZnO surface can be described by

$$N_{XTL} = k_{XTL} (c_2^{eq} - c_2^{s*}) \qquad (B.7)$$

where c_2^{eq} is the equilibrium concentration of zincate ion and k_{XTL} represents the rate constant of the chemical reaction. The surface concentration c_2^{s*} is not necessarily the same as the concentration at the zinc surface, c_2^{s}. The zincate species is expected to diffuse from the ZnO surface (c_2^{s*}) to bulk in the pores (c_2^{b}).

Zincate conservation equation at ξ in the boundary layer becomes

$$\frac{d}{d\xi}\left[\left(a_s + (a-a_s)\,\xi\right) N_2\right] = 0 \qquad (B.8)$$

where the flux of zincate, N_2, refers to equation (B.1).

The boundary conditions are

$$c_2 = c_2^{s*} \quad \text{at} \quad \xi=0$$

$$c_2 = c_2^{b} \quad \text{at} \quad \xi=1$$

The integration of equation (B.8) with (B.1) results in the following concentration profile.

$$\frac{c_2 - c_2^{s*}}{c_2^{b} - c_2^{s*}} = \frac{\ln\left(1 + \left(\frac{a-a_s}{a_s}\right)\xi\right)}{\ln\left(\frac{a}{a_s}\right)}$$

The flux of zincate at $\xi=0$ transferring away from the ZnO area (a_s) or interface area (a) becomes

$$a_s N_2(\xi=0) = a_s\left(-\frac{D_{AA}}{\delta}\frac{dc_2}{d\xi}\right)_{\xi=0} = -\frac{D_{AA}}{\delta}\frac{a-a_s}{\ln\left(\frac{a}{a_s}\right)}(c_2^{b}-c_2^{s*}) \qquad (B.9)$$

It appears to be convenient to express the rate of dissolution

of ZnO per area of a_s ($a_s N_{XTL}$ of equation (B.7)), which is the same as the flux $a_s N_2(\xi=0)$ of equation (B.9), by the following form

$$a_s N_{XTL} = a_s N_2(\xi=0) = a\, k_s^* (c_2^s - c_2^b) \qquad (B.10)$$

Rearranging equations (B.10) together with (B.7) and (B.9) yields the following relationship.

$$\frac{1}{k_s^*} = \frac{1}{k_A^o \dfrac{1 - \frac{a_s}{a}}{\ln\left(\frac{a}{a_s}\right)}} + \frac{1}{\frac{a_s}{a} k_{XTL}} \quad : \quad k_A^o = \frac{D_{AA}}{\delta}$$

APPENDIX C

C-1. Solubility of ZnO in KOH Solution (Reference 85)

The notation c^s represents the saturation concentration of ZnO in KOH solution.

(a) $c_{KOH} \leq 2.0 \times 10^{-3}$ mole/cm^3

$$c^s = 0$$

(b) $2.0 \times 10^{-3} < c_{KOH} < 9.0 \times 10^{-3}$ mole/cm^3

$$c^s = -2.1 \times 10^{-4} + 9.75 \times 10^{-2}\, c_{KOH} + 1.25\, (c_{KOH})^2$$

$$\frac{\partial c^s}{\partial c_{KOH}} = 9.75 \times 10^{-2} + 2.5\, c_{KOH}$$

(c) $c_{KOH} \geq 9.0 \times 10^{-3}$ mole/cm^3

$$c^s = 1.0 \times 10^{-4} + 3.0 \times 10^{-2}\, c_{KOH} + 5.0\, (c_{KOH})^2$$

$$\frac{\partial c^s}{\partial c_{KOH}} = 3.0 \times 10^{-2} + 10.0\, c_{KOH}$$

C-2. Conductivity of KOH Electrolytic Solution (Reference 84)

(a) $c_{KOH} \leq 1.5 \times 10^{-3} (mole/cm^3)$

$$\kappa = 0.03655 + 195.34 \quad (c_{KOH} - 1.513 \times 10^{-4}) \quad mho/cm$$

$$\frac{\partial \kappa}{\partial c_{KOH}} = 195.34 \quad mho\text{-}cm^2/mole$$

(b) $1.5 \times 10^{-3} < c_{KOH} \leq 3.7 \times 10^{-3} \quad (mole/cm^3)$

$$\kappa = 0.3 + 134.10 \quad (c_{KOH} - 1.5 \times 10^{-3}) \quad mho/cm$$

$$\frac{\partial \kappa}{\partial c_{KOH}} = 134.10 \quad mho\text{-}cm^2/mole$$

(c) $3.7 \times 10^{-3} < c_{KOH} < 9.0 \times 10^{-3} \quad (mole/cm^3)$

$$\kappa = 0.6572 \cos \left\{ \frac{\pi}{2} \left(\frac{c_{KOH} - 0.00645}{0.0105} \right) \right\} \quad mho/cm$$

$$\frac{\partial \kappa}{\partial c_{KOH}} = -31.295\, \pi \sin \left\{ \frac{\pi}{2} \left(\frac{c_{KOH} - 0.00645}{0.0105} \right) \right\} \quad mho\text{-}cm^2/mole$$

(d) $c_{KOH} \geq 9.0 \times 10^{-3} \quad (mole/cm^3)$

$$\kappa = 0.61 - 57.805 (c_{KOH} - 0.009) \quad mho/cm$$

$$\frac{\partial \kappa}{\partial c_{KOH}} = -57.805 \quad mho\text{-}cm^2/mole$$

C-3. Activity Coefficients of Potassium Hydroxide and Potassium Zincate

The activity coefficients of electrolytes $A(K_2Zn(OH)_4)$ and B (KOH) are approximated by the following equation (reference 68).

$$\ln \gamma_A = - \frac{2\alpha\sqrt{I}}{1 + Ba\sqrt{I}} + 2\beta_{12}\left(\frac{m_1+2m_2}{3}\right) + \beta_{13}\frac{4m_3}{3}$$

$$\ln \gamma_B = - \frac{\alpha\sqrt{I}}{1 + \sqrt{I}} + \beta_{12} m_2 + \beta_{13}(m_1 + m_3)$$

where m_i is the molality (mole/Kg of water) of species i, and subscripts "1", "2", and "3" denote K^+ ion, $Zn(OH)_4^=$ ion, and OH^- ion, respectively. The ionic strength I is defined by

$$I = \frac{1}{2}\sum_i z_i^2 m_i = \frac{1}{c_o M_o}\frac{1}{2}\sum_i z_i^2 c_i$$

The coefficients α and β_{13} for potassium hydroxide are taken from the reported data (68,106), while the coefficients Ba and β_{12} for potassium zincate were estimated from the data of activity coefficients of K_2CrO_4 (86).

α = 1.1762

Ba = 1.158

β_{12} = - 0.01425

β_{13} = 0.130

APPENDIX D

D-1. Input Data

ALPHA — Kinetic parameter used in equation (33), (α_a=1.5)

ALPHC — Kinetic parameter used in equation (33), (α_c=0.5)

A0 — Initial effective interface area (a^o, taken as 50 cm^2/cm^3 for Figures 2 to 13 and as 300 cm^2/cm^3 for Figures 17 to 20, 24, and 25)

CITOT — Applied superficial current density, amp/cm^2

COB — Initial concentration of KOH, $moles/cm^3$, (c_B^o, taken as 0.008 for Figures 2 to 13 and 0.01 for Figures 17 to 20, 24, and 25)

CONMEM — Effective conductivity of the solution in the membrane (κ^m= 0.5243 mho/cm)

DIFA — Diffusion coefficient of potassium zincate in the solution (D_{AA}, taken as 6.86×10^{-6} cm^2/sec)

DIFB — Diffusion coefficients of KOH in the solution (D_{BB}, 2×10^{-5} cm^2/sec at 10 M KOH solution)

DJS — Parameter characterizing complete coverage of the zinc surface by ZnO (λ, taken as zero)

EPI — Initial porosity of the electrode (ε^o, taken as 0.4 for Figures 2 to 13. For Figures 17 to 20, 24, and 25, ε^o=0.33 and ε^o=0.6 are used for the low porosity and the high porosity electrodes, respectively)

EPGI — Initial volume fraction of the inert conducting material (ε_I^o, taken as zero)

FIO — Exchange current density (i_0^o, taken as 0.06 amp/cm^2 for Figures 2 to 13 and 0.1 amp/cm^2 for Figures 17 to 20, 24, and 25)

FL — Thickness of the Zinc electrode (L=0.1 cm)

FLCOUN — Distance between the membrane and the counter electrode (taken as 1.1 cm)

GAM — Kinetic parameter used in equation (33) (γ =0.75)

QI — Initial volume fraction of ZnO (ε_{ZnO}^o, taken as 0.1 for Figures 2 to 13 and zero for Figures 17 to 20, 24, and 25)

RMO — Mass transfer coefficient of zincate ion defined by equation (44) (k_A^o, taken as 0.001 cm/sec)

ROHO — Mass transfer coefficient of hydroxide ion defined by equation (44) (k_B^o, taken as 0.003 cm/sec)

RXT — Rate constant of the chemical reaction defined by equation (44) (k_{XTL}, taken as 0.005 cm/sec)

SGMO — Conductivity of pure zinc metal (σ_{Zn}^o, 2x10^5 $\Omega^{-1}cm^{-1}$)

SGSO — Conductivity of ZnO (σ_{ZnO}^o= 0.01 $\Omega^{-1}cm^{-1}$)

SGGO — Conductivity of inert conducting material (σ_I^o, taken as 100 $\Omega^{-1}cm^{-1}$)

Si — Stoichiometric coefficients of species i for the charge transfer reaction, defined by equation (10); S1 for K^+ ion (s_1=0), S2 for zincate ion (s_2=-1), S3 for OH^- ion (s_3= 4), and SO for water (s_o=0)

SSi — Stoichiometric coefficients of species i for chemical precipitation or dissolution reaction; SS1 for K^+ ion

(s_1^*=0), SS2 for zincate ion (s_2^*=1), SS3 for OH^- ion (s_3^*=-2), and SSO for water (s_o^*= -1).

T2R — Transference number of zincate ion (t_2^o, taken as 0.05 at 10 M KOH-saturated ZnO solution)

T1R — Transference number of the potassium ion (t_1^o, taken as 0.23 for 10 M KOH-saturated ZnO solution)

TOR
TOT — Tortuosity factor for diffusion coefficients (TOR) and that for conductivity of the solution (TOT) (t=0.5)

TR2M — Transference number of zincate ion in the membrane (t_2^m=0)

TR3M — Transference number of OH^- ion in the membrane (t_3^m=0.5)

VA — Molar volume of potassium zincate ($\bar{V}_A$ =67.0 cm^3/mole)

VB — Molar volume of potassium hydroxide ($\bar{V}_B$=17.8 cm^3/mole)

VM — Molar volume of metallic zinc ($\bar{V}_{Zn}$ = 9.15 cm^3/mole)

VS — Molar volume of ZnO ($\bar{V}_{ZnO}$ =14.51 cm^3/mole)

VO — Molar volume of water ($\bar{V}_{H_2O}$ = 18.07 cm^3/mole)

VOL1 — Partial molar volume of potassium ion ($\bar{V}_{K^+}$, taken as 7.2 cm^3/mole)

VOLUME — Volume of the electrolyte reservoir between the zinc electrode surface and the membrane (V, taken as zero for Figures 2 to 13. For Figures 17 to 20, 24, and 25, V is taken as 0.01 cm^3 (for ZMD) and 0.05 cm^3 (for ZDM))

ZETA — Kinetic parameter used in equation (33) (ζ=0.0)

D-2. Programming Parameters

Control Parameter

N — Number of unknowns (N=6)

NJ — Number of mesh points used (NJ=31)

JP — Has the value of 0 if ϕ_2^s is assumed to be the same as ϕ_2 (see equation (29)), and 1 or 2 if correction for ϕ_2^s is included.

JPLG — Has the value of 1 or 2 if swelling effects are included. Otherwise, JPLG is zero.

L — Specifies the initial mode of operation. Equal to 1 for discharge and 2 for charge.

LMX — Has the value of 1 without inert conducting matrix and 2 with inert conducting material.

LCB — Specifies the initial concentration of the continued half cycle. Equal to zero if c_2^o and c_3^o are used, but equal to 1 if average concentrations of salts A and B resulting from the previous half cycle were used.

LPUN — Has the value of 1 if punched cards for output are desired. Equal to zero if punched data cards are not necessary.

LREP — Activates reading of the punched output cards (obtained from LPUN=1) and continues calculation

NACT — Use of binary activity coefficients for the value of zero and ternary activity coefficients for the value, 2.

NBC — Specifies types of boundary layer. Equal to zero for

solution boundary and 1 for the membrane boundary

NCYCLM — Specifies the number of half cycle. Equal to 0 or 1 for the initial half cycle. The value of 4 activates the run for the two complete cycles.

NT — Has the values greater than zero. The first time step of each half cycle (onset of each half cycle) is divided by the NT number of intervals.

TDEL — Time step duration, seconds

TLIMIT — Fixes maximum of operation time of each half cycle, seconds

TSTOP — Specifies the rest period between two half cycles, seconds

Subroutine

BAND MATINV — Called at each mesh point to solve the set of linearized equations. These are developed by Newman.

EQUIL — Equilibrium or saturation concentration of ZnO in KOH solution and its derivatives with respect to concentrations, c_2 and c_3

RKAY — Active surface area (a_m, a_s, and a), mass transfer coefficients (k_A, k_B, and k_s^*) and their derivatives with respect to concentrations, c_2 and c_3

SACTIV — Activity coefficients of KOH and potassium zincate and their derivatives with respect to concentrations.

SCOND — Conductivity of solution and its derivatives with respect to concentrations, c_2 and c_3

SDIF — Diffusion coefficients of potassium hydroxide and potassium zincate and their derivatives with respect to

concentrations, c_2 and c_3

SDIFP — Second derivatives of the diffusion coefficients with respect to concentrations, c_2 and c_3

SIGMA — Effective conductivity of the solid matrix and its derivatives with respect to volume fractions of zinc, zinc oxide, and inert conducting materials.

Dimensional Parameter

A,B,D,G X,and Y — Coefficients of the linearized equations which were defined by Newman

C(I,J) — Variables I (I=1 to 6) at mesh point J of the present iteration at the present time step. CI(I,J) refer to those of the previous interation at the present time step. Z(I,J) represent the variables at the previous time step.

AMET — Active surface area, a_m, which is active for charge transfer reaction (at the present time step)

AREA — Effective solid-solution interface area, a, of the present time step.

CAS — Ratio of the concentration of zincate ion at the metal surface to that in the bulk of the pores.

CRATIO — Ratio of zincate concentration to hydroxide concentration at the metal surface

CONVRN — Fractional conversion of Zn into ZnO, i.e., moles of the precipitated ZnO divided by the moles of the initial Zn.

EQUL — Zincate concentration of the bulk solution in the pores

minus the saturation concentration of zincate

EP — Porosity of the electrode at the present time step. ZEP (J) refers to that at the previous time step.

OVERP — Overpotentials with respect to the Hg/HgO reference electrode.

Q — Volume fractions of ZnO at the present time step. ZQ(J) are the volume fractions of ZnO at the previous time step.

QM — Volume fractions of Zn at the present time step. ZQM(J) are the volume fractions of Zn at the previous time step.

QMNON — Volume fractions of Zn which is nonactive due to pore plugging.

RS — Product of the specific surface area, a, and the rate constants for chemical reaction, k_s^*. ZRS(J) are the values of ak_s^* at the previous time step.

TRNCUR — Transfer current density, j, at the present time step.

D-3. Computer Program

Computer program used in this work is presented.

```
      IMPLICIT REAL*8 (A-H,O-Z)
      DIMENSION A(6,6),B(6,6),C(6,93),D(6,13),G(6),X(6,6),Y(6,6),
     1 Z(6,93),TRNCUR(93),EP(93),ZEP(93),O(93),CI(6,93),OMNON(93),
     2 AREA(93),ZO(93),CAS(93),AMET(93),RS(93),ZRS(93),OM(93),ZOM(93)
     3 ,EQUL(93),CONVRN(93),OVERP(93),CRATIO(93)
      COMMON/WORKA/A,B,D,G,X,Y
      COMMON/WORKB/N,NJ
      COMMON/WORKC/AO,TIME,R40,RSO,RXT,EPI,EPGI,EPNUCS,EPNUCM,EQUIAB,
     1 EQUMAX,EPLIM,NOZN,MM,J
      COMMON/WORKD/C
      COMMON/WORKE/SGMO,SGSO,SGGO,EMLIM
      COMMON/WORKF/NACT
      COMMON/WORKG/OM,O,EP,H,VOLUME,EPGICC,JPLG
      COMMON/WORKH/TOT,L
      COMMON/WORKI/EFFCND
   98 READ 101,NJ
      READ 104,L,LMX,NCYCLM,LREP,LPUN,NBC,NT,LCB,JP
      READ 105,NOZN,NACT,JPLG,NSTOP
      READ 107,NJDELT,NJDMN,NJDMX,EPLGMN,ESPLG
  101 FORMAT(1I2)
  104 FORMAT(6I1,I2,2I1)
  105 FORMAT(4I1)
  106 FORMAT(/1I14/)
  107 FORMAT(3I2,4X,2F10.5)
  108 FORMAT(5X,I4,F20.5,2I4,F20.5)
      IF(NJ.EQ.0) STOP
      N=6
      READ 102,CITOT,FL,C09,TDEL,TLIM,TSTOP,FLCOUN,CONMEM
      READ 102,ALPHA,ALPHC,GAM,ZETA,TOR,TOT,VM,VS
      READ 102,T2R,T1R,S2,S3,SO,SS2,SS3,SSO
      READ 102,VA,VB,VO,SGMO,SGSO,SGGO,RMO,RXT
      READ 102,FIO,AO,EPI,OI,EPGI,DJS ,VOLI,RGHO
      READ 102,CALML,CALMH,POTLIM ,EPNUCS,EPNUCM,EQUMAX,EPLIM,EMLIM
      READ 102,TR2M,TR3M,DLAAM,DLBBM,VELM,VOLUME,EFFCND
  102 FORMAT(8D10.4)
      FITOT=CITOT
      IF(L.EQ.2) FITOT=-CITOT
      IF(LMX.EQ.1) EPGI=0.0
      EPGICC=EPGI
      OMI=1.0-EPI-OI-EPGI
      TMI=TDEL/200.0
      NJMI=NJ-1
      NJM2=NJ-2
      F=96487.0
      R=8.3143
      T=298.16
      EN=2.0
      MM=1
      TR1=T1R
      TR2=T2R
      TR3=1.0-TR1-TR2
      ASTA = VM/EN/F
      BSTAR=(-2.0*VOLI+S2*VA+S3*VB+SO*VO)/2.0/F
      CSTAR=VS
      DSTAR=SS2*VA+SS3*VB+SSO*VO
      H=FL/DFLOAT(NJ-1)
      TIME=0.0
      CALL EQUIL(C0B,C0B,C0A,EQUAB,EQCBP)
      CALL SCOND(C0A,C0B,CONDO,CONDAA,CONDBB)
      DO 11 J=1,NJ
      O(J)=OI
      EP(J)=EPI
      OM(J)=OMI
      CALL EQUIL(C0A,C0B,EQCB,EQUIAB,EQCBP)
      EQUL(J) = EQUIAB
      C(3,J)=C0A
      C(4,J)=C0B
   11 CONTINUE
      OMMAX=OMI+OI*VM/VS
      OMPLG=OMI-EPI*VM/(VS-VM)
      IF(OMPLG.LE.0.0) OMPLG=0.0
      OMCOV=DJS*(OMMAX-OMPLG)
      OMNONI=OMPLG+OMCOV
      OMO=OMI-OMNONI
      CALL SIGMA(EPGI,EPI,OMO,OI,SIGDM,SIGDS,SIGMI)
      CALL RKAY(TDEL,EPI,OMO,OI,AMO,AMCUR,AMCA,FMI,PSI,PMCUR,RSCUR,
     1 RMCA,RSCA)
      PRINT 106,NJ,L,LMX,NCYCLM,LREP,LPUN,MM,NBC,NT,LCB,JP
      PRINT 106,NOZN,NACT,JPLG,NSTOP
```

```
      PRINT 108,NJDELT,EPLGMN,NJOMN,NJDMX,ESPLG
      PRINT 201,FITOT,FL,COA,COB,TDEL,TLIM,ALPHA,ALPHC,GAM,ZETA,
     1 TOR,VM,VS,VA,VB,VO,TR2,TR3,S2,S3,
     2 SO,SS2,SS3,SSO,FIO,EPI,OMI,OI,EPGI,AO,
     3 RMO,RXT,CONDO,SGMO,SGSO,SGGO,SIGMI,DJS,VOLI,CALML,
     4 CALMH,POTLIM,TR2M,TR3M,DLAAM,DLBBM,EPLIM,EPNUCS,EPNUCM,EQUMAX,
     5 RMI,RSI,AMO,OMNON(1,OMPLG,VELM,VOLUME,ROHO,TOT
     6 ,FLCOUN,CONMEM,EMLIM,EFFCND
  201 FORMAT(1H0/(5F20.8))
C
C
C
      IF(LREP.EQ.0) GO TO 9
      DO 12 J=1,NJ
      READ 103,C(1,J),C(2,J),C(3,J),C(4,J),C(5,J)
      READ 103,C(6,J),EP(J),OM(J),O(J),RS(J)
  103 FORMAT(5D16.8)
   12 CONTINUE
      READ 103,(OMNON(J),J=1,NJ)
      READ 103,(EQUL(J),J=1,NJ)
      NCYC=1
      READ 204,TIME,DELT,TLIM,NTI
      READ 103,SUM4,SUM5
  204 FORMAT(3F10.3,I3)
      IF(LREP.GE.2) GO TO 4
      GO TO 6
    9 CONTINUE
      NTI=0
      DELT=TDEL
      NCYC=1
      SUM4=COA
      SUM5=COB
    4 CONTINUE
      DO 7 J=1,NJ
      OMMAX=OM(J)+O(J)*VM/VS
      OMPLG=OM(J)-EP(J)*VM/(VS-VM)
      IF(OMPLG.LE.0.0) OMPLG=0.0
      OMCOV=DJS*(OMMAX-OMPLG)
      OMNON(J)=OMPLG+OMCOV
    7 CONTINUE
    6   CONTINUE
      IF(TIME.GT.TMI) GO TO 31
      IF(LCB-1) 21,21,22
   21 CAINT=DFLOAT(LCB)*SUM4+DFLOAT(1-LCB)*COA
      CBINT=DFLOAT(LCB)*SUM5+DFLOAT(1-LCB)*COB
      GO TO 24
   22 CBINT=DFLOAT(LCB-2)*SUM5+DFLOAT(3-LCB)*COB
      CALL EQUIL(COA,CBINT,CAINT,EQUAB,ECBQP)
   24 CONTINUE
C  APPROXIMATE SOLUTION FOR TIME=0.0
C
      DO 1 J=1,NJ
      C(3,J)=CAINT
      C(4,J)=CBINT
      OMI=OM(J)-OMNON(J)
      CALL EQUIL(C(3,J),C(4,J),EQCB,EQUIAB,EQCRP)
      CALL SIGMA(EPGI,EP(J),OMI,O(J),SGM,SGS,SIGMJ)
      CALL RKAY(TDEL,EP(J),OMI,O(J),AMJ,AMCUR,AMCA,RMJ,RS(J),RMCUR,
     1 RSCUR,RMCA,RSCA)
      AMET(J)=AMJ
      CAS(J)=C(3,J)/COA
      IF(CAS(J).LE.CALML) CAS(J)=CALML
      IF(CAS(J).GT.CALMH) CAS(J)=CALMH
      EPJ=EP(J)
      CALL SCOND(C(3,J),C(4,J),CONDJ,CNDA,CNDB)
      RPOL=AMJ*FIO*F*(ALPHA+ALPHC)/R/T*CAS(J)**GAM
      RAMS=RPOL*(1.0/SIGMJ/(1.0-EPJ)+1.0/CONDJ/EPJ**(1.0+TOT))
      RAM=DSQRT(RAMS)
      RKAP=RPOL*FITOT/SIGMJ/RAMS/(1.0-EPJ)
      EXPR=DEXP(RAM*FL)-DEXP(-RAM*FL)
      RA=(FITOT-RKAP*(1.0-DEXP(-RAM*FL)))/EXPR
      RB=(-FITOT-RKAP*(DEXP(RAM*FL)-1.0))/EXPR
      EX=DFLOAT(J-1)/DFLOAT(NJ-1)*FL
      C(1,J)=RA*DEXP(RAM*EX)+RB*DEXP(-RAM*EX)+RKAP
      C(6,J)= (RA*DEXP(RAM*EX)/RAM-RB*DEXP(-RAM*EX)/RAM+RKAP*EX
     1 -FITOT*EX-(RA-RB)/RAM)/SIGMJ/(1.0-EPJ)
      C(2,J)=C(6,J)-(RA*RAM*DEXP(RAM*EX)-RB*RAM*DEXP(-RAM*EX))/RPOL
      C(5,J)= -(ASTA +BSTAR)*C(1,J)
```

```
    1    CONTINUE
   31    CONTINUE
         PRINT 217
  217    FORMAT(/20X,'QMNON='/)
         PRINT 205,(QMNON(J),J=1,NJ)
         IF(L.EQ.1) PRINT 211
         IF(L.EQ.2) PRINT 212
  211    FORMAT(//1H ,'THIS IS FOR ANODIC')
  212    FORMAT(//1H ,'THIS IS FOR CATHODIC')
         IF(LMX.EQ.1) PRINT 213,EPGI
         IF(LMX.EQ.2) PRINT 214,EPGI
  213    FORMAT(//1H ,8X,'FOR ZINC MATRIX',20X,'EPGI =',F5.2)
  214    FORMAT(//1H ,8X,'FOR INERT MATRIX',20X,'EPGI =',F5.2)
         PRINT 222,TIME
  222    FORMAT(// 20X,'TIME=',F10.3//)
         DO 5 J=1,NJ
         PRINT 205,C(1,J),C(2,J),C(3,J),C(4,J),C(5,J),C(6,J)
  205    FORMAT(6D20.8)
    5    CONTINUE
         PRINT 29
   29    FORMAT(/15X,'EP=',15X,'QM=',15X,'CHARGE=',12X,'RS',15X,'AM=',20X,
        1 'CAS='/)
         DO 28 J=1,NJ
         PRINT 205,EP(J),QM(J),Q(J),RS(J),AMET(J),CAS(J)
   28    CONTINUE
    2    JCOUNT=0
         DELTI= ASTA *DELT/2.0
         DEL=CSTAR*DELT/2.0
         IF(MM.EQ.0) DEL=0.0
         IF(MM.EQ.0) DELTI=0.0
         DO 3  J=1,NJ
         ZQ(J)=Q(J)
         ZEP(J)=EP(J)
         ZQM(J)=QM(J)
         ZRS(J)=RS(J)
         DO 3 I=1,N
         Z(I,J)=C(I,J)
    3    CONTINUE
    8    JCOUNT=JCOUNT+1
         DO 10 I=1,N
         DO 10 J=1,NJ
   10    CI(I,J)=C(I,J)
C
C
         J=0
         DO 13 I=1,N
         DO 13 K=1,N
         X(I,K)=0.0
   13    Y(I,K)=0.0
   15    J=J+1
         DO 17 I=1,N
         G(I)=0.0
         DO 17 K=1,N
         A(I,K)=0.0
         B(I,K)=0.0
   17    D(I,K)=0.0
         IF(J.EQ.NJ) GO TO 50
         IF(J.NE.1) GO TO 40
C
C  PROGRAM FOR J=1
C
         B(2,1)=1.0
         B(5,5)= 1.0
         B(6,6)= 1.0
         CAF =0.5*(C(3,J)+C(3,J+1))
         CBF =0.5*(C(4,J)+C(4,J+1))
         CURF=0.5*(C(1,J)+C(1,J+1))
         CURPF=(C(1,J+1)-C(1,J))/H
         CAPF =(C(3,J+1)-C(3,J))/H
         CBPF =(C(4,J+1)-C(4,J))/H
         PHIPF=(C(2,J+1)-C(2,J))/H
         CALL SCOND(CAF,CBF,COND,CONDA,CONDB)
         IF(TIME.GT.TMI) GO TO 32
         EPF=0.5*(EP(J)+EP(J+1))
         01=COND*EPF*(1.0+TOT)
         B(1,1)=0.5
         D(1,1)=0.5
         B(1,2)=-01/H
         D(1,2)=01/H
```

```
      B(3,3)=1.0
      B(4,4)=1.0
      G(3)=CAINT
      G(4)=CBINT
      GO TO 34
   32 CONTINUE
      CALL SACTIV(CAF,CBF,ACTA,ACTB,YA,YB,YAA,YAB,YBA,YBB)
      CALL SWATR(T1R,T2R,COA,CAF,CBF,PA,PB,PAA,PAB,PBA,PBB)
      QF=(Q(J)+Q(J+1))/2.0
      QMF1=(QM(J)+QM(J+1))/2.0
      QMNONF=(QMNON(J)+QMNON(J+1))/2.0
      QMF=QMF1-QMNONF
      EPF=(EP(J)+EP(J+1))/2.0
      CALL EQUIL(CAF,CBF,EQCB,EQUIAB,EQCBP)
      CALL RKAY(DELT,EPF,QMF,QF,AMF,AMCUR,AMCA,RMF,RSF,RMCUR,
     1 RSCUR,RMCA,RSCA)
      DELTA=-DEL*RSF
      DELTB=DEL*RSF*EQCBP
      O1=COND*EPF**(1.0+TOT)
      O2= YA*PA/CAF
      O3=YB*PB/CBF
      OAA= CONDA+YAA+PAA
      OBA= CONDA+YBA+PBA
      OAB= CONDB+YAB+PAB
      OBB= CONDB+YBB+PBB
      OE= (1.0+TOT)*O1*(PHIPF+O2*CAPF+O3*CBPF)/EPF
      OA= O1*(CONDA*PHIPF+O2*(OAA-1.0/CAF)*CAPF+O3*OBA*CBPF)
      OB= O1*(CONDB*PHIPF+O2*OAB*CAPF+O3*(OBB-1.0/CBF)*CBPF)
      B(1,1)= 0.5-OE*DELTI/H
      D(1,1)= 0.5+OE*DELTI/H
      D(1,2)=  O1/H
      B(1,2)=-O(1,2)
      B(1,3)=-O1*O2/H+0.5*(OE*DELTA+OA)
      D(1,3)=O1*O2/H+ 0.5*(OE*DELTA+OA)
      B(1,4)=-O1*O3/H+(OB+OE*DELTB)/2.0
      D(1,4)= O1*O3/H+(OB+OE*DELTB)/2.0
      G(1)= OE*DELTI*CURPF+OE*DELTA*CAF+OA*CAF+OB*CBF+OE*DELTB*CBF
      B(3,3)=-3.0
      D(3,3)=4.0
      X(3,3)=-1.0
      B(4,4)=-3.0
      D(4,4)=4.0
      X(4,4)=-1.0
   34 CONTINUE
      CALL BAND(J)
      GO TO 15
C
C
C
C  PROGRAM FOR  J.GT.1 AND J.LT.NJ
   40 CONTINUE
      CAF =0.5*(C(3,J)+C(3,J+1))
      CBF =0.5*(C(4,J)+C(4,J+1))
      CURF=0.5*(C(1,J)+C(1,J+1))
      CURPF=(C(1,J+1)-C(1,J))/H
      CAPF =(C(3,J+1)-C(3,J))/H
      CBPF =(C(4,J+1)-C(4,J))/H
      PHIPF=(C(2,J+1)-C(2,J))/H
      CALL SCOND(CAF,CBF,COND,CONDA,CONDB)
      IF(TIME.GT.TMI) GO TO 42
      EPF=0.5*(EP(J)+EP(J+1))
      O1=COND*EPF**(1.0+TOT)
      B(1,1)=0.5
      D(1,1)=0.5
      B(1,2)=-O1/H
      D(1,2)=O1/H
      B(3,3)=1.0
      B(4,4)=1.0
      G(3)=CAINT
      G(4)=CBINT
      GO TO 44
   42 CONTINUE
      CALL SACTIV(CAF,CBF,ACTA,ACTB,YA,YB,YAA,YAB,YBA,YBB)
      CALL SWATR(T1R,T2R,COA,CAF,CBF,PA,PB,PAA,PAB,PBA,PBB)
      QMF1=(QM(J)+QM(J+1))/2.0
      QMNONF=(QMNON(J)+QMNON(J+1))/2.0
      QMF=QMF1-QMNONF
      QF=(Q(J)+Q(J+1))/2.0
      EPF=(EP(J)+EP(J+1))/2.0
```

```
      CALL EQUIL(CAF,CBF,EQCB,EQUIAB,EQCBP)
      CALL RKAY(DELT,EPF,QMF,QF,AMF,AMCUR,AMCA,RMF,RSF,RMCUR,
     1 RSCUR,RMCA,RSCA)
      DELTA=-DEL*RSF
      DELTB= DEL*RSF*EQCBP
      01=COND*EPF**(1.0+TOT)
      02=YA*PA/CAF
      03=YB*PB/CBF
      OAA=CONDA+YAA+PAA
      OBA=CONDA+YBA+PBA
      OAB= CONDB+YAB+PAB
      OBB=CONDB+YBB+PBB
      OE= (1.0+TOT)*01*(PHIPF+02*CAPF+03*CBPF)/EPF
      OA= 01*(CONDA*PHIPF+02*(OAA-1.0/CAF)*CAPF+03*OBA*CBPF)
      OB= 01*(CONDB*PHIPF+02*OAB*CAPF+03*(OBB-1.0/CBF)*CBPF)
      B(1,1)=0.5-OE*DELTI/H
      D(1,1)=0.5+OE*DELTI/H
      D(1,2)= 01/H
      B(1,2)=-D(1,2)
      B(1,3)=-01*02/H+0.5*(OE*DELTA+OA)
      D(1,3)=01*02/H+ 0.5*(OE*DELTA+OA)
      B(1,4)=-01*03/H+(09+OE*DELTB)/2.0
      D(1,4)= 01*03/H+(09+OE*DELTB)/2.0
      G(1)= OE*DELTI*CURPF+OE*DELTA*CAF+OA*CAF+OB*CBF+OE*DELTB*CBF
      CURP =(C(1,J+1)-C(1,J-1))/2.0/H
      PHIP =(C(2,J+1)-C(2,J-1))/2.0/H
      CAP  =(C(3,J+1)-C(3,J-1))/2.0/H
      CBP  =(C(4,J+1)-C(4,J-1))/2.0/H
      VELP =(C(5,J+1)-C(5,J-1))/2.0/H
      ZVELP=(Z(5,J+1)-Z(5,J-1))/2.0/H
      PHI1P=(C(6,J+1)-C(6,J-1))/2.0/H
      ZCURP=(Z(1,J+1)-Z(1,J-1))/2.0/H
      ZPHIP=(Z(2,J+1)-Z(2,J-1))/2.0/H
      ZCAP =(Z(3,J+1)-Z(3,J-1))/2.0/H
      ZCBP =(Z(4,J+1)-Z(4,J-1))/2.0/H
      CURPP=(C(1,J+1)+C(1,J-1)-2.0*C(1,J))/H/H
      CAPP =(C(3,J+1)+C(3,J-1)-2.0*C(3,J))/H/H
      CBPP =(C(4,J+1)+C(4,J-1)-2.0*C(4,J))/H/H
      ZCURPP=(Z(1,J+1)+Z(1,J-1)-2.0*Z(1,J))/H/H
      ZCAPP =(Z(3,J+1)+Z(3,J-1)-2.0*Z(3,J))/H/H
      ZCBPP =(Z(4,J+1)+Z(4,J-1)-2.0*Z(4,J))/H/H
      EPPC=(EP(J+1)-EP(J-1))/2.0/H
      ZEPPC=(ZEP(J+1)-ZEP(J-1))/2.0/H
      CAC=C(3,J)
      CBC=C(4,J)
      ZAC=Z(3,J)
      ZBC=Z(4,J)
      VELC=C(5,J)
      ZVEL=Z(5,J)
      QC=Q(J)
      QMC1=QM(J)
      QMNONC=QMNON(J)
      EPC=EP(J)
      ZEPC=ZEP(J)
      QMC=QMC1-QMNONC
      CALL EQUIL(CAC,CBC,EQCB,EQUIAB,EQCBP)
      CALL EQUIL(ZAC,ZBC,ZEQCB,ZEQUAB,ZEQCBP)
      CALL RKAY(DELT,EPC,QMC,QC,AMC,AMCUR,AMCA,RMC,RSC,RMCUR,RSCUR,
     1 RMCA,RSCA)
      DELTA=-DEL*RSC
      DELTB=DEL*RSC*EQCBP
      CMD=CSTAR-OSTAR
      APB=ASTA +BSTAR
      CALL SDIF(CAC,CBC,DIFA,DIFB,DIFAA,DIFAB,DIFBA,DIFBB)
      CALL SDIF(ZAC,ZBC,ZDIFA,ZDIFB,ZDIFAA,ZDIFAB,ZDIFBA,ZDIFBB)
      CALL 3DIFP(CAC,CBC,DIFAAA,DIFABA,DIFABB,DIFBAA,DIFBAB,DIFBBB)
      EPT=EPC**TOR
      ZEPT=ZEPC**TOR
      TR2=T2R*CAC/C0A
      TR3=1.0-TR1-TR2
      Q1=DIFA*EPT*CAPP
      Q2= EPT*CAP*CAP
      Q3= EPT*CAP*CBP
      Q4= (1.0+TOR)*EPT*DIFA*CAP/EPC
      Q5=(-TR2+S2)/2.0/F/EPC-CAC*QSTAR/EPC
      Q6=(SS2-CAC*QSTAR)*(VELC+ASA*CURP)/CMD/EPC
      ZQ1=ZDIFA*ZEPT*ZCAPP
      ZQ2=ZEPT*ZCAP*ZCAP
```

```
      ZQ3= ZEPT*ZCAP*ZCBP
      ZQ4=(1.0+TOR)*ZEPT*ZDIFA*ZCAP/ZEPC
      ZQ5=(-TR2+S2)/2.0/F/ZEPC-ZAC *BSTAR/ZEPC
      ZQ6=(SS2-ZAC*DSTAR)*(ZVELP+APB*ZCURP)/CMD/ZEPC
      Q7=VELC*CAP/EPC+TOR*Q1+(TOR-1.0)*EPPC*Q4+CURP*Q5+ Q6
     1 +TOR*Q2*DIFA*DIFAA +TOR*Q3*DIFA*DIFAB
      QIP=DELTI*Q7/EPC
      QCAP=-VELC/EPC      +EPT*DIFA*(CAP*DIFAA+CBP*DIFAB)
      QCA=DELTA*Q7/EPC+DIFAA*(Q1+EPPC*Q4)+(VELP+APB*CURP)*DSTAR/CMD/EPC
     1 +Q2*DIFAAA+Q3*DIFABA+BSTAR*CURP/EPC
      QCB= DELTB*Q7/EPC+DIFAB*(Q1+EPPC*Q4)
     1+Q2*DIFABA+Q3*DIFABB
      QVEY=(SS2-CAC*DSTAR)/CMD/EPC
      ZQVEY=(SS2-ZAC*DSTAR)/CMD/ZEPC
      A(3,1)=-(Q5+QVEY*APB-QIP)/4.0/H
      D(3,1)=+(Q5+QVEY*APB-QIP)/4.0/H
      Q8=QCAP+EPT*DIFA*(1.0+TOR)*EPPC/EPC
      A(3,3)= -0.5*DIFA*EPT/H/H+Q8/4.0/H+0.5/DELT-QCA/4.0
      D(3,3)= -0.5*DIFA*EPT/H/H-Q8/4.0/H +0.5/DELT-QCA/4.0
      B(3,3)=DIFA*EPT/H/H
      A(3,4)=-QCB/4.0
      D(3,4)=-QCB/4.0
      A(3,5)= -QVEY/4.0/H+CAP/EPC/4.0
      D(3,5)= QVEY/4.0/H+CAP/EPC/4.0
      G(3)=ZAC/DELT    +0.5*(-ZCAP*ZVEL/ZEPC+ZQ1+(ZQ2*ZDIFAA+ZQ3*
     1 ZDIFAB)*ZDIFA+ZEPPC*ZQ4   -ZCURP*ZQ5-ZQVEY*(ZVELP+APB*ZCURP)
     2 -QIP*CURP-QCA*CAC-QCB*CBC+CAP*VELC/EPC)
      R1= DIFB*EPT*CBPP
      R2=EPT*CBP*CBP
      R3=EPT*CAP*CBP
      R4=(1.0+TOR)*EPT*DIFB*CBP/EPC
      R5=(-TR3/F+0.5*S3/F-CBC*BSTAR)/EPC
      R6=(SS3-CBC*DSTAR)*(VELP+APB*CURP)/CMD/EPC
      R7=VELC*CBP/EPC  +TOR*R1+(TOR-1.0)*EPPC*R4+CURP*R5+R6
     1 +TOR*R3*DIFB*DIFBA+TOR*R2*DIFB*DIFBB
      RIP=DELTI*R7/EPC
      RCA=DELTA*R7/EPC  +DIFBA*(R1+EPPC*R4)
     1 +R2*DIFBAB+R3*DIFBAA
      RCBP=-VELC/EPC      +EPT*DIFB*(DIFBA*CAP+DIFBB*CBP)
      RCB= DELTB*R7/EPC+DIFBB*(R1+EPPC*R4)+DSTAR*(VELP+APB*CURP)/CMD/EPC
     1+R2*DIFBBB+R3*DIFBAB+BSTAR*CURP/EPC
      ZR1= ZDIFB*ZEPT*ZCBPP
      ZR2=ZEPT*ZCBP*ZCBP
      ZR3=ZEPT*ZCAP*ZCBP
      ZR4=(1.0+TOR)*ZEPT*ZDIFB*ZCBP/ZEPC
      ZR5=(-TR3/F+S3/2.0/F-ZBC*BSTAR)/ZEPC
      ZR6=(SS3-ZBC*DSTAR)*(ZVELP+APB*ZCURP)/CMD/ZEPC
      RVEY=(SS3-CBC*DSTAR)/CMD/EPC
      ZRVEY=(SS3-ZBC*DSTAR)/CMD/ZEPC
      A(4,1)=-(R5+RVEY*APB-RIP)/4.0/H
      D(4,1)=+(R5+RVEY*APB-RIP)/4.0/H
      A(4,3)=-RCA/4.0
      D(4,3)=-RCA/4.0
      A(4,4)=-0.5*DIFB*EPT/H/H +R5/4.0/H-RCB/4.0 +0.5/DELT
      D(4,4)=-0.5*DIFB*EPT/H/H -R5/4.0/H-RCB/4.0 +0.5/DELT
      B(4,4)=DIFB*EPT/H/H
      R8=RCBP+(1.0+TOR)*EPT*DIFB*EPPC/EPC
      A(4,5)= -RVEY/4.0/H+CBP/EPC/4.0
      D(4,5)= RVEY/4.0/H+CBP/EPC/4.0
      G(4)= ZBC/DELT   +0.5*(-ZCBP*ZVEL/ZEPC+ZR1+(ZR2*ZDIFBB+
     1ZR3*ZDIFBA)*ZDIFB+ZEPPC   *ZR4-ZCURP*ZR5-ZRVEY*(ZVELP+APB*ZCURP)
     2 -RIP*CURP-RCA*CAC-RCB*CBC+CBP*VELC/EPC)


 44   CONTINUE
      CURB =0.5*(C(1,J)+C(1,J-1))
      PHIB =0.5*(C(2,J)+C(2,J-1))
      CAB  =0.5*(C(3,J)+C(3,J-1))
      CBB  =0.5*(C(4,J)+C(4,J-1))
      VELB =0.5*(C(5,J)+C(5,J-1))
      PHI1B=0.5*(C(6,J)+C(6,J-1))
      CURPB=(C(1,J)-C(1,J-1))/H
      PHI1PB=(C(6,J)-C(6,J-1))/H
      QMB1=(QM(J)+QM(J-1))/2.0
      QMNONB=(QMNON(J)+QMNON(J-1))/2.0
```

```
      QMB=QMB1-QMNONB
      QR=(Q(J)+Q(J-1))/2.0
      EPB=(EP(J)+EP(J-1))/2.0
      CALL EQUIL(CAB,CBB,EQCB,EQUIAB,EQCBP)
      CALL RKAY(DELT,EPB,QMB,Q3,AMB,AMCUR,AMCA,RMB,RSB,RMDI,RSDI,
     1 RMCA,RSCA)
      AMCB=-AMCA*EQCBP
      RMCB=-RMCA*EQCBP
      RSCB=-RSCA*EQCBP
      DELTA=-DEL*RSB
      DELTB=DEL*RSB*EQCBP
      AMET(J)=AMB
      IF(TIME.GT.TMI) GO TO 35
      AEPN=DEXP(ALPHA*(PHI(I)-PHI(I-1))*F/R/T)
      CEPN=DEXP(-ALPHC*(PHI(I)-PHI(I-1))*F/R/T)
      EXR=AEPN-CEPN
      EXPO=(ALPHA*AEPN+ALPHC*CEPN)*F/R/T
      G4=FIO*(CAB/C0A)**GAM*(CBB/C0B)**ZETA
      A(2,1)=-1.0/H
      B(2,1)= 1.0/H
      A(2,2)= AMB*G4 *EXPO/2.0
      B(2,2)= AMB*G4 *EXPO/2.0
      A(2,6)=-AMB*G4 *EXPO/2.0
      B(2,6)=-AMB*G4 *EXPO/2.0
      G(2)=AMB*G4 *(EXR-EXPO*PHI(I)+EXPO*PHI(I-1))
      GO TO 43
   35 CONTINUE
      ROMB=RMB*RCMO/RMO
      ROMCUR=RMDI
      ROMCA=RMCA
      ROMCB=RMCB
      IF(CAB.LE.CALML) CAB=CALML
      IF(CBB.LE.CALML) CBB=CALML
      ASAK=1.0-S2*CURPB/EN/F/CAB/RMB
      BSBK=1.0-S3*CURPB/EN/F/CBB/ROMB
      ASAKM2=S2/EN/F/CAB/RMB
      BSBKM2=S3/EN/F/CBB/ROMB
      ASAKM1=ASAKM2*CURPB
      BSBKM1=BSBKM2*CURPB
      IF(ASAK.LE.CALML) ASAK=CALML
      IF(BSBK.LE.CALML) BSBK=CALML
      IF(ASAK.GE.CALMH) ASAK=CALMH
      IF(BSBK.GE.CALMH) BSBK=CALMH
      CAS(J)=ASAK
      CRATIO(J)=ASAK/BSBK
      CRATIO(1)=CRATIO(2)
      CAAV=(ASAK*CAB+CAB)/2.0
      CBAV=(BSBK*CBB+CBB)/2.0
      CALL SACTIV(CAAV,CBAV,ACTA,ACTB,YA,YB,YAA,YAB,YBA,YBB)
      TR2=T2R*CAB/C0A
      TR3=1.0-T1R-TR2
      ZZETA=1.5*(1.0+TR2)*YA
      ZZETB=-(4.0-2.0*TR3)*YB
      IF(JP.EQ.2) GO TO 45
      ZZETA=1.5*(1.0+TR2)
      ZZETB=-(4.0-2.0*TR3)
      IF(JP.EQ.1) GO TO 45
      ZZETA=0
      ZZETB=0
   45 CONTINUE
      ZETAA=GAM -ALPHA*ZZETA
      ZETBA=ZETA-ALPHA*ZZETB
      ZETAC=GAM +ALPHC*ZZETA
      ZETBC=ZETA+ALPHC*ZZETB
      CAAM1=ASAK**(ZETAA-1.0)
      CBAM1=BSBK**(ZETBA-1.0)
      CACM1=ASAK**(ZETAC-1.0)
      CBCM1=BSBK**(ZETBC-1.0)
      CONAA=ASAK*CAAM1
      CONBA=BSBK*CBAM1
      CONAC=ASAK*CACM1
      CONBC=BSBK*CBCM1
      EXPONA=DEXP(ALPHA*F*(PHI(I)-PHI(I-1))/R/T)
      EXPONC=DEXP(-ALPHC*F*(PHI(I)-PHI(I-1))/R/T)
      EXPO=CONAA*CONBA*EXPONA-CONAC*CONBC*EXPONC
      CZNM1=(CAB/C0A)**(GAM-1.0)
      COHM1=(CBB/C0B)**(ZETA-1.0)
      CZN=CZNM1*CAB/C0A
      COH=COHM1*CBB/C0B
```

```
      PREXPA=AMB*FIO*CZN*COHM1
      PREXPB=AMB*FIO*COH*CZNM1
      PREXPO=AMB*FIO*CZN*COH
      PANOD=PREXPO*CAAM1*COAM1*EXPONA
      PCATD=PREXPO*CACM1*COCM1*EXPONC
      BPHI=PREXPO*(ALPHA*CONAA*CONBA*EXPONA
     1 +ALPHC*CONAC*CONBC*EXPONC)*F/R/T
      BANI=(PANOD*ZETAA-PCATD*ZETAC)*BSBK
      BCTI=(PANOD*ZETBA-PCATD*ZETHC)*ASAK
      GI1=PREXPO*EXPO*AMCUR/AMB+BANI*ASAKM2*(-1.0+CURPB*RMDI)
     1 +BCTI*BSBKM2*(-1.0+CURPB*ROHCUR)
      GA2=PREXPO*EXPO*AMCA/AMB+PREXPB*EXPO*GAM/COA
     1 +BANI*ASAKMI*(1.0/CAB+RMCA)+BCTI*BSBKMI*ROHCA
      GB3=PREXPO*EXPO*AMCB/AMB+PREXPA*EXPO*ZETA/COB
     1 +BANI*ASAKMI*RMCB +BCTI*BSBKMI*(1.0/CBB+ROHCB)
      A(2,1)=-1.0/H+GI1/H
      B(2,1)=-A(2,1)
      A(2,2)=BPHI/2.0
      B(2,2)=BPHI/2.0
      A(2,3)=-GA2/2.0
      B(2,3)=-GA2/2.0
      A(2,4)=-GB3/2.0
      B(2,4)=-GB3/2.0
      A(2,6)=-BPHI/2.0
      B(2,6)=-BPHI/2.0
      G(2)=PREXPO*EXPO-BPHI*PHI18+BPHI*PHIB-GI1*CURPB-GA2*CAB-GB3*CBB
 43   CONTINUE
      TI=RSB*(CSTAR-OSTAR)
      T2=TI*EQUIAB
      TR2=T2R*CAB/COA
      TR3=1.0-TR2-TR1
      ZCURPB=(Z(I,J)-Z(I,J-1))/H
      CALL SIGMA(EPGI,EPB,QMB,QB,SGZN,SGZNO,SIGMI)
      IF(TIME.GT.TMI) GO TO 47
      A(5,1)= -(ASTA +BSTAR)/H
      B(5,1)=-A(5,1)
      A(5,5)=-1.0/H
      B(5,5)=1.0/H
      G(5)=T2
      A(6,1)=-0.5
      B(6,1)= -0.5
      A(6,6)= -(1.0-EPB)*SIGMI/H
      B(6,6)= -A(6,6)
      G(6)= -FITOT
      GO TO 49
 47   CONTINUE
      A(5,1)= -(ASTA +BSTAR)/H + T2*RSDI/H
      B(5,1)=-A(5,1)
      A(5,3)=-0.5*TI-0.5*T2*RSCA
      B(5,3)= A(5,3)
      A(5,4)=0.5*TI*EQCBP-0.5*T2*RSCB
      B(5,4)= A(5,4)
      A(5,5)=-1.0/H
      B(5,5)=1.0/H
      G(5)=T2-TI*CAB+TI*EQCBO*CBB-T2*(RSCA*CAB+RSCB*CBB)-T2*RSDI*CURPB
      A(6,1)=-0.5-SGZN*(-DELTI)*PHIIPB*(1.0-EPB)/H+SIGMI*PHIIPB*DELTI/H
      B(6,1)=-0.5+SGZN*(-DELTI)*PHIIPB*(1.0-EPB)/H-SIGMI*PHIIPB*DELTI/H
      A(6,3)=0.5*SGZNO*(-DELTA)*PHIIPB*(1.0-EPB)-0.5*SIGMI*PHIIPB*DELTA
      B(6,3)= A(6,3)
      A(6,4)=0.5*SGZNO*(-DELTB)*PHIIPB*(1.0-EPB)-0.5*SIGMI*PHIIPB*DELTB
      B(6,4)= A(6,4)
      A(6,6)=-SIGMI*(1.0-EPB)/H
      B(6,6)= SIGMI*(1.0-EPB)/H
      G(6)= -FITOT+PHIIPB*(SGZN*(-DELTI)*CURPB +SGZNO*(-DELTA)*CAB
     1 +SGZNO*(-DELTB)*CBB)*(1.0-EPB)-SIGMI*PHIIPB*(DELTI*CURPB+DELTA*
     2 CAB+DELTB*CBB)
 49   CONTINUE
      CALL BAND(J)
      GO TO 15

  PROGRAM FOR J=NJ
 50   CONTINUE
      B(1,1)=1.0
      G(1)= FITOT
      CURB =0.5*(C(1,J)+C(1,J-1))
      PHIB =0.5*(C(2,J)+C(2,J-1))
      CAB  =0.5*(C(3,J)+C(3,J-1))
      CBB  =0.5*(C(4,J)+C(4,J-1))
      VELB =0.5*(C(5,J)+C(5,J-1))
```

```
      PHI1B=0.5*(C(6,J)+C(6,J-1))
      CURPB=(C(1,J)-C(1,J-1))/H
      PHI1PB=(C(6,J)-C(6,J-1))/H
      QB=(Q(J)+Q(J-1))/2.0
      EPB=(EP(J)+EP(J-1))/2.0
      QMB1=(QM(J)+QM(J-1))/2.0
      QMNONB=(QMNON(J)+QMNON(J-1))/2.0
      QMB=QMB1-QMNONB
      CALL EQUIL(CAB,CBB,EQCB,EQUIAB,EQCBP)
      CALL RKAY(DELT,EPB,QMB,QB,AMB,AMCUR,AMCA,RMB,RSB,RMDI,RSDI,
     1 RMCA,RSCA)
      AMCB=-AMCA*EQCBP
      RMCB=-RMCA*EQCBP
      RSCB=-RSCA*EQCBP
      DELTA=-DEL*RSB
      DELTA=DEL*RSB*EQCBP
      AMET(J)=AMB
      IF(TIME.GT.TMI) GO TO 36
      AEPN=DEXP(ALPHA*(PHI1B-PHI1)*F/R/T)
      CEPN=DEXP(-ALPHC*(PHI1B-PHI1)*F/R/T)
      EXR=AEPN-CEPN
      EXPO=(ALPHA*AEPN+ALPHC*CEPN)*F/R/T
      G4=F10*(CAB/C0A)**GAM*(CBB/C0B)**ZETA
      A(2,1)=-1.0/H
      B(2,1)= 1.0/H
      A(2,2)= AMB*G4 *EXPO/2.0
      B(2,2)= AMB*G4 *EXPO/2.0
      A(2,6)=-AMB*G4 *EXPO/2.0
      B(2,6)=-AMB*G4 *EXPO/2.0
      G(2)=AMB*G4 *(EXR-EXPO*PHI1B+EXPO*PHIB)
      GO TO 60
36    CONTINUE
      ROHB=RMB*RCHO/RMO
      ROHCUR=RMDI
      ROHCA=RMCA
      ROHCB=RMCB
      IF(CAB.LE.CALML) CAB=CALML
      IF(CBB.LE.CALML) CBB=CALML
      ASAK=1.0-S2*CURPB/EN/F/CAB/RMB
      BSBK=1.0-S3*CURPB/EN/F/CBB/ROHB
      IF(ASAK.LE.CALML) ASAK=CALML
      IF(BSBK.LE.CALML) BSBK=CALML
      IF(BSBK.GE.CALMH) BSBK=CALMH
      IF(ASAK.GE.CALMH) ASAK=CALMH
      CAS(J)=ASAK
      CRATIO(J)=ASAK/BSBK
      ASAKM2=S2/EN/F/CAB/RMB
      BSBKM2=S3/EN/F/CBB/ROHB
      ASAKM1=ASAKM2*CURPB
      BSBKM1=BSBKM2*CURPB
      CAAV=(ASAK*CAB+CAB)/2.0
      CBAV=(BSBK*CBB+CBB)/2.0
      CALL SACTIV(CAAV,CBAV,ACTA,ACTB,YA,YB,YAA,YAB,YBA,YBB)
      TR2=T2R*CAB/C0A
      TR3=1.0-T1R-TR2
      ZZETA=1.5*(1.0+TR2)*YA
      ZZETB=-(4.0-2.0*TR3)*YB
      IF(JP.EQ.2) GO TO 55
      ZZETA=1.5*(1.0+TR2)
      ZZETB=-(4.0-2.0*TR3)
      IF(JP.EQ.1) GO TO 55
      ZZETA=0
      ZZETB=0
55    CONTINUE
      ZETAA=GAM -ALPHA*ZZETA
      ZETBA=ZETA-ALPHA*ZZETB
      ZETAC=GAM +ALPHC*ZZETA
      ZETBC=ZETA+ALPHC*ZZETB
      CAAM1=ASAK**(ZETAA-1.0)
      CBAM1=BSBK**(ZETBA-1.0)
      CACM1=ASAK**(ZETAC-1.0)
      CBCM1=BSBK**(ZETBC-1.0)
      CONAA=ASAK*CAAM1
      CONBA=BSBK*CBAM1
      CONAC=ASAK*CACM1
      CONBC=BSBK*CBCM1
      EXPONA=DEXP(ALPHA*F*(PHI1B-PHIB)/R/T)
      EXPONC=DEXP(-ALPHC*F*(PHI1B-PHIB)/R/T)
```

```
      EXPO=CONAA*CONBA*EXPONA-CONAC*CONBC*EXPONC
      CZNM1=(CAB/C0A)**(GAM-1.0)
      COHM1=(CBB/C0B)**(ZETA-1.0)
      CZN=CZNM1*CAB/C0A
      COH=COHM1*CBB/C0B
      PREXPA=AMB*FIO*CZN*COHM1
      PREXPB=AMB*FIO*COH*CZNM1
      PREXPO=AMB*FIO*CZN*COH
      PANOD=PREXPO*CAAM1*C3AM1*EXPONA
      PCATD=PREXPO*CACM1*C4CM1*EXPONC
      BPHI=PREXPO*(ALPHA*CONAA*CONBA*EXPONA
     1  +ALPHC*CONAC*CONBC*EXPONC)*F/R/T
      BAN1=(PANOD*ZETAA-PCATD*ZETAC)*BSSK
      BCT1=(PANOD*ZETBA-PCATD*ZETBC)*ASAK
      GI1=PREXPO*EXPO*AMCUR/AMB+BAN1*ASAKM2*(-1.0+CURPB*RMDI)
     1  +BCT1*BSBKM2*(-1.0+CURPB*ROHCUR)
      GA2=PREXPO*EXPO*AMCA/AMB+PREXPB*EXPO*GAM/C0A
     1  +BAN1*ASAKM1*(1.0/CAB+RMCA)+BCT1*BSAKM1*ROHCA
      GB3=PREXPO*EXPO*AMCB/AMB+PREXPA*EXPO*ZETA/C0B
     1  +BAN1*ASAKM1*RMCB +BCT1*BSBKM1*(1.0/CBB+ROHCB)
      A(2,1)=-1.0/H+GI1/H
      B(2,1)=-A(2,1)
      A(2,2)=BPHI/2.0
      B(2,2)=BPHI/2.0
      A(2,3)=-GA2/2.0
      B(2,3)=-GA2/2.0
      A(2,4)=-GB3/2.0
      B(2,4)=-GB3/2.0
      A(2,6)=-BPHI/2.0
      B(2,6)=-BPHI/2.0
      G(2)=PREXPO*EXPO-BPHI*PHI1B+BPHI*PHIB-GI1*CURPB-GA2*CAB-GB3*CBB
60    CONTINUE
      T1=RSB*(CSTAR-DSTAR)
      T2=T1*EQUIAB
      TR2=T2R*CAB/C0A
      TR3=1.0-TR2-TR1
      ZCURPB=(Z(I,J)-Z(I,J-1))/H
      CALL SIGMA(EPGI,EPB,AMB,QB,SGZN,SGZNO,SIGMI)
      IF(TIME.GT.TMI) GO TO 53
      B(3,3)=1.0
      B(4,4)=1.0
      G(3)=CAINT
      G(4)=CBINT
      A(5,1)= -(ASTA +BSTAR)/H
      B(5,1)= -A(5,1)
      B(5,5)=1.0/H
      A(5,5)=-1.0/H
      G(5)=T2
      A(6,1)=-0.5
      B(6,1)= -0.5
      A(6,6)= -(1.0-EPB)*SIGMI/H
      B(6,6)= -A(6,6)
      G(6)= -FITOT
      GO TO 52
53    CONTINUE
      A(5,1)= -(ASTA +BSTAR)/H + T2*RSDI/H
      B(5,1)=-A(5,1)
      A(5,3)=-0.5*T1-0.5*T2*RSCA
      B(5,3)= A(5,3)
      A(5,4)=0.5*T1*EQCBP-0.5*T2*RSCB
      B(5,4)= A(5,4)
      A(5,5)=-1.0/H
      B(5,5)=1.0/H
      G(5)=T2-T1*CAB+T1*EQCBP*CBB-T2*(RSCA*CAB+RSCB*CBB)-T2*RSDI*CURPB
      A(6,1)=-0.5-SGZN*(-DELTI)*PHI1PB*(1.0-EPB)/H+SIGMI*PHI1PB*DELTI/H
      B(6,1)=-0.5+SGZN*(-DELTI)*PHI1PB*(1.0-EPB)/H-SIGMI*PHI1PB*DELTI/H
      A(6,3)=0.5*SGZNO*(-DELTA)*PHI1PB*(1.0-EPB)-0.5*SIGMI*PHI1PB*DELTA
      B(6,3)= A(6,3)
      A(6,4)=0.5*SGZNO*(-DELTB)*PHI1PB*(1.0-EPB)-0.5*SIGMI*PHI1PB*DELTB
      B(6,4)= A(6,4)
      A(6,6)=-SIGMI*(1.0-EPB)/H
      B(6,6)= SIGMI*(1.0-EPB)/H
      G(6)= -FITOT+PHI1PB*(SGZN*(-DELTI)*CURPB +SGZNO*(-DELTA)*CAB
     1 +SGZNO*(-DELTB)*CBB)*(1.0-EPB)-SIGMI*PHI1PB*(DELTI*CURPB+DELTA*
     2 CAB+DELTB*CBB)
      CALL SDIF(C(3,J),C(4,J),DIFA,DIFB,DIFAA,DIFAB,DIFBA,DIFBB)
      CALL SDIF(Z(3,J),Z(4,J),ZDIFA,ZDIFB,ZDIFAA,ZDIFAB,ZDIFBA,ZDIFBB)
      CALL EQUIL(C(3,J),C(4,J),EQCB,EQUIAB,EQCBP)
      QMM=QM(J)-QMNON(J)
```

```
      CALL RKAY(DELT,EP(J),QMM,Q(J),AM,AMCUR,AMCA,RM,RS(J),RMCUR,RSCUR
     1 ,RMCA,RSCA)
      DELTA=-DEL*RS(J)
      DELTB=DEL*RS(J)*EQCBP
      CAP=(3.0*C(3,J)-4.0*C(3,J-1)+C(3,J-2))/2.0/H
      CBP=(3.0*C(4,J)-4.0*C(4,J-1)+C(4,J-2))/2.0/H
      ZCAP=(3.0*Z(3,J)-4.0*Z(3,J-1)+Z(3,J-2))/2.0/H
      ZCBP=(3.0*Z(4,J)-4.0*Z(4,J-1)+Z(4,J-2))/2.0/H
      CURP=(3.0*C(1,J)-4.0*C(1,J-1)+C(1,J-2))/2.0/H
      EPT=EP(J)**TOR
      ZEPT=ZEP(J)**TOR
      Q4=(1.0+TOR)*EPT*DIFA*CAP
      R4=(1.0+TOR)*EPT*DIFB*CBP
      IF(NBC.EQ.0) GO TO 82
      C3NJ=C(3,NJ)
      C4NJ=C(4,NJ)
      IF(L.EQ.1) VELMEM=VELM
      IF(L.EQ.2) VELMEM=-VELM
      VELDIF=VELMEM-C(5,J)
      VELZIF=VELMEM-Z(5,J)
      TRN2D=TR2M-TR2
      TRN3D=TR3M-TR3
      IF(NBC.EQ.1) GO TO 85
      IF(NBC.EQ.2) TRN2D=0.0
      IF(NBC.GE.3) TRN3D=0.0
      IF(NBC.EQ.4) TRN2D=0.0
      GO TO 85
   82 CONTINUE
      C3NJ=0.0
      C4NJ=0.0
      VELDIF=0.0
      VELZIF=0.0
      TRN2D=0.0
      TRN3D=0.0
   85 CONTINUE
      Y(3,1)= Q4*DELTI/2.0/H
      A(3,1)=-Q4*DELTI*4.0/2.0/H
      B(3,1)= Q4*DELTI*3.0/2.0/H
      B(3,4)=EP(J)*EPT*CAP*DIFA*DIFAB+Q4*DELTB
      B(3,5)=-C3NJ
      Y(3,3)= EP(J)*EPT*DIFA/2.0/H
      A(3,3)=-EP(J)*EPT*DIFA*4.0/2.0/H
      B(3,3)= EP(J)*EPT*DIFA*3.0/2.0/H+2.0*VOLUME/DELT+DLAAM+VELDIF
     1       +EP(J)*EPT*CAP*DIFA*DIFAA+Q4*DELTA
      G(3)=2.0*VOLUME*Z(3,J)/DELT+2.0*TRN2D*FITOT/2.0/F+2.0*DLAAM*C0A
     1 -ZDIFA*ZEP(J)*ZEPT*ZCAP -(DLAAM+VELZIF      )*Z(3,J)
     2 +EP(J)*EPT*CAP*DIFA*(DIFAA*C(3,J)+DIFAB*C(4,J)) +Q4*(DELTI*
     3 CURP+DELTA*C(3,J)+DELTB*C(4,J)) -C3NJ*C(5,J)
      Y(4,1)= R4*DELTI/2.0/H
      A(4,1)=-4.0*R4*DELTI/2.0/H
      B(4,1)= 3.0*R4*DELTI/2.0/H
      B(4,3)=EP(J)*EPT*CBP*DIFB*DIFBA+R4*DELTA
      B(4,5)=-C4NJ
      Y(4,4)= EP(J)*EPT*DIFB/2.0/H
      A(4,4)=-EP(J)*EPT*DIFB*4.0/2.0/H
      B(4,4)= EP(J)*EPT*DIFB*3.0/2.0/H+2.0*VOLUME/DELT+DLBBM+VELDIF
     1       +EP(J)*EPT*CBP*DIFB*DIFBB +R4*DELTB
      G(4)=2.0*VOLUME*Z(4,J)/DELT +2.0*DLBBM*C0B-ZEP(J)*ZEPT*ZDIFB*ZCBP
     1 -(DLBBM+VELZIF      )*Z(4,J) +EP(J)*EPT*CBP*DIFB*(DIFBA*C(3,J)+
     2 DIFBB*C(4,J)) + R4*(DELTI*CURP+DELTA*C(3,J)+DELTB*C(4,J))
     3 -C4NJ*C(5,J)     +2.0*TRN3D*FITOT/F
   52 CONTINUE
      CALL BAND(J)
      IF(TIME.GT.TM1) GO TO 475
      DO 476 J=2,NJM1
  476 TRNCUR(J)=(C(1,J+1)-C(1,J-1))/(A0*2.0*H)
      TRNCUR(1)=(-C(1,3)+4.0*C(1,2)-3.0*C(1,1))/(A0*2.0*H)
      TRNCUR(NJ)=(C(1,NJM2)-4.0*C(1,NJM1)+3.0*C(1,NJ))/(A0*2.0*H)
      IF(JCOUNT.GT.20) GO TO 59
      DO 479 I=1,N
      DO 479 J=2,NJM1
      IF(DABS(C(I,J)).LT.1.0D-10) GO TO 479
      IF(DABS(C(I,J)-CI(I,J)).GT.1.0D-5*DABS(C(I,J))) GO TO 8
  479 CONTINUE
      GO TO 59
  475 CONTINUE
      DO 71 J=1,NJ
      CALL EQUIL(C(3,J),C(4,J),EQCB,EQUL(J),EQCBP)
   71 CONTINUE
      DO 72 J=1,NJ
      QMM=Q4(J)-QMNON(J)
      CALL EQUIL(C(3,J),C(4,J),EQCB,EQUIAB,EQCBP)
```

```
      CALL RKAY(DELT,EP(J),QMM,Q(J),AM,AMCUR,AMCA,RM,RS(J),RMCUR,RSCUR,
     1 RMCA,RSCA)
      AMET(J)=AM
72    CONTINUE
      QDELI=ASTA*DELT/2.0
      QDEL=CSTAR*DELT/2.0
      DO 70 J=2,NJM1
      CURP =(C(1,J+1)-C(1,J-1))/2.0/H
      ZCURP=(Z(1,J+1)-Z(1,J-1))/2.0/H
      CALL EQUIL(Z(3,J),Z(4,J),ZEQCB,ZEQUAB,ZEQCBP)
      QM(J)=ZQM(J)-QDELI*(CURP+ZCURP)
      Q(J)=ZQ(J)+QDEL*(RS(J)*EQUL(J)+ZRS(J)*ZEQUAB)
      EP(J)=ZEP(J)+QDELI*(CURP+ZCURP)-QDEL*(RS(J)*EQUL(J)+ZRS(J)*ZEQUAB)
70    CONTINUE
      CURF=(-C(1,3)+4.0*C(1,2)-3.0*C(1,1))/2.0/H
      ZCURF=(-Z(1,3)+4.0*Z(1,2)-3.0*Z(1,1))/2.0/H
      CALL EQUIL(Z(3,1),Z(4,1),ZEQCB,ZEQUAB,ZEQCBP)
      QM(1)=ZQM(1)-QDELI*(CURF+ZCURF)
      Q(1)=ZQ(1)+QDEL*(RS(1)*EQUL(1)+ZRS(1)*ZEQUAB)
      EP(1)=ZEP(1)+QDELI*(CURF+ZCURF)-QDEL*(RS(1)*EQUL(1)+ZRS(1)*ZEQUAB)
      CURB=(C(1,NJM2)-4.0*C(1,NJM1)+3.0*C(1,NJ))/2.0/H
      ZCURB=(Z(1,NJM2)-4.0*Z(1,NJM1)+3.0*Z(1,NJ))/2.0/H
      CALL EQUIL(Z(3,NJ),Z(4,NJ),ZEQCB,ZEQUAB,ZEQCBP)
      QM(NJ)=ZQM(NJ)-QDELI*(CURB+ZCURB)
      Q(NJ)=ZQ(NJ)+QDEL*(RS(NJ)*EQUL(NJ)+ZRS(NJ)*ZEQUAB)
      EP(NJ)=ZEP(NJ)+QDELI*(CURB+ZCURB)-QDEL*(RS(NJ)*EQUL(NJ)+ZRS(NJ)*
     1 ZEQUAB)
      DO 73 J=1,NJ
      IF(QM(J).LE.0.0) QM(J)=0.0
      IF(Q(J).LE.0.0) Q(J)=0.0
      EP(J)=1.0-QM(J)-Q(J)-EPGI
73    CONTINUE
      IF(JPLG.EQ.0) GO TO 96
      IF(JPLG.EQ.1) GO TO 93
      MEP=0
      DO 92 J=1,NJ
      IF(Q(J).GE.ESPLG)MEP=MEP+1
      IF(MEP.EQ.1) NJMIN=J
92    CONTINUE
      NJMAX=NJMIN+MEP-1
      IF(MEP.LE.NJDMN)GO TO 96
      IF(MEP.GE.NJDMX) GO TO 96
      CALL SWELL(NJMIN,NJMAX)
      GO TO 96
93    CONTINUE
      MEP=0
      DO 94 J=1,NJ
      IF(EP(J).LE.EPLGMN) MEP=MEP+1
94    CONTINUE
      IF(MEP.EQ.0) GO TO 96
      IF(MEP.GE.NJDELT) GO TO 96
      DO 95 J=1,NJ
      IF(EP(J).GT.EPLGMN) GO TO 95
      EP(J)=EPLGMN
      Q(J)=1.0-QM(J)-EP(J)-EPGI
95    CONTINUE
96    CONTINUE
      DO 97 J=1,NJ
      QMMAX=QM(J)+Q(J)*VM/VS
      QMPLG=QM(J)-EP(J)*VM/(VS-VM)
      IF(QMPLG.LE.0.0) QMPLG=0.0
      QMCOV=DJS*(QMMAX-QMPLG)
      QMNON(J)=QMPLG+QMCOV
      QMM=QM(J)-QMNON(J)
      CALL EQUIL(C(3,J),C(4,J),EQCB,EQUL(J),EQCBP)
      CALL RKAY(DELT,EP(J),QMM,Q(J),AM,AMCUR,AMCA,RM,RS(J),RMCUR,RSCUR,
     1 RMCA,RSCA)
      AMET(J)=AM
97    CONTINUE
      DO 481 J=2,NJM1
      AREA(J)=A0*((1.0-EP(J))/(1.0-EPI))**(2.0/3.0)
      TRNCUR(J)=(C(1,J+1)-C(1,J-1))/(AREA(J)*2.0*H)
481   CONTINUE
      AREA(1)=A0*((1.0-EP(1))/(1.0-EPI))**(2.0/3.0)
      AREA(NJ)=A0*((1.0-EP(NJ))/(1.0-EPI))**(2.0/3.0)
      TRNCUR(1)=(-C(1,3)+4.0*C(1,2)-3.0*C(1,1))/(AREA(1)*2.0*H)
      TRNCUR(NJ)=(C(1,NJM2)-4.0*C(1,NJM1)+3.0*C(1,NJ))/(AREA(NJ)*2.0*H)
      IF(JCOUNT.LT.15) GO TO 54
      WRITE(6,202)
```

```
  202  FORMAT(/// 20X,' DID NOT CONVERGE'///)
       GO TO 59
   54  DO 58 I=1,N
       DO 58 J=2,NJM1
       IF(DABS(C(I,J)).LT.1.0D-9 ) GO TO 58
       CHECK=1.0D-5
       IF(DABS(C(I,J)-CI(I,J)).GT.CHECK *DABS(C(I,J))) GO TO 8
   58  CONTINUE
   59  CONTINUE
       DO 78 J=1,NJ
       CALL SACTIV(C(3,J),C(4,J),ACTA,ACTB,YA,YB,YAA,YAB,YBA,YBB)
       CALL SACTIV(C0A,C0B,ACTA0,ACTB0,YA,YB,YAA,YAB,YBA,YBB)
       RTNF=R*T/F/2.0
       OVERP(J)=C(6,1)-C(2,J)-RTNF*DLOG(ACTA0*ACTB**4/ACTA/ACTB0**4)
   78  CONTINUE
       CALL SACTIV(C(3,NJ),C(4,NJ),ACTAL,ACTBL,YA,YB,YAA,YAB,YBA,YBB)
       CALL SCOND(C0A,C0B,CONDO,CONDA,CONDB)
       OHMMEM=FITOT/CONMEM
       VOLTM=OHMMEM-RTNF*DLOG(ACTA0*ACTBL**4/ACTAL/ACTB0**4)
       OHMCT=OHMMEM+FITOT*FLCOUN/CONDO
       VOLTCT=VOLTM+FITOT*FLCOUN/CONDO
       DO 74 J=1,NJ
   74  CONVRN(J)=Q(J)/(VS*(QM(J)/VM + Q(J)/VS))
       PRINT 203,JCOUNT,TIME,DELT
  203  FORMAT(// 10X,'JCOUNT=',I5,20X,'TIME=',F15.5,20X,'DELT=',F10.5//)
       PRINT 248
  248  FORMAT(7X,'CURRENT',7X,'PHI-2',12X,'C-ZINC',12X,'C-KOH',12X,
      1 'VEL',12X,'PHI-M',12X,'CONVRN',12X,'OVERP'/)
       DO 57 J=1,NJ
       PRINT 208,C(1,J),C(2,J),C(3,J),C(4,J),C(5,J),C(6,J),CONVRN(J)
      1 ,OVERP(J)
   57  CONTINUE
  208  FORMAT(8D16.7)
       PRINT 207
  207  FORMAT(/1H ,8X,'POROSITY',10X,' QM',11X,'CHARGE',11X,'TRN CUR',
      112X,'CAS',17X,'RS',10X,'AM   ',11X,'EQUL'/)
       CAS(1)=CAS(2)
       DO 75 J=1,NJ
       PRINT 209,EP(J),QM(J),Q(J),TRNCUR(J),CAS(J),RS(J),AMET(J),EQUL(J)
  209  FORMAT(7D17.7,1D13.4)
   75  CONTINUE
       SUM1=0.0
       SUM2=0.0
       SUM3=0.0
       SUM4=0.0
       SUM5=0.0
       SUM6=0.0
       DO 88 J=1,NJ
       SUM1=SUM1+EP(J)
       SUM2=SUM2+QM(J)
       SUM3=SUM3+Q(J)
       SUM4=SUM4+C(3,J)
       SUM5=SUM5+C(4,J)
       SUM6=SUM6+CONVRN(J)
   88  CONTINUE
       DFNJ=DFLOAT(NJ)
       SUM1=SUM1/DFNJ
       SUM2=SUM2/DFNJ
       SUM3=SUM3/DFNJ
       SUM4=SUM4/DFNJ
       SUM5=SUM5/DFNJ
       SUM6=SUM6/DFNJ
       PRINT 206,OVERP(1),OVERP(NJ),OHMMEM,OHMCT,VOLTM,VOLTCT
  206  FORMAT(/' PB=',D16.7,2X,'PF=',D16.7,2X,'MOHM',D16.7,2X,'COHM',
      1 D16.7,2X,'MTOT',D16.7,2X,'CTOT',D16.7/)
       PRINT 87,SUM1,SUM2,SUM3,SUM4,SUM5,SUM6
   87  FORMAT(/' EP=',D16.7,2X,'QM=',D16.7,2X,'Q=',D16.7,2X,'CA=',D16.7,
      1 2X,'CB=',D16.7,3X,'CONV=',D16.7/)
       IF(TIME.GT.TLIM) GO TO 63
       IF(DABS(C(2,NJ)).GT.POTLIM) GO TO 990
       NPOT=0
       DO 61 J=1,NJ
   61  IF(C(2,J).GT.0.0) NPOT=NPOT+1
       IF(NPOT.GE.NJM1) GO TO 63
       IF(NPOT.LE.1) GO TO 63
       TM=TIME-TDEL
       PRINT 62,TM
   62  FORMAT(// 10X,'OSCILLATION AT TIME=',F20.10//)
       IF(NSTOP.EQ.0) GO TO 63
       GO TO 998
   63  CONTINUE
       IF(TIME.GT.(TLIM+TSTOP)) GO TO 980
       DELT=TDEL
```

```
      NTM1=NT-1
      IF(NTI.LT.NTM1) DELT=TDEL/2.0**(NT-NTI)
      IF(NTI.EQ.NTM1) DELT=TDEL-TIME
      NTI=NTI+1
      IF(TIME.GT.(TLIM-TDEL)) GO TO 999
      TIME=TIME+DELT
      GO TO 2
  999 CONTINUE
      IF(NCYCLM.EQ.0) GO TO 990
      DO 129 J=1,NJ
      C(1,J)=0.0
      C(3,J)=SUM4
      C(4,J)=SUM5
  129  CONTINUE
      FITOT=0.0
      IF(TIME.GT.(TLIM+TSTOP)) GO TO 988
      TIME=TIME+DELT
      GO TO 2
  988 CONTINUE
      IF(NCYC.GE.NCYCLM) GO TO 990
      L=L+1
      IF(L.EQ.3) L=1
      TIME=0.0
      NTI=0
      DELT=TDEL/2.0**(NT-NTI)
      IF(NCYCLM.EQ.0) GO TO 990
      NCYC=NCYC+1
      IF(L.EQ.1) FITOT=CITOT
      IF(L.EQ.2) FITOT=-CITOT
      IF(L.EQ.1) PRINT 132,TIME
      IF(L.EQ.2) PRINT 131,TIME
  131 FORMAT(//1H ,20X,'THIS IS FOR CATHODIC STARTING TIME=',F10.5//)
  132 FORMAT(//1H ,20X,'THIS IS FOR ANODIC   STARTING TIME=',F10.5//)
      IF(L.EQ.2) GO TO 6
      GO TO 4
  990 CONTINUE
      IF(LPUN.EQ.0) GO TO 998
      DO 99 J=1,NJ,LPUN
      WRITE(7,103) C(1,J),C(2,J),C(3,J),C(4,J),C(5,J)
      WRITE(7,103) C(6,J),EP(J),QM(J),Q(J),RS(J)
   99 CONTINUE
      WRITE(7,103)(QMNON(J),J=1,NJ,LPUN)
      WRITE(7,103)(EQUL(J),J=1,NJ,LPUN)
      WRITE(7,204) TIME,DELT,TLIM,NTI
      WRITE(7,103) SUM4,SUM5
  998 STOP
      END
C
C
C
      SUBROUTINE BAND(J)
      IMPLICIT REAL*8(A-H,O-Z)
      DIMENSION A(6,6),B(6,6),C(5,93),D(6,13),G(6),X(6,6),Y(6,6),
     1 E(6,7,93)
      COMMON/WORKA/A,B,D,G,X,Y
      COMMON/WORKD/C
      COMMON/WORK8/N,NJ
  101 FORMAT(15HODETERM=0 AT J=,I4)
      IF(J-2) 1,6,8
    1 NP1=N+1
      DO 2 I=1,N
      D(I,2*N+1)=G(I)
      DO 2 L=1,N
      LPN = L+N
    2 D(I,LPN)= X(I,L)
      CALL MATINV(N,2*N+1,DETERM)
      IF(DETERM)4,3,4
    3 WRITE (6,101) J
    4 DO 5 K=1,N
      E(K,NP1,1)=D(K,2*N+1)
      DO 5 L=1,N
      E(K,L,1)=-D(K,L)
      LPN=L+N
    5 X(K,L)=-D(K,LPN)
      RETURN
    6 DO 7 I=1,N
      DO 7 K=1,N
      DO 7 L=1,N
```

```
 7  D(I,K)=D(I,K)+A(I,L)*X(L,K)
 8  IF(J-NJ) 11,9,9
 9  DO 10 I=1,N
    DO 10 L=1,N
    G(I)=G(I)-Y(I,L)*E(L,NP1,J-2)
    DO 10 M=1,N
10  A(I,L)=A(I,L)+Y(I,M)*E(M,L,J-2)
11  DO 12 I=1,N
    D(I,NP1)=-G(I)
    DO 12 L=1,N
    D(I,NP1)=D(I,NP1)+A(I,L)*E(L,NP1,J-1)
    DO 12 K=1,N
12  B(I,K)=B(I,K)+A(I,L)*E(L,K,J-1)
    CALL MATINV(N,NP1,DETERM)
    IF (DETERM) 14,13,14
13  WRITE(6,101) J
14  DO 15 M=1,NP1
    DO 15 K=1,N
15  E(K,M,J)=-D(K,M)
    IF(J-NJ) 20,16,16
16  DO 17 K=1,N
17  C(K,J)=E(K,NP1,J)
    DO 18 JJ=2,NJ
    M=NJ-JJ+1
    DO 18 K=1,N
    C(K,M)=E(K,NP1,M)
    DO 18 L=1,N
18  C(K,M)=C(K,M)+E(K,L,M)*C(L,M+1)
    DO 19 L=1,N
    DO 19 K=1,N
19  C(K,1)=C(K,1)+X(K,L)*C(L,3)
20  RETURN
    END

    SUBROUTINE MATINV(N,M,DETERM)
    IMPLICIT REAL*8(A-H,O-Z)
    DIMENSION A(6,6),B(6,6),C(6,93) ,D(6,13),G(6),X(6,6),Y(6,6),ID(6)
    COMMON/WORKA/A,B,D,G,X,Y
    COMMON/WORKD/C
    DETERM=1.0
    DO 1 I=1,N
 1  ID(I)=0
    DO 18 NN=1,N
    BMAX=0.0
    DO 6 I=1,N
    IF(ID(I)) 2,2,6
 2  DO 5 J=1,N
    IF(ID(J)) 3,3,5
 3  IF(DABS(B(I,J))-BMAX) 5,5,4
 4  BMAX=DABS(B(I,J))
    IROW=I
    JCOL=J
 5  CONTINUE
 6  CONTINUE
    IF(BMAX) 7,7,8
 7  DETERM=0.0
    RETURN
 8  ID(JCOL)=1
    IF(JCOL-IROW) 9,12,9
 9  DO 10 J=1,N
    SAVE=B(IROW,J)
    B(IROW,J)=B(JCOL,J)
10  B(JCOL,J)=SAVE
    DO 11 K=1,M
    SAVE=D(IROW,K)
    D(IROW,K)=D(JCOL,K)
11  D(JCOL,K)=SAVE
12  F=1.0/B(JCOL,JCOL)
    DO 13 J=1,N
13  B(JCOL,J)=B(JCOL,J)*F
    DO 14 K=1,M
14  D(JCOL,K)=D(JCOL,K)*F
    DO 18 I=1,N
    IF(I-JCOL) 15,18,15
15  F=B(I,JCOL)
    IF(DABS(F).LE.1.00-25) F=0.0
    DO 16 J=1,N
16  B(I,J)=B(I,J)-F*B(JCOL,J)
```

```
      DO 17 K=1,M
   17 D(I,K)=D(I,K)-F*D(JCOL,K)
   18 CONTINUE
      RETURN
      END
      SUBROUTINE SCOND(XA,XB,CND,CNDA,CNDB)
      IMPLICIT REAL*8(A-H,O-Z)
      COMMON/WORK1/EFFCND
      CNDA=0.0
      IF(XB.GE.0.009) GO TO 3
      IF(XB.GE.0.0037) GO TO 2
      IF(XB.GE.0.0015) GO TO 1
      B1=195.3362
      CND=0.03655+B1*(XB-1.513*10.0**(-4))
      CNDB=B1/CND
      GO TO 4
    1 B1=134.0975
      CND=0.300+ B1*(XB-0.0015)
      CNDB=B1/CND
      GO TO 4
    2 B1=3.14159*(XB-0.00645)/0.0105/2.0
      CND=0.6572*DCOS(B1)
      CNDB=-31.295*3.14159*DSIN(B1)/CND
      GO TO 4
    3 CND=0.61-57.805*(XB-0.009)
      CNDB=-57.805/CND
    4 CONTINUE
      CND=CND*EFFCND
      RETURN
      END
      SUBROUTINE EQUIL(CA,CB,EQB,EQAB,EQP)
      IMPLICIT REAL*8(A-H,O-Z)
      COMMON/WORKH/TOT,L
      IF(CB.GE.0.009) GO TO 2
      IF(CB.GE.0.002) GO TO 1
      EQB=0.0
      EQAB=CA-EQB
      EQP=0.0
      GO TO 3
    1 EQB=-2.0*10.0**(-4)+0.0975*CB+1.25*CB*CB
      IF(EQB.LT.0.0) EQB=0.0
      EQAB=CA-EQB
      EQP=0.0975+2.5*CB
      GO TO 3
    2 EQB=1.0*10.0**(-4)+0.030*CB+5.0*CB*CB
      EQAB=CA-EQB
      EQP=0.03+10.0*CB
    3 CONTINUE
      IF(L.EQ.1.AND.EQAB.LT.0.0) EQAB=0.0
      IF(L.EQ.2.AND.EQAB.GT.0.0) EQAB=0.0
      RETURN
      END
C
      SUBROUTINE SACTIV(XA,XB,ACTA,ACTB,YA,YB,YAA,YAB,YBA,YBB)
      IMPLICIT REAL*8(A-H,O-Z)
      COMMON/WORKF/NACT
      BA=1.1580
      BET12=-0.01425
      BET13 = 0.130
      ALPH=1.1762
      WMA=211.58
      WMB=56.10
      WMW=18.016
      VOLW=18.07
      B1DEN=46.70
      B2DEN=-625.90
      A1DEN=128.475
      A2DEN=-401.68
      DENTY=1.0+B1DEN*XB+B2DEN*XB**2+A1DEN*XA+A2DEN*XA**2
      CONW=(DENTY-XA*WMA-XB*WMB)/WMW
      XMOLA=(XA/CONW/WMW)*1000.0
      XMOLB=(XB/CONW/WMW)*1000.0
      IF(NACT.NE.0) GO TO 1
      SQTTA=(3.0*XMOLA)**0.50
      SQTTB=XMOLB**0.50
      COEFA=-2.0*ALPH*SQTTA/(1.0+BA*SQTTA)+6.0*BET12*XMOLA/3.0
      COEFB=-ALPH*SQTTB/(1.0+SQTTB)+2.0*BET13*XMOLB
      SQLM=10.0**(-5)
      IF(SQTTA.LE.SQLM) GO TO 2
      GA=8.0*BET12/3.0 - 3.0*ALPH/SQTTA/(1.0+BA*SQTTA)**2
      YA0=1.0+GA*XMOLA
      GO TO 3
    2 YA0=1.0
```

```
    3   IF(SQTTB.LE.SQLM) GO TO 4
        GB=2.0*BET13 - ALPH/2.0/SQTTB/(1.0+SQTTB)**2
        YB0=1.0+GB*XMOLB
        GO TO 5
    4   YB0=1.0
        GO TO 5
    1   CONTINUE
        TOTAL=XMOLB+3.0*XMOLA
        SQTOT=(TOTAL)**0.50
        COEFA=-2.0*ALPH*SQTOT/(1.0+BA*SQTOT)+8.0*BET12*XMOLA/3.0
       1 +2.0*(BET12+2.0*BET13)*XMOLB/3.0
        COEFB=-ALPH*SQTOT/(1.0+SQTOT)+2.0*BET13*XMOLB
       1 +(BET12+2.0*BET13)*XMOLA
        GA=8.0*BET12/3.0 - 3.0*ALPH/SQTOT/(1.0+BA*SQTOT)**2
        GB=2.0*BET13 - ALPH/2.0/SQTOT/(1.0+SQTOT)**2
        YA0=1.0+GA*XMOLA
        YB0=1.0+GB*XMOLB
    5   CONTINUE
        GAMA=DEXP(COEFA)
        GAMB=DEXP(COEFB)
        ACTA=XMOLA*GAMA
        ACTB=XMOLB*GAMB
        YA=YA0/CONW/VOLW
        YB=YB0/CONB/VOLW
        CONWTR=CONW*WMW*CONW*VOLW
        YBB=GB*1000.0/CONWTR -YB*(3.1DEN-WMB+A2DEN*2.0*XB)/WMW/CONW
        YAA=0.0
        YAB=0.0
        YBA=0.0
        RETURN
        END
C
C
        SUBROUTINE SWATR(T1,T2,C0,XA,XB,YA,YB,YAA,YAB,YBA,YBB)
        IMPLICIT REAL*8(A-H,O-Z)
        RTF=8.3143*298.16/96487.0
        TR2=T2*XA/C0
        TR3=1.0-T1-TR2
        YA=1.5*RTF*(-1.0-TR2)
        YAA=-1.5*RTF*T2/C0/YA
        YB=RTF*(4.0-2.0*TR3)
        YBA=2.0*RTF*T2/C0/YB
        YAB=0.0
        YBB=0.0
        RETURN
        END
C
C
C
C
        SUBROUTINE SDIF(CA,CB,YA,YB,YAA,YAB,YBA,YBB)
        IMPLICIT REAL*8(A-H,O-Z)
        XA=CA*1000.0
        XB=CB*1000.0
        YA=0.686*10.0**(-5)
        WMKOH=56.10
        WMH2O=18.016
        VISC=0.889812+0.073531*XB+0.016601*XB**2
        IF(XB.LE. 3.866) VISC=0.33370+0.090549*XB+0.011962*XB**2
        IF(XB.GT.7.333) VISC=7.434-1.57482*XB+0.119677*XB**2
        DENS=1.0156+0.03576*XB
        IF(XB.LE.5.0) DENS=0.9971+0.03959*XB
        CW=(DENS-CB*WMKOH)/WMH2O
        CT=CW+ 2.0*CB
        YB=7.358*10.0**(-8)*298.16*CT/CW/VISC
        YAA=0.0
        YAB=0.0
        YBA=0.0
        YBB=0.0
        RETURN
        END
C
C
        SUBROUTINE SDIFP(XA,XB,YAAA,YAAB,YABB,YBAA,YBAB,YBBB)
        IMPLICIT REAL*8(A-H,O-Z)
        YAAA=0.0
        YAAB=0.0
        YABB=0.0
```

```
      YBAA=0.0
      YBAB=0.0
      YBBB=0.0
      RETURN
      END
C
C
      SUBROUTINE SIGMA(EG,EPI,EM,ES,SGDM,SGDS,SIG)
      IMPLICIT REAL*8(A-H,O-Z)
      COMMON/WORKE/SGM0,SGS0,SGG0,EMLIM
      COMMON/WORKH/TOT,L
      TT=TOT
      TTM1=TT-1.0
      EMTM1=0.0
      ESTM1=0.0
      EGTM1=0.0
      IF(EM.GT.EMLIM) EMTM1=EM**TTM1
      IF(ES.GT.0.0) ESTM1=ES**TTM1
      IF(EG.GT.0.0) EGTM1=EG**TTM1
      SIG=SGM0*EMTM1*EM+SGS0*ESTM1*ES+SGG0*EG*EGTM1
      SGDM=SGM0*TT*EMTM1
      SGDS=SGS0*TT*ESTM1
      RETURN
      END
C
      SUBROUTINE RKAY(DELT,EPSOL,EPZN,EPZNO,AM,AMDCUR,AMDCA,RM,RS,
     1 RMDCUR,RSDCUR,RMDCA,RSDCA)
      IMPLICIT REAL*8(A-H,O-Z)
      COMMON/WORKC/A0,TIME,RM0,RS0,RXT,EPI,EPGI,EPNUCS,EPNUCM,EQUIAB,
     1 EQUMAX,EPLIM,NOZN,MM,J
      COMMON/WORKH/TOT,L
      P=2.0/3.0
      S=2.0/3.0
      EPG=EPGI
      RS0=RM0
      RXTAL=RXT
      ATOT=A0*((1.0-EPSOL)/(1.0-EPI))**P
      IF(EPZN.LE.EPLIM) EPZN=EPLIM
      IF(EPZNO.LE.EPLIM) EPZNO=EPLIM
      EPM=EPZN
      EPS=EPZNO
      IF(L.EQ.1) EPS=EPZNO+EPG
      IF(L.EQ.2) EPM=EPZN+EPG
      EPMP=EPM**P
      EPSQ=EPS**S
      EPMS=EPMP+EPSQ
      EPMFRN=EPMP/EPMS
      EPSFRN=EPSQ/EPMS
      NEPM=0
      NEPS=0
      IF(L.EQ.2) GO TO 4
      IF(EPSFRN.GE.EPNUCS) GO TO 7
      IF(EQUIAB.LE.1.0D-10) EQUIAB=1.0D-10
      IF(EQUIAB.GE.EQUMAX) EQUIAB=EQUMAX
      EPSFRN=EPNUCS*(EQUIAB/EQUMAX)**NEPS
      GO TO 7
    4 CONTINUE
      IF(NOZN.EQ.0) GO TO 6
      IF(EPMFRN.GE.EPNUCM) GO TO 7
      EQUFRN=1.0-DABS(EQUIAB)/EQUMAX
      IF(EQUFRN.LE. 1.0D-10) EQUFRN=1.0D-10
      EPMFRN=EPNUCM*EQUFRN**NEPM
      GO TO 7
    6 CONTINUE
      IF(J-1) 11,11,12
   11 EPMMTX=1.0-EPSQ
      IF(EPMFRN.LE.EPMMTX) EPMFRN=EPMMTX
      GO TO 7
   12 IF(EPMFRN.GE.EPNUCM) GO TO 7
      EQUFRN=1.0-DABS(EQUIAB)/EQUMAX
      IF(EQUFRN.LE. 1.0D-10) EQUFRN=1.0D-10
      EPMFRN=EPNUCM*EQUFRN**NEPM
    7 CONTINUE
      AM=ATOT*EPMFRN
      AS=ATOT*EPSFRN
      RM=RM0*(ATOT-AM)/DLOG(ATOT/AM)
      RS1=RS0*(ATOT-AS)/DLOG(ATOT/AS)
      RS=1.0/(1.0/AS/RXTAL+1.0/RS1)
      DT=DELT
```

```
      IF(MM.LE.1) DT=0.0
      ASTAR=9.15/2.0/96487.0
      DEL=14.51*DT/2.0
      DELTI=ASTAR*DT/2.0
      DELTA=-DEL*RS
      PORO=-2.0/3.0/(1.0-EPI)
      ATOTI=ATOT*PORO*DELTI
      ATOTA=ATOT*PORO*DELTA
      AMDCUR=(PORO-P*EPSFRN/EPM)*AM*DELTI
      AMDCA=(PORO+S*EPSFRN/EPS)*AM*DELTA
      ASI=(PORO+P*EPMFRN/EPM)*AS*DELTI
      ASA=(PORO-S*EPMFRN/EPS)*AS*DELTA
      RMC1=1.0/(ATOT-AM)-1.0/ATOT/DLOG(ATOT/AM)
      RMC2=1.0/AM/DLOG(ATOT/AM)-1.0/(ATOT-AM)
      RMDCUR=RMC1*ATOTI+RMC2*AMDCUR
      RMDCA=RMC1*ATOTA+RMC2*AMDCA
      ASC0=1.0/(ATOT-AS)-1.0/ATOT/DLOG(ATOT/AS)
      ASCU=1.0/(ATOT-AS)-1.0/AS  /DLOG(ATOT/AS)
      RSC1=ASC0*(1.0-RS/AS/RXTAL)
      RSC2=-ASCU+ASC0*RS*ATOT/RXTAL/AS/AS
      RSDCUR=RSC1*ATOTI +RSC2*ASI
      RSDCA =RSC1*ATOTA+ RSC2*ASA
      RETURN
      END
      SUBROUTINE SWELL(NJMN,NJMX)
      IMPLICIT REAL*8(A-H,O-Z)
      DIMENSION C(6,93),QM(93),Q(93),EP(93)
      COMMON/WORKB/N,NJ
      COMMON/WORKD/C
      COMMON/WORKG/QM,Q,EP,H,VOLUME,EPGICC,JPLG
      COMMON/WORKH/TOT,L
      NJM1=NJ-1
      SUMQM=0.0
      SUMQS=0.0
      DO 1 J=NJMN,NJM1
      SUMQM=SUMQM+0.5*H*(QM(J)+QM(J+1))
      SUMQS=SUMQS+0.5*H*(Q(J)+Q(J+1))
    1 CONTINUE
      NJSWL=NJMN+SUMQS/H/Q(NJMN) +0.50
      QM(NJSWL)=2.0*SUMQM/H/DFLOAT(NJSWL-NJMN) -QM(NJMN)
      NJSWM=NJSWL
      IF(QM(NJSWL).GT.0.0) GO TO 2
      NJSWM=2.0*SUMQM/H/QM(NJMN) +NJMN +0.50
    2 CONTINUE
      DO 3 J=NJMN,NJSWL
      Q(J)=Q(NJMN)
      IF(NJSWM.GE.NJSWL) GO TO 4
      QM(J)=QM(NJMN)-QM(NJMN)*DFLOAT(J-NJMN)/DFLOAT(NJSWM-NJMN)
      IF(QM(J).LE.0.0) QM(J)=0.0
      GO TO 5
    4 CONTINUE
      QM(J)=QM(NJMN)+(QM(NJSWL)-QM(NJMN))*DFLOAT(J-NJMN)/DFLOAT(NJSWL
     1 -NJMN)
    5 CONTINUE
      IF(J.LT.NJ) GO TO 6
      EP(J)=1.0-QM(J)-Q(J)-EPGICC
      C(3,J)=C(3,NJ)
      C(4,J)=C(4,NJ)
      C(1,J)=C(1,NJ)
      C(5,J)=C(5,NJ)
      CALL SCOND(C(3,J),C(4,J),CONDNJ,CONDA,CONDB)
      C(2,J)=C(2,NJ)-C(1,J)*DFLOAT(J-NJ)*H/CONDNJ/EP(J)**(1.0+TOT)
      C(6,J)=C(6,NJ)
    6 CONTINUE
    3 CONTINUE
      VOLUME=VOLUME-H*DFLOAT(NJSWL-NJ)
      NJ=NJSWL
      RETURN
      END
```